

https://dspace.org/

Increasing geotechnical data confidence through the Integration of laser scanner face mapping data into the Sishen iron ore mine geotechnical database

Russell, Timothy Michael

2018

https://hdl.handle.net/10539/25215

Russell, Timothy Michael (2018) Increasing geotechnical data confidence through the Integration of laser scanner face mapping data into the Sishen iron ore mine geotechnical database, University of the Witwatersrand, Johannesburg, <http://hdl.handle.net/10539/25215>

Downloaded from a DSpace repository. https://dspace.org/

Increasing Geotechnical Data Confidence through the Integration of Laser Scanner Face Mapping Data into the Sishen Iron Ore Mine Geotechnical Database

Timothy Michael Russell

A research report submitted to the Faculty of Engineering and the Built Environment, University of the Witwatersrand, Johannesburg, in partial fulfilment of the requirements for the degree of Master of Science in Engineering.

Johannesburg 2018

Declaration

I am aware that plagiarism (the use of someone else's work without their permission and/or without acknowledging the original source) is wrong. I confirm that ALL the work submitted for assessment for this research report is my own unaided work except where I have explicitly indicated otherwise. I have followed the required conventions in referencing the thoughts and ideas of others. I understand that the University of the Witwatersrand may take disciplinary action against me if there is a belief that this is not my own unaided work or that I have failed to acknowledge the source of the ideas or words in my writing.

Signature: _____ Date: _____

ABSTRACT

Face mapping is a simple but invaluable means of geological and geotechnical data acquisition whereby intact rock properties, rock mass properties, discontinuity properties and structural orientation can be assessed. Although traditionally done via direct contact with the mapping face through techniques such as line mapping or window mapping, remote face mapping using various digital techniques has become increasingly popular in recent years. Sishen Mine is a large open pit mining operation requiring a comprehensive geotechnical data set to evaluate pit wall design and stability with the necessary level of confidence. Geotechnical borehole data, face mapping data, geotechnical lab testing data and implicit structural models provide the main sources of this information. Although a large geotechnical borehole database has always been maintained at the mine, face mapping has in the past been restricted to sporadic and isolated stability assessments. In 2013 the mine acquired a Maptek 8810 terrestrial laser scanner with the resolution, photographic capabilities and software required to carry out geotechnical face mapping. The aims of this research project were to evaluate the capabilities of the Maptek scanner and system, set up a standard face mapping procedure, integrate face mapping data in the mine's geotechnical database and compare face mapping acquired rock mass data with the mine's existing borehole data set. Further potential uses for the laser scanner system and face mapping data were also explored throughout the course of the dissertation. A face mapping procedure was set up and faces were mapped from 86 individual scans, acquired between October 2015 and April 2017. The mapping data obtained from the scans was integrated into the Acquire Geological Data Management System, a purpose designed Structured Query Language (SQL) database system used for storing the mine's geotechnical data. Open Database Connectivity (ODBC) database links with the Micromine Computer Aided Design (CAD) package allowed for spatial overlays of mapping data with other geotechnical data as well as survey and mine planning data. In terms of data analysis mapping parameters such as joint spacing, Rock Quality Designation and Rock Mass Rating could be directly compared with borehole logging values for the same rock types. The comparison indicated that in general borehole measurements tend to slightly under estimate joint spacing and rock mass rating values while face mapping assessments tend to slightly over estimate these values. This is due to various intricacies of the two data capture techniques that tend to skew the data in one way or the other. Face mapping data was compared with Sishen's existing structural model, which is based mainly on interpretation and implicit data. Structural orientations and features correlate well between the implicit model and actual mapped values gathered during the data collection phase of this project. Within the geotechnical design process, having actual mapping data in combination with increased confidence in the structural model allows for better definition of geotechnical design sectors. Overall the face mapping and geotechnical analysis features of the Maptek 8810 terrestrial laser scanner make it an invaluable geotechnical data capture tool, providing a system is in place to store mapping data in a manner that allows for meaningful rock mass and structural information to be produced.

ACKNOWLEDGEMENTS

I would like to acknowledge my supervisor for this research, Professor Dick Stacey for his input and advice, and the knowledge that he imparted during the course of my research. I would also like to thank Kumba Iron Ore for the financial support that they provided and for allowing me to use their facilities, equipment and data. Marnus Bester, Kumba's Principal Geotechnical Engineer and Richard Carey, Sishen Mine's Chief Geotechnical Engineer both gave invaluable advice and logistical support that allowed me to carry out this research. The Sishen Mine Survey Department played a crucial role in field data collection and equipment maintenance while the staff of Sishen's Geotechnical Engineering Section were invaluable in assisting with data capture. I would finally like to thank my wife and parents for the support I received from them while completing this research project.

TABLE OF CONTENTS

DECLARATION i
ABSTRACT ii
ACKNOWLEDGEMENTS iii
LIST OF FIGURES viii
LIST OF TABLES xiv
LIST OF ABREVIATIONS AND SYMBOLS xv

CHAPTER 1: INTRODUCTION AND RESEARCH OBJECTIVES 1
1.1. INTRODUCTION 1
1.2. RESEARCH OBJECTIVES 2
1.3. SISHEN IRON ORE MINING OPERATION 2

CHAPTER 2: GEOLOGICAL SETTING 6
2.1. REGIONAL GEOLOGICAL SETTING 6
2.1.1. Camblerand Subgorup Dolomites (Transvaal Supergroup) 9
2.1.2. Wolharkop Formation Chert Breccia (Transvaal Spergroup) 9
2.1.3. Manganore Iron Formation (Transvaal Supergroup) 10
2.1.4. Gamagara Formation (Olifantshoek Supergroup) 11
2.1.5. Postmasburg Formation (Transvaal Supergroup) 12
2.1.6. Kalahari Group 12
2.2. STRUCTURAL EVOLUTION 14
2.3. INTRUSIVE EVENTS 15

CHAPTER 3: GEOTECHNICAL FACE MAPPING THEORY 16
3.1. DISCONTINUITY PROPERTIES AND THE INFLUENCE ON A ROCK MASS 16
3.1.1. Definition and Engineering Significance 16
3.1.2. Origin and nature of Natural Discontinuities 17
3.1.3. Discontinuity Strength 18
3.1.3.1. Joint Roughness Coefficient (JRC) 20
3.1.3.2. Joint Compressive Strength (JCS) 23
3.1.4. Discontinuity Orientation 25
3.1.5. Discontinuity Spacing 25
3.1.6. Discontinuity Persistency 27
3.2. ROCK MASS CLASSIFICATION SYSTEMS 28
3.2.1. Geological Strength Index (GSI) 31

3.2.2. Tunneling Q Index (GSI) 31
3.2.3. Rock Mass Rating (RMR) 32
3.2.4. Mining Rock Mass Rating (MRMR) 34
3.3. FACE MAPPING BACKGROUND AND TECHNIQUES 36
3.3.1. Mapping Parameters 36
3.3.2. Manual Face Mapping Techniques 37
3.3.3. Digital Face Mapping Techniques 37
3.3.4. Disadvantages of Face Mapping 39
3.4. KINEMATIC SLOPE STABILITY ANALYSIS 40
3.4.1. Plane Failure Analysis 41
3.4.2. Wedge Failure Analysis 42
3.4.3. Toppling Failure Analysis 43

CHAPTER 4: PROJECT METHODOLOGY 46
4.1. THEORETICAL FACE MAPPING DATA FLOW PROCESS 47
4.2. FACE MAPPING PROCEDURE 47
4.2.1. Mapping Face Selection 47
4.2.2. Laser Scanning 48
4.2.3. Data Analysis 49
4.2.4. Setup and Features of the I-Site Studio Software 50
4.2.5. Face Mapping Protocol 52
4.2.6. Data Processing in Microsoft Excel 67
4.2.6.1. Data Import From I-Site Studio 67
4.2.6.2. Discontinuity Roughness Calculation and Import 69
4.2.6.3. Mapping Data Analysis 70
4.2.6.3.a. Stereographic Projection 71
4.2.6.3.b. Stereonet Kinematic Analysis Functionality 73
4.2.6.3.c. Plane Failure Analysis 75
4.2.6.3.d. Wedge Failure Analysis 76
4.2.6.3.e. Designating Major Planes 77
4.2.6.3.f. Rock Mass Classification 78
4.2.6.4. Data Export from Excel to Acquire 80
4.2.7. Data Import into Acquire 81
4.2.7.1. Front End Software 81
4.2.7.2. Geotechnical Database Structure 82
4.2.7.3. The Acquire Data Model (ADM) 82
4.2.7.4. Accommodating Mapping Data 85

4.2.7.5. Theoretical Face Mapping Database Table Scheme 87
4.2.7.6. Methodology For Exchange of data between Excel and Acquire 89
4.2.7.7. Accessing, Querying and Reporting of Mapping Data Stored in Acquire 91
4.2.7.7.a. Accessing Data Directly Within Acquire 91
4.2.7.7.b. Creating a Database Link for Third Party Software 91
4.2.7.7.c. Accessing Mapping Data Using Microsoft Excel 92
4.2.7.7.d. Accessing Mapping Data Using Micromine Software 92
4.3. INTERGRATION OF MAPPING DATA IN THE GEOTECHNICAL DESIGN PROCESS 93
4.3.1. Linking of Sishen's Geotechnical Data Sources with Micromine 94
4.3.2. Integration of Mapping Data With Other Geotechnical Data Sources 95
4.3.3. Influence of an Integrated Face Mapping Database on the Design Process 98
4.4. REPORTING AND ANALYSIS OF ACQUIRE BOREHOLE AND MAPPING DATA 99
4.4.1. Tracking of Mapping Progress 99
4.4.2. Reconciliation of Mapping and Borehole Data Statistics 100
4.5. GEOTECHNICAL HAZARD IDENTIFICATION 104

CHAPTER 5: RESULTS AND DISCUSSION 106
5.1. OBSERVED ADVANTAGES AND DISADVANTAGES OF THE SYSTEM 106
5.1.1. Mapping of Scanned Faces and Data Capture 106
5.1.1.1. Safety and Accessibility 106
5.1.1.2. Data Capture Process 107
5.1.1.3. Idealized I-Site Studio Kinematic Analysis Process 108
5.1.2. Economic and Practical Aspects of Laser Scanning 113
5.2. COMPARISON OF BOREHOLE AND FACE MAPPING DERIVED ROCK MASS RATING PARAMETERS 114
5.2.1. Discontinuity Spacing / Fracture Frequency 114
5.2.1.1. Bedding Spacing 114
5.2.1.2. Joint Spacing 117
5.2.2. RQD 119
5.2.3. Discontinuity Persistency 124
5.2.4. Roughness Measurements 126
5.2.5. Rock Mass Rating Systems 130
5.2.5.1. Input Variability Between Face Mapping and Borehole Data 130
5.2.5.2. Comparison of Face Mapping and Borehole Derived RMR and GSI Data 131
5.3. SYNTHETIC ROCK MASS MODELLING 135
5.4. FACE MAPPING FOR STRUCTURAL MODEL RECONCILLIATION 137
5.5. POTENTIAL FUTURE DEVELOPMENTS 141

5.5.1. Geotechnical Block Modelling 141
5.5.2. Blastability Evaluation 142

CHAPTER 6: CONCLUSIONS 145

LIST OF FIGURES

		Page
Figure 1.1:	Location of Kumba Iron Ore mining operations.	3
Figure 1.2:	Sishen mining area.	3
Figure 1.3:	Illustration of the mining areas within the Sishen mining complex.	4
Figure 1.4:	Illustration of the actual mined out area versus the planned final pit shells for the Sishen Northern Mining area.	4
Figure 1.5:	Illustration of the actual mined out area versus the planned final pit shells for the Sishen Central and Southern Mining area.	4
Figure 2.1:	Southern African Archean and Proterozoic.	6
Figure 2.2:	Locality of the Sishen Mine relative to the Kaapvaal craton and the Griqualand West and Transvaal structural basins.	7
Figure 2.3:	Geological setting of the Maremane Dome area.	8
Figure 2.4:	Stratigraphy of the Maremane Dome Area.	8
Figure 2.5:	Hand sample and field exposure of Wolhaarkop Formation Chert Breccia at Sishen Mine.	9
Figure 2.6:	Hand and core samples of Banded Iron Formation as well as field exposure at Sishen Mine.	10
Figure 2.7:	Hand sample of massive hematite ore.	10
Figure 2.8:	Interbedded Gamagara Formation Quartzite and Shale at Sishen Mine.	11
Figure 2.9:	Kalahari Group sediments at Sishen Mine.	13
Figure 2.10:	Diabase dyke intruded into Banded Iron Formation, cross cutting the Sishen mining area.	15
Figure 3.1:	Illustration of jointing patterns on the limb of an asymmetrical anticline.	18
Figure 3.2:	Illustration of the Patton (1966) saw tooth.	19
Figure 3.3:	Joint roughness profiles for estimation of the Joint Roughness Coefficient.	20
Figure 3.4:	Chart for estimation of Joint Roughness Coefficient from the amplitude of asperities.	21
Figure 3.5:	Illustration of the compass disc-clinometer roughness measurement method.	22
Figure 3.6:	Illustration of the straight edge roughness measurement method.	23
Figure 3.7:	Palmström classification of roughness and waviness based on the amplitude of joint asperities.	23
Figure 3.8:	Chart for estimation of Joint Compressive Strength based on Schmidt Hammer rebound values.	24
Figure 3.9:	Illustration of dip, dip direction, strike, trend and plunge measurements.	25
Figure 3.10:	Illustration of the effect of scale on rock mass stability.	26

Figure 3.11: Illustration of a continuous failure surface (a) and stepped path failure surface (b). 27
Figure 3.12: Illustration of the effect of persistency on rock mass stability. 28
Figure 3.13: Relationship between RQD and joint spacing based on the relationship TRQD = 100 $e^{t\lambda}$ ($t\lambda$ + 1). 29
Figure 3.14: Application of the MRMR system. 35
Figure 3.15: Haines and Terbrugge slope stability chart. 36
Figure 3.16: Idealized modes of slope failure and associated stereonet pole plots. 41
Figure 3.17: Plane failure analysis stereonet. 42
Figure 3.18: Illustration of a failure wedge. 43
Figure 3.19: Wedge failure analysis stereonet. 43
Figure 3.20: Illustration of block toppling (a), flexural Toppling (b) and block flexural toppling (c). 44
Figure 3.21: Toppling failure analysis stereonet. 45
Figure 4.1: Theoretical process flow for development, implementation and assessment of the results from laser scanner face mapping. 46
Figure 4.2: Theoretical face mapping data flow process. 47
Figure 4.3: Maptek 8810 laser scanner using a vehicle-mounted setup (left) and a high resolution point cloud for use in face mapping (right). 48
Figure 4.4: Illustration of the process to create a mapping face from a point cloud in the I-Site Studio software. 49
Figure 4.5: Illustration of the selection of discontinuity planes in the I-Site Studio software. 49
Figure 4.6: Illustration of a joint surface mapped by amplitude of asperities for roughness determination. 50
Figure 4.7: Example of the folder tree within an I-Site Studio project. 51
Figure 4.8: A scan showing unconnected scan points (above) and connected points with a photographic overlay (below). 52
Figure 4.9: High resolution with many points defining the mapping plane. 53
Figure 4.10: Low resolution with few points defining the mapping plane. 53
Figure 4.11: Examples of good and poor face mapping faces. 54
Figure 4.12: Data captured from a single scan allowing for mapping of both the exposed final pit boundary and legacy slopes up to 400m away from the scanner location. 55
Figure 4.13: Examples of a curved highwall divided into two separate mapping faces. 55
Figure 4.14: Raw scan data (left) versus mapping face viewed from the scan origin, ready for mapping of discontinuities (right). 56
Figure 4.15: Selection of a joint plane for mapping. 56

Figure 4.16: Discontinuity storage with the I-Site Studio Database. 56
Figure 4.17: Automated discontinuity extraction using the I-Site 'Extract Discontinuities' tool. 57
Figure 4.18: Erroneous automated discontinuity plane extractions. 58
Figure 4.19: Joint plane extraction with automated joint spacing measurements indicated in red and true joint spacing including 'hidden' planes indicated in blue for a prominent sub vertical joint set. 59
Figure 4.20: Illustration of joint spacing measurements on a mapping face. 60
Figure 4.21: Interpretation of joint persistency's on a mapping face. 61
Figure 4.22: Persistent discontinuity terminating below the floor of the face – not suitable for measurement. 61
Figure 4.23: Roughness measurement process using the built in I-Site Studio Discontinuity Waviness tool. 62
Figure 4.24: Joint roughness trace lines plotted between two points on the Face surface. 63
Figure 4.25: Face profile showing trace length versus amplitude of irregularities. 64
Figure 4.26: Face profile on known flat surfaces illustrating deviations in the surface created from laser scanner data from the true surface. 64
Figure 4.27: Illustration of the area of the Barton (1982) chart where roughness values are considered unreliable due to the relative scale of the scanner inaccuracy. 65
Figure 4.28: Face orientation, length and area determination in I-Site Studio. 66
Figure 4.29: Example of Excel data import template with face mapping data imported. 68
Figure 4.30: Example of orientation, spacing and frequency data imported into Microsoft Excel. 68
Figure 4.31: Illustration of data plotted on a digital version of the Barton (1982) JRC Chart. 69
Figure 4.32: Joint roughness assessment from roughness measurement taken from a single mapping face. 70
Figure 4.33: Illustration of the projection of a plane on the lower hemisphere of a stereonet onto a flat surface. 71
Figure 4.34: Illustration of plotting and rotating a stereonet point on an Excel chart. 72
Figure 4.35: Illustration of the apparent dip of a point on the great circle of a plane. 72
Figure 4.36: Illustration of a stereonet plotted on a Microsoft Excel chart. 74
Figure 4.37: Illustration of a stereonet plotted on a Microsoft Excel chart with contoured data. 74
Figure 4.38: Major planes plotted on the analysis stereonet (dashed orange) for plane failure analysis. 75
Figure 4.39: Mapping analysis report sheet wedge failure analysis stereonet and statistics. 76

Figure 4.40: Intersections of major planes selected by the user on the mapping analysis sheet. 77
Figure 4.41: Process of selecting discontinuity sets for export into Acquire. 78
Figure 4.42: Rock Mass Rating and GSI output on the face mapping report sheet. 80
Figure 4.43: Mapping data stored as CSV files after export. 81
Figure 4.44: Simplified representation of how geotechnical data is stored in Acquire. 82
Figure 4.45: Example of how geotechnical data is stored in Acquire. 84
Figure 4.46: Theoretical geotechnical slope design process showing potential face mapping data input points. 87
Figure 4.47: Basic schematic face mapping database layout. 88
Figure 4.48: Theoretical mapping data flow path between I-Site Studio and Acquire. 90
Figure 4.49: Geotechnical spatial data flow path at Sishen Mine. 93
Figure 4.50: Data flow between Acquire and Micromine allowing for the automatic updating of Micromine plots as Acquire data is added. 95
Figure 4.51: Geotechnical face mapping and borehole data overlain on Sishen's design pit shell. 95
Figure 4.52: Section through the Sishen North pit structural geological interpretation. 96
Figure 4.53: Process used to estimate bedding dip and dip direction based on modelled lithological contacts per fault block. 96
Figure 4.54: Inferred versus measured dip directions, green arrows represents bedding stereonet best fits per mapping faces, red/blue arrows represent inferred dip and dip directions. 97
Figure 4.55: Measured versus interpreted fault planes overlain on an aerial photograph of the Sishen final pit boundary. 97
Figure 4.56: Summary of the potential face mapping inputs into the geotechnical design process. 98
Figure 4.57: Summary faces scanned per month between October 2015 and May 2017. 99
Figure 4.58: Summary of mapping measurement per lithology (Green – Total Measurements; Blue – Bedding Planes; Red – Joint Planes). 100
Figure 4.59: Mine divisions used for laboratory test, logging and mapping data queries. 101
Figure 4.60: Mapping / Logging data query sheet. 102
Figure 4.61: Laboratory testing data query sheet. 103
Figure 4.62: Face mapping analysis report. 104
Figure 5.1: Conceptual changes to the I-Site Studio discontinuity orientation capture process. 108
Figure 5.2: Conceptual addition of spacing and persistency query functions to I-Site Studio. 109

Figure 5.3: Conceptual addition to allow spacing and persistency measurements to be added to stereonet object for later reporting. 109
Figure 5.4: Actual I-Site Studio stereonet functionality. 110
Figure 5.5: Possible I-Site Studio stereonet functionality extensions. 110
Figure 5.6: Potential GSI rating system to be incorporated into mapping analysis. 111
Figure 5.7: Example face mapping report header section. 111
Figure 5.8: Example face mapping report rock mass statistics section. 112
Figure 5.9: Example face mapping report kinematic analysis section. 112
Figure 5.10: Comparison of bedding spacing data distributions for mapping and borehole logging data – laminated units. 115
Figure 5.11: Comparison of bedding spacing data distributions for mapping and borehole logging data – non-laminated unit. 116
Figure 5.12: Comparison of joint spacing data distributions for mapping and borehole logging data – laminated units. 118
Figure 5.13: Comparison of joint spacing data distributions for mapping and borehole logging data – non-laminated unit. 119
Figure 5.14: Comparison of RQD data distributions for mapping and borehole logging data. 120
Figure 5.15: Relationship between RQD and Joint Spacing according to the equation RQD = 115 – 3.3Jv. 121
Figure 5.16: Cumulative joint spacing for Banded Iron Formation from mapping data with Arithmetic and Log Normal mean positions indicated. 122
Figure 5.17: Comparison of face mapping RQD values derived from the Arithmetic and Log Normal discontinuity spacing mean of each mapping face. 122
Figure 5.18: Actual RQD values measured from borehole core versus theoretical joint spacing values back calculated from the Palmström (1982) and Palmström (2005) formulae (assuming 3 joint sets + random). 123
Figure 5.19: Distribution of bedding and joint persistency measurement taken during face mapping for Shale and BIF. 125
Figure 5.20: All discontinuity roughness data from the data collection phase of this project plotted on the Barton (1982) JRC calculation chart. 127
Figure 5.21: Roughness distribution for Banded Iron Formation and Shale. 128
Figure 5.22: Borehole and mapping subjective roughness descriptions. 129
Figure 5.23: Difference between calculated RMR and GSI values for the same geotechnical zone or mapping face. 131
Figure 5.24: Face mapping and borehole derived GSI and RMR data for BIF and Shale. 133

Figure 5.25: Illustration of the process used for modeling of slope stability with anisotropic strength. 136
Figure 5.26: Sishen North Mine measured (Red) versus inferred (Green) bedding orientation data. 137
Figure 5.27: Sishen Middle Mine measured (Red) versus inferred (Green) bedding orientation data. 138
Figure 5.28: Sishen South Mine measured (Red) versus inferred (Green) bedding orientation data. 138
Figure 5.29: Interpreted (Red) and mapped (Green) bedding dip directions. 139
Figure 5.30: Difference in interpreted versus measured dip direction. 139
Figure 5.31: Percentage of inferred dip direction values within 45 degrees of measured values considering data points at a range of 20m, 40m, 60m, 80m and 100m 140
Figure 5.32: Distribution of error in interpreted data points from corresponding measured dip direction data. 140
Figure 5.33: Design parameters from the Sishen geotechnical block model. 141
Figure 5.34: Illustration of populating a geotechnical block model with bedding orientation data. 142
Figure 5.35: Conceptual process for determining limit block blast design from face mapping data. 143
Figure 5.36: Conceptual process for determining production block blast design and carrying out post blast analysis. 144

LIST OF TABLES

		Page
Table 3.1:	RMR A1, A2 and A3 Ratings.	33
Table 3.2:	RMR Joint Condition A4 Rating.	33
Table 3.3:	RMR Groundwater A5 Rating.	34
Table 3.4:	RMR Orientation B Rating.	34
Table 3.5:	Slope design angles based on MRMR.	35
Table 4.1:	Approximate point spacing on a surface 50m from the Maptek 8810 Scanner at different scan resolution settings.	53
Table 4.2:	Rock Strength Classification.	79
Table 4.3:	Summary of face mapping statistics for faces scanned between September 2015 and May 2017.	99
Table 4.4:	Rock Types / Geotechnical Zones used for geotechnical purposes as Sishen. Groupings of logging codes are based on the geological groupings of rock types used in the mine's geological model.	101
Table 5.1:	Statistical bedding spacing parameters for data acquired from borehole logging and face mapping.	115
Table 5.2:	Statistical bedding spacing parameters for data acquired from borehole logging and face mapping for the non-laminated Wolhaarkop Formation.	116
Table 5.3:	Statistical joint spacing parameters for data acquired from borehole logging and face mapping.	117
Table 5.4:	Statistical joint spacing parameters for data acquired from borehole logging and face mapping for non-laminated manganese marker unit.	118
Table 5.5:	Statistical RQD parameters for data acquired from borehole logging and face mapping.	120
Table 5.6:	RQD statistics derived from the arithmetic and lognormal discontinuity spacing mean of each mapping face.	122
Table 5.7:	Bedding persistency statistics.	124
Table 5.8:	Joint persistency statistics.	125
Table 5.9:	Overall discontinuity Joint Roughness Coefficient statistics.	127
Table 5.10:	Joint and bedding plane Joint Roughness Coefficient statistics for Banded Iron Formation and Shale.	128
Table 5.11:	Comparison of subjective roughness assessments for RMR input from borehole core and mapping faces.	129
Table 5.12:	Comparison of borehole and face mapping derived RMR and GSI values.	132

LIST OF ABREVIATIONS AND SYMBOLS

Φ	Angle of Internal Friction
ADM	Acquire Data Model
BIF	Banded Iron Formation
C	Cohesion
CAD	Computer Aided Design
CSIR	Centre for Scientific and Industrial Research
CSV	Comma separated value file
DFN	Discrete Fracture Network
DRMS	Laubscher (1994) Design Rock Mass Strength
DTM	Digital Terrain Model
FOS	Factor of Safety
GSI	Geological Strength Index
IRS	Intact Rock Strength
JCS	Joint Compressive Strength
JRC	Joint Roughness Coefficient
Jv	Volumetric Joint Count
MRMR	Laubscher (1994) Mining Rock Mass Rating
ODBC	Open Database Connectivity
POF	Probability of Failure
Q	Barton et al. (1974) Q-System Rock Mass Rating Number
RMR	Bieniawski (1989) Rock Mass Rating
RMS	Laubscher (1994) Rock Mass Strength
RQD	Rock Quality Designation
SRM	Synthetic Rock Mass
UCS	Uniaxial Compressive Strength
VBA	Visual Basic for Applications

CHAPTER 1: INTRODUCTION AND RESEARCH OBJECTIVES

1.1. INTRODUCTION

Fundamental to the Geotechnical Design Process is the acquisition of a reliable and complete geotechnical dataset. Geotechnical data acquisition will typically commence during the early stages of a project and continue well into the operational life of the mine, with the data confidence progressively increasing as the amount of data captured increases.

Kumba Iron Ore currently bases all open pit geotechnical designs and geotechnical risk assessment on geotechnical borehole data in conjunction with interpreted structural models. Boreholes are logged and the data is captured as an ongoing process in each of the company's operations. This process forms the initial step in the geotechnical design and risk assessment process whereby the raw data is used to classify the strength properties for each lithology, provide inputs for geotechnical block models and ultimately provide the inputs for slope design analyses. To date borehole data has provided the only large scale, organized dataset for input into geotechnical analyses at Sishen Mine and throughout Kumba. Although borehole data forms the best and most comprehensive form of geotechnical data, there are some shortfalls that can be addressed by other data collection methods. These shortfalls are as follows:

- Boreholes are generally not orientated; although orientated drilling has been attempted at Sishen Mine, it has proven to be slow, costly and generally unreliable.
- Most boreholes drilled from surface are vertical, capturing limited data pertaining to sub-vertical and inclined features. As with orientated boreholes, inclined borehole drilling has been attempted, with limited success on Sishen Mine.
- Borehole drilling is a relatively slow and expensive means of data capture.
- Boreholes capture limited and potentially unreliable data pertaining to discontinuity orientation, spacing and persistency.

The shortfalls in geotechnical borehole data collection relate specifically to the fact that borehole core represents a small, relatively disturbed sample of the overall rock mass. The purpose of the research in this dissertation is to eliminate the shortfalls of relying on borehole data alone by devising a practical means of adding face mapping to the geotechnical data collection, storage and analysis process.

Various face mapping projects have been undertaken in the past at Sishen using the Sirovision Face Mapping system. These have however been restricted to case specific studies in specific areas of the mine, without any formal system of data capture and storage. Data collection on a large scale requires an organized database system whereby large amounts of raw input data can be stored,

analyzed and queried according to the required output parameters or spatial divisions. In December of 2013 each of the Kumba Iron Ore mining operations purchased a Maptek 8810 laser scanner for the specific purpose of geotechnical face mapping. The scanner allows for the rapid collection and analysis of face mapping data and has the potential to add significant value to the geotechnical dataset of each site.

Kumba currently uses the Acquire Geological Database for the storage of geotechnical borehole data. While the system has proven to be a robust means of capturing, storing and querying borehole data, it has become clear over time that there is a need to supplement the borehole data in the database with other forms of geotechnical information. This will be addressed by investigating a practical means of integrating face mapping data into a borehole based geotechnical database.

1.2. RESEARCH OBJECTIVES

- To investigate the process of geotechnical face mapping using laser scanning technology and to establish a method for integration of face mapping data into a borehole based geotechnical database.

- To analyze the effect that adding face mapping data to geotechnical borehole data has on calculated rock mass parameters, geotechnical data uncertainty and the geotechnical design process.

- To examine further practical applications of geotechnical face mapping in geotechnical risk mitigation.

1.3. SISHEN IRON ORE MINING OPERATION

Sishen Iron Ore Mine is located approximately 5km to the south west of the town of Kathu in South Africa's Northern Cape Province. At the time of preparing this dissertation the mine was under the ownership of Kumba Iron Ore and formed one of two active mining operations together with Kolomela Mine, approximately 90km to the south of Sishen. A third mining operation at the town of Thabazimbi in South Africa's Limpopo Province reached its end of life at the beginning of 2016.

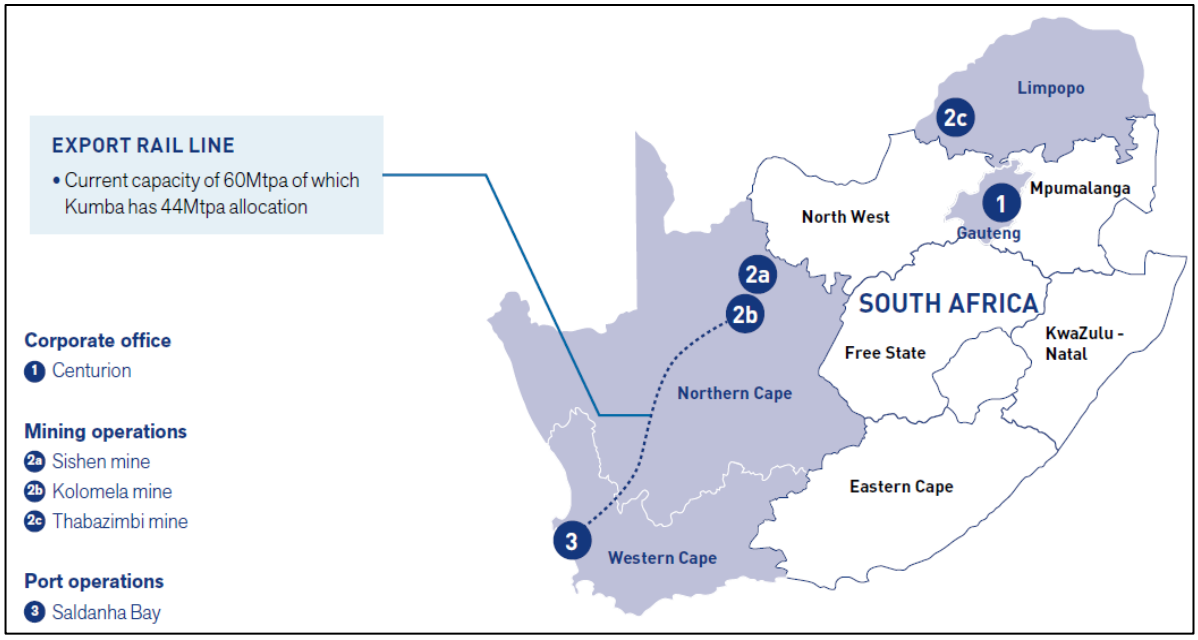

Figure 1.1: Location of Kumba Iron Ore mining operations (After Kumba Iron Ore Integrated Annual Report, 2015).

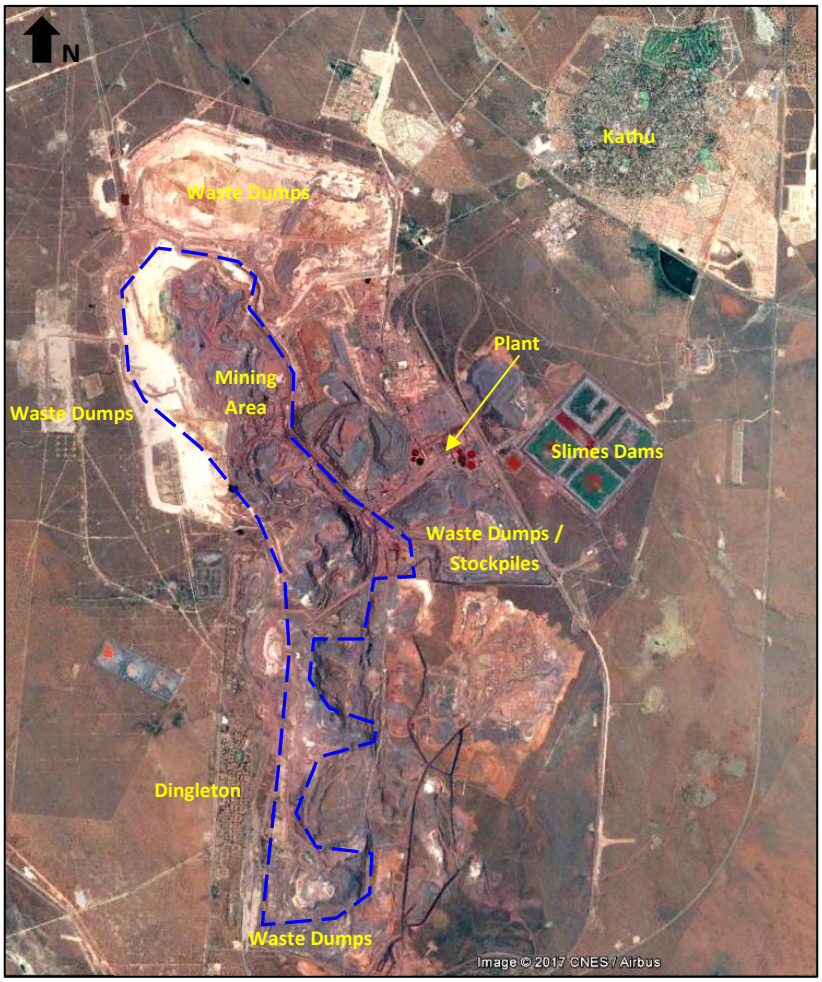

Figure 1.2: Sishen mining area (Google Earth, 2017).

Sishen mine is one of the largest single open pit mining operations in the world, consisting of a series of interconnected pits extending approximately 12km in a north-south direction. The pit width varies between approximately 1km and 3km, with a maximum depth in 2016 of approximately 260m.

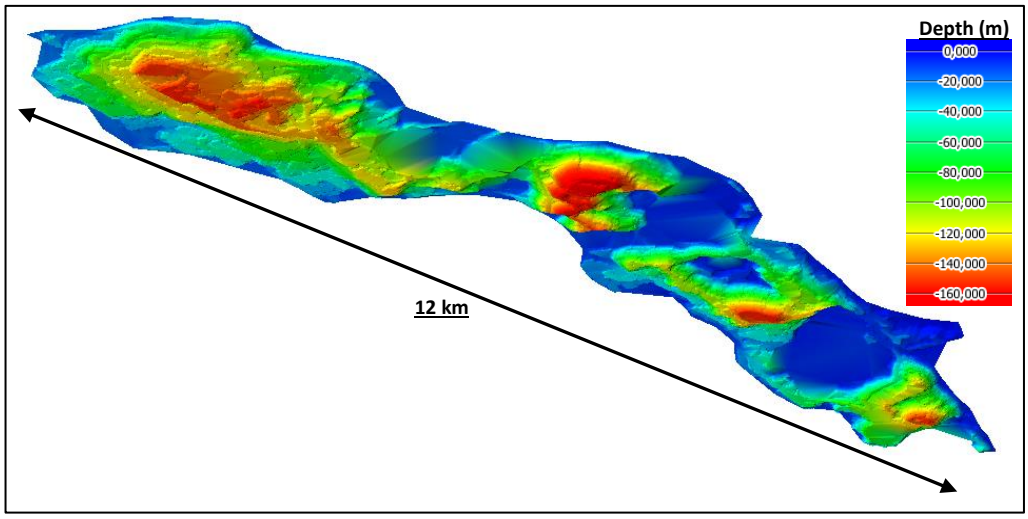

Figure 1.3: Illustration of the mining areas within the Sishen mining complex.

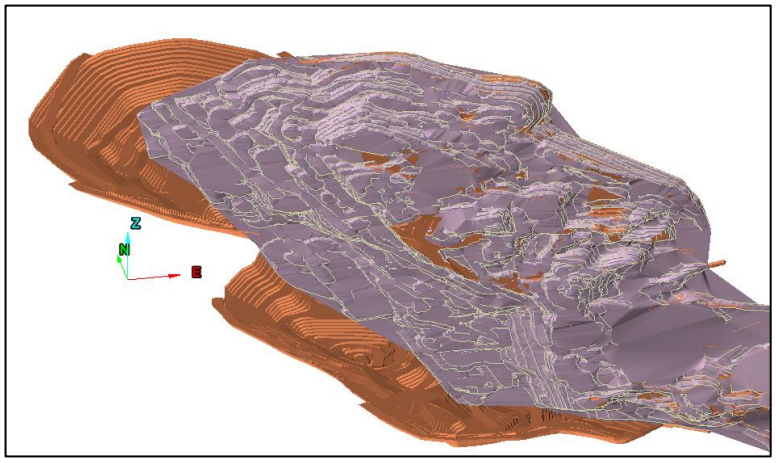

Figure 1.4: Illustration of the actual mined out area versus the planned final pit shells for the Sishen Northern Mining area.

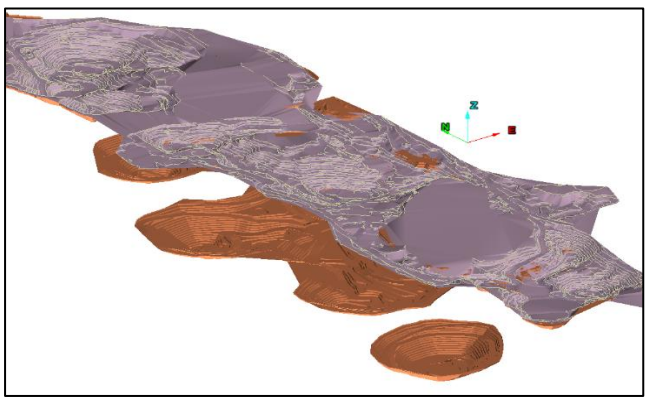

Figure 1.5: Illustration of the actual mined out area versus the planned final pit shells for the Sishen Central and Southern Mining area.

The mine exploits a high quality hematite orebody hosted within Banded Iron Formation belonging to the Asbestos Hills Subgroup of the Transvaal Supergroup. The mining operation beneficiates the raw product through Jig and Dense Medium Separation (DMS) plants to produce 64%Fe lump ore and 63.5%Fe high quality sinter fines for the export market. Iron ore produced at Sishen is transported via the approximately 800km long Sishen – Saldanha railway line where it is exported from the Saldanha Port Operation. The majority of the iron ore produced at Sishen is currently exported to China, with other destinations including Japan, South Korea, India and various European destinations.

CHAPTER 2: GEOLOGICAL SETTING

This chapter provides a review of the local and regional geological setting of the Sishen Mining area. Rock types and structural features occurring on the mine are discussed in terms of the broader regional scale stratigraphic and structural setting. The aim of this is to provide context to the research presented in this dissertation by giving a degree of insight into the rock mass under investigation.

2.1. REGIONAL GEOLOGICAL SETTING

On a regional scale Sishen Mine is located on the western edge of the Archean crustal block of the Kaapvaal Craton, as illustrated in Figure 2.1. The western edge of the cratonic basement is overlain by the Neo Archean-Paleoproterozoic (2600 – 2100 Ma) rocks of the Transvaal-Griqualand West Supergroup. These rocks represent a thick sequence of chemical and clastic sediments deposited in two main fault controlled basins, namely the Transvaal Basin and the Griqualand West Basin. The basins are separated by a north-south trending paleo-high referred to as the Vryburg Rise/Arch (Mortimer, 1995; Alchin and Botha, 2005; Friese and Alchin, 2007; Alchin, 2008; Basson, 2010).

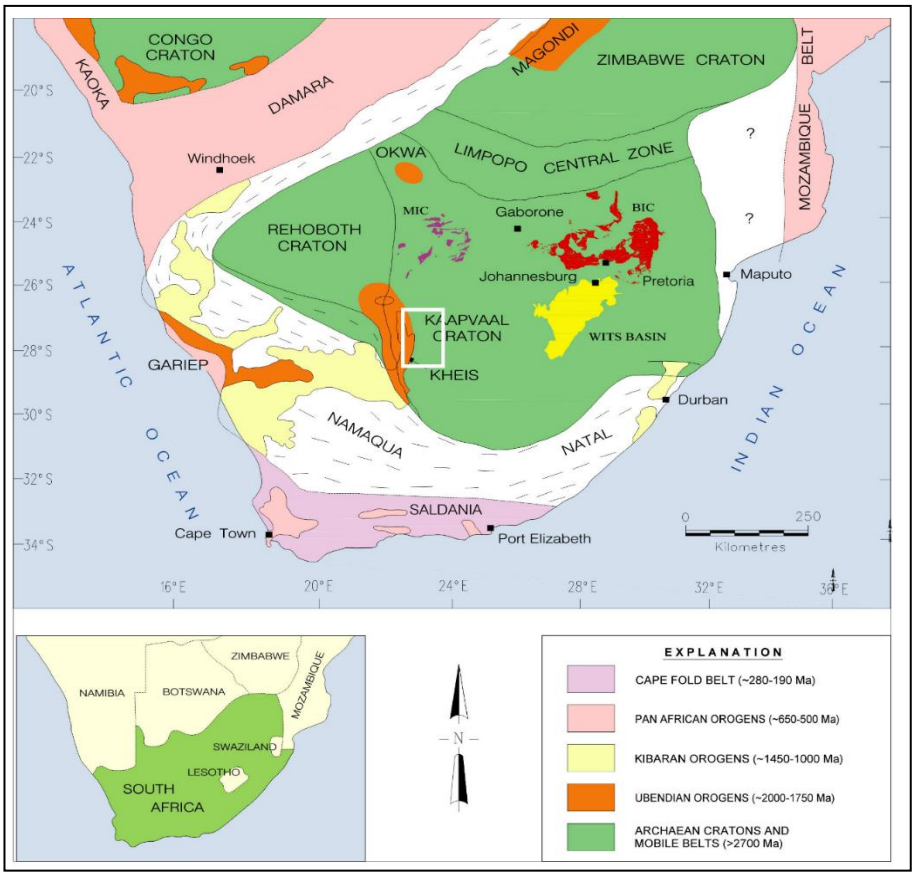

Figure 2.1: Southern African Archean and Proterozoic (From Friese, 2007).

Sishen is located in an area of the Griqualand West Basin referred to as the Maremane Dome, as indicated in Figure 2.2. Within the Maremane Dome area Transvaal Supergroup strata consist of the 2590 – 2430 Ma Ghaap Group and the 2350 – 2220 Ma Postmasburg Group, as illustrated in Figure 2.4 (Friese and Alchin, 2007).

Stratigraphy overlying the Cratonic Basement in the Maremane Dome consists of the basal dolomitic deposits of the 2590 – 2520 Ma Camblerand Subgroup of the Ghaap Group which is unconformably overlain by the brecciated manganiferous chert of the Wolhaarkop Formation. The Wolhaarkop Chert Breccia is in turn unconformably overlain by the 2465 – 2430 Ma Manganore Iron Formation of the Asbestos Hill Subgroup (Ghaap Group). Manganore Formation Units are unconformably overlain by 2050 – 1930 Ma Gamagara/Mapedi Formation strata of the Olifantshoek Supergroup which is in turn unconformably overlain by the 2350 – 2220 Ma Postmasburg Group of the Transvaal Supergroup. Postmasburg Group strata have been locally thrust over the younger Olifantshoek Supergroup units (Friese and Alchin, 2007; Alchin and Botha, 2005; Mortimer, 1994; Alchin, 2008; Basson, 2010).

The Carboniferous – Permian age glacial deposits of the 310 – 280 Ma Dwyka Group of the Karoo Supergroup unconformably overlie the Postmasburg Group sediment in the area. Karoo Supergroup Sediments are in turn unconformably overlain by Paleogene, Neogene and Quaternary deposits of the Kalahari Group (Basson, 2010; Norman and Whitfield, 2006).

Transvaal and Olifantshoek Supergroup sediments have been intruded by a series of 2060 Ma Diabase dykes and sills (Friese and Alchin, 2007).

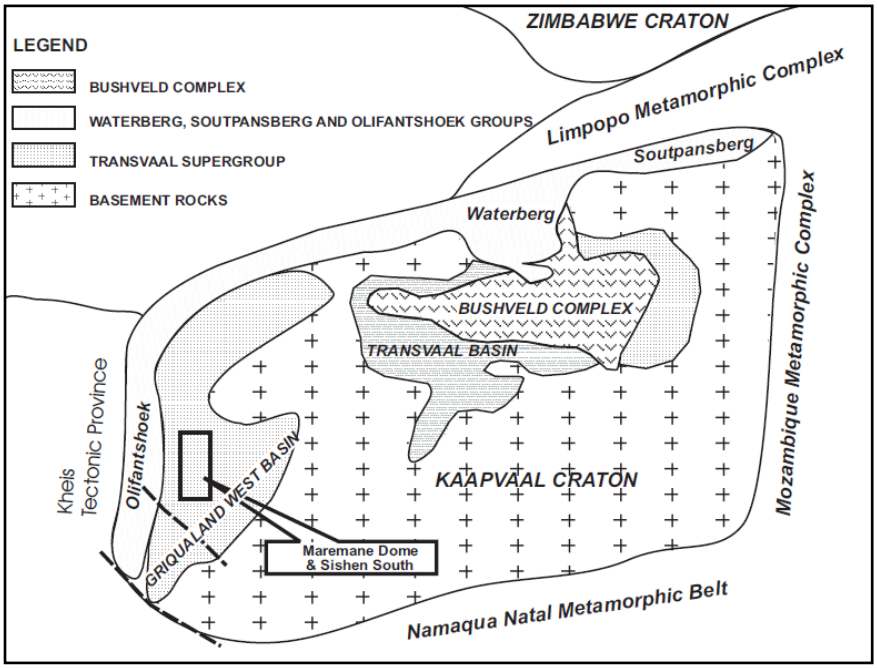

Figure 2.2: Locality of the Sishen Mine relative to the Kaapvaal craton and the Griqualand West and Transvaal structural basins (From Alchin and Botha, 2005).

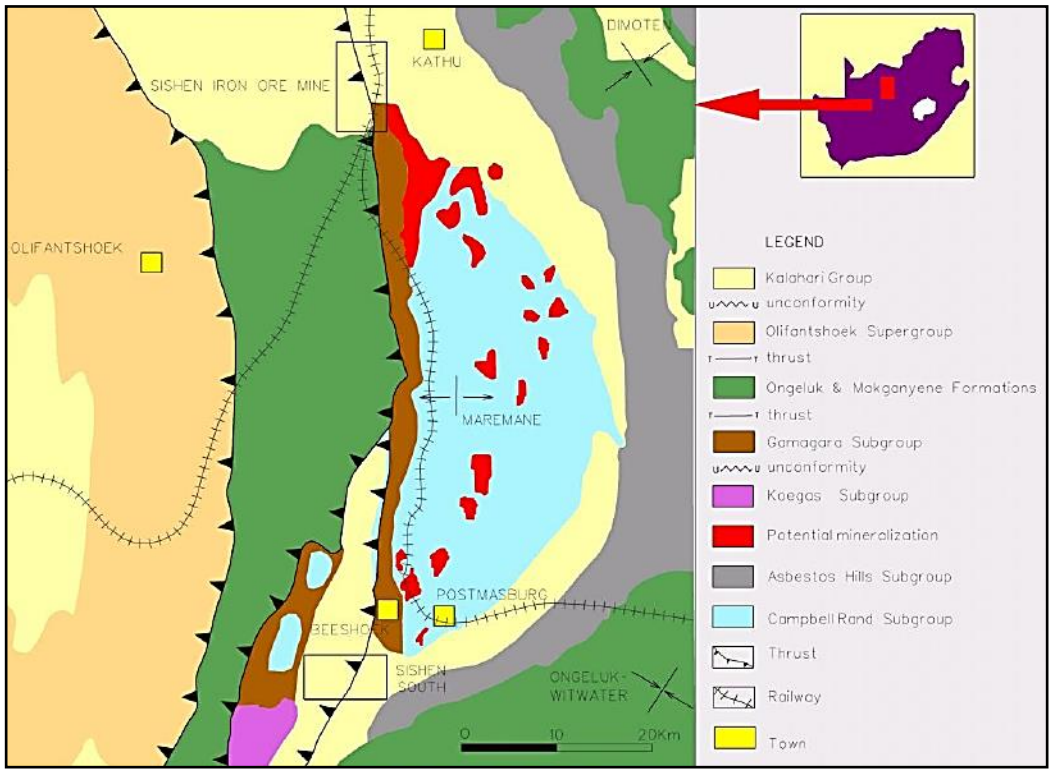

Figure 2.3: Geological setting of the Maremane Dome area (After Friese, 2007).

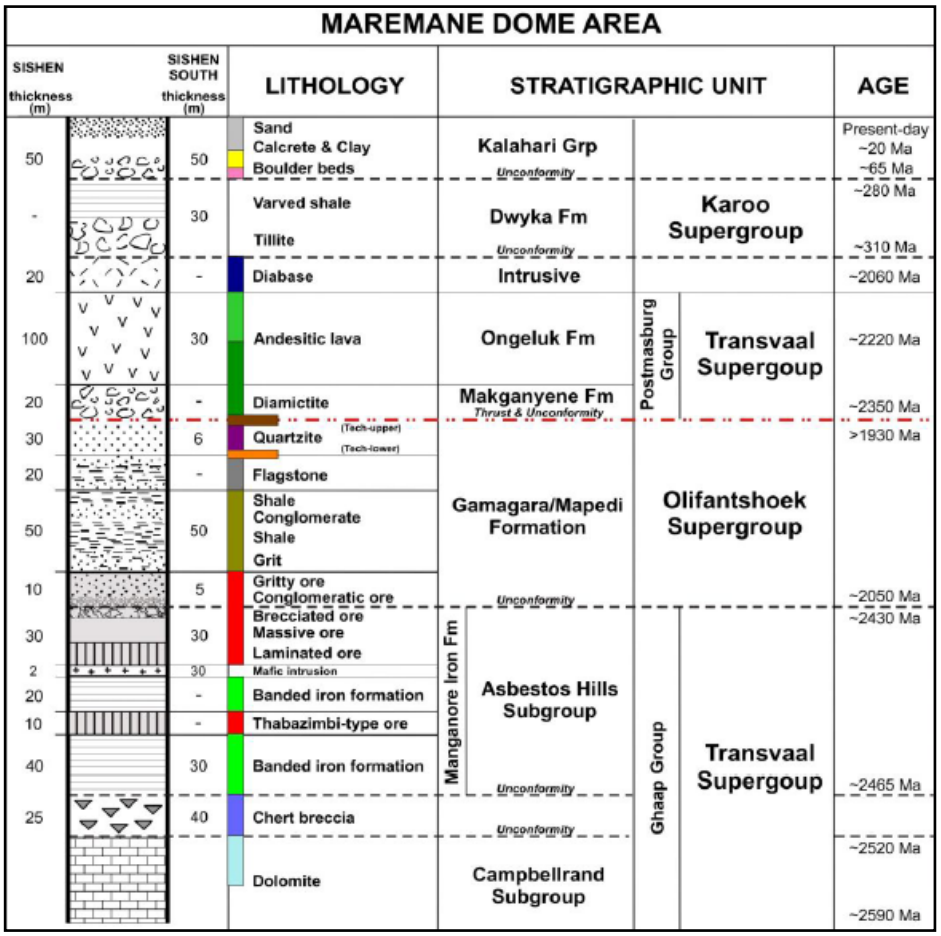

Figure 2.4: Stratigraphy of the Maremane Dome Area (After Friese and Alchin, 2007; Basson, 2010).

Lithologies of the stratigraphic units outlined in Figure 2.2 are summarised in Sections 2.1.1 to 2.1.6.

2.1.1. Campbellrand Subgroup Dolomites (Transvaal Supergroup)

The basal dolomitic unit in the area typically comprises clastic textured feruginised dolomite containing localised beds of ankerite rich chert (Beukes, 1983). There is limited exposure of this unit in the Sishen Mining area as mining is generally terminated in the overlying Wolhaarkop and Manganore Formation sediments. Depth to the Campbellrand Subgroup dolomites generally decreases to the south of the mine and there are large areas (as illustrated in Figure 2.3) where dolomite occurs directly below its residual by-products and Quaternary windblown sediments across the central portion of the Maremane Dome. There are occurrences of sub surface cavities as well as sinkhole and doline development in the area where dolomite occurs at shallow depth.

2.1.2. Wolhaarkop Formation Chert Breccia (Transvaal Supergroup)

The Wolhaarkop Formation, which unconformably overlies the Campbellrand Subgroup dolomites consists of chert breccias that are generally siliceous but are locally rich in manganese and hematite (Basson, 2010; Friese and Alchin, 2007, Alchin, 2009). The manganese content of the material has a profound effect on its geotechnical properties with siliceous breccias generally hard and competent in contrast with manganese rich material that is weaker and prone to rapid weathering on exposure. The make-up of the breccias suggests that they either formed in a relict cast topography or are solution collapse breccias formed in a shallow water environment with periodic atmospheric exposure (Van Wyk, 1980; Van Schalkwyk & Beukes, 1986). Figure 2.5 shows typical hand specimen and field exposure of the Wolhaarkop Formation at Sishen Mine.

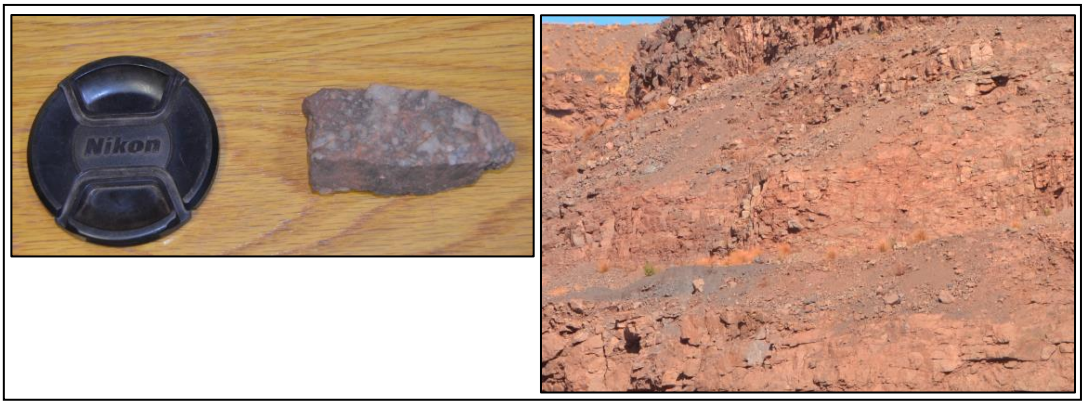

Figure 2.5: Hand sample and field exposure of Wolhaarkop Formation Chert Breccia at Sishen Mine.

2.1.3. Manganore Iron Formation (Transvaal Supergroup)

The Wolhaarkop formation grades upward into a unit of partially folded and brecciated to undisturbed Banded Iron Formation (Figure 2.6) with interstratified shales that represents the lower portion of the 2520 – 2430 Ma Asbestos Hills Subgroup of the Transvaal Supergroup (Beukes, 1983; Alchin 2008; Alchin and Botha, 2005). This unit is known locally as the Manganore Iron Formation and contains the mineralised ore bearing zones that have an Fe content that is economically viable to be mined (Beukes, 1983). The Banded Iron Formation in this unit at Sishen Mine generally occurs in bands of 3mm to 20mm thick and are interpreted as sediments deposited in a sub-aqueous setting with a fluctuating iron and silica rich depositional environment (Mortimer, 1994).

The stratigraphic thickness of the banded ironstones forming the lower portion of this unit ranges between 20m and 50m in the Sishen mining area, although it is in places absent altogether (Mortimer, 1995). The upper portion of the Manganore Iron Formation at Sishen consists of a mineralised zone consisting of a series of ore horizons interbedded with Banded Iron Formation and shales. Hematite ore is divided into three broad sub-categories based on the texture of the ore, namely 'Thabazimbi Type / Massive Ore' (Figure 2.7), Laminated Ore' and 'Conglomeratic Ore' (Basson, 2010).



Figure 2.6: Hand and core samples of Banded Iron Formation as well as field exposure at Sishen Mine.



Figure 2.7: Hand sample of massive hematite ore.

2.1.4. Gamagara Formation (Olifantshoek Supergroup)

The 2050 – 1930 Ma Gamagara Formation that unconformably overlies the Manganore Iron Formation represents the basal unit of the Olifantshoek Supergroup in the area. The unconformity represents a period of 380Ma of erosion, likely resulting from uplift of the area (Mortimer, 1994; Basson, 2010)

The formation consists of a basal conglomerate unit that represents channel fill or valley fill deposits, which levelled out the uneven topographic surface of the unconformable contact with the underlying geology. The conglomerates form an inconsistent layer confined to low lying areas of the paleo topographic surface and are overlain by a unit of reworked iron rich sandstone know as flagstone. This topographic surface most likely represented pre-existing folds in the underlying geology which would have taken the form of a series of elongated hills making up the erosion surface at the time. The conglomerates generally represent a proximal sedimentary deposit made up of iron rich particles from the underlying units (Mortimer, 1994; Alchin and Botha, 2005).

The flagstone unit is conformably overlain by a thin unit of tectonised shale which is in turn overlain by a generally 15 to 25m thick layer of quartzite (Figure 2.8). This is in turn overlain by a second thin and sporadic tectonised shale unit (Basson, 2010; Mortimer, 1994; Alchin and Botha, 2005).

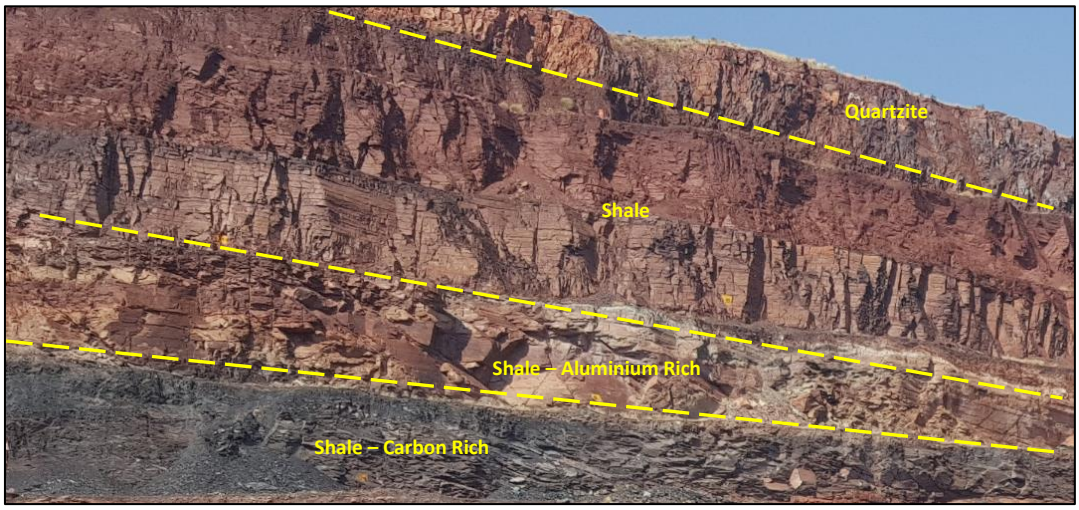

Figure 2.8: Interbedded Gamagara Formation Quartzite and Shale at Sishen Mine.

2.1.5. Postmasburg Formation (Transvaal Supergroup)

The Gamagara Formation quartzites and shales at Sishen are overlain by andesitic lava. There are differing opinions as to the origins of the lava and the relationship between the lava and the underlying Gamagara Formation. Mortimer (1994) suggests that the lavas post-date the Gamagara Formation, representing a volcanic event occurring after an extended erosion period.

The general consensus is however that the lavas are older than the Gamagara Formation and represent the 2350 – 2100 Ma Postmasburg Group of the Transvaal Supergroup. According to this theory the older Postmasburg Group rocks have been placed above the Gamagara Formation in the stratigraphic column by low angle thrusting (Van Schalkwyk & Beukes, 1986; Alchin and Botha, 2005; Friese, 2007; Friese and Alchin, 2007; Basson, 2010). According to Friese (2007) the Postmasburg Group has been removed by erosion over the main portion of the Maremane Dome area, but is present along the western edge of the dome in the form of a basal diamictite unit overlain by andesitic lavas that can be correlated with the Ongeluk Group of the Transvaal Supergroup (Friese, 2007). This unit is prominent on the western side of the north-south elongated Sishen Pit where lavas outcrop in the western highwall. The lavas exposed at Sishen generally consist of an unweathered lower portion and a weathered upper portion. The lavas are logged and modelled as an unweathered basal unit and weathered upper unit by Sishen's geologists. There is no significant exposure of the Postmasburg Group diamictites at the mine.

2.1.6. Kalahari Group

Kalahari Group sediments were deposited between 65 Ma and present. In the Sishen mining area these sediments are made up of a sequence of boulder beds, clays and calcretes capped by a superficial layer of aeolian sand. At its base the Kalahari group in the Sishen mining area consists of a sporadic and variable conglomeratic layer representing alluvial channel deposits from ancient river channels, and the depressions left by graben structures (Jones, 1982). This basal pebble layer is referred to as the Wessels Formation. The Wessels Formation is overlain by a thick clay layer making up the Boudin Formation. These clays are generally brown to red brown and lacking any significant stratification. The clays are calcretised to varying degrees in some areas and show mottling in places due to fluctuating ground water levels. Although regionally not persistent (Haddon, 2005) they occur in most of the Sishen mining area with thicknesses of up to 60m (Basson, 2010).

The Boudin Formation clays are a prevalent feature in the highwalls of the Northern portion of Sishen Mine referred to as the GR80 pit (Figure 2.9). The clays are significant from a geotechnical perspective as they have a marked influence on ground water flow within the shallow aquifer in the area. Furthermore the clays essentially represent an unconsolidated soil in what is otherwise a hard rock mining environment. They play a pivotal role in the overall stability of the pit slopes and therefore on the slope designs at the mine.

There is some uncertainty as to the origin of the Boudin Formation clays. According to Bootsman (1998) the clays were deposited in a lacustrine environment created by the blocking of the southward flowing Proto-Molopo River during the Cretaceous Period. There are however areas where the clays may represent the in-situ weathering of the underlying bedrock strata (Farr et al., 1981; Bootsman, 1998).

Capping the Boudin Formation Clays at Sishen Mine is a thick, persistent layer of hardpan calcrete which represents the most common of the duricrusts that are widespread throughout the Kalahari Basin (Haddon, 2005; Netterberg, 1980). The calcretes are thought to have formed initially with lime accumulation at the base of the zone of leaching in soils with a decreasing degree of compaction with depth. In more permeable soils the zone of lime accumulation will have developed into a hardpan, creating an impermeable base for further calcrete accumulation (Haddon, 2005).

Kalahari Group calcretes encountered at Sishen generally extend from surface level to depths of between 20m to 40m, consisting of flat lying, widely bedded and jointed layers of cemented granular material. From a geotechnical perspective calcretes on the mine generally represent competent highwall material. Stability problems are however often encountered when mining passes through the calcrete layer and into the underlying clays. As clay material is exposed in the pit highwall it tends to spall out under weight of the calcrete. Support for the otherwise competent overlying calcrete will be lost resulting in toppling failure of large blocks of calcrete.

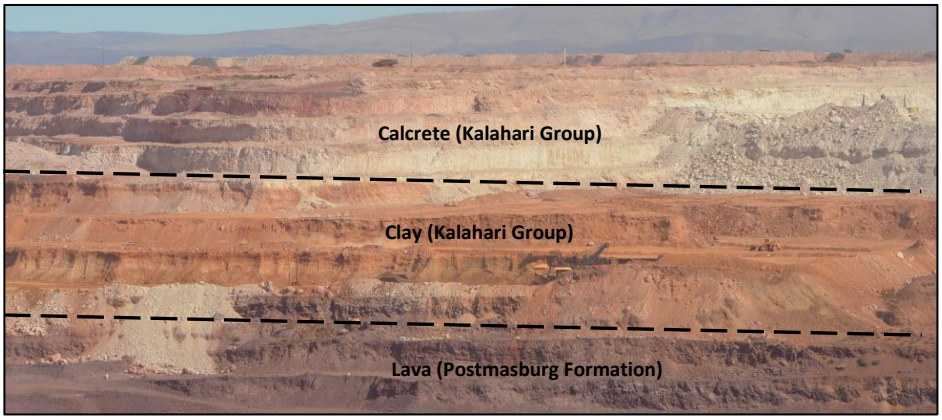

Figure 2.9: Kalahari Group sediments at Sishen Mine.

2.2. STRUCTURAL EVOLUTION

Sishen Mine is located in the Maremane Dome area on the eastern edge of the Kaapvaal Craton. The Transvaal Supergroup strata in the area show polyphase deformation with three main phases of compressional deformation identifiable. These are the Paleoproterozoic Pre-Kheis and Kheis Orogenic events that occurred prior to the accretion of the Namaqua-Natal Province, and the Mesoproterozoic Namaqua-Natal Orogeny (Stowe, 1986; Altermann and Hälbich, 1991; Hälbich et al, 1993).

The first phase of deformation affecting the area occurred at approximately 2000Ma prior to the accretion of the Kheis Subprovince to the western edge of the Kaapvaal Craton. This phase was characterised by extensive thrusting. This was followed by the Kheis Orogeny at about 1750 Ma, an event characterised by coincident thrusting and folding. This was in turn followed by the accretion of the Namaqua Metamorphic Province at approximately 1350 – 1000 Ma during an event in which four phases of crustal shortening were identified (Stowe, 1986; Altermann and Hälbich, 1991).

Friese (2007) further divides the structural evolution of the Sishen Mining Area into 11 separate events. Structural features evident at the mine from various structural mapping exercises (Mortimer, 1994; Friese, 2007; Basson, 2010) are as follows.

- North-South and East-West trending interference folding that has combined to form the Maremane Dome structure.
- Superimposed East-North-East trending folds with associated strike-slip faulting.
- A low angle westerly dipping thrust structure referred to as the Black Ridge Thrust represents a tectonic unconformity between the Gamagara Group shales and quartzites and the overlying Postmasburg Group lavas.
- Extensive block faulting of the Pre-Gamagara Group lithologies with identifiable sets
    - North-South trending inverted normal faults
    - ENE and ESE trending strike-slip faults
    - Identifiable major fault structures such as the North-South trending ‘Sloep Fault’ zone that runs along the eastern margin of the mine.

Interference folding has created a series of dome and basin like synclinal and anticlinal structures within the Pre Gamagara lithology of the area. Faulting has further superimposed a series of horst and graben structures on the aforementioned domes and depressions. The location and grade of the hematite ore mined at Sishen has been influenced to a large degree by these structures with ore tending to be concentrated in the synclinal and graben type depressions (Friese 2007, Basson, 2010).

2.3. INTRUSIVE EVENTS

Magnetic surveys indicate that the Maremane Dome area has been intruded by several pre-Karoo and post-Karoo aged dolerite and diabase dykes and sills (Friese, 2007). Two large sub vertical diabase Dykes (approximately 50-150m wide) have been exposed in the northern and central portions of the mining area (Figure 2.10). The dykes run in a south west to north east direction and are significant in terms of slope stability due to their relatively high rate of weathering and weak altered contact margin.

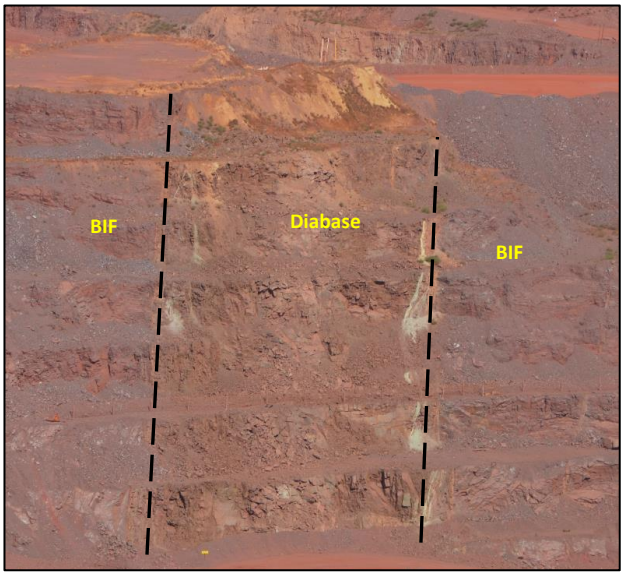

Figure 2.10: Diabase dyke intruded into Banded Iron Formation, cross cutting the Sishen mining area.

This chapter gives an outline of the regional and local geological setting for Sishen Mine in which a brief summary of stratigraphic and structural geological setting is given. The aim of including this information is to provide context to the following chapters that deal with geotechnical face mapping and data capture in the context of the rockmass exposed at Sishen Mine.

The following chapter is a review of the literature covering discontinuities in rock masses, rock mass properties, rock mass classifications and geotechnical face mapping theory. In this chapter laser scanner face mapping is reviewed as a mapping technique, and is compared with photogrammetry techniques and traditional contact face mapping.

CHAPTER 3: GEOTECHNICAL FACE MAPPING THEORY

The previous chapter gave a brief outline of the geological setting of Sishen Mine. In this chapter a review of literature relevant to rock mass and natural discontinuity properties, rock mass classification systems and geotechnical face mapping theory is given. The use of terrestrial laser scanner technology for geotechnical face mapping is reviewed and compared with conventional face mapping techniques.

3.1. DISCONTINUITY PROPERTIES AND THE INFLUENCE ON A ROCK MASS

3.1.1. Definition and Engineering Significance

In order to develop an effective and meaningful face mapping data collection system a review of the nature of rock mass discontinuities and the effect that such features have on the engineering behaviour of the rock mass is required. Hoek and Marinos (2007) state that failure in rock slopes is frequently controlled by the presence of and interactions between discontinuities within the rock mass.

According to Priest (1993) the term 'discontinuity' can be categorised as a broad definition encompassing a wide range of mechanical defects within a rock mass. These include defects originating from a wide range of geological processes including bedding planes, faults, joints, fissures and fractures within the rock mass. Significantly, from an engineering perspective, discontinuities typically have little or no tensile strength, low shear strength and high fluid conductivity compared with the surrounding rock material (Priest, 1993). Priest (1993) makes a further division between natural discontinuities, resulting from geological processes, and artificial discontinuities that are created by disruption to the rock mass during excavation.

According to Piteau (1970 and 1973) in general terms the discontinuity properties that have the greatest significance on the design stage of an excavation are as follows.

1. Orientation
2. Size
3. Persistency
4. Surface Geometry
5. Generic Type
6. Infill Material

The significance of these properties are highlighted by how they are incorporated into and weighted in the various empirical rock mass rating systems such as the RMR (Bieniawski, 1989), MRMR (Laubscher, 1994) and Q (Barton et al., 1974) systems.

In low stress environments unfavourably orientated discontinuities or discontinuity sets can result in rigid block type failures resulting from sliding, toppling or falling mechanisms while in high stress environments discontinuities can provide weakness planes for shear displacement and failure (Hoek and Brown, 1980; Brady and Brown, 1985).

3.1.2. Origin and Nature of Natural Discontinuities

In terms of general geological terminology natural discontinuities can be broadly divided into faults, joints, bedding, fissures and fractures, and cleavage (Priest, 1993).

According to Price (1966) a fault can be defined as a plane of shear failure within a rock mass that displays significant displacement of the material on either side of the plane. Faults are typically identified by offsetting of features across the fault plane such as bedding or veins within the rock mass, as well as the generation of slickensides or fault gouge (Priest, 1993). Formation of faults can be attributed to tectonic stresses, with slipping occurring when the shear stresses exceed the shear strength along a particular plane within the rock mass (Kersten, 1969). According to Whitten and Brooks (1972) faults rarely form a single planar feature within the rock mass and usually form as a zone of sub parallel fracture sets. Gouge and brecciated material commonly occurs within a fault zone (Priest, 1993)

A joint can be defined as a geological discontinuity along which there has been little or no displacement (Price, 1966; Priest, 1993). Joints develop due to a variety of common geological processes ranging from cooling of intrusive rocks (columnar jointing), stresses induced by uplift and erosion, tectonic stresses and stress relief within a rock mass (Priest, 1993). Joints can be divided into systematic joints, which form well defined parallel sets within a rock mass and non-systematic joints, which are randomly orientated within the rock mass. As illustrated in Figure 3.1 systematic joints can often be correlated with other geological features related to the same tectonic event, such as faulting and folding (Price, 1966; Whitten, 1966; Ramsay, 1967).

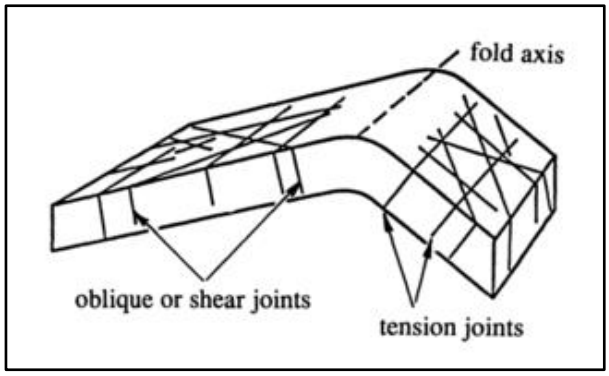

Figure 3.1: Illustration of jointing patterns on the limb of an asymmetrical anticline (Priest, 1993).

Priest (1993) defines bedding as a surface created by a change in grain size, grain orientation, minerology or chemistry during the deposition of a sedimentary rock. Bedding planes may represent a change in colour or texture and do not necessarily represent a discontinuity (Priest, 1993). The shear features of a bedding plane are influenced by a number of factors including mineralogy, grain size distribution and grain orientations (Giani, 1992).

Rock cleavage can be defined as a secondary planar feature whereby mineralogical alignment creates a fabric within a rock that results in mechanical anisotropy of the material. Cleavage and mechanical anisotropy within a rock develops as a result of metamorphic processes during which elongated or platy minerals within the rock are aligned according to the applied stress field (Giani, 1992; Ghosh, 1993).

3.1.3. Discontinuity Strength

As discontinuities generally have little or no tensile strength and a shear strength that is far lower than that of the surrounding intact rock they generally form preferential failure planes within the rock mass. This type of structurally controlled failure is prevalent in the low stress environment of an open or near surface excavation. Within a rock mass the discontinuities will have a significant weakening effect, dependant on their spacing, persistency, orientation and shear strength (Hoek and Marinos, 2007; Priest, 1993).

The strength properties of a discontinuity are influenced by the roughness of the discontinuity surface, the compressive strength of the joint walls and the nature of any infilling material. In the case of joints where little or no infill material is present and the joint walls are in direct contact with each other, joint strength is dictated primarily by the roughness of the joint surface and compressive strength of the joint walls (Hoek and Marinos, 2007; Priest, 1993; Barton, 1976). Patton (1966) demonstrated the effects of

roughness on shear strength though the shear testing of idealised saw tooth samples to quantify the relationship between the two, as illustrated in Figure 3.2.

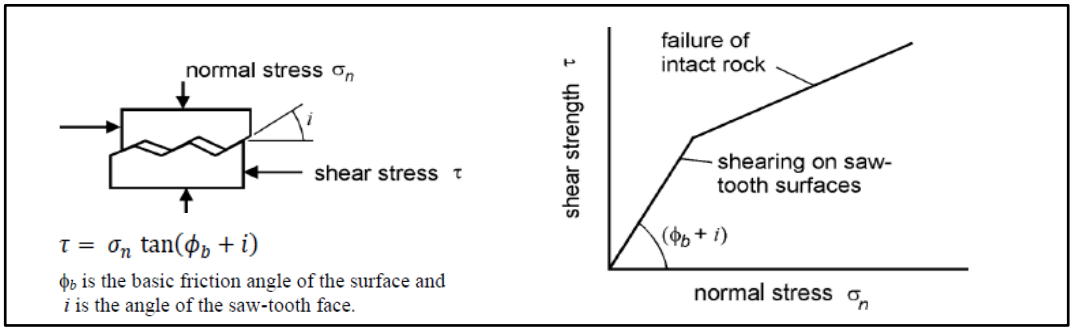

Figure 3.2: Illustration of the Patton (1966) saw tooth (From Hoek and Marinos, 2007).

Although a simplification of joint surface interactions, the saw tooth experiment does illustrate the behaviour of the joint walls at a low normal stress level, where the roughness will result in an increased friction angle and dilation of the joint plane as the teeth move over each other. At higher normal stresses the shear stress will reach a point where the strength of the teeth is exceeded and they shear off, at which point the friction angle will revert back to the base friction angle of the material. Barton (1973, 1976) advanced the theory of Patton (1966) to provide an empirical estimate of the behaviour of natural joint surfaces as opposed to an idealised saw tooth. Barton observed that joints tend to show a gradual transition from the initial roughness controlled shear strength, to the high normal stress base friction angle strength exhibited by a joint plane.

Barton (1973) initially developed an empirical failure criterion for rock joints without infilling material, incorporating the normal stress, joint compressive strength, joint roughness and base friction angle. This was later refined by Barton and Choubey (1977), replacing the base friction angle of the joint surface with an estimated residual friction angle. This equation forms part of the Barton and Bandis (1990) rock joint strength and deformability criterion.

$$\tau = \sigma_n tan\left[\sigma_b + JRC\ log_{10}\left(\frac{JCS}{\sigma_n}\right)\right] \qquad \text{(Barton, 1973; 1976)}$$

$$\tau = \sigma_n tan\left[\sigma_r + JRC\ log_{10}\left(\frac{JCS}{\sigma_n}\right)\right] \qquad \text{(Barton and Choubey, 1977)}$$

$$\sigma_r = (\sigma_b - 20) + 20\left(\frac{r}{R}\right) \qquad \text{(Barton and Choubey, 1977)}$$

$\tau = Shear\ Strength$

$\sigma_n = Normal\ Stress$

$\sigma_b = Base\ Friction\ Angle$

$\sigma_r = Residual\ Friction\ Angle$

$JRC = Joint\ Roughness\ Coefficient$

$JCS = Joint\ Compressive\ Strength$

$r = Shmidt\ Hammer\ Rebound\ Number\ on\ a\ wet\ and\ weathered\ fracture\ surface$

$R = Shmidt\ Hammer\ Rebound\ Number\ on\ a\ dry\ saw\ cut\ surface$

The preceding equations provide a means of calculating the shear strength of a discontinuity under a given normal stress. Inputs for the equations are derived by empirical means by Barton (1973, 1976), Barton and Choubey (1977) and Barton and Bandis (1990).

3.1.3.1. Joint Roughness Coefficient (JRC)

The JRC is an empirical value defining the effect that the roughness of a joint surface will have on joint shear strength. A visual method for estimating joint roughness based on comparison with pre-defined joint surface profiles is given by Barton and Choubey (1977).

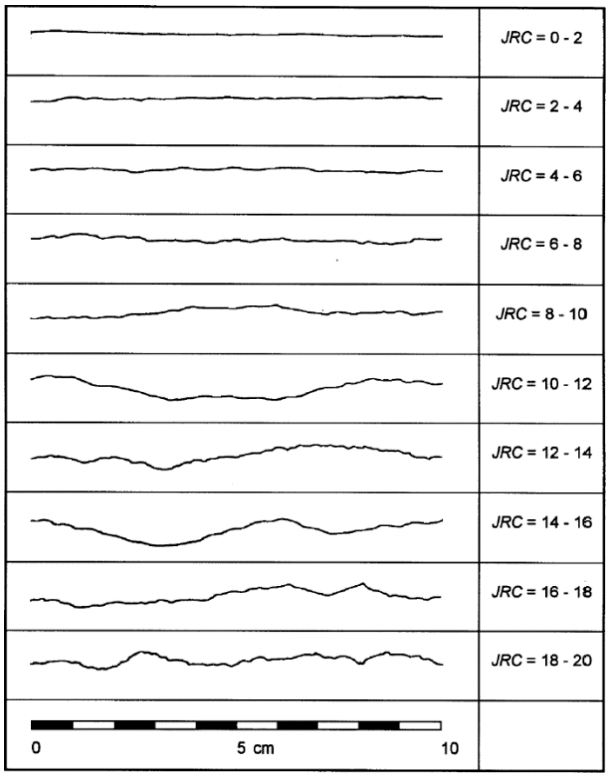

Figure 3.3: Joint roughness profiles for estimation of the Joint Roughness Coefficient (After Barton and Choubey, 1977).

The joint profiles illustrated in Figure 3.3 are based on a 10cm sample length. In order to take the effects of scale into account Barton and Bandis (1982) proposed the following equation.

$$JRC_n = JRC_0 \left(\frac{L_n}{L_0}\right)^{-0.02L_0}$$ (Barton and Bandis, 1982)

An alternative method for estimating JRC whereby a measurement of the amplitude of the asperities is used was proposed by Barton (1982).

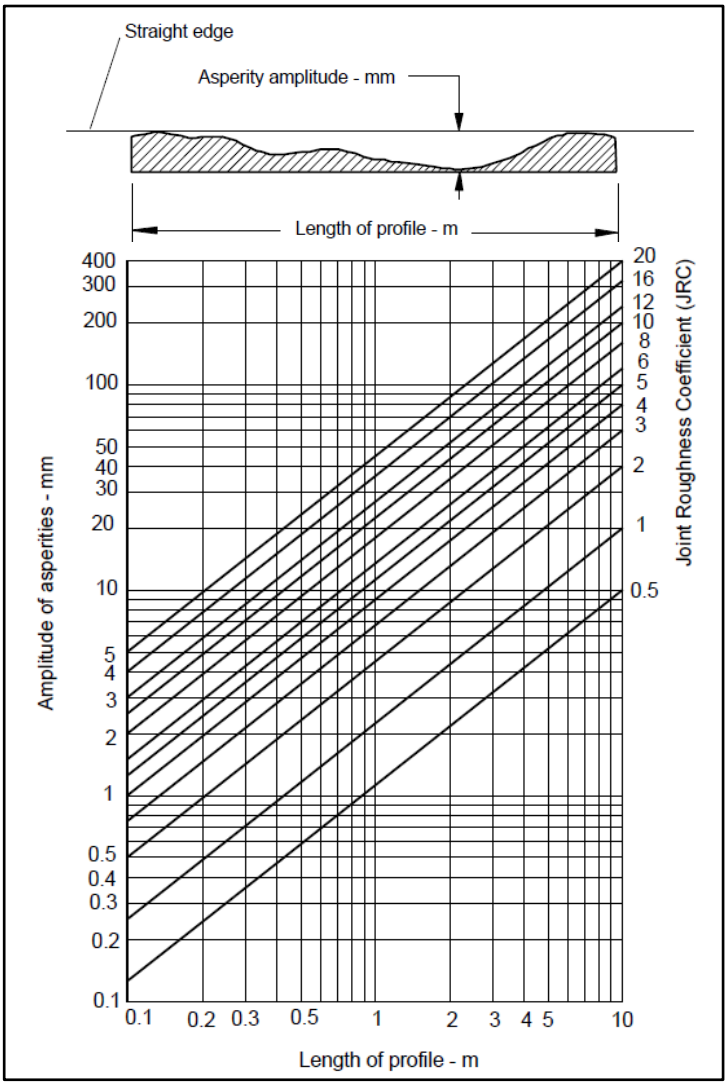

Figure 3.4: Chart for estimation of Joint Roughness Coefficient from the amplitude of asperities (After Barton, 1982).

There are various methods for measuring joint roughness, either by direct contact with the discontinuity surface or through remote sensing methods such as laser scanning or photogrammetry. Contact profiling methods include the use of a

compass disc-clinometer to determine the surface angle to the normal (Figure 3.4) at various scales while the straight edge method (Figure 3.4) is used to determine the amplitude of large scale roughness / waviness of a discontinuity (Tesfamariam, 2007). For smaller scale roughness estimations a joint comb, as well as a direct visual assessment can be used for comparison with standardised profiles (Barton and Choubey, 1977)

When measuring roughness using the compass disc-clinometer method discs of varying size (typically 5, 10, 20 and 40 cm diameter) are placed on the discontinuity surface in different positions (Figure 3.5). At each position the dip and dip direction created by the flat disc surface is recorded. A minimum of 25 readings are taken for each disk size. Disc orientation data is then plotted on a stereonet where the maximum angle between different readings can be determined in any potential sliding direction (Fecker and Rengers, 1971; ISRM, 1978).

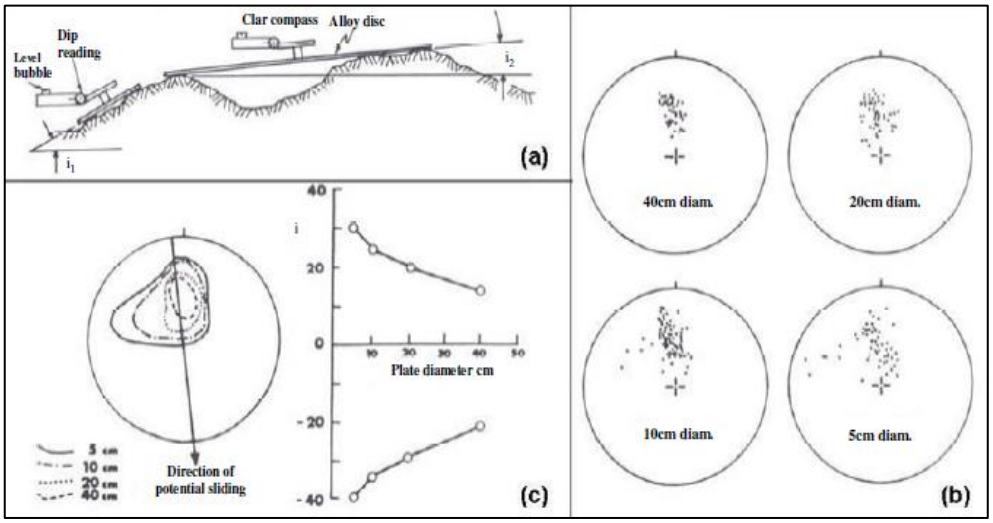

Figure 3.5: Illustration of the compass disc-clinometer roughness measurement method (Fecker and Rengers, 1971).

The straight edge method requires that a straight edge be placed against the discontinuity surface. With the edge in place the depth of the irregularities can then be measured off, as illustrated in Figure 3.6. The measured deviations from the straight line can then be applied to the Barton (1982) discontinuity roughness chart given in Figure 3.4 to determine the JRC of the discontinuity (Palmström, 2001, Piteau, 1970). Palmström (1995) gives a qualitative classification of joint roughness and waviness based on the Barton (1982) JRC chart as indicated in Figure 3.7.

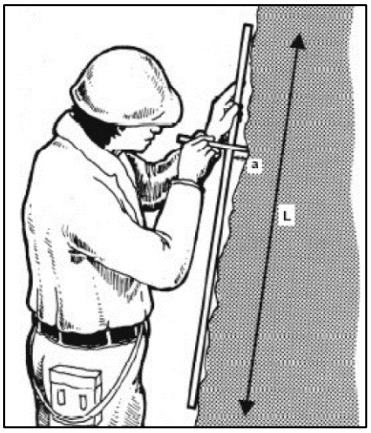

Figure 3.6: Illustration of the straight edge roughness measurement method (After Milne et al., 1992).

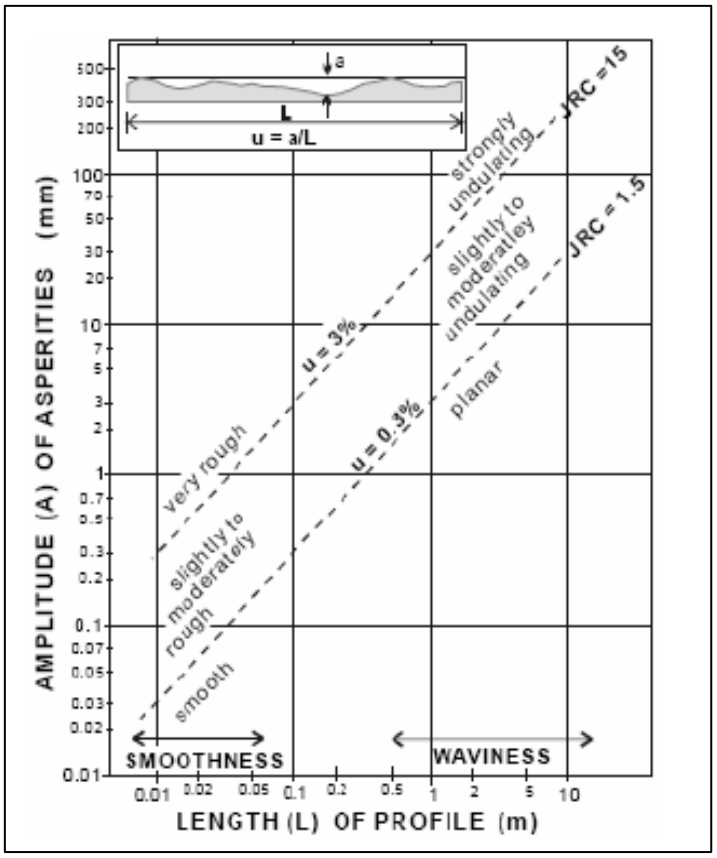

Figure 3.7: Palmström classification of roughness and waviness based on the amplitude of joint asperities (Palmström, 1995).

3.1.3.2. Joint Compressive Strength (JCS)

The JCS is a value representing the compressive strength of the wall rock immediately adjacent to the joint surface that has been affected by factors such as weathering and water ingress. This can range from fresh joint walls, with a

compressive strength equal to that of the intact rock, to highly weathered joint walls with a significantly reduced joint wall strength (Gumede, 2005). The JCS can be estimated from Schmidt Hammer rebound numbers using the following chart (Figure 3.8) proposed by Barton and Choubey (1977).

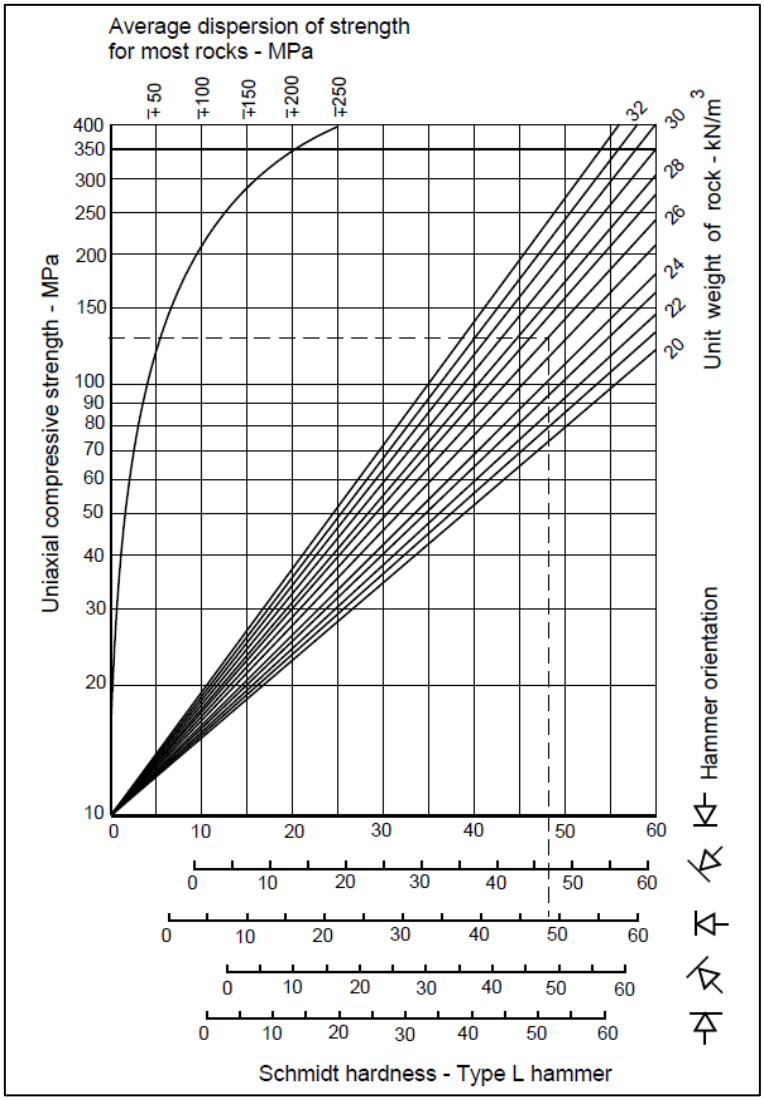

Figure 3.8: Chart for estimation of Joint Compressive Strength based on Schmidt Hammer rebound values (After Barton and Choubey, 1977).

The scale of the discontinuity has an impact on the influence that the joint compressive strength will have on the shear strength of the plane. In theory there will be more defects and a greater potential for weaknesses across a larger surface that a small scale laboratory sample (Hoek and Marinos, 2007). Barton and Bandis (1982) derived the following equation to upscale from small scale lab tests to field discontinuity measurements.

$$JCS_n = JCS_0 \left(\frac{L_n}{L_0}\right)^{-0.03L_0}$$ (Barton and Bandis (1982)

3.1.4. Discontinuity Orientation

Discontinuity orientation refers to the orientation that discontinuity planes form in space and is measured in terms of two aspects. The first is the angle that the plane forms in the horizontal to vertical orientation, typically referred to as the dip of the plane and measured in degrees from the horizontal. The second is the orientation in which the plane dips relative to compass direction. This is generally either quoted as the dip direction, referring to the direction of maximum dip along the plane surface or strike, referring to the orientation of zero dip (perpendicular to the dip direction). When referring to a linear feature such as the intersection line between two planes, the line is measured in term of plunge, which is the angle between the line and the horizontal in the horizontal-vertical plane, and trend, referring to the direction of the line in terms of compass orientation (Wylie and Mah, 2004). Discontinuity measurement conventions are illustrated in Figure 3.9.

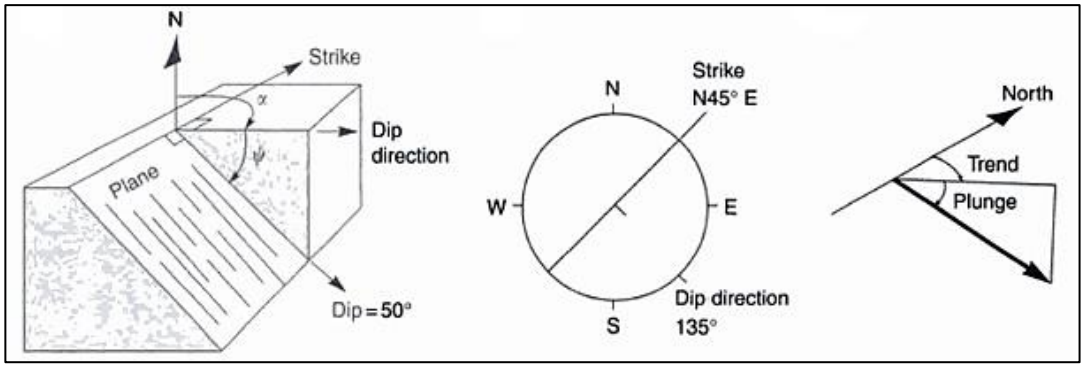

Figure 3.9: Illustration of dip, dip direction, strike, trend and plunge measurements (After Wylie and Mah, 2004).

3.1.5. Discontinuity Spacing

In the most general sense, discontinuity spacing represents the distance between individual discontinuities within a rock mass (Priest, 1993). Discontinuities delineate the boundaries between individual rock blocks. The spacing, persistency and relative orientation of the discontinuities plays a major role in the freedom of individual blocks within the rock-mass to move and rotate (Marinos et al. 2005). Block size and the spacing of discontinuities are key factors in most of the major rock mass classification systems that are used in quantifying rock mass strength for slope design.

Rock Quality Designation (RQD) is a measure of the sum of the length of borehole core pieces longer than 10cm out of a total borehole core run length, represented as a percentage. The RQD gives a basic measure of the joint spacing in the rock mass and is

used within rock mass rating systems such as the Bieniawski (1989) RMR and Barton (1974) Q systems (Priest, 1993).

The spacing of the discontinuities in a rock mass in combination with the number of discontinuity sets, as well as the relative orientation of the sets to each other, determines the size and shape of the individual rock blocks within the rock mass. Joint spacing and rock block size within a rock mass also need to be considered in the context of the scale of the scenario under consideration, as illustrated in Figure 3.10 (Hoek et al. 2013).

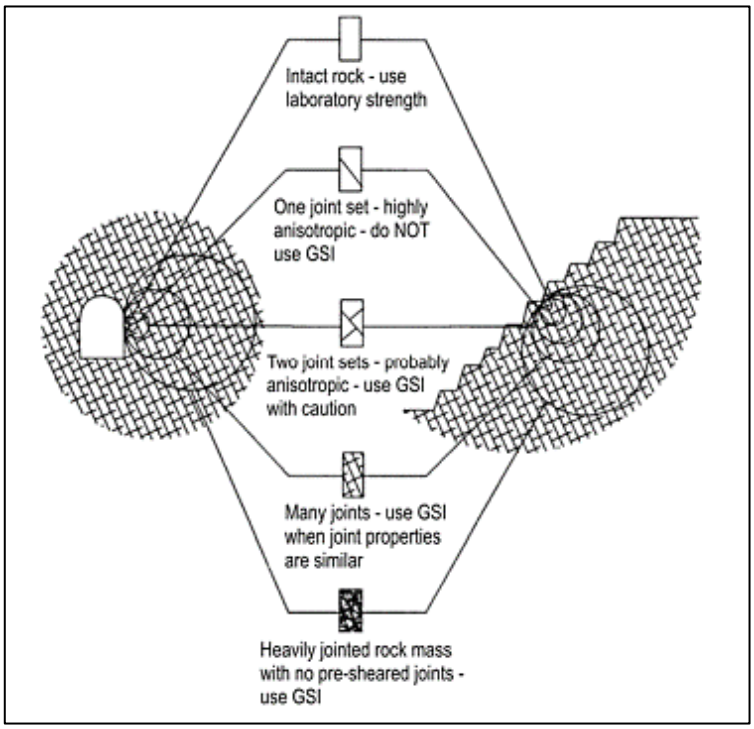

Figure 3.10: Illustration of the effect of scale on rock mass stability (From Hoek et al. 2013).

The spacing of discontinuities within a rock mass will always have a degree of variability, with a population of different joint spacing values. In most cases a typical normal distribution with the population evenly spread above and below the mean value does not accurately describe the joint spacing within a rock mass. Joint spacing distributions generally show more values at the lower end of the population range and are best described by log-normal or exponential distributions (Mohajerani and Aust, 1989). Analysis carried out by Priest and Hudson (1976) on joint spacing distributions in siltstone, sandstone and chalk showed a best fit to a negative exponential distribution while spacing study on the jointing in schists by Sen and Kazi (1984) complied best with a lognormal distribution.

3.1.6. Discontinuity Persistency

Discontinuity persistency can be defined as a measure of the extent of the development of a discontinuity surface (Singhal and Gupta, 2010). Within a rock mass the persistency of discontinuities will, in conjunction with the joint spacing, determine the sizes of individual blocks and the interconnectivity of joints, as well as the distribution of potential sliding planes and rock bridges (Figure 3.11). The shear strength of rock bridges is typically one to two orders of magnitude greater than that of discontinuity planes, meaning that their presence within a rock mass will have a profound effect on shear strength and overall stability (Giani, 1992). Typically rock slope stability analysis assumes a joint persistency of 100%; however if measured persistency indicates that this is not the case, a stepped path type failure that incorporates discontinuous failure planes and rock bridges needs to be assessed (ISRM, 1978; Giani, 1992).

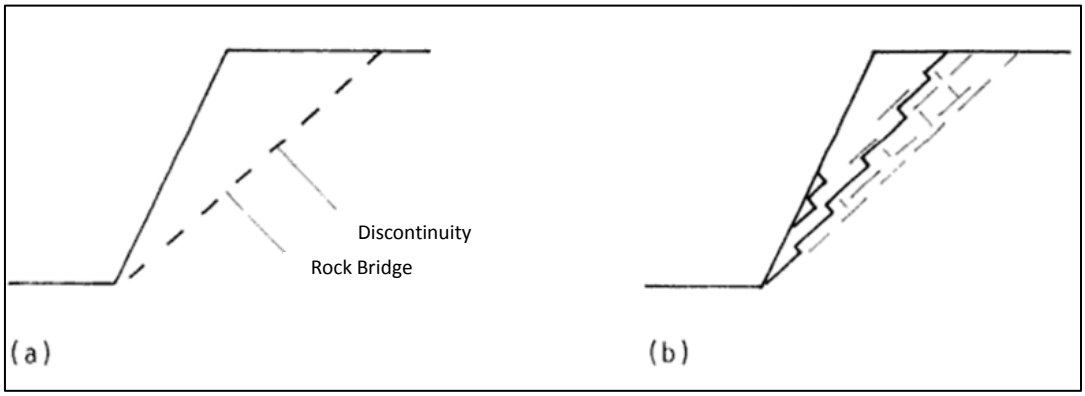

Figure 3.11: Illustration of a continuous failure surface (a) and stepped path failure surface (b) (After Giani, 1992).

Although playing a role in the strength of failure surfaces that may develop behind slopes of any scale, the effect of discontinuity persistence is particularly significant on bench to stack scale sized failures on hard rock mines such as Sishen. In these situations the overall stress levels are relatively low and failures are typically controlled by the interaction of discontinuity sets within the rock mass.

Figure 3.12 illustrates the effect of discontinuity persistency and spacing on the distribution of potential failure planes and rock bridges behind a slope.

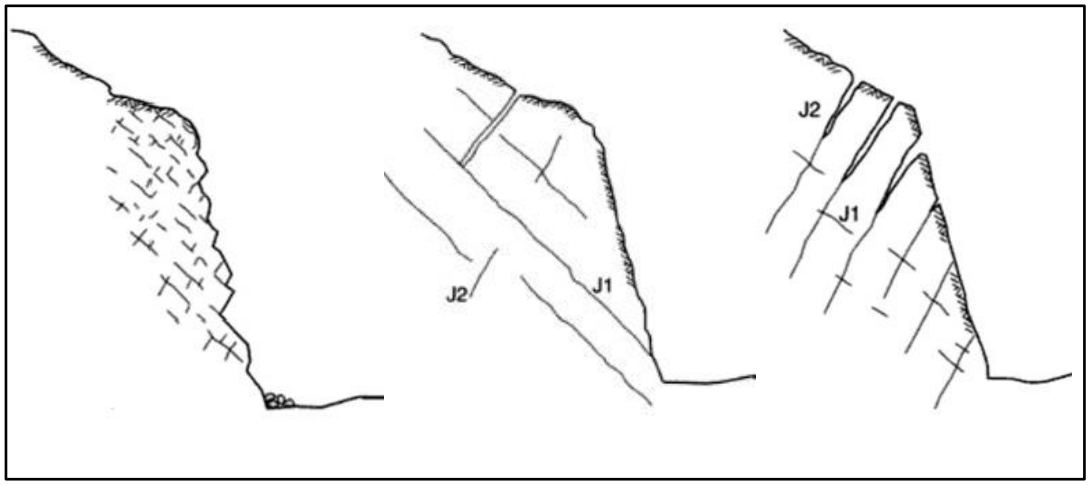

Figure 3.12: Illustration of the effect of persistency on rock mass stability (After Wylie and Mah, 2004).

3.2. ROCK MASS CLASSIFICATION SYSTEMS

Rock mass classification systems are considered relevant to this research report, as one of the aims of the research is to assess the effect that adding face mapping data to a borehole based geotechnical data set will have on such classification. Face mapping data is a potential input into rock mass rating systems, which in turn represent an input into slope stability analysis**.**

The most basic form of rock mass classification is the Rock Quality Designation (RQD) first introduced by Deere et al. (1967). The system rates borehole core based on the sum of core pieces longer than 10cm in a core run, expressed as a percentage of the total core run length. Although the RQD system is based on borehole core measurements, several formulae have been introduced to estimate RQD values based on face mapping data.

Palmström (1982) introduced the concept of the volumetric joint count (Jv) which is the total number of joints crossing a cubic metre of rock. The Jv value can be correlated with RQD through the following empirical formulae:

RQD = 115 – 3.3 Jv	Palmström (1982)
RQD = 110 – 2.5 Jv	Palmström (2005)

Priest and Hudson (1976) proposed an empirical relationship between RQD and discontinuity spacing based on the premise that discontinuity spacings conform to a negative exponential distribution. According to Priest and Hudson (1976) the RQD along a scanline can be derived by taking the sum of values, from a randomly selected negative exponentially distributed sample

set, for a given dataset falling above a threshold value. The sum of discontinuity lengths above the given threshold is represented as a percentage of the total scan line length to derive TRQD (Figure 3.13). Priest and Hudson (1976) defined the relationship between RQD and fracture frequency as follows.

$TRQD = 100\, e^{t\lambda}\, (t\lambda + 1)$

Where λ = Fracture Frequency and t = Minimum spacing threshold value

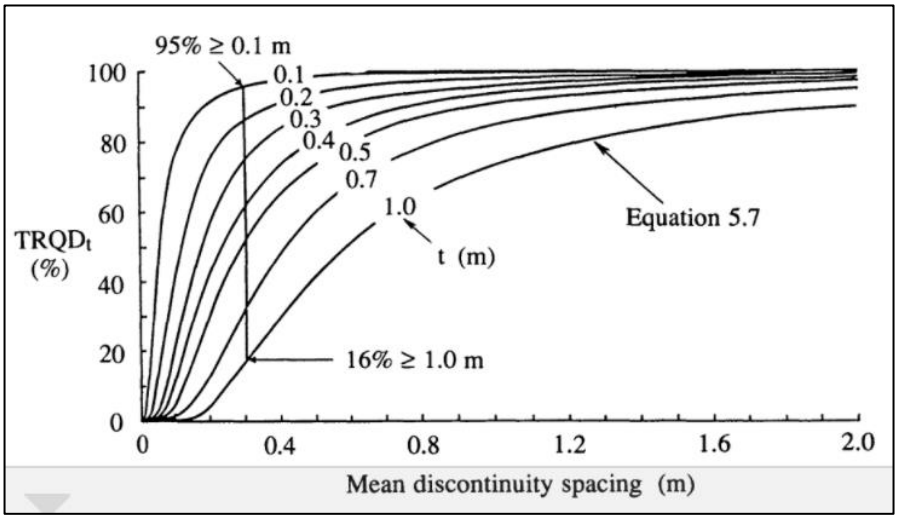

Figure 3.13: Relationship between RQD and joint spacing based on the relationship TRQD = $100\, e^{t\lambda}\, (t\lambda + 1)$, (After Priest and Hudson, 1976).

According to Priest and Hudson (1976), the conventional RQD lower threshold for RQD measurements of 0.1m will only be sensitive to mean discontinuity spacing values of less than 0.3m. Higher thresholds are suggested to effectively downgrade the RQD value for large excavations where joint spacing is likely to negatively impact stability or water inflow (Priest, 1993).

Priest and Hudson (1976) state that a threshold value of 0.1m is appropriate for fracture frequency values in the range of 2 to 38, as such the above generic equation can be re-written as follows.

$RQD = 100\, e^{-0.1\lambda}\, (0.1\lambda + 1)$

The RQD rating forms part of more complicated rock mass rating systems, that incorporate parameters such as UCS and joint spacing, persistency and condition as well as measures such as ground water conditions and the stress environment, to predict the behavior of a rock mass. Commonly used rock mass rating systems include the following:

- Rock Mass Rating (RMR) by Bieniawski (1976; 1989)
- Geological Strength Index (GSI) by Hoek (1994), Hoek et al. (2013)
- Tunneling Q Index by Barton et al. (1974)
- The Mining Rock Mass Rating (MRMR) system by Laubscher (1994)

All of the above systems use input measurements from the rock mass to generate an empirical strength classification that can be used to predict the behavior of the rock mass under different circumstances (Milne, 2007; Potvin et al., 2012). Systems relevant to this project are those that attempt to predict the behaviour and stability of slopes in open pit mines. This may be through an empirical system that gives a direct stability estimate, such as the slope design chart developed by Haines and Terbrugge (1991), or the Coal slope berm width chart proposed by Butcher et al. (2001). Alternatively, empirical rock mass strength estimates can also be derived from rock mass classification systems. A commonly used system that is incorporated into many modern slope stability software packages is the Generalized Hoek Brown failure criterion developed by Hoek and Brown (1988). This criterion uses GSI to predict the strength characteristics of a rock mass and is defined by the following equations:

$$\sigma_1 = \sigma_3 + \sigma_{ci}\{m_b.\frac{\sigma_3}{\sigma_{ci}} + S\}^a$$

$$m_b = m_i exp\{(GSI - 100)/(28 - 14D)\}$$

$$s = exp\{(GSI - 100)/(9 - 3D)\}$$

$$a = 1/2 + \{exp(-GSI/15) - exp(-20/3)\}/6$$

In the above equations, m_b represents a reduced value of the material constant m_i, D is a factor relating to blast damage and $\boldsymbol{\sigma_{ci}}$ is the intact material UCS (Hoek and Brown, 1988).

3.2.1. Geological Strength Index (GSI)

The GSI system was initially developed to allow for easy determination of rating values using the GSI chart, whereby a GSI rating is determined by visual comparison of the rock mass structure and discontinuity surface conditions with a set of descriptive values (Hoek et al. 1998; Marinos and Hoek 2000, 2001). It is however not practical to apply this type of subjective visual assessment when dealing with a large geotechnical dataset captured using standard logging procedures. In such cases other empirical estimates that take the measured logging parameters into account need to be considered. According to Hoek and Brown (1997), a correlation with RMR for competent rock masses (GSI > 25, RMR > 23) can be obtained using the following formula:

$$\boldsymbol{GSI = RMR_{89} - 5}$$

In the above formula RMR_{89} is the basic RMR value from the Bieniawski (1989) system, with the Groundwater rating set to 15 (dry), and the joint orientation adjustment set to 0 (very favourable).

Another method of deriving the GSI from measured input data was proposed by Hoek et al. (2013). The GSI is derived using the RQD and the Joint Condition rating from the RMR System (Bieniawski, 1989) through the following formula.

$$\boldsymbol{GSI = 1.5 \times Joint\ Condition + {RQD}/{2}}$$

3.2.2. Tunnelling Q Index (GSI)

The tunnelling Q Index is a system originally developed by Barton et al. (1974) as a means of quantifying the quality of a rock mass in terms of tunnelling support requirements. The system is divided into 6 separate components as follows.

- RQD is an index used to define the joint spacing of the rock mass.
- Joint Number (Jn) is a measure of the number of joint sets defining the rock mass.
- Joint Roughness (Jr) and Joint Alteration (Ja) define the joint surface conditions.
- Joint Water (Jw) defines the ground water conditions.
- The Strength Reduction Factor (SRF) defines the in situ stress environment.

These six input parameters are each assigned a score which is then entered into the following equation to attain a Tunnelling Q value.

$$Tunneling\ Q = \frac{RQD}{Jn} . \frac{Jr}{Ja} . \frac{Jw}{SRF}$$

According to Barton et al. (1974) the first portion of the equation (RQD / Jn) represents a rough measure of the block size, the second portion (Jr / Ja) is a measure of the inter-block shear strength and the third portion (Jw / SRF) a measure of the active stress state.

The Q System was specifically developed in the underground tunnelling environment to quantify rock mass conditions and estimate support requirements. The system was developed based on observations of rock mass conditions, tunnel stability and support of 200 separate tunnels located in the Alps mountain range (Barton et al, 1974, Palmström and Broch, 2006). The numbers applied to each of the categories in the Q system are derived from the observed data in the case studies.

Although it currently has little use as a direct input in slope design it does provide a useful cross reference to check against calculated RMR values. Q can be correlated with RMR through the following formulas.

$RMR = 9 \ln Q + 44$ (Bieniawski, 1989)

$RMR = 15 \log Q + 50$ (Barton, 1995)

3.2.3. Rock Mass Rating (RMR)

The Rock Mass Rating system was first published by Bieniawski (1973) as a quantitative empirical measure of rock mass quality. The system was initially developed at the South African Council of Scientific and Industrial Research (CSIR) for use in tunnelling in the Civil Engineering Industry and is based on observations in shallow tunnel excavations into sandstones (Dyke, 2006; Singh and Goel, 1999). The system has undergone revisions in 1974, 1975, 1976 and 1989 as more case study data has become available. The 1976 and 1989 versions of the system are most commonly used (Palmström, 2009). The system is based on a series of empirical rating numbers for various parameters considered to play an important role in determining rock mass strength and stability. The scores for each of the individual parameters are added up to give an overall RMR rating out of 100.
The original 1973 system incorporated the following rating parameters.

- Rock Quality Designation (RQD)
- Weathering
- Intact Rock Strength (UCS)

- Joint Spacing
- Joint Separation
- Joint Continuity
- Groundwater
- Strike and Dip Orientations (Tunnels / Foundations)

Modifications during the various revisions of the System involved changes in rating scores, parameters and parameter descriptions (Dyke, 2006). The most up to date (1989) version of the RMR System, as used on Sishen Mine, is summarised in Tables 3.1 to 3.4 below. From the tabulated values the RMR is calculated using the following formula.

$$RMR = A1\ Rating + A2\ Rating + A3\ Rating + A4\ Rating + A5\ Rating - B\ Rating$$

Table 3.1: RMR A1, A2 and A3 Ratings (Modified After Bieniawski, 1989).

UCS (MPa)	A1 Rating
> 250	15
100 – 250	12
50 – 100	7
25 – 50	4
5 – 25	2
1 - 5	1

RQD %	A2 Rating
90 - 100	20
75 - 90	17
50 - 75	13
25 - 50	8
0 - 25	3

Minimum average discontinuity spacing (cm)	A3 Rating
> 200	20
60 – 200	17
20 – 60	13
6 – 20	8
<=6	5

Table 3.2: RMR Joint Condition A4 Rating (Modified After Bieniawski, 1989).

A4 = E1 +E2 +E3 + E4 + E5				
Persistence E1	**Fill Thickness E2**	**Surface Roughness E3**	**Infilling or Gouge E4**	**Joint Wall Weathering E5**
< 1m E1 = 6	None E2 = 6	Very Rough E3 = 6	None E4 = 6	Unweathered E5 = 6
1 – 3m E1 = 4	< 0.1mm E2 = 5	Rough E3 = 5	Hard infilling < 5mm E4 =4	Slightly Weathered E5 = 5
3 – 10m E1 = 2	0.1 – 1.0mm E2 = 4	Slightly Rough E3 = 3	Hard infilling > 5mm E4 = 2	Moderately Weathered E5 = 3
10 – 20m E1 = 1	1 – 5mm E2 = 1	Smooth E3 = 1	Soft infilling < 5mm E4 = 2	Highly Weathered E5 = 1
> 20m E1 = 0	> 5 mm E2 = 0	Slickensided E3 = 0	Soft infilling > 5mm E4 = 0	Decomposed E5 = 0

Table 3.3: RMR Groundwater A5 Rating (Modified After Bieniawski, 1989).

Inflow in l/10m tunnel length	Joint Water Pressure per Major principal stress	General Conditions	A5 Rating
None	0	Dry	15
< 10	< 0.1	Damp	10
10 – 25	0.1 – 0.2	Wet	7
25 – 125	0.2 – 0.5	Dripping	4
> 125	> 0.5	Flowing	0

Table 3.4: RMR Orientation B Rating (Modified After Bieniawski, 1989).

Orientation of critical joint set with respect to tunnel or mine excavation	Rating
Very Favourable	0
Favourable	-2
Fair	-5
Unfavourable	-10
Very Unfavourable	-12

The above parameters can be gathered through geotechnical borehole logging or face mapping of exposed surfaces.

3.2.4. Mining Rock Mass Rating (RMR)

The Mining Rock Mass Rating system was first introduced in 1974 as a mining applicable extension to Rock Mass Rating system. The system is based on the same principle as the RMR with rating values assigned to the following basic rock mass parameters based on the assessed parameter condition (Laubscher, 1990).

- Rock Quality Designation (RQD)
- Rock Strength (UCS)
- Joint Spacing
- Joint Condition and Water

As for the RMR, the rating scores for each parameter are added up to give an overall rating out of 100.

Where the MRMR differs from the RMR system is that adjustments specific to the mining environment are applied to adjust the initial rating out of 100 for use in mine planning and

design. The following adjustments are applied by multiplying the original rating by each of the adjustment ratings.

- Weathering Adjustment
- Mining Induced Stress Adjustment
- Orientation Adjustment
- Blasting Adjustment

Like the RMR system, MRMR input values can be acquired from boreholes and exposed rock surfaces (Laubscher, 1990).

Several practical mining related applications of the MRMR system have been described by Laubscher, 1990), centred mainly around the cavability / stability of excavations in the massive underground mining environment. A schematic overview of the application of the MRMR system in the mining environment is given in Figure 3.3.

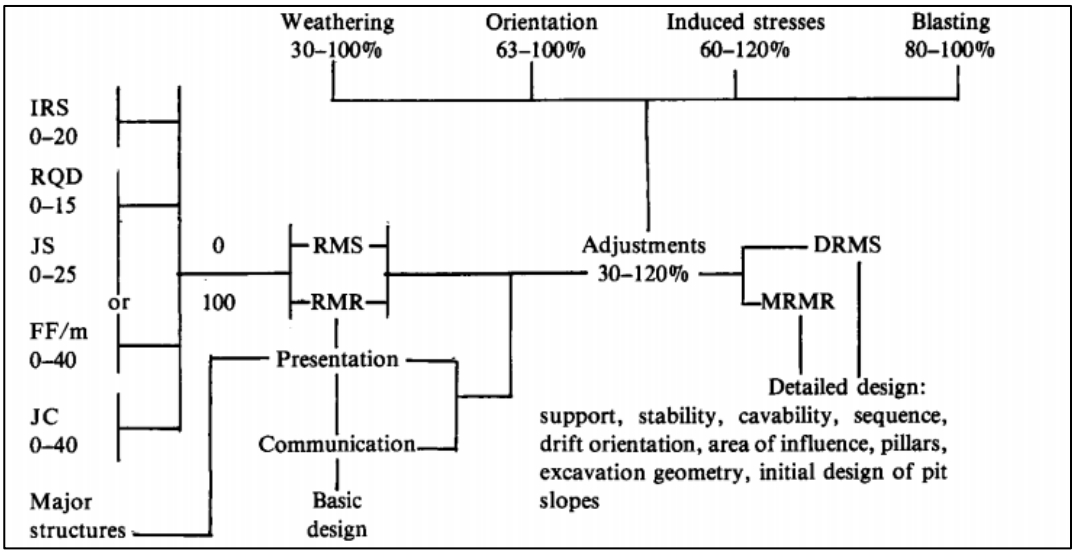

Figure 3.14: Application of the MRMR system (From Laubscher, 1990).

With respect to open pit slopes, initial slope design angles can be estimated using the MRMR of the rock mass as per Table 3.5 (Laubscher, 1990).

Table 3.5: Slope design angles based on MRMR (After Laubscher, 1990).

MRMR	100-80	80-61	41-60	21-40	0-20
Slope Angle (Degrees)	75	65	55	45	35

Haines and Terbrugge (1991) produced an empirical chart allowing for the estimation of slope factor of safety (FOS) based on slope height, slope angle and MRMR (Figure 3.15).

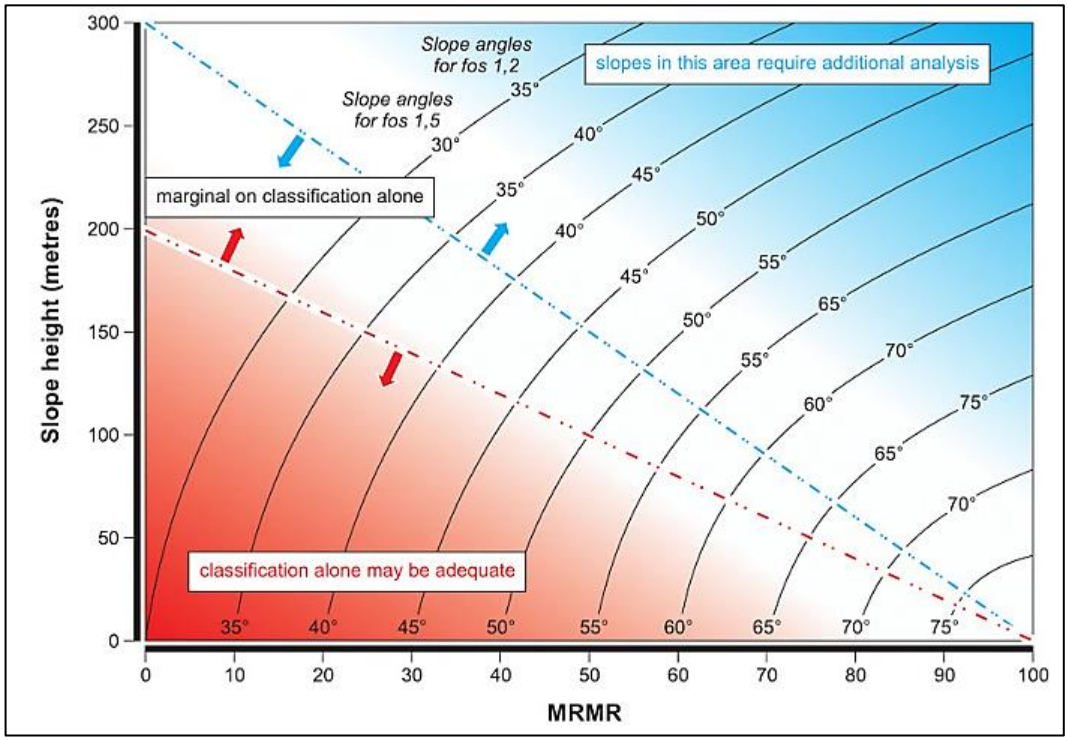

Figure 3.15: Haines and Terbrugge slope stability chart (From Lorig et al. (2009).

3.3. FACE MAPPING BACKGROUND AND TECHNIQUES

3.3.1. Mapping Parameters

The purpose of geotechnical face mapping is to gather data pertaining to the strength and condition of a rock mass through measurements taken from an exposed rock face. Conventionally, a geologist or geotechnical engineer does face mapping by giving a descriptive assessment and by taking measurements directly from an exposed face. These typically include the rock type, weathering and strength of the intact material as well as measurements of orientation, spacing, persistency and condition of the discontinuities present (Read et al., 2009).

Face mapping parameters are generally described according to standard classification systems of hardness, weathering as well as discontinuity condition, spacing and persistency (Read et al., 2009). According to Read et al. (2009) a complete field face mapping sheet will typically have data pertaining to the following.

- Identification, location and size of the exposure/face being mapped.
- A description of rock type, degree of weathering and rock strength.
- Orientation, frequency, persistency and condition of discontinuities.
- Moisture condition and seepage.
- Rock mass classification such as RMR (Bieniawski, 1989) or GSI (Hoek, 1994).
- A sketch/plan of the face showing the distribution of features mapped.

Structural face mapping is specifically aimed at gathering information pertaining to the discontinuities in an exposed face. This is vital for kinematic analyses and as an input into limit equilibrium and numerical modelling analyses. Structural face mapping includes Scanline Mapping, Cell/Window Mapping and digital mapping techniques such as digital photogrammetry or laser scanning mapping (Read et al., 2009; McQuillan, 2013).

3.3.2. Manual Face Mapping Techniques

Scanline mapping is a sampling method in which measurements are manually taken for all the features on an exposed face that intersect the sampling line. Typically, several sampling lines are taken in orientations as close to perpendicular to the prominent discontinuity sets as possible to reduce sampling bias. Feature properties such as orientation, length, roughness, and infill type are recorded for each feature along the scan line (Read et al., 2009; Simangunson et al., 2004; Wines and Lilly, 2001; Bye and Bell, 2001; Call, 1992; Hoek and Bray, 1981).

Cell or window mapping is a manual face mapping method where an outcrop or face is divided into cells. Discontinuity sets are identified within each cell and the orientation, spacing, persistency and properties of the discontinuities within each set are measured. Typically, the cells will make up 10 to 25% of the total exposed area of face (Read et al., 2009; Call, 1992; Priest, 1993).

Fundamental disadvantages of any manual face mapping technique are that they are labour intensive, time consuming and require physical contact with the rock face (Gumede, 2005). Direct access to the rock face is often limited in the mining environment making direct face mapping impractical (Gumede, 2005, Simangunson et al., 2004; Wines and Lilly, 2001). Manual face mapping also introduces a rockfall hazard to personnel conducting the mapping as they have to come in contact with the rock face.

3.3.3. Digital Face Mapping Techniques

The practical problems associated with manual face mapping have been addressed with advances in technology that allow for face mapping using a digital image that has been draped over a 3D point cloud of the mapping face.

Most literature refers to 3D photogrammetry techniques for this purpose whereby stereo photos are used to generate the required point cloud of the face (Read et al., 2009; Gumede, 2005; Little, 2006; Reid and Harrison, 2000; Beer et al, 1999; Harrison, 1993;

Franklin et al., 1988). Although more practical than manual face mapping digital photogrammetry does have drawbacks in as much as a surveyed reference point needs to be positioned on the face and two camera tripod positions need to be accurately surveyed.

A newer technique for digital face mapping comes in the form of mapping using 3D terrestrial laser scanning data. In comparison with photogrammetry, laser scanner mapping is fast and efficient. With the ability to sample several hundred thousand points per second a terrestrial laser scanner can create a high resolution point cloud covering several hundred square metres in the space of a couple of minutes. The scan points themselves typically include X, Y, Z and intensity information, and can include true colours through the use of concurrent digital photography. Geo-referencing using various techniques, in conjunction with the use of concurrent digital photography allows for an accurate representation of a rock face in real 3D space (Feng and Roshoff, 2006; Slob and Hack, 2007).

Various methods for extracting geotechnical data trends from laser scanner point clouds have been examined since the inception of the technology. These include automated techniques that examine orientation trends to derive structural information about mapping faces and semi-automated techniques that rely on user structural interpretations of specific features of a mapping face (Feng and Roshoff, 2006; Slob and Hack, 2007).

An automated approach outlined by Slob and Hack (2007) involves creating a Digital Terrain Model (DTM) from the scan points of a scanned face and using the orientation of the individual DTM facets to derive structural trends. The theory behind this is that if all facet orientations for a face are plotted on a stereonet, major planes will be exposed as point concentrations due to the predominant facet orientations on the mapping face.

The more commonly accepted semi-automated approach follows on from the digital photogrammetry technique, with the user selecting geological features on the 3D digital representation of the mapping face and the software calculating parameters such as orientation, area and length for the selected portion of the scan (Feng, 2001; Feng and Roshoff, 2006; Slob and Hack, 2007). In reality, modern software packages have the functionality to further automate such features by intuitively selecting planes of similar orientation to the user selected plane (Maptek, 2013).

McQuillan (2013) gives a direct comparison between laser scanner face mapping using the Maptek system with photogrammetry face mapping using the Siro Vision system. The laser scanner system was generally found to be superior in terms of the following.

- The laser scanner provided faster and easier data collection.
- The laser scanner provided faster data processing and was less demanding on software systems.
- More accurate discontinuity orientation measurements were obtained using the laser scanner (up to 15° difference in dip measurements between the two techniques was observed).
- Planes oblique to the exposed face were more readily observable with the laser scanner.

3.3.4. Disadvantages of Face Mapping

Geological and geotechnical face mapping fundamentally involves measuring and interpreting various parameters from exposed faces to estimate or infer various rock mass parameters. The fundamental disadvantages of the technique arise from the fact that no mapping face will ever be completely representative of the rock mass. Some of the main disadvantages and potential sources of error during face mapping can be summarised as follows.

- Blast induced fracturing – Blasting inevitably leads to some degree of fracturing on most excavation surfaces, even when limit blasting techniques are used. As these fractures are induced by blasting they are not representative for the general degree of jointing in the rock mass. Wines and Lilly (2001) highlight that in some cases it is difficult to distinguish between blast induced and natural discontinuities in a mapping face. The experience and awareness of the face mapper plays an important role in distinguishing between the two.

- Orientation Bias – The probability of a particular discontinuity being exposed in a mapping face is dependent on the relationship between the orientation of the discontinuity and the face (Zhang, 2006). In many mining operations, limited exposure of orthogonal faces introduces an orientation bias into the face mapping process (Wines and Lilly, 2001).

- Size Bias – A size bias tends to favour larger discontinuities in a mapping exercise as these are more regularly exposed in a mapping face than less persistent discontinuity surfaces (Zhang, 2006).

- Truncation Bias – Very small joints become difficult to measure and are often ignored below a lower cut-off length (Zhang, 2006). Excluding the measurement of the lower

end of the population of joint trace length within a mapping face will have the effect of increasing the overall mean length of the measured joint traces (Gumede, 2005).

- Censoring Bias – Converse to the truncation bias, correct trace length measurements for persistent discontinuities are often difficult to establish as they tend to extend past the ends of the exposed mapping face or mapping window. If both ends of the discontinuity cannot be seen, only a truncated measurement of the joint plane length can be taken (Zhang, 2006).

- Scanline Specific disadvantages

    - Orientation bias – Specifically in the case of scan line mapping an orientation bias is introduced into the fracture frequency / joint spacing measurements if the joint orientation of a particular set is not perpendicular to the direction of the scanline (Gumede, 2005). This can however be corrected trigonometrically through the Terzaghi (1965) weighting as per the following formula where N_{corr} is the corrected fracture spacing, N is the measured fracture spacing and α is the angle between the scanline and the discontinuity set.

$$N_{corr} = N \frac{1}{cos\alpha}$$

    - Size Bias – In the context of mapping along a scanline a size bias can be introduced due to the fact that longer discontinuity traces are more likely to be intersected by the scanline than shorter traces (Einstein et al, 1983).

3.4. KINEMATIC SLOPE STABILITY ANALYSIS

Kinematic analysis is a method for determining the influence that the interactions between discrete planes and surfaces will have on the stability of an excavation. In the context of an excavated rock slope this involves assessing the potential for the development of a structurally controlled failure based on the orientation of predominant discontinuity planes relative to the rock face. Stereonet pole plots for various idealized modes of slope failure are given in Figure 3.16 (Wyllie and Mah, 2004).

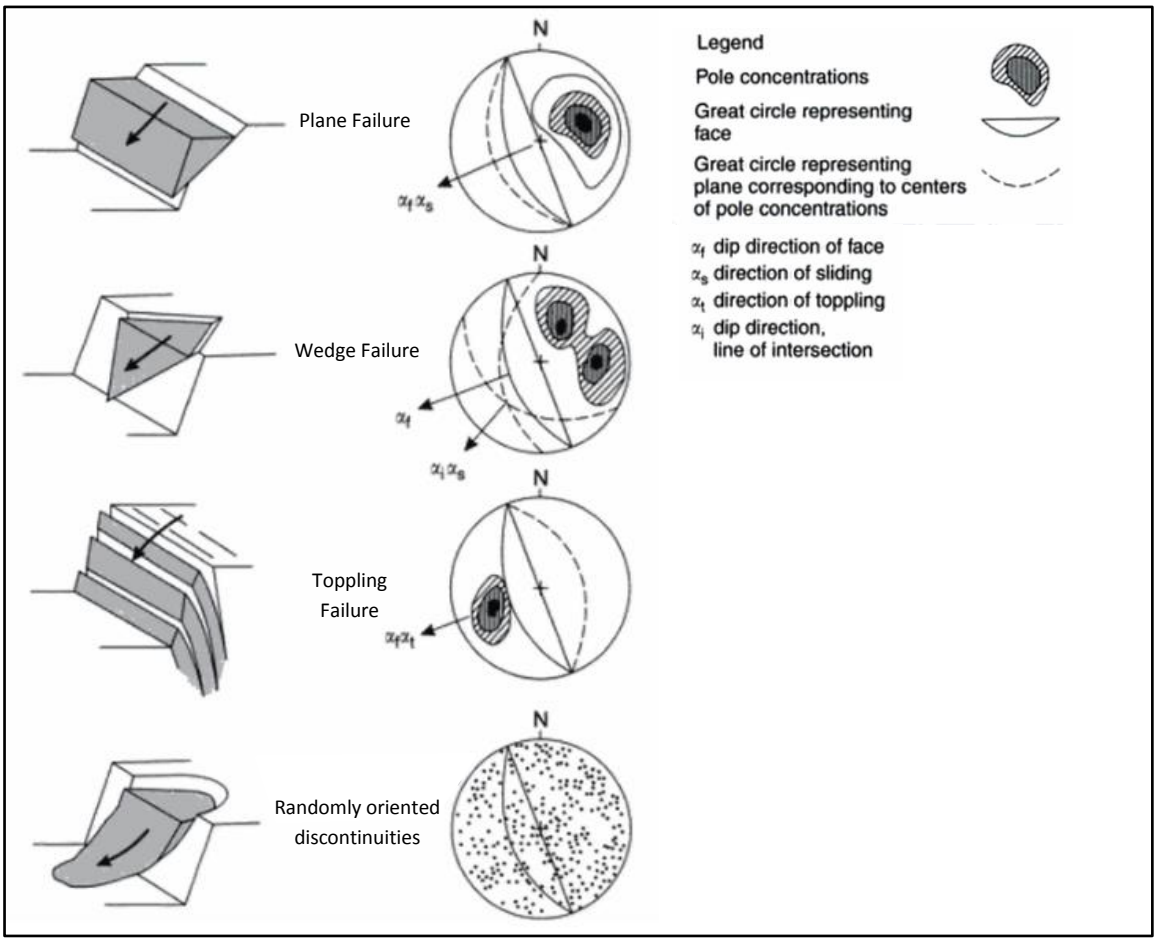

Figure 3.16: Idealized modes of slope failure and associated stereonet pole plots (After, Wyllie and Mah, 2004).

Tests carried out by Markland (1972) and Hocking (1976) have been used to establish major stereonet pole concentrations associated with typical structurally controlled failure types. Structurally controlled rock slope failures can be divided into either plane, wedge or toppling failures. Structurally controlled failure will usually occur by one or a combination of the aforementioned mechanisms, depending on the relative orientation of the slope face and predominant discontinuities (Wylie and Mah, 2004).

3.4.1. Plane Failure Analysis

Plane failure occurs when a slope fails along a continuous surface that conforms to the following (Hoek and Brady, 1981; Eberhardt, 2016).

- The plane and slope face have sub-parallel dip directions, within approximately 20 degrees of each other.
- The plane must 'daylight' in the slope face.
- The dip of the plane must be greater than the friction angle of the sliding surface.

- The upper end of the sliding surface must terminate either at the slope crest or at a tension crack.
- Releasing planes must be present to allow sliding to occur.

In order to assess kinematic feasibility in terms of the pole data representing a discontinuity plane, the daylight envelope and polar friction cone must also be plotted on the stereonet. The daylight envelope represents a zone on the stereonet in which the poles to all daylighting planes lie, while the polar friction cone is a circular plot offset by the friction angle of the potential failure plane from the vertical. Any poles falling outside the polar friction cone while inside the daylight envelope and lateral limits are kinematically feasible for plane failure, as illustrated in Figure 3.17.

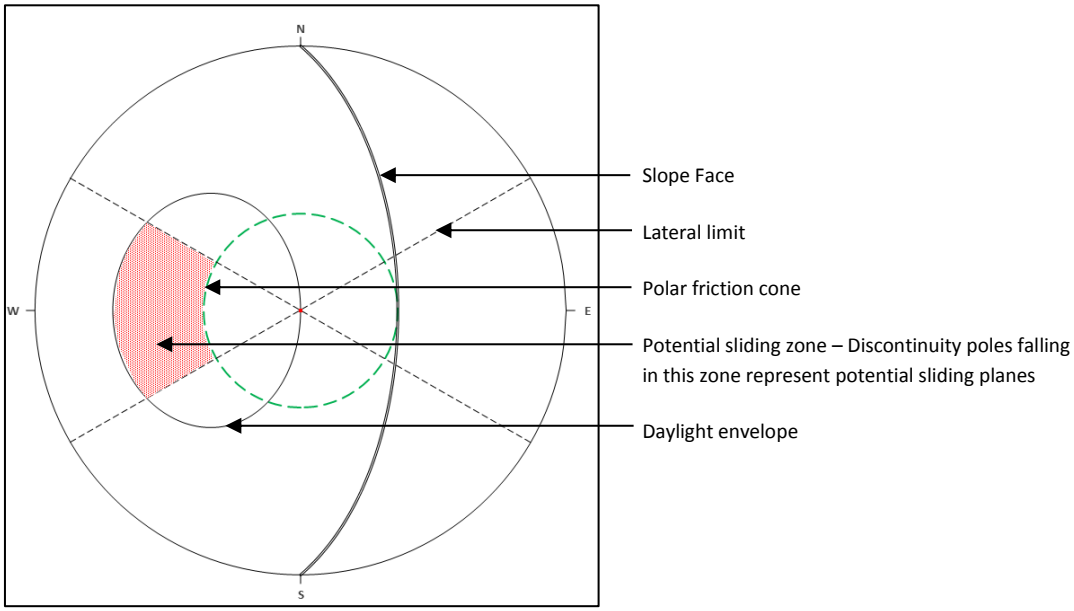

Figure 3.17: Plane failure analysis stereonet.

3.4.2. Wedge Failure Analysis

Wedge failure occurs when the interaction of the slope face and two unfavourably dipping discontinuities results in the formation of a failure wedge (Figures 3.18 and 3.19). For wedge failure to occur the following conditions need to be met (Eberhardt, 2016).

- The slope dip must be greater than the plunge of the line of intersection between the two failure planes.
- The line of intersection must 'daylight' out of the slope face.
- The dip of the line of intersection must be such that the shear strength of the two failure planes is overcome.

- The upper end of the intersection line must either 'daylight' at the slope crest or terminate at a tension crack.

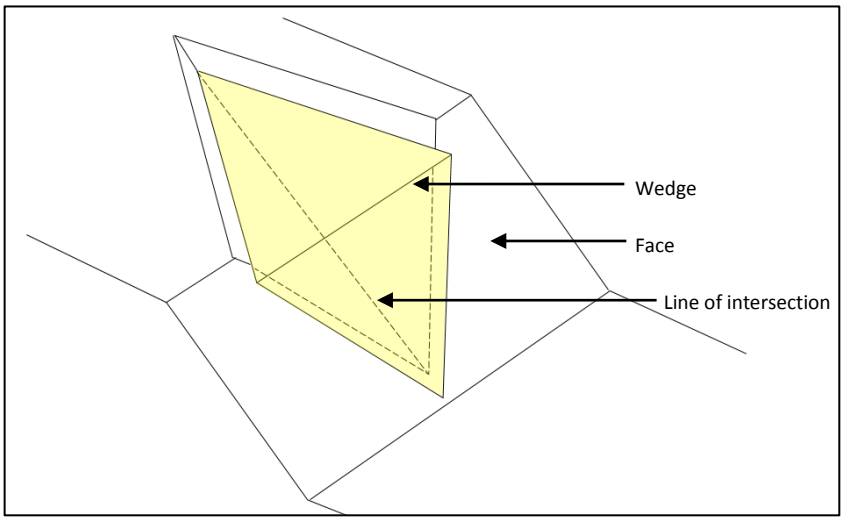

Figure 3.18: Illustration of a failure wedge (After Eberhardt, 2016).

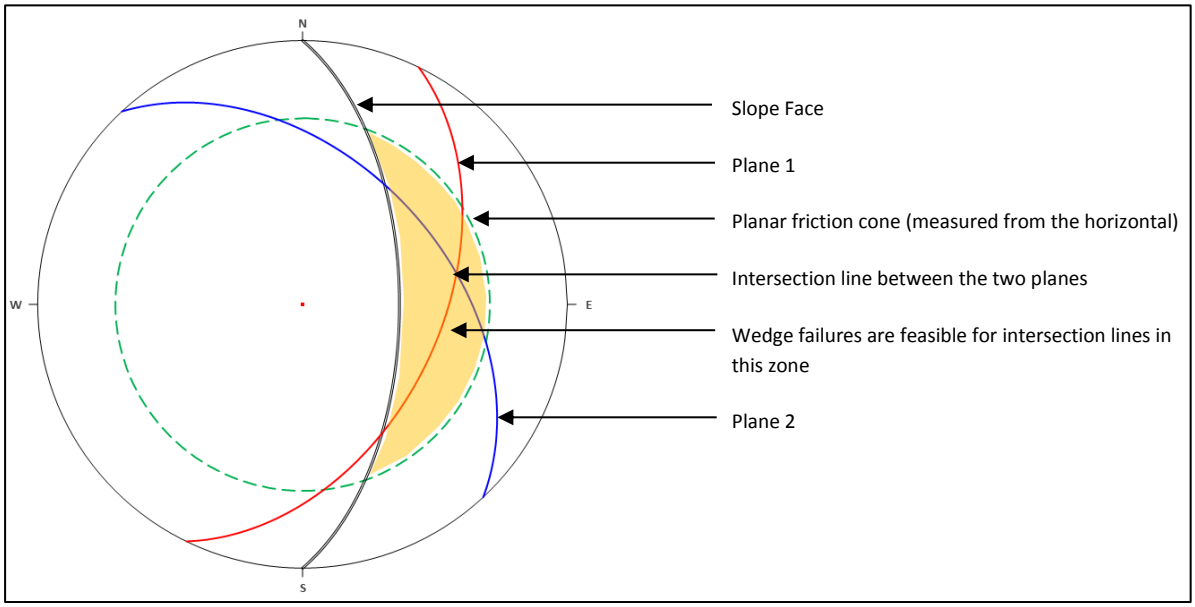

Figure 3.19: Wedge failure analysis stereonet.

3.4.3. Toppling Failure Analysis

In contrast to other kinematically controlled failure mechanisms that involve sliding along a failure plane, toppling failure occurs when blocks or elongated columns of rock rotate outwards from a fixed base. Common classes of toppling failure include block toppling, flexural toppling and block flexural toppling, as illustrated in Figure 3.20 (Wylie and Mah, 2004).

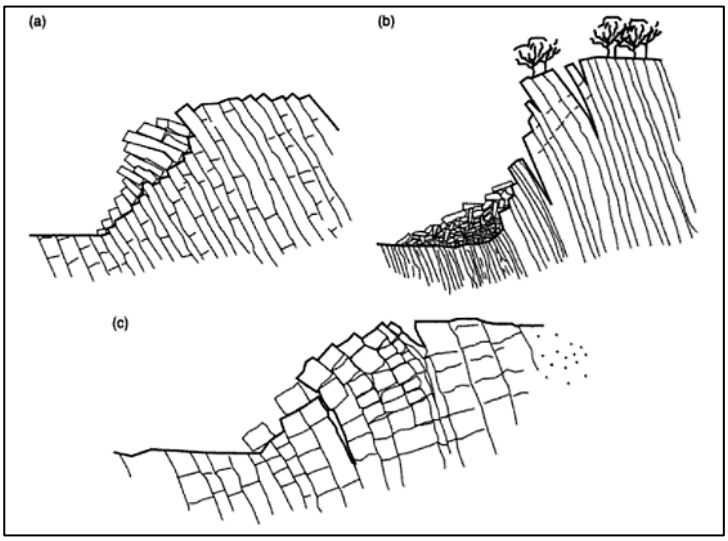

Figure 3.20: Illustration of block toppling (a), flexural Toppling (b) and block flexural toppling (c) (After Wylie and Mah, 2004).

As illustrated in Figure 3.20, flexural toppling involves toppling and flexural failure of elongated blocks while with direct toppling discrete pre-defined blocks are created by orthogonal joints prior to toppling (Goodman, 1980; Wyllie and Mah, 2004).

For toppling failure to occur the following conditions need to be met (Wylie and Mah, 2004).

- The discontinuity defining the toppling plane must strike within approximately 10° of the slope face.
- The centre of gravity of the block must lie outside of its base.
- Frictional forces between adjacent toppling blocks must be overcome.

Kinematic analysis of toppling failure assesses the orientation of blocks with respect to the slope face and whether this will create conditions that will allow for toppling failure. Further analysis of block shape and inter-layer slip is used to assess stability (Wylie and Mah, 2004). Figure 3.21 illustrates the zone of kinematically feasible toppling failure for discontinuity poles on a stereonet.

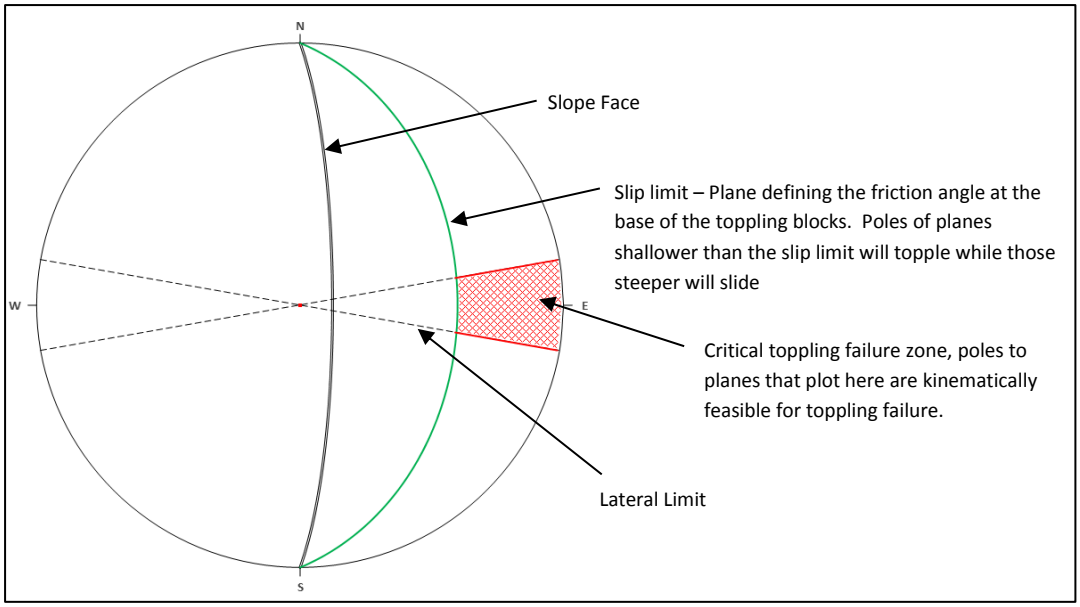

Figure 3.21: Toppling failure analysis stereonet.

This chapter outlines various aspects of rock mechanics theory relating to rock mass and discontinuity strength. Rock mass classification systems are reviewed and the theory behind geotechnical face mapping as a means of data capture is outlined. The use of terrestrial laser scanner technology in geotechnical face mapping is reviewed as a technique, and compared with conventional face mapping methods.

The following chapter documents the methodology adopted for this research dissertation. The laser scanner system and associated software is reviewed as a geotechnical face mapping tool, and the complete face mapping and data management process developed for use on Sishen Mine is documented.

CHAPTER 4: PROJECT METHODOLOGY

The previous chapter outlined various theoretical aspects relating to rock mass strength, discontinuities in rock masses and rock mass rating systems. Conventional geotechnical face mapping methodologies were outlined and laser scanner technology was reviewed as a tool for use in geotechnical face mapping.

In this chapter the terrestrial laser scanner system used during this research project will be discussed and reviewed. The laser scanner geotechnical face mapping process developed for Sishen Mine will be discussed from the face mapping process, to data management and reporting.

The main aim of the research described in this research report is to assess the potential for incorporating laser scanner derived face mapping data into a geotechnical database and in doing so answer the following research objectives.

- Investigate the process of geotechnical face mapping using laser scanning technology and establish a method for integrating face mapping data into a borehole based geotechnical database.

- Analyze the effect that adding face mapping data to geotechnical borehole data has on calculated rock mass parameters, geotechnical data uncertainty and stability analysis results.

- Examine further practical applications of geotechnical face mapping in geotechnical risk mitigation.

A theoretical process flow showing the steps required to achieve the desired research outcomes is outlined in Figure 4.1.

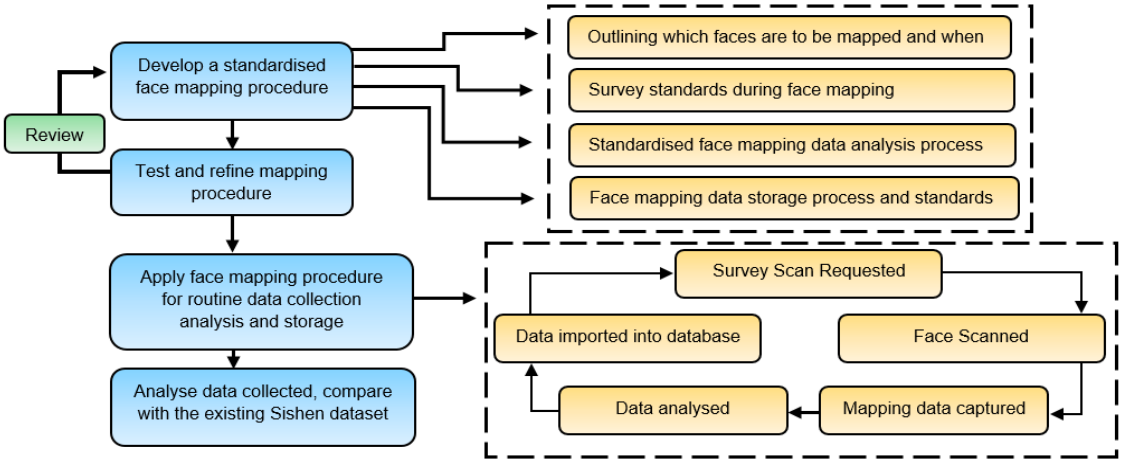

Figure 4.1: Theoretical process flow for development, implementation and assessment of the results from laser scanner face mapping.

4.1. THEORETICAL FACE MAPPING DATA FLOW PROCESS

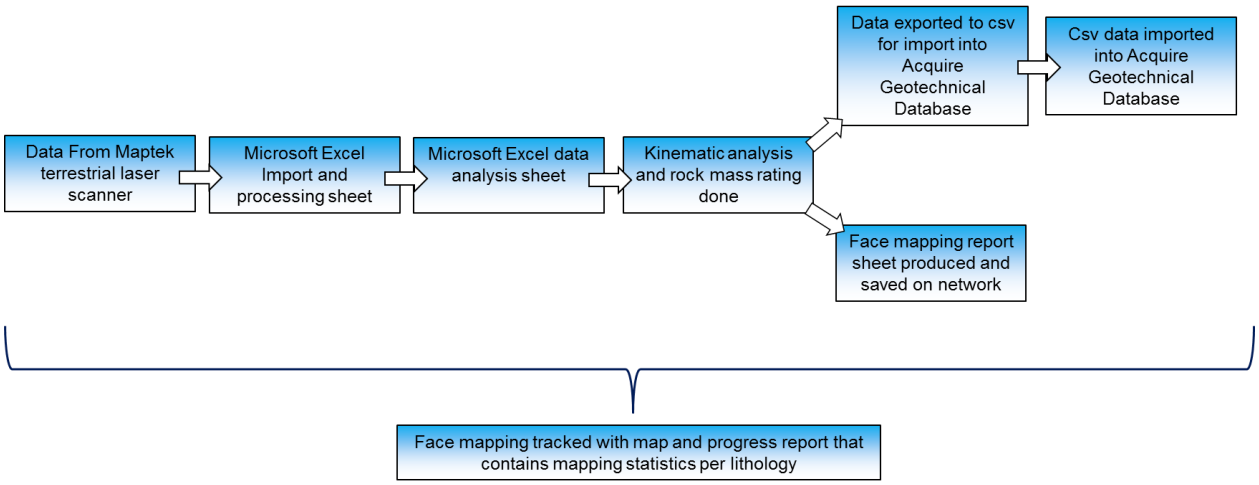

Figure 4.2: Theoretical face mapping data flow process.

4.2. FACE MAPPING PROCEDURE

As outlined in Figure 4.2 the first stage in the methodology of this project is to develop a standardised procedure for the collection and storage of geotechnical face mapping data. A review of the literature pertaining to geotechnical face mapping techniques is given in Chapter 3 of this dissertation. These include the traditional techniques whereby geotechnical data is collected directly from the mapping face and digital mapping techniques in which a digital point cloud representing the highwall face is analysed.

4.2.1. Mapping Face Selection

Sishen Mine is a complex mining operation made up of of several separate mining areas in an elongated series of interconnected pits. The mining process and final product requirements necessitate blending of different grades of ore from different areas within the orebody. This type of mining has led to the development of a large mining area consisting of a mix of relatively flat interim pit boundaries, steep final pit boundaries, large open waste stripping operations and generally confined loading areas. The mine has been in operation for more than 50 years and a range of highwall conditions exists with varying slope angles, slope heights, and overall slope quality.

Further complicating the geotechnical conditions encountered on the mine is the complicated geological environment that hosts the Sishen ore body.

Selection criteria for choosing appropriate faces for geotechnical face mapping must take the geotechnical data requirements, geological conditions and practical circumstances of the operation into account. Appropriate coverage and scale of face mapping based on the phase of the project are outlined by Stacey (2009). Data collection for this research project took place during the operational phase of a large open pit mine, with the purpose of supplementing an already large on-site geotechnical data set. Face mapping scale and coverage in this instance took the site specific conditions and geotechnical data needs into account. Further detail regarding the face mapping selection procedure is given in Section 4.2.5.

4.2.2. Laser Scanning

Laser scanning for this research report was done using the Maptek I-Site 8810 Laser Scanner. The scanning unit is vehicle mounted (Figure 4.3) and is operated from inside the vehicle via a Wi-Fi connection using a Toughbook tablet device. All scans can be carried out over a horizontal range of between 0 and 360 degrees with a fixed vertical range of 80 degrees. In terms of distance the scanner has ranges of 500m, 1000m and 1400m for surfaces with low reflectivity (10% - 40%), medium reflectivity (40% - 80%) and high reflectivity (>80%) respectively. In practical terms scans are usually done within 200m of the target surface, with several scans from different scanning positions making up the overall scan image for larger areas. Laser scans are taken in conjunction with a high resolution panoramic photograph which is tied in with the laser scanning data to provide a photographic image overlay in the analysis software.

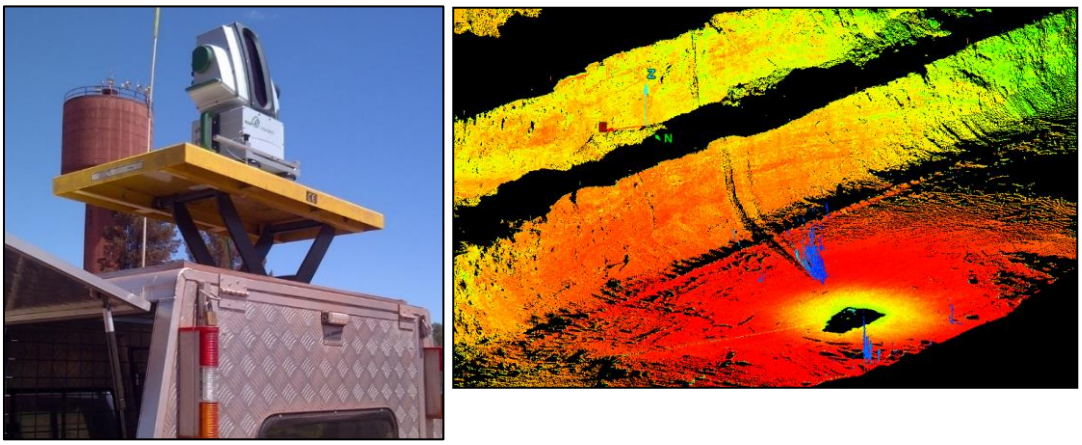

Figure 4.3: Maptek 8810 laser scanner using a vehicle-mounted setup (left) and a high resolution point cloud for use in face mapping (right).

4.2.3. Data Analysis

The Maptek I-Site Studio software is used to carry out face mapping on the laser scanning data. The software drapes a digital image over the laser scanner point cloud (Figure 4.4) allowing the user to accurately measure discontinuity orientation, spacing and persistence (Figure 4.5). The software also has functionality that allows for determination of the roughness of larger discontinuity surfaces as illustrated in Figure 4.6.

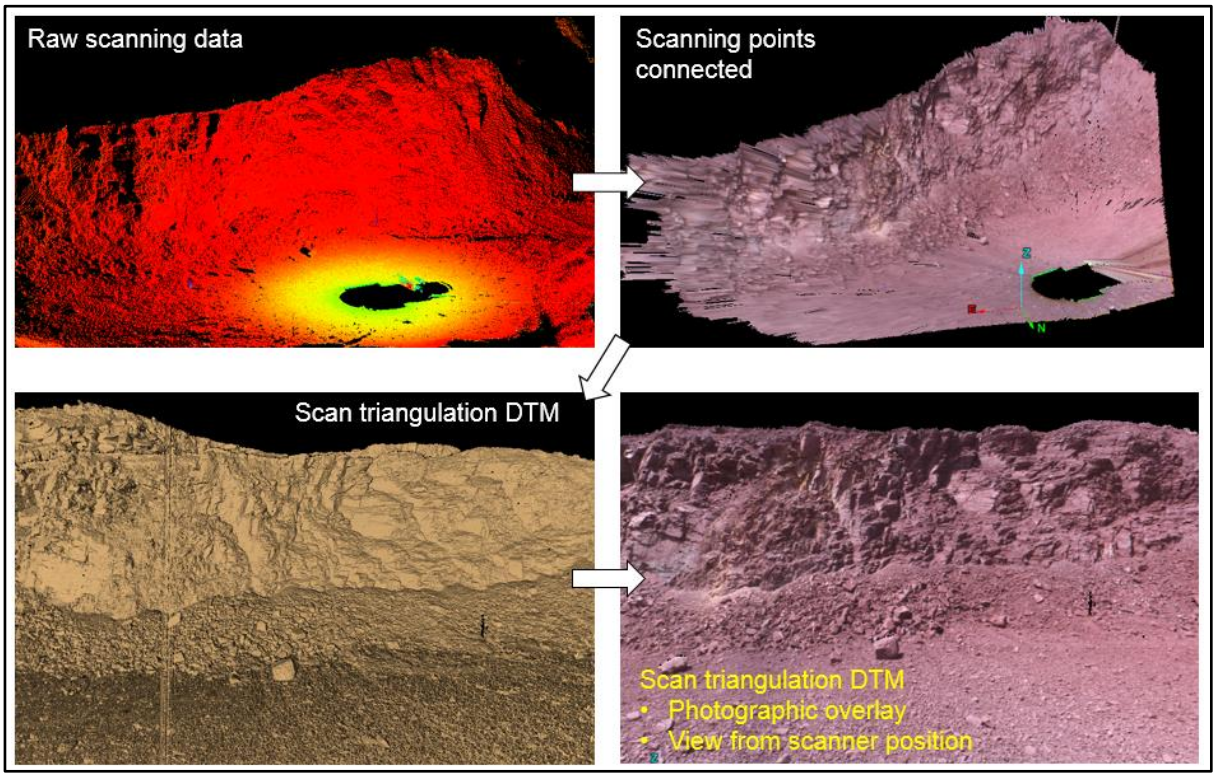

Figure 4.4: Illustration of the process to create a mapping face from a point cloud in the I-Site Studio software.

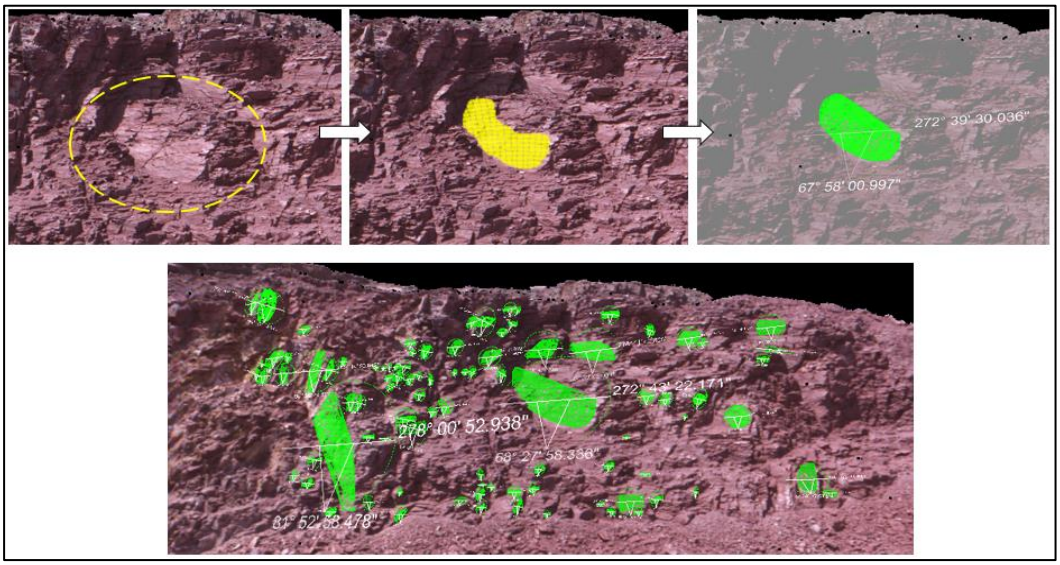

Figure 4.5: Illustration of the selection of discontinuity planes in the I-Site Studio software.

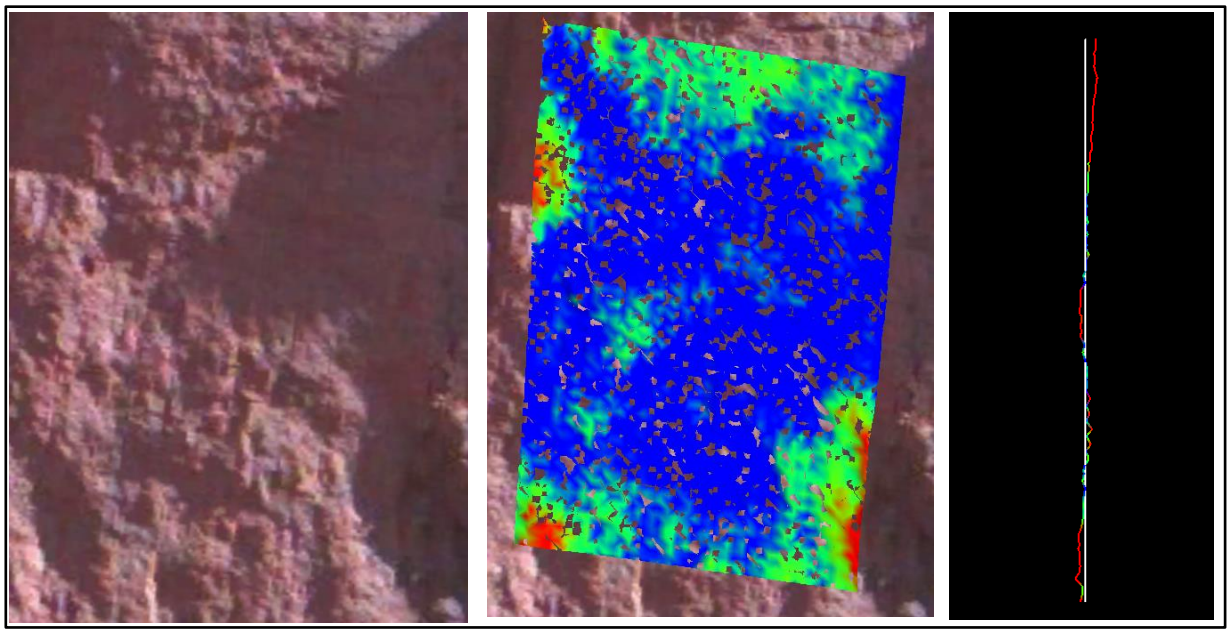

Figure 4.6: Illustration of a joint surface mapped by amplitude of asperities for roughness determination.

4.2.4. Setup and Features of the I-Site Studio Software

The I-Site Studio setup is based on a project database with a pre-set filing system for the management of the various types of spatial data used in the software. Folders within the project folder tree are referred to as containers. The system works in the same way within the I-Site project database as the general Microsoft Windows filing system with the same general file management rules (Figure 4.7). The pre-defined containers for different data types are as follows.

- Scan – Laser scanner data
- Survey – Survey point data
- Surface – DTM data
- CAD – All CAD objects including lines, polygons, extrusions and planes
- Contours – Strings representing contour data and cross sections
- Legend – Legends relating to various built-in I-Site objects
- Geotechnical – Discontinuity objects, stereonets and rose plots
- Scrapbook – A general use folder for import of miscellaneous objects and general storage

The above mentioned folder names cannot be changed as they are automatically used as the initial storage point for the relevant object when created or imported into the software. When working in I-Site studio, sub-containers relevant to the specific task are generally

created and named accordingly. Objects are cut and pasted from their automated storage locations (for example a newly created DTM will automatically be stored in the 'Surface' container) into the relevant 'Scrapbook' container.

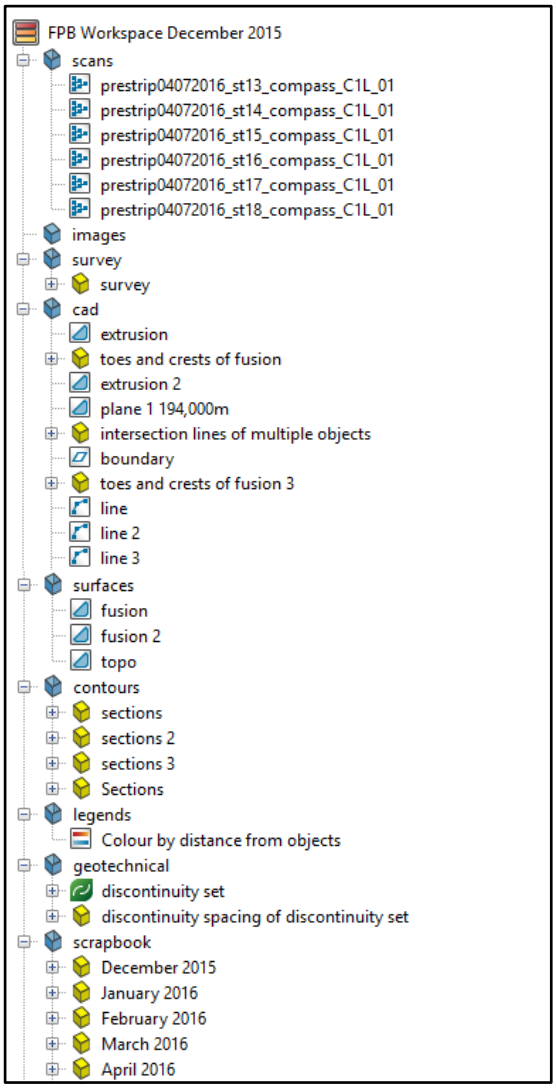

Figure 4.7: Example of the folder tree within an I-Site Studio project.

Scans imported into the software can be registered and georeferenced through various means such as back bearing alignment or matching of points from adjacent scan positions. At Sishen Mine this type of data processing is carried out by the mine's survey department.

The I-Site Studio software has a function that connects adjacent scan points to create an accurate 3D surface that can accommodate the scanner produced concurrent photographic overlay of the face, and can be used for face mapping. The 'Connect Points' function essentially connects points that are next to each other when viewed from the perspective of the scan origin (Figure 4.8). The software bases the connectivity on the acquisition order / topology of the scan.

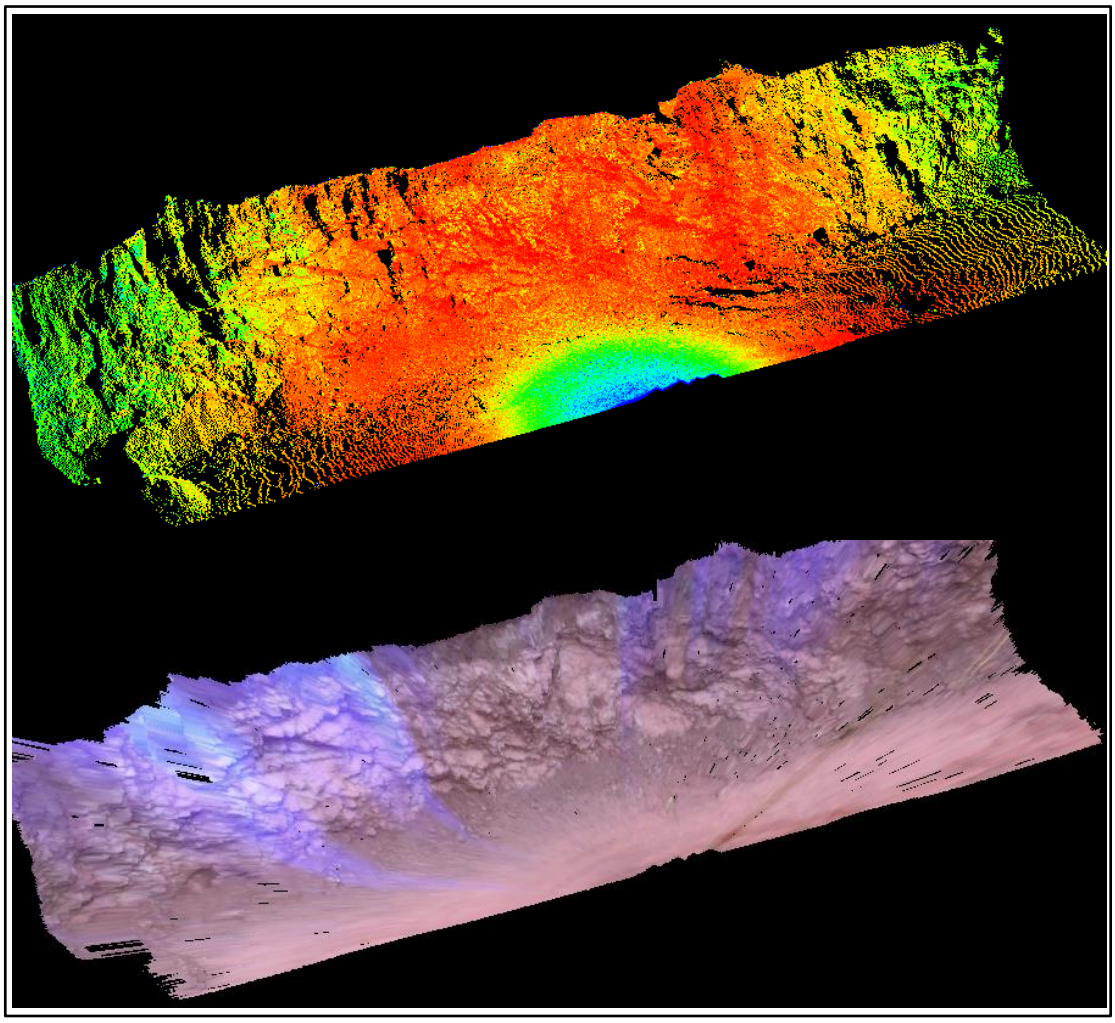

Figure 4.8: A scan showing unconnected scan points (above) and connected points with a photographic overlay (below).

4.2.5. Face Mapping Protocol

Based on the mine's face mapping data requirements, accepted face mapping methodology and the capabilities of the Maptek system the following face mapping protocol was developed for data capture. The following procedure refers to the face mapping procedure itself, and data processing and analysis will be covered in Sections 4.2.6 and 4.2.7.

Step 1 – Scanning

Scans are either requested specifically for mapping by Sishen's Geotechnical Engineering Section or by the mining team for routine final pit boundary design compliance. Once a request is received the mine's Survey Department will carry out the scans using a vehicle mounted set-up, as illustrated in Figure 4.3. The Maptek 8810 Scanner has 4 resolution

settings, and a rough guide to the distance between points on a face 50m away from the scanner is given in Table 4.1.

Table 4.1: Approximate point spacing on a surface 50m from the Maptek 8810 Scanner at different scan resolution settings.

Resolution Setting	Distance between points (mm).
C1	200
C2	100
C4	50
C8	25

There is a trade-off between resolution and file size with the C4 and C8 resolution setting producing scan files that are relatively large, resulting in reduced graphics performance on slower PC's. Based on trial and error during the testing phase of this project it was established that scans of resolutions C1 and C2 are adequate for faces within a range of 100m while C2 and C4 scans work adequately for faces between 100m and 200m from the scanner. Whether the scan resolution is adequate is, however, dependant more on whether there are enough points to define the discontinuity surfaces on the face in question than on the resolution setting (Figures 4.9 and 4.10). Although a minimum of 3 points is required to define the orientation of a plane, this is not ideal in terms of accuracy and should be avoided during face mapping.

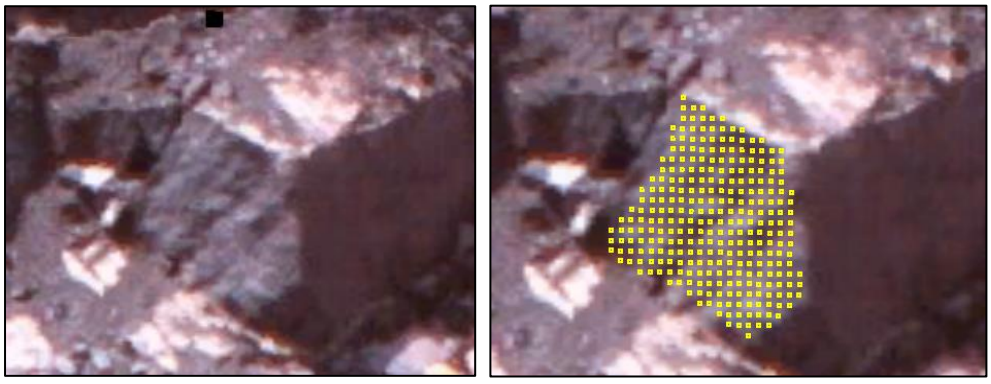

Figure 4.9: High resolution with many points defining the mapping plane.



Figure 4.10: Low resolution with few points defining the mapping plane.

Step 2 – Scan Review and Mapping Face Selection

As standard procedure, Sishen's survey department scan final pit boundaries when exposed and send the data to the Geotechnical Engineering Section. These scans are reviewed and checked for faces that can be mapped. Highwall faces that have been exposed by the survey scan must be mapped if possible.

When evaluating the scan, it is viewed while 'connected' with the concurrent scanner photograph overlain over the scan surface. Highwall faces are evaluated viewing the 'connected' scan image from the scan origin. Faces that are undisturbed, without considerable blast damage, and where structural features are clearly visible may be selected for mapping. Examples of faces that are considered adequate and inadequate for mapping are given in Figure 4.11.

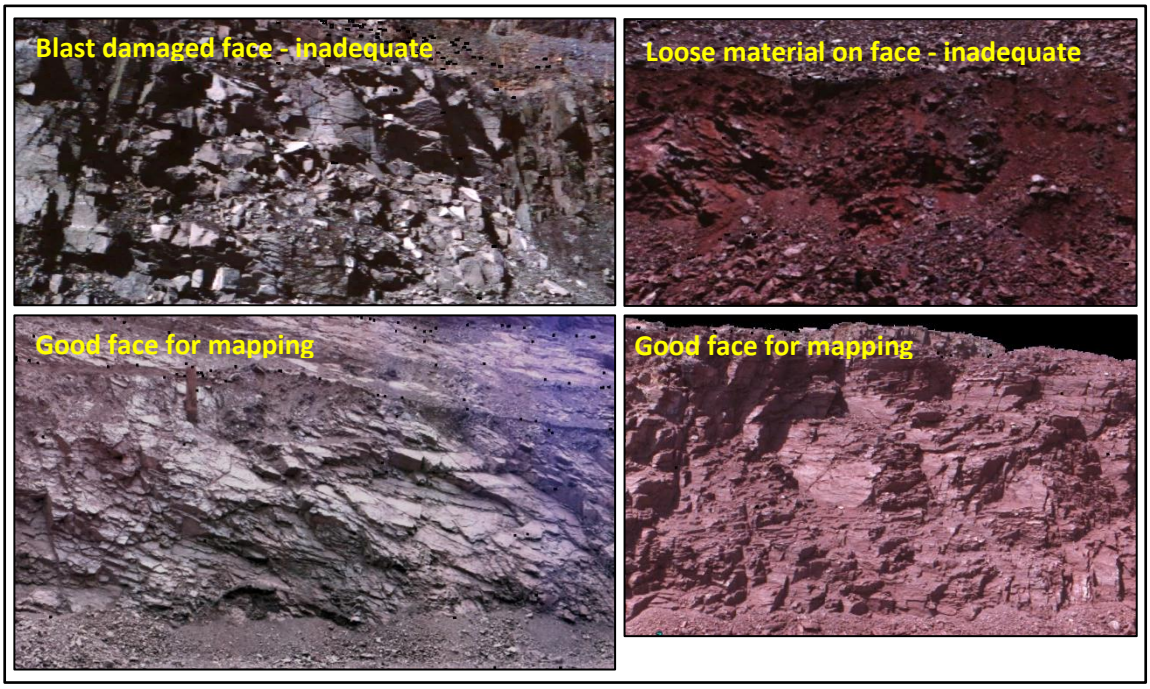

Figure 4.11: Examples of good and poor face mapping faces.

The laser scanner generally captures a wide area and there is often adequate scanning data to map legacy slopes surrounding the primary mapping face, as illustrated in Figure 4.12.

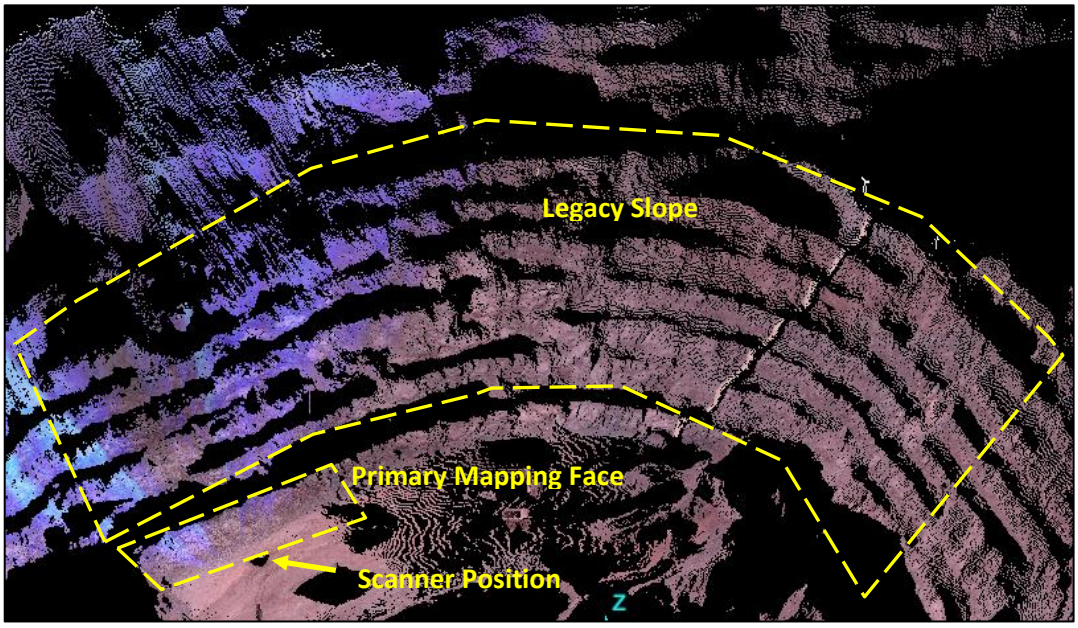

Figure 4.12: Data captured from a single scan allowing for mapping of both the exposed final pit boundary and legacy slopes up to 400m away from the scanner location.

In order to minimise truncation and size bias the Sishen mapping protocol does not include the delineation of a specific mapping window, but rather requires that mapping be restricted to a face of a particular orientation. If a scan has captured data from a curved pitwall or on two sides of a separate pit, the mapping face must be divided into separate approximately linear mapping surfaces (Figure 4.13).

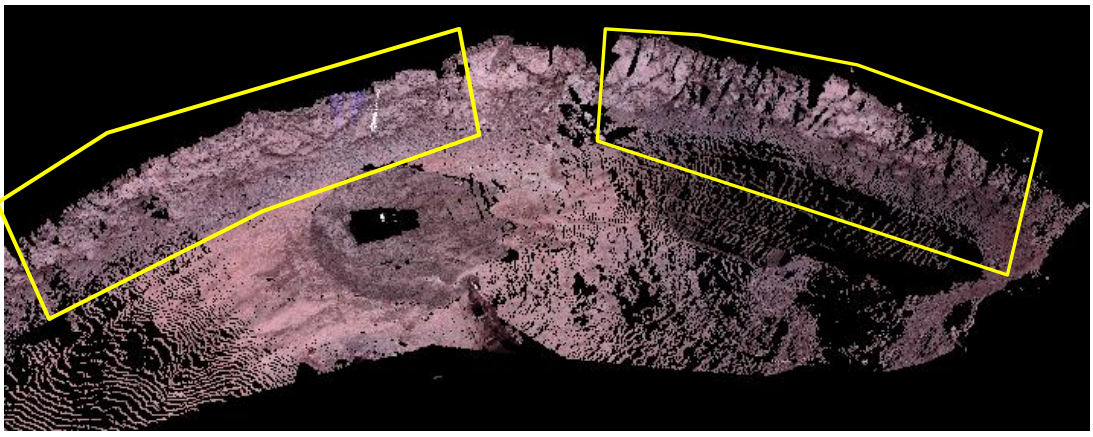

Figure 4.13: Examples of a curved highwall divided into two separate mapping faces.

Step 3 – Mapping Orientation Data

The first step in the face mapping process is to identify and map all visible discontinuity surfaces in the exposed area of concern. The scan points are 'connected' for face mapping and the photographic overlay is applied. The scan is then viewed from the scan origin to give the most realistic view of the scan face (Figure 4.14).

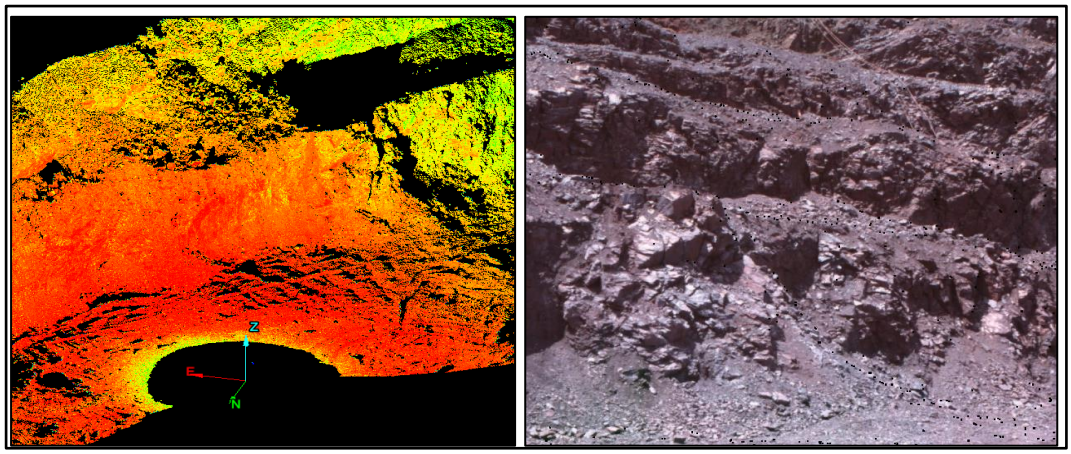

Figure 4.14: Raw scan data (left) versus mapping face viewed from the scan origin, ready for mapping of discontinuities (right).

When a discontinuity is selected, as illustrated in Figure 4.15, it is automatically saved and named sequentially as a discontinuity object within the I-Site Studio project database. Each discontinuity that is mapped must be classified as either 'Bedding', 'Joint', 'Fault' or 'Other'. It is easier to map the different discontinuity types separately (e.g.: bedding first followed by joints) and to take note of the sequential numbering of the discontinuities during mapping, as opposed to renaming each individual discontinuity object.

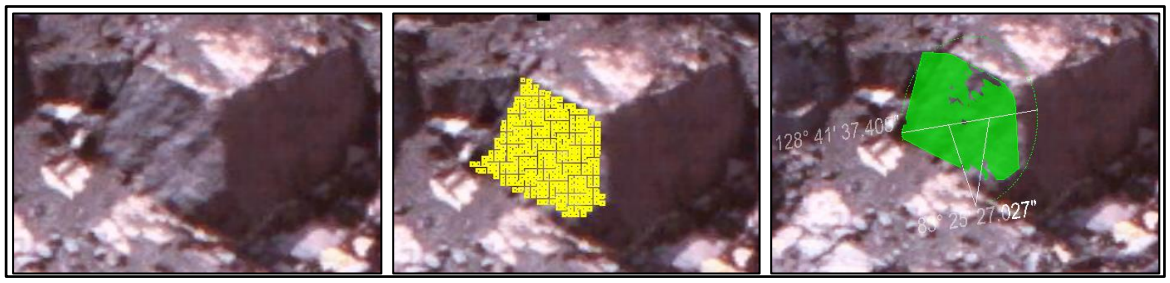

Figure 4.15: Selection of a joint plane for mapping.

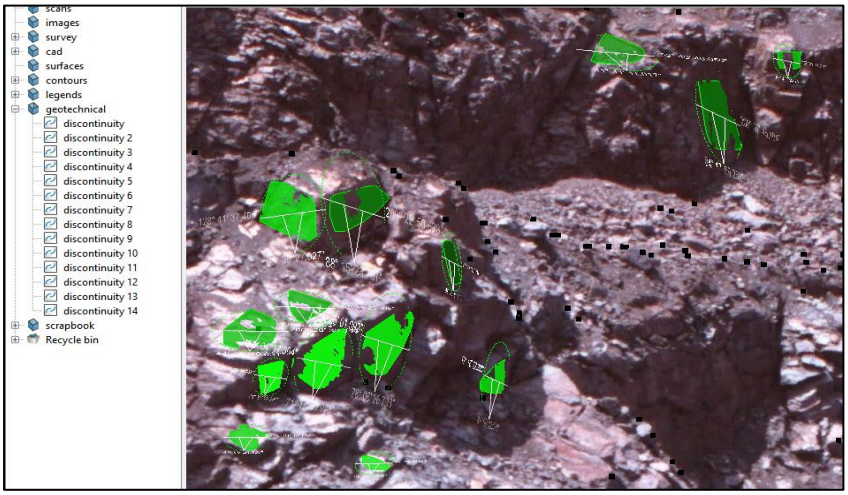

Figure 4.16: Discontinuity storage with the I-Site Studio Database.

I-Site Studio has built in features aimed at automating and assisting in discontinuity orientation mapping. The first feature that can help identify mapping planes is referred to as 'smart select'. This feature allows the user to extend a group of points manually selected on a plane to the entire area of that particular plane. While the 'smart select' tool may be used to assist in defining planes for mapping it is not specifically required in the protocol developed for mapping at Sishen. Experience during the development phase of the mapping procedure has shown that the simplest and most reliable means of selecting a reliable and representative grouping of points to delineate a particular plane is to outline the desired plane using the software's 'freehand selection' tool. A second feature built into the I-Site Studio software aimed at automating discontinuity mapping is the 'Extract Discontinuity' tool (Figure 4.17). If a plane is selected on the mapping face the tool will scan the face, looking for all planes falling within set orientation limits to the selected plane as well as a set plane size limit.

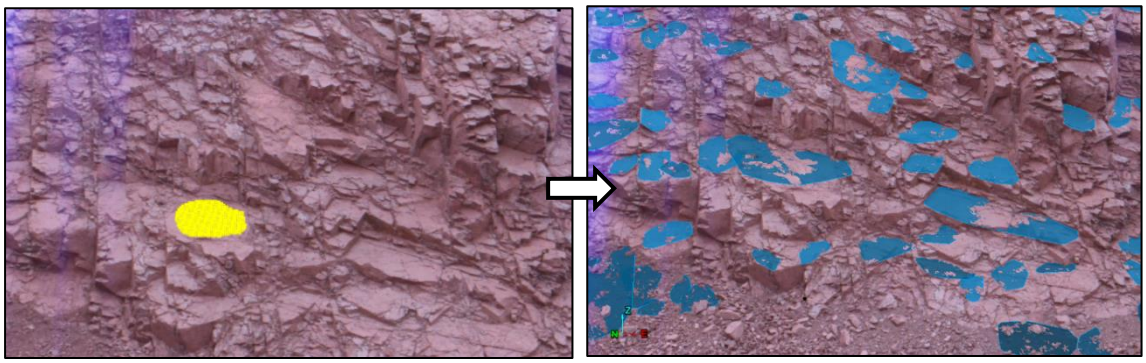

Figure 4.17: Automated discontinuity extraction using the I-Site 'Extract Discontinuities' tool.

While extracting discontinuities speeds up the process of face mapping, testing of the system during the development of the Sishen mapping protocol revealed two potential problems with automated plane selection.

Firstly, the software cannot recognize a true geological discontinuity on the mapping face in the manner in which a geologist or technician can by interpreting a photographic overlay. The software simply searches for planar surfaces in a particular orientation. These may include features such as scree slopes, excavator cut planes, partially obscured portions of the face and the edges of loose rock blocks. An illustration of erroneous automatically generated planes is given in Figure 4.18.



Figure 4.18: Erroneous automated discontinuity plane extractions.

Secondly, the software has the potential to magnify sampling bias by specifically looking for surfaces within a certain threshold of a particular plane. A person may interpret the planes that they are mapping on a face and apply judgement as to which planes are representative of the prevailing discontinuity sets. The computer cannot make such interpretations, and experience has shown that a search relating to an insignificant random joint may produce several results, creating the illusion of a prominent joint set.

Usage of the 'Extract Discontinuities' tool can be effective when used with a good appreciation of its limitations and extensive proofing and editing of the discontinuity extraction results.

In order to ensure data integrity, the Sishen face mapping protocol prescribes manual discontinuity plane selection with the use of the automated feature only for guidance in identifying potential mapping planes.

Step 4 – Mapping Spacing Data

Methods for determining fracture frequency from geological faces and exposures are outlined in Chapter 3 of this research report. Typically discontinuity spacing will be measured through counting of discontinuities along a scan line in direct measurement methods such as face mapping or window mapping. Although this method is practical when dealing with the constraints of working at the mapping face it does introduce significant sampling biases. The CAD and measurement features available in the I-Site Studio software easily allow for a digital replication of a mapping scanline. However, given that accurate measurements can be made directly on the 3D face mapping surface, a direct joint spacing measurement method was considered more appropriate.

I-Site Studio Version 6.0 and newer have a built in joint spacing measurement function that uses extracted discontinuities to determine joint spacing. Joint spacing measurements are taken by determining the perpendicular distance between extracted planes. The obvious drawback of this is that in most cases all the joints within a particular set are not exposed as open planes in a mapping face. If discontinuities fall between exposed planes the measured spacing will be incorrect, as illustrated in Figure 4.19.

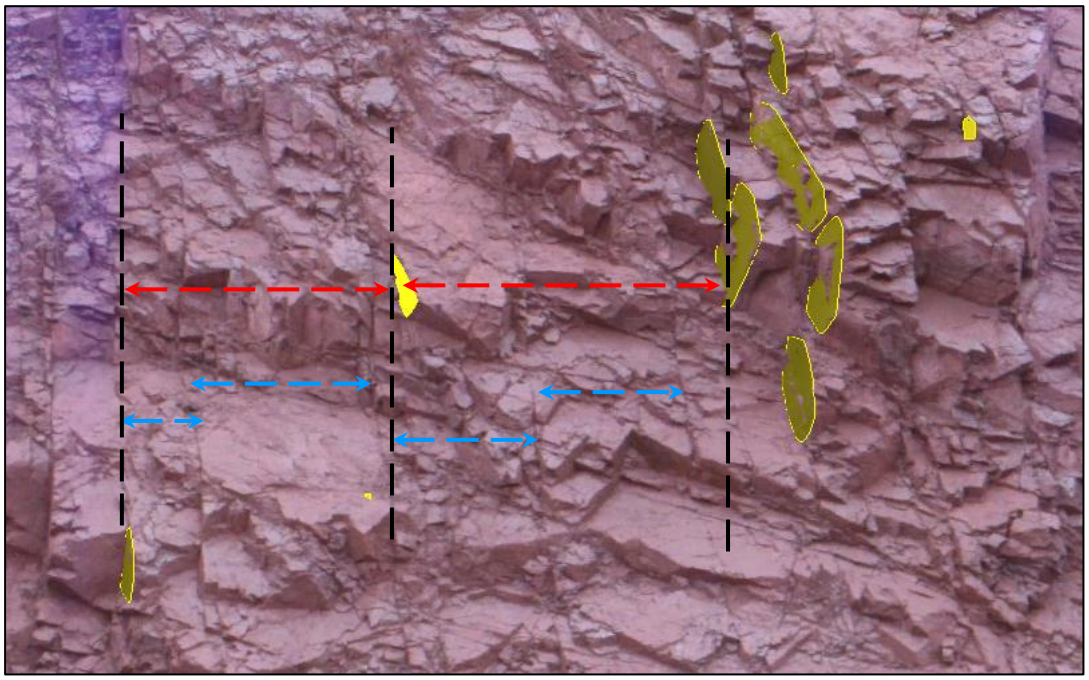

Figure 4.19: Joint plane extraction with automated joint spacing measurements indicated in red and true joint spacing including 'hidden' planes indicated in blue for a prominent sub vertical joint set.

Based on the available functionality of the software, the best approach for measuring fracture frequency for the Sishen face mapping protocol was considered to be a direct measurement method where the perpendicular distance between individual fractures is measured. I-Site studio has CAD functionality that allows for easy selection and measurement of the distance between points on the digital mapping surface. During the mapping process the mapper identifies adjacent discontinuities and creates a simple two point line between fractures, as close to perpendicular to the fracture planes as possible (Figure 4.20). No specific joint sets are defined in this process as this is done in the data processing stage of the protocol, as described in Section 4.2.6.

I-Site Studio stores and sequentially names the individual lines representing discontinuity spacing measurements under the CAD folder in the I-Site Studio project database. As for orientation data, the mapper must distinguish between bedding planes and joint planes when measuring spacing as this information will be required during processing in Microsoft Excel and storage in the Acquire Database.

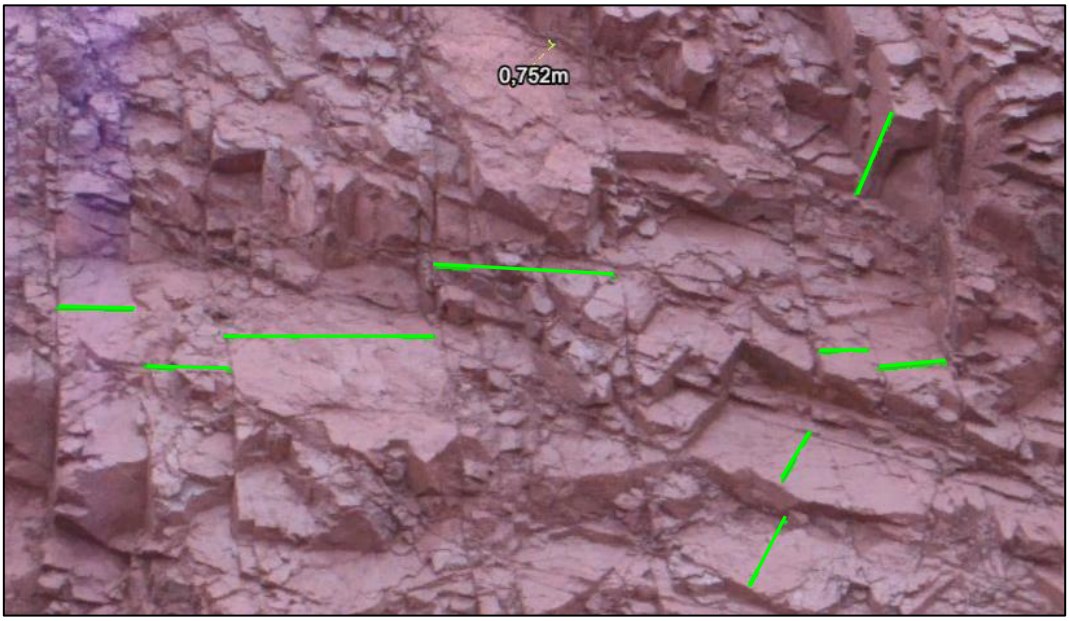

Figure 4.20: Illustration of joint spacing measurements on a mapping face.

Step 5 – Mapping Persistency Data

Discontinuity persistency plays an important role in rock mass behaviour and is a valuable input during analysis of how a rock mass will respond to an excavation. Boreholes cut a small section through the rock mass and do not provide data regarding the persistency of discontinuities. Face mapping provides a means of measuring discontinuity persistency, however the shortfalls and sampling bias outlined in Chapter 3 need to be taken into account when attempting to take persistency measurements. As for measurement of joint spacing, the Sishen face mapping protocol bases persistency measurements on a direct measurement along a line defined by two points. In the case of persistency measurements these points are defined by the termination points of the specific discontinuity (Figure 4.21).

Persistency measurements are only taken for discontinuities where both termination points are clearly visible in the highwall face. From experience during the development of the mapping protocol there are often very few or no well-defined discontinuity termination points, especially on single bench mapping faces (Figure 4.22).

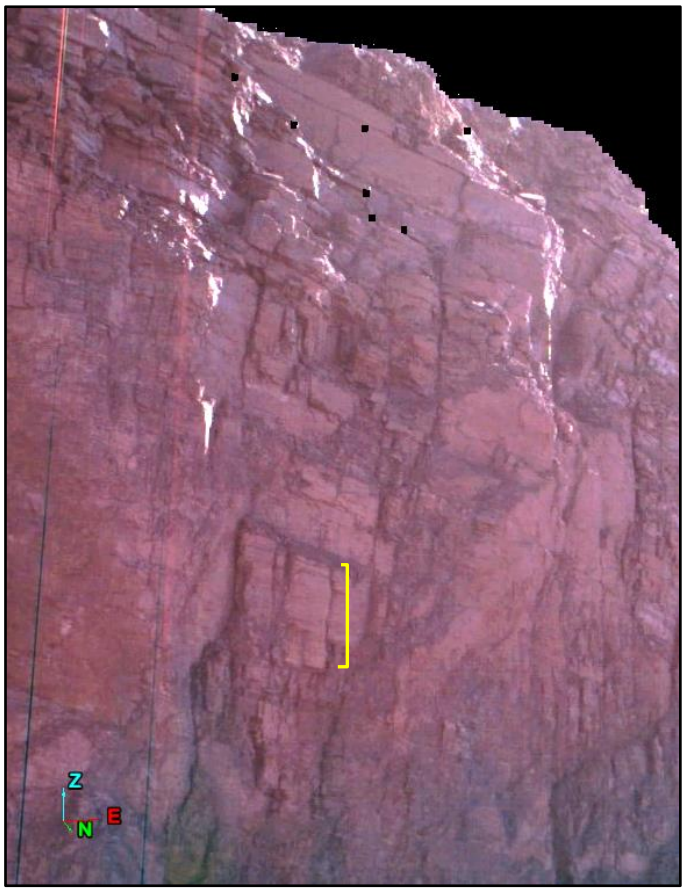

Figure 4.21: Interpretation of joint persistency's on a mapping face.



Figure 4.22: Persistent discontinuity terminating below the floor of the face – not suitable for measurement.

Data is stored and organised in the same manner as for joint spacing data in the I-Site Studio project database with all measurements stored as separate CAD line objects, divided based on the discontinuity type.

Step 6 – Measuring Discontinuity Roughness

There are several methods for both qualitatively and quantitatively measuring discontinuity roughness through either direct contact with the mapping face or remote sensing methods. One of the goals when creating the Sishen face mapping protocol was to develop a roughness profiling method that could be easily applied by personnel carrying out face mapping, and thus provide meaningful data for rock mass strength estimates, numerical modelling inputs and slope stability analysis.

I-Site Studio 6.0 was released with a built in function to evaluate and quantify the roughness of an exposed discontinuity surface (Figure 4.23). The function requires that the user selects an input area of points representing the exposed plane, which is then analysed by the software to determine the degree of waviness of the plane. The user sets input parameters allowing the software to divide the surface into cells for analysis, determine the analysis section orientation and set the minimum number of analysis points.

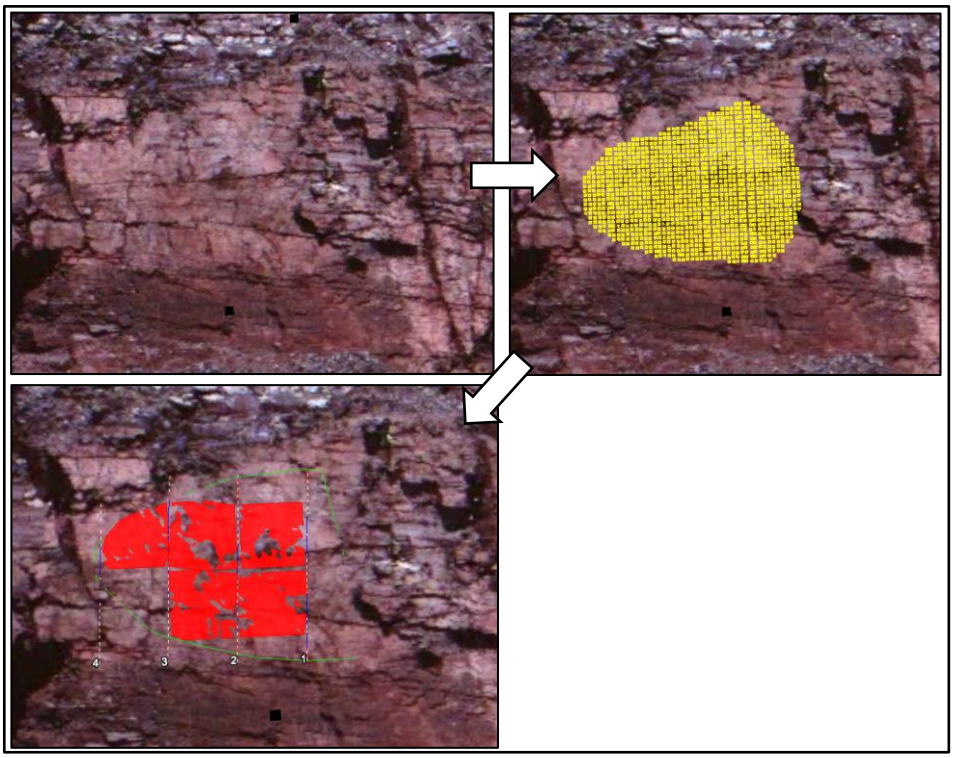

Figure 4.23: Roughness measurement process using the built in I-Site Studio Discontinuity Waviness tool.

A report is then generated giving a histogram showing the variation in dip across the analysis plane and giving section lines through the plane. The ultimate goal of evaluating roughness of the discontinuities on mapping faces is to arrive at a joint roughness rating value that can be applied to empirical joint strength and rock mass classification systems.

Two means of determining the Joint Roughness Coefficient (JRC) value for a discontinuity surface are discussed in Chapter 3. Firstly, according to the Barton and Choubey (1982) joint profiles the JRC can be estimated using a visual assessment. Secondly, with the use of the Barton (1982) Joint roughness chart the JRC can be estimated using the ratio of the amplitude of the asperities to the length of the joint profile. The above mentioned Discontinuity Waviness tool produces a report with joint profiles that can be compared with the Barton and Choubey (1982) standard profiles.

Although the Discontinuity Waviness tool can produce useful joint roughness information, using it is a relatively time consuming and complicated process, not ideally suited to a routine face mapping protocol. A more effective and objective means of incorporating joint roughness values was developed using the generic distance measurement functionality of the I-Site Studio software in conjunction with the Barton (1982) asperity amplitude chart. The following procedure was created to allow for joint profile data to be exported from I-Site Studio.

- Straight lines (CAD line objects) are plotted on the face in the positions of the desired trace measurements for a particular joint set. The starting and end points of the trace line are snapped to the face surface (Figure 4.24).

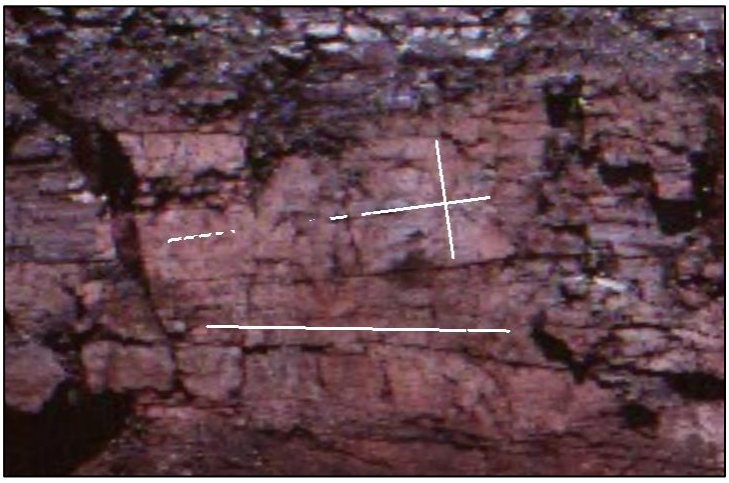

Figure 4.24: Joint roughness trace lines plotted between two points on the Face surface.

- Each line is divided into 10cm intervals using the 'Smooth Line' tool to provide measurement points.

- The 'Colour by distance' tool is then used to measure the most direct distance between each point on the straight trace line and the mapping face. The 'export to file' option is selected to export the trace data in CSV format for further analysis in Microsoft Excel. Different discontinuity types are exported as separate CSV files for a particular mapping face. As illustrated in Figure 4.25, this is effectively creating a digital version of the straight edge measurement method discussed in Section 3.1.3.1.

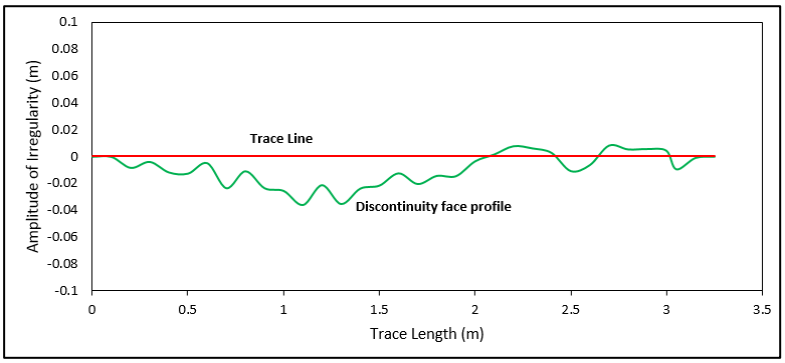

Figure 4.25: Face profile showing trace length versus amplitude of irregularities.

During development of the roughness measurement procedure, fundamental accuracy limitations with the laser scanning data became apparent. In order to trace a representative roughness profile over the surface of a mapping face, the spatial data representing the face needs to be highly accurate. According to Maptek the 8810 laser scanner is accurate to within 8mm at a scanner distance of 200m, under controlled conditions. Various environmental factors affect the accuracy of laser scanner data, and direct tests of data reflected from known flat surfaces (Figure 4.26) revealed an apparent irregularity, approximately consistent with the quoted accuracy of the equipment.

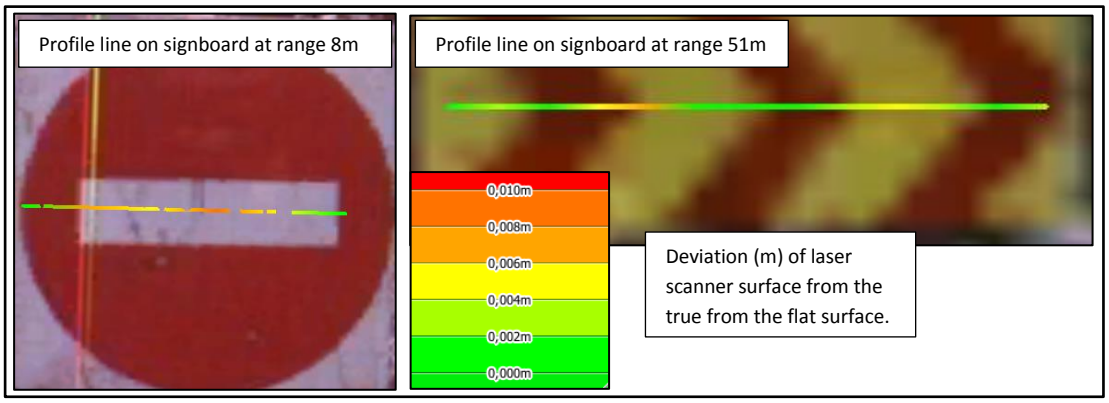

Figure 4.26: Face profile on known flat surfaces illustrating deviations in the surface created from laser scanner data from the true surface.

When considering the inherent inaccuracy of the system, roughness values at the lower end of the Barton (1982) chart for small scale discontinuities are considered unreliable. As illustrated in Figure 4.27, JRC values at a small scale for discontinuities of less than a metre in length can be attributed as much to the inherent inaccuracy of the equipment as the natural irregularity of the surface being analysed.

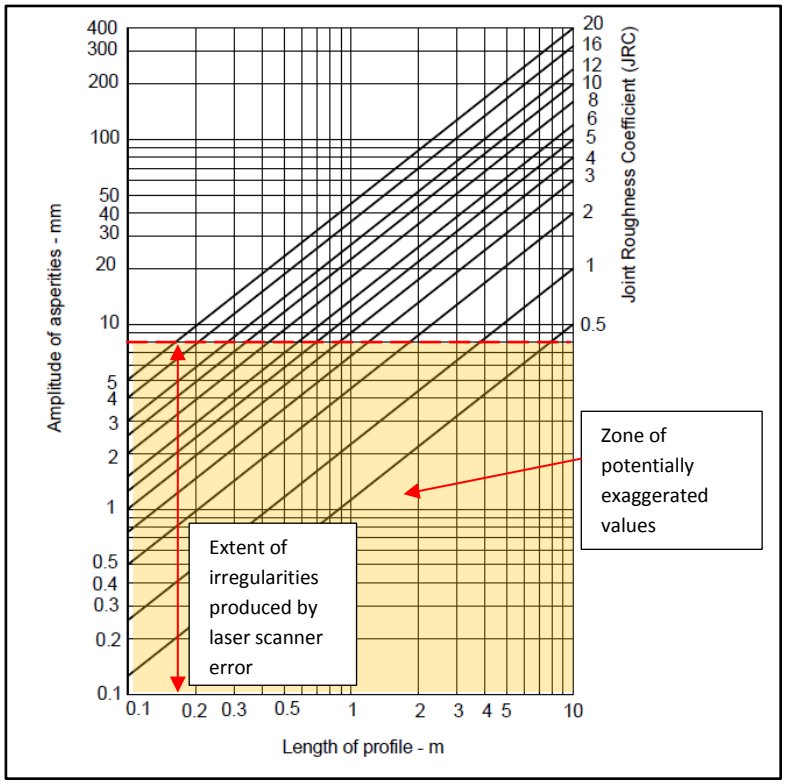

Figure 4.27: Illustration of the area of the Barton (1982) chart where roughness values are considered unreliable due to the relative scale of the scanner inaccuracy.

Due to the inaccuracies of the equipment, JRC values obtained for discontinuity traces of less than 2m in length are considered meaningless. For the mapping protocol only discontinuity traces of 2m and longer are considered for roughness analysis. An analysis macro in Microsoft Excel applies an 8mm reduction in the measured maximum amplitude of irregularity to try to give a more conservative estimate and best account of the effect of scanner inaccuracy.

Step 7 – Face Orientation Measurement

The orientation of the mapping face needs to be recorded and stored when an area is mapped. In order to do this all orientation, spacing and persistency measurements are re-imported into the mapping view in I-Site studio. A trace is then made around the extent of the mapping measurement to select all scan points within the mapped area. The query discontinuity tool is then applied to the selection. This saves the face as a discontinuity object with a dip, strike, length and area (Figure 4.28).

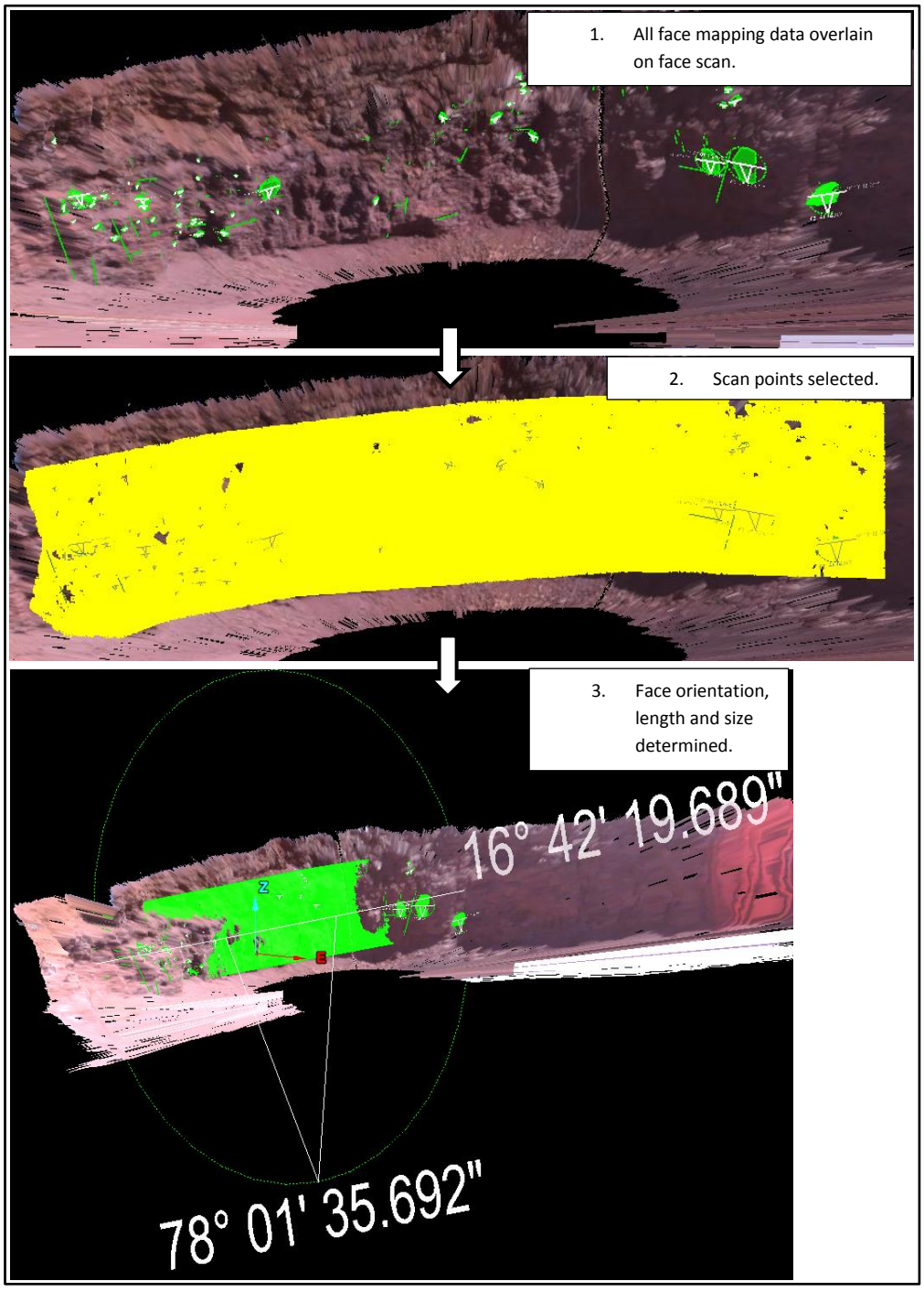

Figure 4.28: Face orientation, length and area determination in I-Site Studio.

Step 8 – Data Export from I-Site Studio

Once all discontinuities have been mapped and the face orientation determined, all data is exported into a network folder for further processing in Microsoft Excel. Network sub-folders corresponding with the I-Site Studio storage 'containers' are set up in preparation for export. Discontinuity objects are exported as separate files as opposed to a single CSV file listing the discontinuity measurements. They are by default exported as text files. Spacing and persistency measurements are exported as individual text files that contain the co-ordinate information for each of the measurements. The face orientation measurement is exported as an individual text file in the same manner as the discontinuity orientation measurements.

4.2.6. Data Processing in Microsoft Excel

Once a face has been mapped and all relevant data has been exported from I-Site Studio, the data needs to be incorporated into a geotechnical database, namely the Acquire Geological Database System in the case of Sishen Mine and Kumba Iron Ore. Furthermore, a kinematic stability assessment and rock mass classification on the individual face needs to be carried out. A standard Microsoft Excel template was set up to import data from I-Site Studio, to carry out the required analysis and classification and incorporate the data into the Acquire Database. Macro Instructions written in the Visual Basic for Applications (VBA) programming language were heavily relied on to Import, manipulate and analyse the mapping data from I-Site Studio in Excel.

4.2.6.1. Data Import From I-Site Studio

As outlined in Section 4.2.5, mapping data is exported from I-Site studio as individual text files. These text files are incorporated into Excel through a series of import macros that read the text data to compile a data list on an import sheet in Excel. The mapping face as well as discontinuity orientation, spacing and persistency measurements, are all imported separately. For orientation, spacing and persistency measurements the user has the option to select individual text files representing bedding planes, joints, faults or 'other' referring to other types of feature that may have been mapped. The macros make use of the VBA Line Input object to read the information in the individual text files for input into Excel. In the case of the spacing and persistency measurements the CAD lines drawn in I-Site are represented by a start and end set of X, Y and Z co-ordinates. These are not imported directly, but calculations within the import macro produce a single set of

co-ordinates representing the centre point of the line. Further calculations determine the length and the plunge of the line. For spacing measurements, the implied dip of the discontinuity is considered to be at 90 degrees to the plunge of the measurement line, as measurements are generally taken approximately perpendicular to the discontinuity.

In addition to the imported data, the user is required to enter the rock type, mapping location and estimated friction angle of the discontinuity surfaces. Rock types are restricted to the standard geological codes used on Sishen Mine.

Figures 4.29 show the macro linked Excel data import template, Figure 4.30 shows text data from I-Site studio exports that has been imported into Excel.

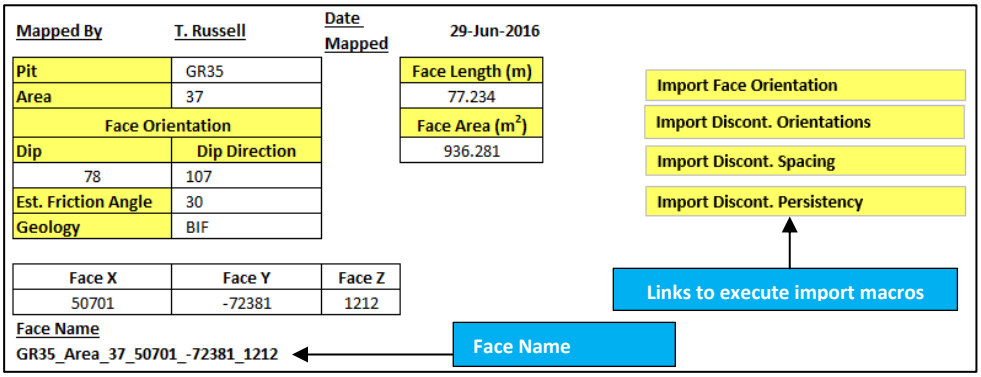

Figure 4.29: Example of Excel data import template with face mapping data imported.

Orientation

File Name	Discont. Type	X	Y	Z	Dip	Direction	Strike	Length	Area
discontinuity 1.txt	Bedding	50697.22	-72397.6	1213.129	33.546	99.582	9.582	2.025	0.968
discontinuity 2.txt	Bedding	50697.51	-72398	1212.631	41.736	98.594	8.594	0.391	0.057
discontinuity 3.txt	Bedding	50698.04	-72391.9	1211.812	30.992	108.199	18.199	1.228	0.337
discontinuity 4.txt	Bedding	50698.56	-72392.1	1211.412	33.072	103.348	13.348	0.86	0.126

Spacing

File Name	Discont.Type	X1	Y1	Z1	X2	Y2	Z2	Length (m)	Dip
line 1.txt	Bedding	50697.95	-72396.6	1212.182	50698.07	-72396.8	1212.671	0.54	25
line 2.txt	Bedding	50697.1	-72398.9	1212.126	50697.31	-72399	1212.651	0.58	25
line 3.txt	Bedding	50697.09	-72399	1212.721	50696.95	-72399.4	1213.223	0.69	43
line 4.txt	Bedding	50698.87	-72396.7	1210.666	50698.96	-72396.7	1210.9	0.26	24

Persistency

File Name	Discont.Type	X1	Y1	Z1	X2	Y2	Z2	Length (m)	Dip
line 1.txt	Bedding	50693.75	-72406.5	1214.034	50697.73	-72390.4	1213.238	16.62	3
line 2.txt	Bedding	50700.69	-72380	1210.5	50699.4	-72386.6	1211.432	6.77	8
line 3.txt	Bedding	50704.71	-72367.3	1206.99	50704.71	-72365.4	1207.093	1.94	3
line 4.txt	Bedding	50704.92	-72358.7	1213.587	50703.45	-72364	1214.146	5.53	6

Figure 4.30: Example of orientation, spacing and frequency data imported into Microsoft Excel.

4.2.6.2. Discontinuity Roughness Calculation and Import

As discussed in Section 4.2.5, discontinuity roughness values are exported from I-site Studio as a set of straight line traces. Each trace is divided into 0.1m intervals with each interval used as a measurement point to determine the distance between the straight trace line and the irregular discontinuity surface, effectively representing the amplitude of irregularity at that point.

The exported roughness text file from I-Site Studio containing the discontinuity roughness data for a particular set of discontinuities from a mapping face is imported using a VBA macro in Excel. The following data is extracted from the text file for each individual discontinuity trace contained within the file.

- Trace Centre Point Co-ordinates (X, Y, Z)
- Trace Type – 'Bedding' / 'Joint' / 'Fault' / 'Other'
- Trace line plunge
- Trace Length (m)
- Maximum Amplitude of Irregularity (mm)
- Barton's JRC Number

The import Macro calculates the Barton (1982) JRC Number using the Chart from Barton (1982) in Figure 3.4. Chart values were tabulated and incorporated into the import macro to allow JRC values to be read off the chart numerically, as illustrated in Figure 4.31 and 4.32.

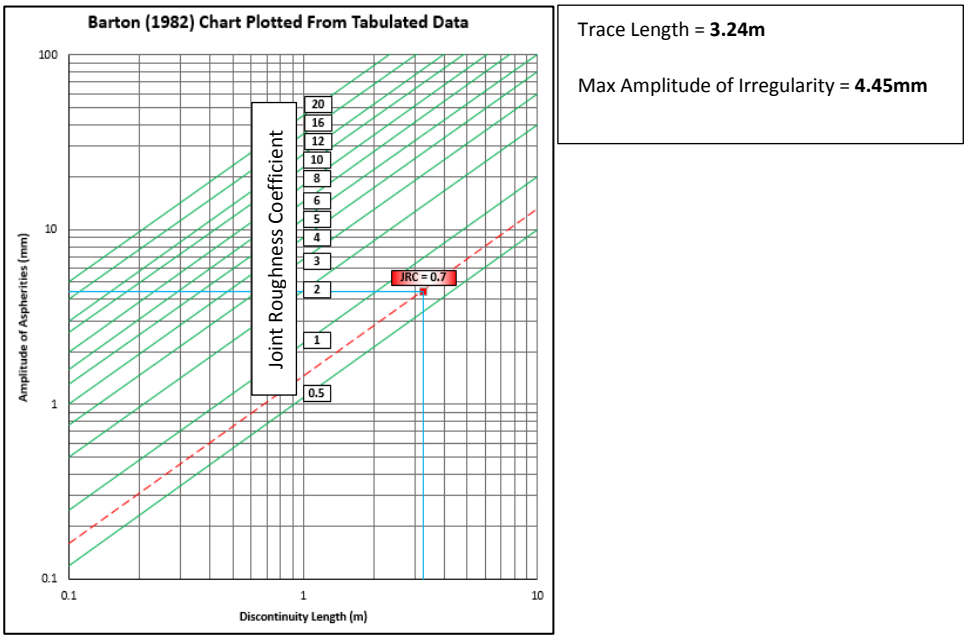

Figure 4.31: Illustration of data plotted on a digital version of the Barton (1982) JRC Chart.

Type	Length (m)	Amplitue (mm)	JRC
Joint	2.04	47.8	10.8
Bedding	2.06	45.8	10.2
Bedding	2.30	77.0	15.9
Bedding	2.74	58.7	9.9
Bedding	2.35	62.6	12.5
Bedding	2.70	57.1	9.8

	Total	Bedding	Joint
Count	6	5	1
Min	9.8	9.8	10.8
Max	15.9	15.9	10.8
Average	11.5	11.7	10.8
St.Dev	2.4	2.6	-
CV 9%)	20%	22%	-

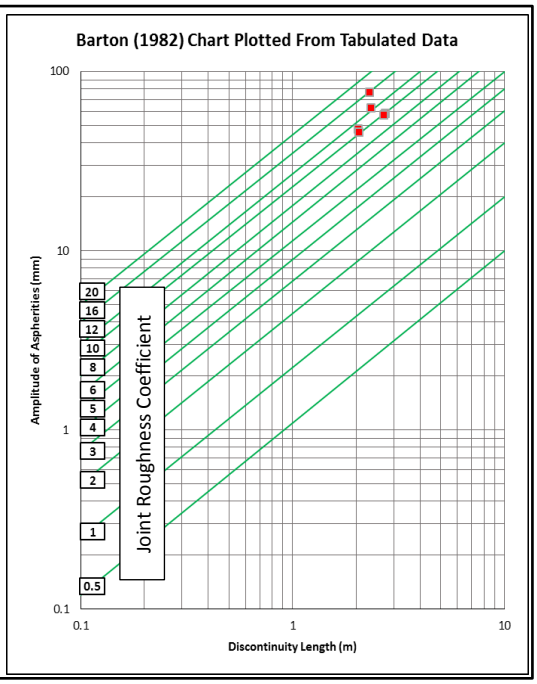

Figure 4.32: Joint roughness assessment from roughness measurement taken from a single mapping face.

A variety of statistical methods are available for the analysis of joint roughness, as outlined in Chapter 3. This kind of analysis is outside the scope of this research report but may be relevant to more in-depth joint roughness studies on the mine. For this reason, in addition to exporting the JRC and relevant joint parameters to Acquire for each mapped joint profile, the raw profile co-ordinate data is stored during the mapping process for future access and analysis.

4.2.6.3. Mapping Data Analysis

I-Site Studio has built in functionality to plot orientation data on a stereonet and carry out kinematic analysis. Kinematic analysis can also be carried out using specialised software packages such as Dips, produced by the software vendor Rocscience (2012). Specialised software packages generally have a wide variety of functions, with several settings allowing for the type of in-depth analysis that is not always necessary during analysis of a single mapping face. For this project, the approach taken was to build the required stereonet functionality directly into Excel to carry out the necessary routine kinematic analysis. The reasoning behind this was to create a streamlined and repeatable reporting process that incorporates both kinematic and rock mass data.

4.2.6.3.a. Stereographic Projection

Plotting a stereonet in an Excel chart or any other flat surface requires projecting points from the lower (or upper) hemisphere of a sphere onto a Cartesian plane. Stereonets can either be projected as an equal angle (Wulff) projection, where angular relationships between points are preserved at the expense of an areal distortion, or an equal area (Schmidt) projection, where area across the extent of the stereonet is better preserved. For plotting polar densities and analysing trends in face mapping data, the equal area stereonet is more appropriate (Hoek and Bray, 1981; Kliche, 1999).

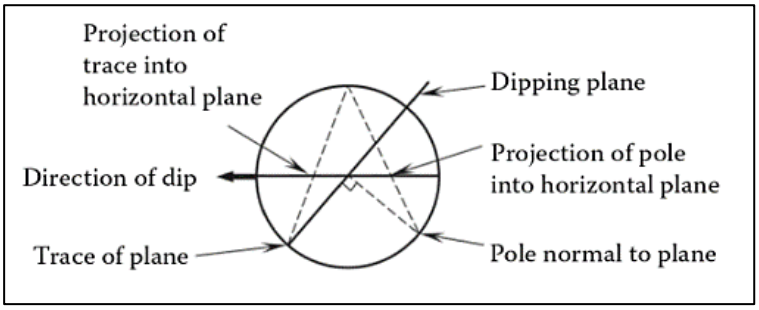

Figure 4.33: Illustration of the projection of a plane on the lower hemisphere of a stereonet onto a flat surface (From Kliche, 1999).

For the projection illustrated in the above the following formula is used to determine the distance from the origin on a Cartesian plane relating to a specific dip on the stereonet.

$$Projected\ Point = 2 \times Radius\left(0.5 \times dip \Big/ \sqrt{2}\right)$$

A full review of the derivation of this calculation can be found in Marshak and Mitra (1988), Chapter 8.

Once the dip of the point has been established, it can be rotated on the stereonet through the use of trigonometric functions to determine the Cartesian co-ordinates of the point. An example of a point plotted on a stereonet in an Excel chart is given in Figure 4.34. For convenience the stereonet has been set up with the origin representing the middle of the net and the radius of the circle set to 90 units in Cartesian space. The example point illustrated in red in Figure 4.34 is dipping at 30 degrees. When the above equation is applied, a distance from the origin of 32.9 units on the projection plane is calculated. This is the projected point dip on the flat stereonet surface. When rotating the point to represent a particular dip direction, the distance of 32.9 units on the Cartesian plane can be considered as the hypotenuse of a right angled triangle. By

multiplying this distance by the cosine and sine of the rotation angle the rotated X and Y co-ordinates relating to the dip and dip direction of the point can be derived. For this example, the point is rotated 20 degrees anticlockwise from the original point on the X-axis illustrated in Figure 4.34. In this case the rotated co-ordinates are X = 30.9; Y = 11.26, which corresponds to a dip of 30° and a dip direction of 070°.

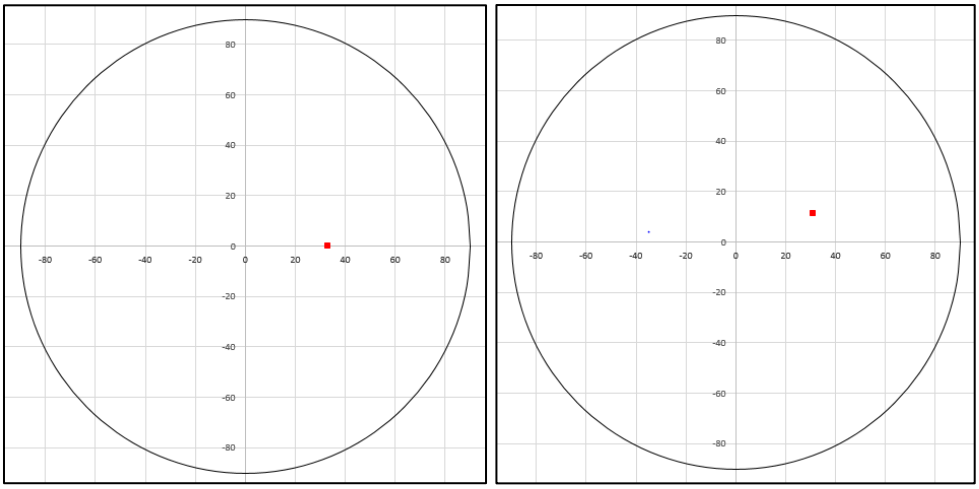

Figure 4.34: Illustration of plotting and rotating a stereonet point on an Excel chart.

A great circle representing a plane on a stereonet can be defined as a line joining all points where the plane intersects the stereonet sphere. When projecting a great circle, each incremental point where the plane intersects the stereonet sphere can be considered as having an apparent dip relative to the plane itself, as illustrated in Figure 4.35.

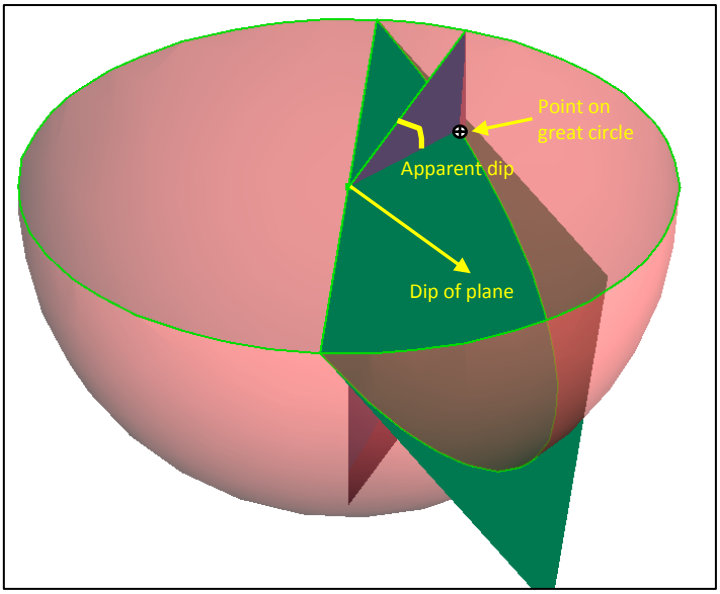

Figure 4.35: Illustration of the apparent dip of a point on the great circle of a plane.

The apparent dip of each point defining the great circle can be calculated using the difference between the true dip direction of the plane and the dip direction defining the point. The apparent dip is calculated using the following equation (Lisle, 2004)

$$\tan(apparent\ dip) = \tan(true\ dip) \times (obliquity\ angle)$$

The apparent dip of the great circle point and the obliquity angle from the dip direction of the plane in question are used to determine the overall position of the point on the stereonet. Once this has been established, the co-ordinates of the point on the flat Cartesian plane can be established as per the method described previously in this section for a single point. By repeating the calculation for a series of points with dip directions varying between -90 degrees and 90 degrees relative to the plane, the outline of the plane's great circle can be traced and plotted on an Excel chart.

4.2.6.3.b. Stereonet Kinematic Analysis Functionality

In order to evaluate mapping data on a built-in Excel stereonet, some additional features needed to be added, namely:

- The daylight envelope relating to the slope face plane.
- The lateral limits defining the range of orientations where plane failure is kinematically feasible.
- A contouring function to contour the density of polar data on the stereonet.
- A function set up to calculate the plunge and trend of the intersection line between two planes.
- Functionality that allows the user to select a point on the stereonet representing a major plane based on the mouse pointer location.

The above mentioned calculations and functions were added to the Excel analysis stereonet, either through direct calculations embedded in the spreadsheet, or through a procedure written into VBA macros. Stereonets plotted as Excel chart objects are illustrated in Figures 4.36 and 4.37.

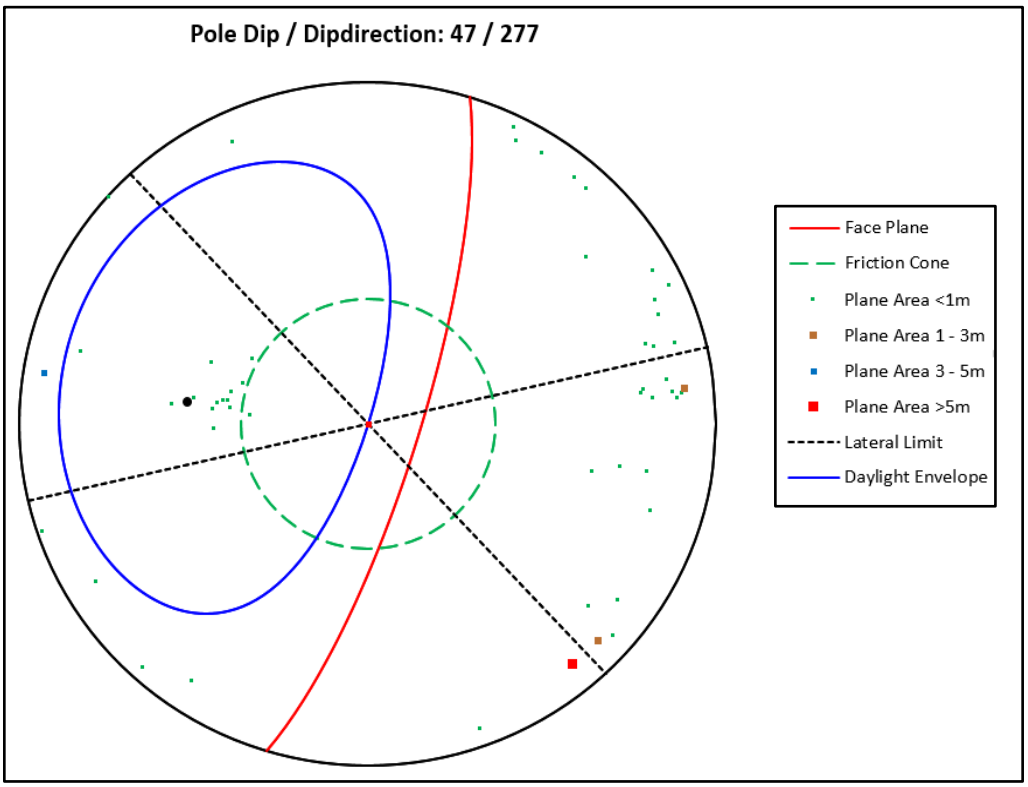

Figure 4.36: Illustration of a stereonet plotted on a Microsoft Excel chart.

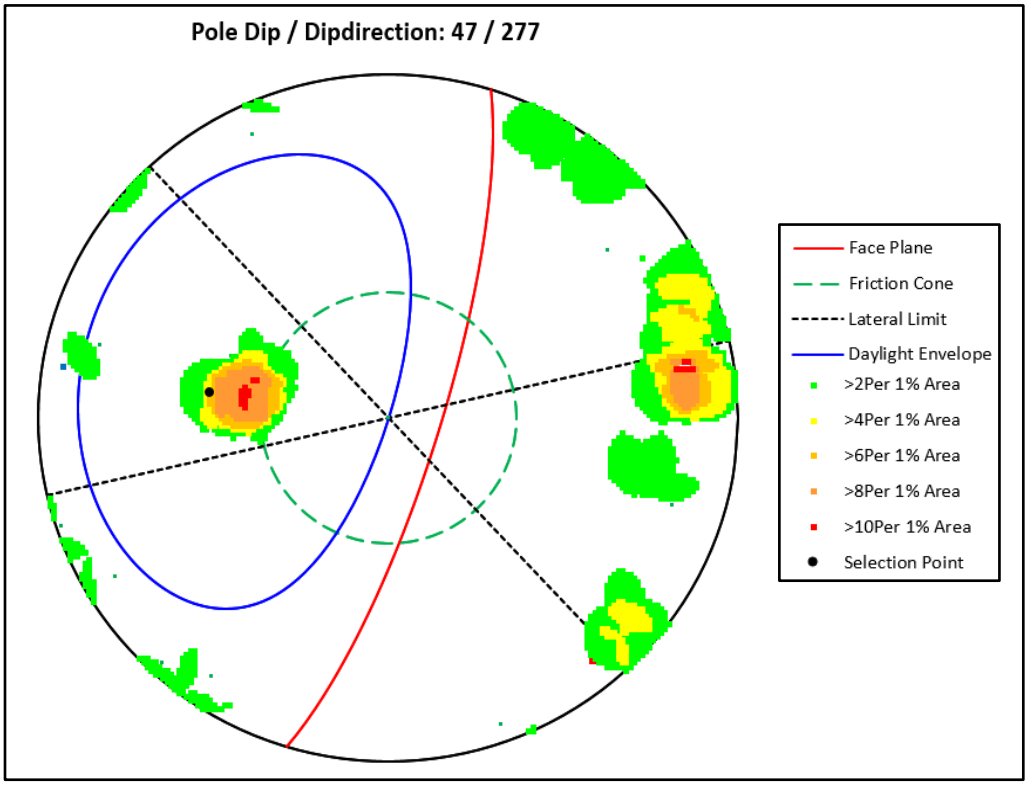

Figure 4.37: Illustration of a stereonet plotted on a Microsoft Excel chart with contoured data.

4.2.6.3.c. Plane Failure Analysis

The Excel analysis sheet incorporated into the Sishen face mapping protocol has been set up to carry out basic plane failure analysis. The methodology of kinematic plane failure analysis is outlined in Chapter 3 of this dissertation. For reporting, the analysis sheet was set up to calculate and plot the following for a mapping face.

- Calculate the percentage of kinematically feasible planes within a pre-set lateral limit of 30% from the face dip direction.
- Plot all poles on a stereonet with poles colour coded according to the size of the mapped plane.
- Plot lateral limits, the polar friction cone and daylight envelope on a stereonet.
- Provide a density contour plot of mapped poles.
- Allow the user to select major planes and calculate if the selected planes are feasible for plane failure based on the input face orientation and friction angle.

An example of plane failure analysis reporting is given in Figure 4.38.

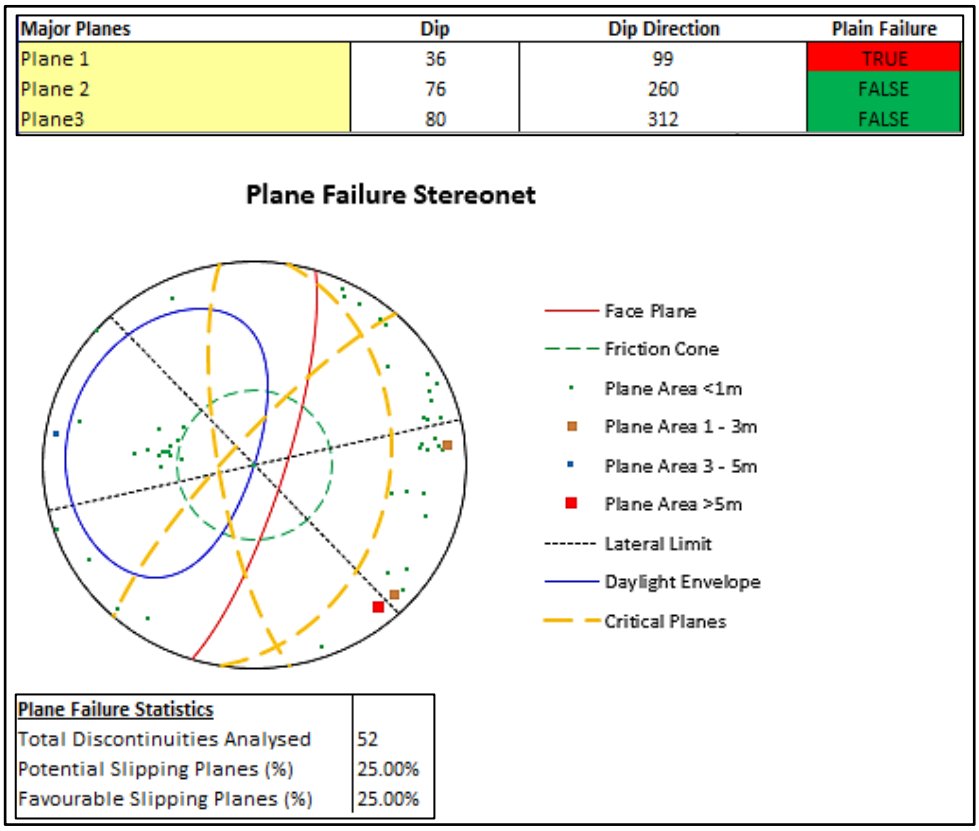

Figure 4.38: Major planes plotted on the analysis stereonet (dashed orange) for plane failure analysis.

4.2.6.3.d. Wedge Failure Analysis

Wedge failure analysis was incorporated into the mapping analysis report template in a similar manner to the analysis for plane failures. A function was derived and written into a visual basic procedure to determine mathematically the plunge and plunge direction of the intersection line of two planes with given dips and dip directions.

The analysis report was set up to cross reference all mapped planes with each other; in each case the intersection trend line orientation is calculated and the kinematic feasibility of a wedge failure developing for the given friction angle and face orientation is determined. The percentage of kinematically feasible wedge intersections is quoted in the report as a percentage of the total wedge intersection analysed. This calculation is similar to the wedge failure analysis function in the Dips kinematic analysis program developed by Rocscience (2012). Overall and feasible wedge intersections are plotted on a stereonet embedded as a chart within the Excel analysis sheet (Figure 4.39).

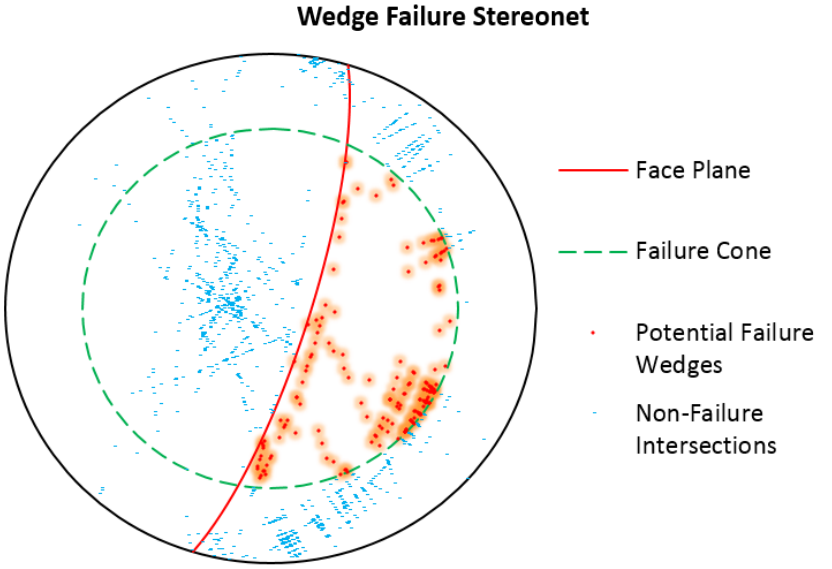

Wedge Failure Analysis	Number	Percent
Total Intersection	1326	
Shallow Plunging (0 - 30 deg.)	549	41.40%
Medium Plunging (30 - 60 deg.)	315	23.76%
Steep Plunging (60 - 90 deg.)	462	34.84%
Kinematically Feasable Wedges	171	12.90%
Large (>2m^2 area) Kinematically Feasable Wedges	14	1.06%

Figure 4.39: Mapping analysis report sheet wedge failure analysis stereonet and statistics.

As mentioned in the preceding section, as part of the analysis process the user can select major planes based on the distribution of the poles of the mapped planes of the stereonet. The intersections of the major planes selected by the user are automatically evaluated for wedge failure feasibility (Figure 4.40).

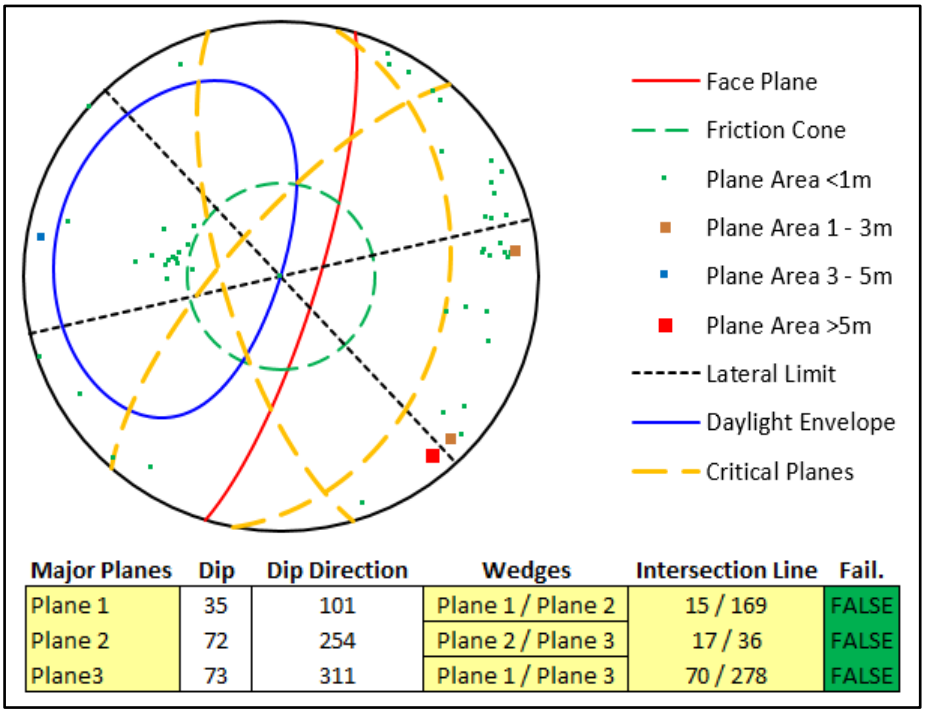

Major Planes	Dip	Dip Direction	Wedges	Intersection Line	Fail.
Plane 1	35	101	Plane 1 / Plane 2	15 / 169	FALSE
Plane 2	72	254	Plane 2 / Plane 3	17 / 36	FALSE
Plane3	73	311	Plane 1 / Plane 3	70 / 278	FALSE

Figure 4.40: Intersections of major planes selected by the user on the mapping analysis sheet.

4.2.6.3.e. Designating Major Planes

When establishing structural trends for geotechnical design sectors, predominant joint and bedding orientations are more relevant than individual planes. Overlaying a large volume of individual joint and bedding orientation measurements from different mapping faces within a pit may be misleading when trying to establish the orientations of dominant discontinuity sets. Broad structural trends and spatial variations in discontinuity orientations will tend to be hidden by a wide spread of individual pole plots. A greater degree of clarity in determining structural orientation trends during the delineation of design sectors can be gained by assessing only the identified major discontinuity sets from each mapping face.

Major planes selected by the geotechnical face mapper are designated in the same manner as for individual mapping planes as either ‘Bedding’, ‘Joint’, ‘Fault’

or other (Figure 4.41). These major planes are then exported to the Acquire Database where their orientation and discontinuity type are stored.

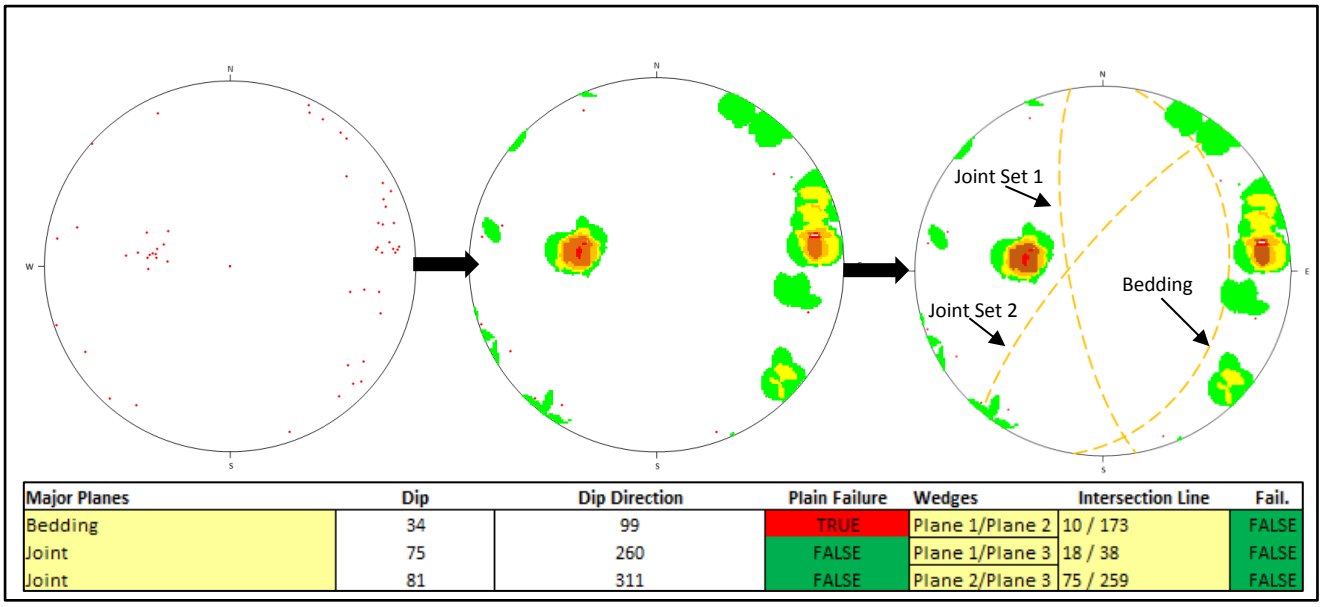

Major Planes	Dip	Dip Direction	Plain Failure	Wedges	Intersection Line	Fail.
Bedding	34	99	TRUE	Plane 1/Plane 2	10 / 173	FALSE
Joint	75	260	FALSE	Plane 1/Plane 3	18 / 38	FALSE
Joint	81	311	FALSE	Plane 2/Plane 3	75 / 259	FALSE

Figure 4.41: Process of selecting discontinuity sets for export into Acquire.

4.2.6.3.f. Rock Mass Classification

The face mapping procedure outlined in the preceding sections includes the measurement of discontinuity spacing, persistency and roughness. As part of the analysis and reporting phase of the mapping protocol these values are combined with estimates based on the known rock mass properties on the mine to calculate RMR and GSI values (Figure 4.42). In order to derive a rock mass rating value for a mapping face, the following inputs are required, some of which are available directly from the mapping data and others have to be estimated based on observation of the scan photo and known values for the mine. The Bieniawski (1989) Rock Mass Rating gives rating scores based on UCS, RQD, Joint Spacing, Joint Condition and Ground Water. These values are derived in the following manner from face mapping data in the Sishen face mapping protocol.

- **UCS –** Estimated by the geotechnical engineer / technician mapping the face as per Standard South African Core Logging strength estimates (Brink and Bruin, 2002) used on Sishen Mine (Table 4.2).

Table 4.2: Rock Strength Classification (From Brink and Bruin, 2002).

Classification	Field Test	Range of Minimum compressive strength (MPa)
Very soft rock	Can be peeled with a knife; material crumbles under firm blow with the sharp end of a geological pick.	1 to 3
Soft rock	Can just be scraped with a knife; indentations of 2mm to 4mm with firm blows of the pick point.	3 to 10
Medium hard rock	Cannot be scraped or peeled with a knife; hand-held specimen breaks with firm blows of the pick.	10 to 25
Hard rock	These materials are usually only broken with some difficulty and ring when struck. Classification can be assessed by Schmidt hammer/point load test and verified by uniaxial compressive strength testing.	25 to 70
Very hard rock		70 to 200
Extremely hard rock		>200

- **RQD –** is calculated from the joint spacing measurement captured during face mapping using the formula.

  RQD = 115 – 3.3 Jv Palmström (1982)

  The above formula was selected over the Palmström (2005) revision as it produces slightly more conservative results.

- **Joint Spacing –** Is calculated from the captured joint spacing measurement.

- **Joint Condition**
  - **Persistency –** Is calculated from persistency measurements captured during face mapping.
  - **Aperture –** Is estimated by the face mapper.
  - **Roughness –** Is estimated by the face mapper, with the assistance of the Barton (1982) JRC roughness chart when suitable surfaces are available for extracting joint roughness traces.
  - **Weathering –** Is estimated by the face mapper.

- **Groundwater –** Is estimated by the face mapper from observed seepage on the scan photograph.

The same input data used for RMR (Bieniawski, 1989) is used to calculate the GSI value through the following formula (Hoek et al., 2013).

$$GSI = 1.5 \times Joint\ Condition + {}^{RQD}/_{2}$$

RMR Inputs	Value	Rating	Joint Condition	Input	Rating
Calc.RQD (3 Sets + Rand. assumed)	93	20	Persistency (m)	17.05	1
Estimated Rock Strength	Strong rock	7	Appeture	Closed	6
Calculated Joint Spacing	0.60	10	Roughness	Rough	5
Estimated Ground Water	Dry	15	Weathering	Slightly Weath.	9
RMR		**73**	Joint Condition Rating		21
GSI		**78**			

Figure 4.42: Rock Mass Rating and GSI output on the face mapping report sheet.

4.2.6.4. Data Export from Excel to Acquire

The Sishen Acquire Geological Database is a SQL Server Database that is accessed and managed through a database specific software suite. Data that needs to be imported into an Acquire Database is done so through an import object, linked to a comma separated value (CSV) file with a pre-defined format. For each mapping face, the relevant information is exported from the Excel data processing sheet to a CSV file that is in a format that can be accepted by a corresponding import object within the Acquire Data Management System. A VBA macro has been set up within the Excel face mapping template to export the following data for each face, once all data has been imported and the face has been analysed.

- Face ID (The unique identifier for the mapping face)
- Face Length, Face Area, Estimated Friction Angle, Face Lithology.
- RQD, RMR, GSI, Average Joint Spacing, Average Joint Persistency, IRS
- The Northing, Easting and Elevation of the Face Midpoint.
- Northing, Easting, Elevation, Measurement Type, Discontinuity Type, Dip, Strike, Dip Direction, Plane Length and Plane Area for each orientation measurement.
- Northing, Easting, Elevation, Measurement Type, Discontinuity Type, Trace Plunge and Measurement Length for each discontinuity spacing and persistency measurement.
- Northing, Easting, Elevation, Measurement Type, Dip and Dip Direction for each major plane identified by the geotechnical face mapper.

For each mapping face the export data is written to an individual CSV file on the mine's network drive which is given the face ID as a file name (Figure 4.43). In addition to this a set of central CSV files containing all mapping data is updated to include all data from the current mapping face. These files form the access point for import into Acquire; each time data from a new mapping face is added, the

export macro reads through the file to ensure no repeat data is included (for instance when a mapping face is erroneously re-exported). By including this process of data quality verification on the CSV export file, errors upon importing into Acquire are avoided. The methodology behind this process is discussed in Section 4.2.7.6.



Figure 4.43: Mapping data stored as CSV files after export.

4.2.7. Data Import into Acquire

As outlined in the previous section Kumba Iron Ore uses the Acquire Geological Data Management System to capture, store and analyse geotechnical data. The Acquire database system is a relational database built around a set database structure specifically designed to accommodate geological borehole data and laboratory test samples. Data is stored on a back end SQL server database while data is accessed through front end Acquire software.

4.2.7.1. Front End Software

The Acquire software accesses data through a set of software specific objects which are developed and customised according to the specific needs of a particular site. Development of these objects takes a relatively in-depth knowledge of the Acquire software, the Acquire Data Model and SQL programming. This is typically done by Acquire support staff when a database is set up on site.

4.2.7.2. Geotechnical Database Structure

Data captured and entered during the geotechnical logging process is best summarised by the following broad categories.

- Data captured per project / site
- Data captured per borehole
- Data captured per core run
- Data captured per geotechnical zone
- Data captured per laboratory test sample
- Data captured per face mapping zone

Each of the above categories of data is stored according to compound definitions that have been predefined according to the Acquire Data Model. Relevant compound definitions for end users using the Geotechnical Databases within Kumba are the Collar Compound Definition (Data per borehole), Geology (Data per core run, per geotechnical zone and per face mapping zone), and CorpAssay (Data per sample). Figure 4.44 illustrates how geological data is organised within the Acquire Data Model.

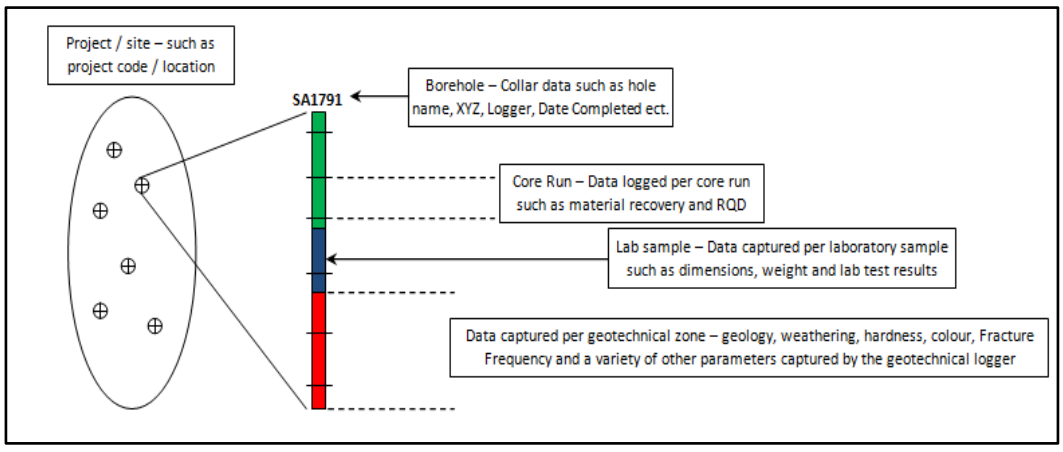

Figure 4.44: Simplified representation of how geotechnical data is stored in Acquire.

4.2.7.3. The Acquire Data Model (ADM)

The Acquire Data Model (ADM) refers to the model used by the Acquire Database System to store geological data. Within the data model, similar data (as indicated in Figure 4.44) has been grouped in tables under the various compound definitions. The ADM database is a relational database, meaning that different

tables across the database are linked via key data fields. The following terms are used to describe the main elements of the Acquire ADM.

Acquire Specific Terms Database Terms

Data Entry Object: A form that allows users to enter values directly into the Acquire Database.

Fixed Field: A field that appears within the Acquire Database Model. Fixed field are pre-defined in the model using generic field names that cannot be changed. Fixed fields are used for input of generic information such as borehole names. These fields cannot be added, removed or modified.

Virtual Fields: Virtual fields are data entry fields created for the specific data capture needs of a site such as Geotechnical Zones, UCS values and RQD. Virtual fields are captured in the Acquire Database as records within the database structure.

Derived Field: A derived field consists of calculated values that are created by Acquire from a SQL script. Derived fields are calculated when included in a form or report object. Derived fields typically contain data such as RMR values that are not entered into the database, but rather calculated from other data such as RQD and UCS strength values for each geotechnical zone.

Compound Definition: In Acquire a Compound Definition represents a group of associated tables. A compound definition can be used to define a form or data client view, thereby allowing the user access to the virtual and derived fields within the tables grouped under the compound definition in question. For example the **'Collar'** compound definition groups tables with virtual and derived fields relating to borehole collar information such as co-ordinates, end depth and drilling status, while the **'Geology'** compound definition contains fields relating to logging information such as lithology, joint descriptions and RQD. Compound definitions are pre-defined as part of the Acquire Data Model (ADM).

Form: A form is a means of viewing, editing and exporting selected data from the Acquire Database using the Acquire front end software. A form is created by defining selected fixed, virtual and derived fields which are displayed in a tabular format when the form is opened.

Data Client View: A data client view is a virtual table in the acquire database that contains data fields set up by the user. The purpose of data client views is to allow external software such as Micromine or Excel access to selected data from within the acquire database.

Data Import Object: An Acquire data object is used to import data into an Acquire Database from an external file source such as a CSV file.

From an end user perspective, data that is to be entered into the database is stored in either fixed or virtual fields. Fixed fields within the ADM appear within the tables represented in the diagram in Figure 4.45. The field names written in capital letters refer to fixed fields where user entered data is stored directly while the field names written in lower case italics are there to store information pertaining to the virtual fields within the database. Virtual fields are defined by the user and allow for storage of site specific data.

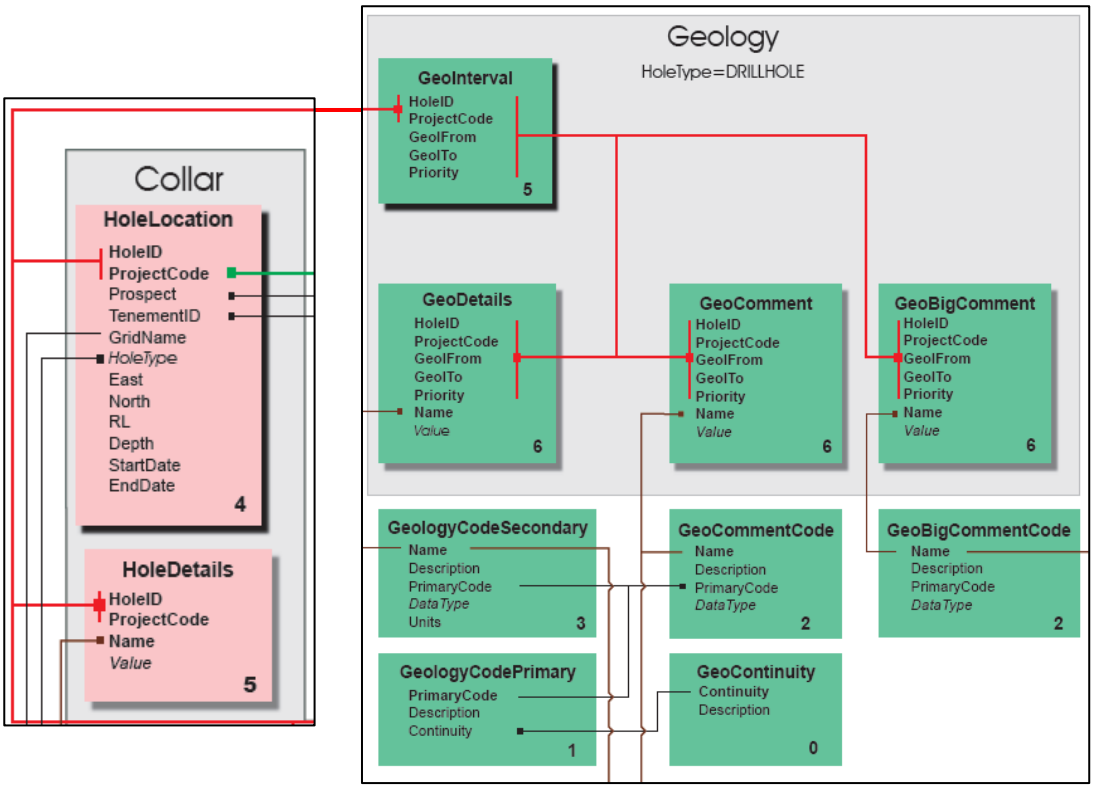

Figure 4.45: Example of how geotechnical data is stored in Acquire.

4.2.7.4. Accommodating Mapping Data

The Acquire database structure is designed to accommodate borehole data, meaning that specific adaptions were required to set up a system in the database to incorporate the mapping data produced during face mapping. As discussed in Section 4.2.6 the data flow process developed to accommodate face mapping data involves first exporting the mapped entities from I-Site Studio as individual text files. These files are then imported and collated into appropriate tables in a standard Microsoft Excel template using a set of import macros.

When transferring the data from Excel to Acquire, the face mapping data first needs to be converted into a format compatible with the Acquire system, this essentially involves treating individual mapping faces as boreholes, with a unique face identifier acting as the borehole collar and individual mapping entities stored in customised virtual fields within the database.

Face mapping data can be accommodated within the Acquire Data Model under the **Collar** and **Geodetails** compound definitions.

The modifications to the database were made to allow each individual mapped face to be treated as a borehole collar. The following Fixed Fields were used in the **Collar** compound definition.

- HOLEID - A unique identifier for the face as follows Pit_Area_X_Y_Z
- EASTING – Face center point X co-ordinate
- NORTHING – Face center point Y co-ordinate
- RL – Face center point Z co-ordinate
- PROJECT CODE – ‘Sishen’
- PROSPECT – ‘MAP’
- HOLETYPE – ‘Mapping Face’

The following Virtual Fields were added under the Collar compound definition. All face mapping virtual fields under the collar compound definition were assigned the prefix ‘Face’.

- Face_Pit – Pit in which the mapping face is located
- Face_Area – Area / sector within the pit where the mapping face is located
- Face_Date_Mapped – Mapping date
- Face_Mapper – Name of the person carrying out the mapping
- Face_Length_m – Length of the mapping face
- Face_Area_m^2 – Total area mapped

- Face_Dip – Dip of the mapping face
- Face_Dip_Direction – Dip direction of the mapping face
- Face_Est_Friction – An estimate of dominant discontinuity friction angle
- Face_Geol – Lithology of the mapped face
- Face_RQD – Estimated from joint spacing
- Face_Joint_Spacing – Average from measured values
- Face_Joint_Persistency – Average from measured values
- Face_IRS – Estimated from logging standards (R0 – R6) as per Table 4.2
- Face_Joint_Weathering
- Face_RMR
- Face_GSI
- Face_MajPlane1_Dip
- Face_MajPlane1_DipDrx
- Face_MajPlane1_Desc
- Face_MajPlane2_Dip
- Face_MajPlane2_DipDrx
- Face_MajPlane2_ Desc
- Face_MajPlane3_Dip
- Face_MajPlane3_DipDrx
- Face_MajPlane3_ Desc

Parameters associated with major planes selected from the mapping stereonet

The following fields have been added under the **Geology** compound definition to accommodate mapping data gathered for each specific face. All mapping virtual fields created in the **Geology** compound definition carry the prefix 'FaceM'.

- FaceM_Measure_Type – "Orientation", "Spacing", "Persistency", "Roughness"
- FaceM_Discont_Type – "Bedding", "Joint", "Fault", "Other"
- FaceM_X – Easting Co-Ordinate
- FaceM_Y – Northing Co-Ordinate
- FaceM_Z - Elevation
- FaceM_Dip – Discontinuity Dip
- FaceM_Dip_Direction – Discontinuity Dip Direction
- FaceM_Strike – Discontinuity Strike
- FaceM_Area_m^2 – Area of discontinuity
- FaceM_Length_m – Length of discontinuity Plane / Spacing / Persistence
- FaceM_JRC

4.2.7.5. Theoretical Face Mapping Database Table Scheme

The preceding section describes how mapping data has been incorporated into the Acquire Data Model. An adaption had to be made to adequately accommodate mapping data within a database model specifically designed for borehole data. When designing a face mapping data storage system the intended database outputs and information that will potentially be drawn from the database needs to be considered. Required outputs for the Sishen face mapping database can be considered in terms of the general requirements in the open pit geotechnical design process (Figure 4.46).

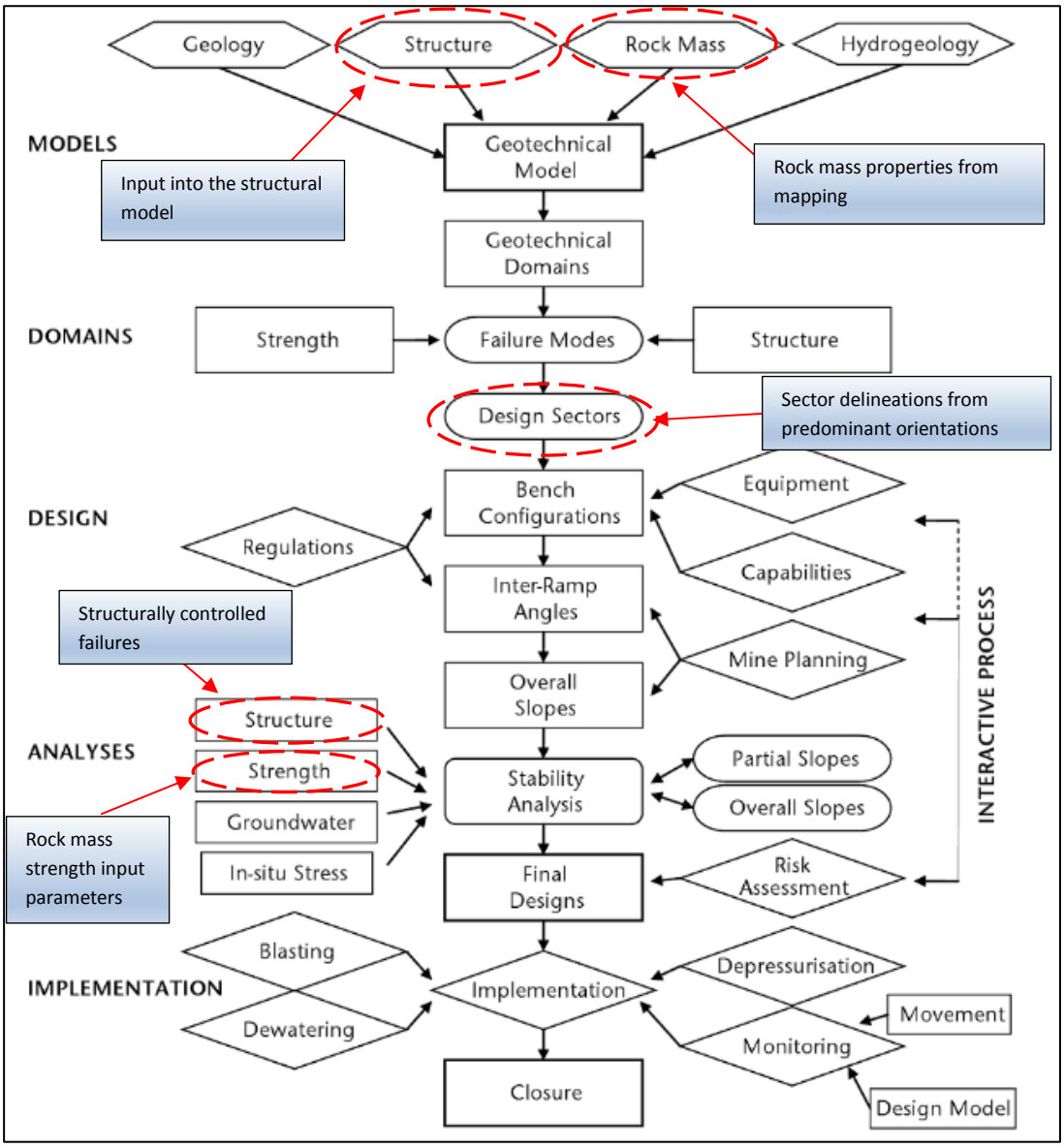

Figure 4.46: Theoretical geotechnical slope design process showing potential face mapping data input points (From Stacey, 2009).

A face mapping database has the potential to add value and reduce uncertainty within the design process illustrated in Figure 4.46. This however requires that the data is organised in such a manner that it can be accessed and queried to produce relevant and meaningful information to aid in the design process.

The following generic relational data model was applied to fit into the Acquire Data Model, used to accommodate Sishen's geotechnical data. The schematic table layout represented in Figure 4.47 was found to represent a simple and robust method of storing mapping data. The **Face Mapping Collar** Table is a parent table containing information pertaining to each mapping face as a whole, this is related to the **Face Mapping Detail** table through the Face ID field which represents the primary key. Other relevant parameters can either be added to the **Face Mapping Collar** Table if a single record is applicable to the face as a whole or to the **Face Mapping Detail** table if several values (e.g.: Schmidt Hammer test) are to be added.

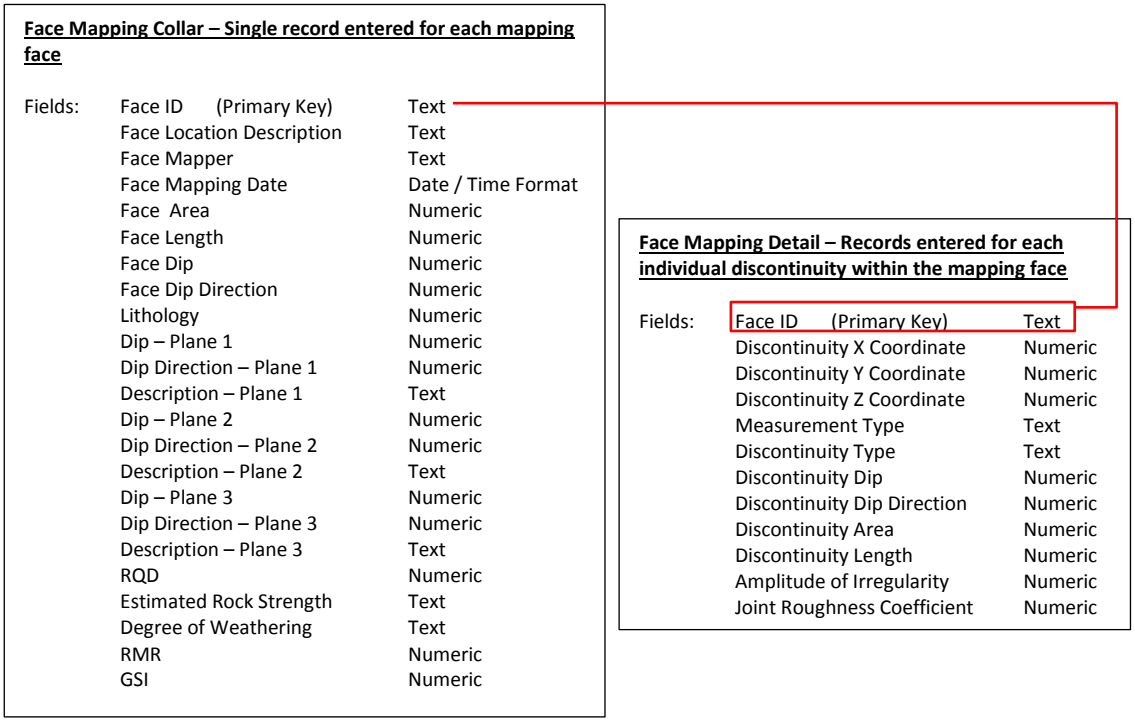

Figure 4.47: Basic schematic face mapping database layout.

4.2.7.6. Methodology For Exchange of data between Excel and Acquire

A reliable system for transferring data between Microsoft Excel and the Acquire Database needed to be developed. The functionality of Acquire and Microsoft Excel allows for two possible means of data transfer. Firstly, data can be transferred directly through a VBA macro that links with the database and executes the required export into Acquire. Secondly, data can be exported from Excel to a template CSV file and imported from there through an Acquire data import object. When developing a system for adding data from an individual mapping worksheet to the dataset stored in the database, the following needed to be considered to ensure data integrity.

- The mapping face name is the primary key and a unique identifier for that face. If a face were to be remapped or revised the database would not allow re-entry of the mapping face name.
- There is the potential for users to erroneously re-enter duplicate values for individual mapping records, for example if the incorrect text files are exported from I-Site Studio.
- Acquire data tables have various required data formats and data validation conditions that must be adhered to for data to be successfully imported.

In order to ensure no conflicts occur when importing data, and only the correct, unique mapping values are allowed into the database, a data transfer system was designed to incorporate pre transfer data integrity checks to ensure that imports are successful and that duplicate values are not allowed into the database. The flow diagram in Figure 4.48 illustrates the data flow path in the system that was developed to transfer mapping data from Excel into the Acquire Database. Within the Excel mapping data analysis template an export Macro validates the mapping data and adds it to an intermediary CSV file that mirrors the mapping data in the database. The CSV file is then imported into the Acquire database using an Acquire Import Object that performs a merge operation to import outstanding data from the CSV file to the database, effectively ‘syncing’ the two datasets.

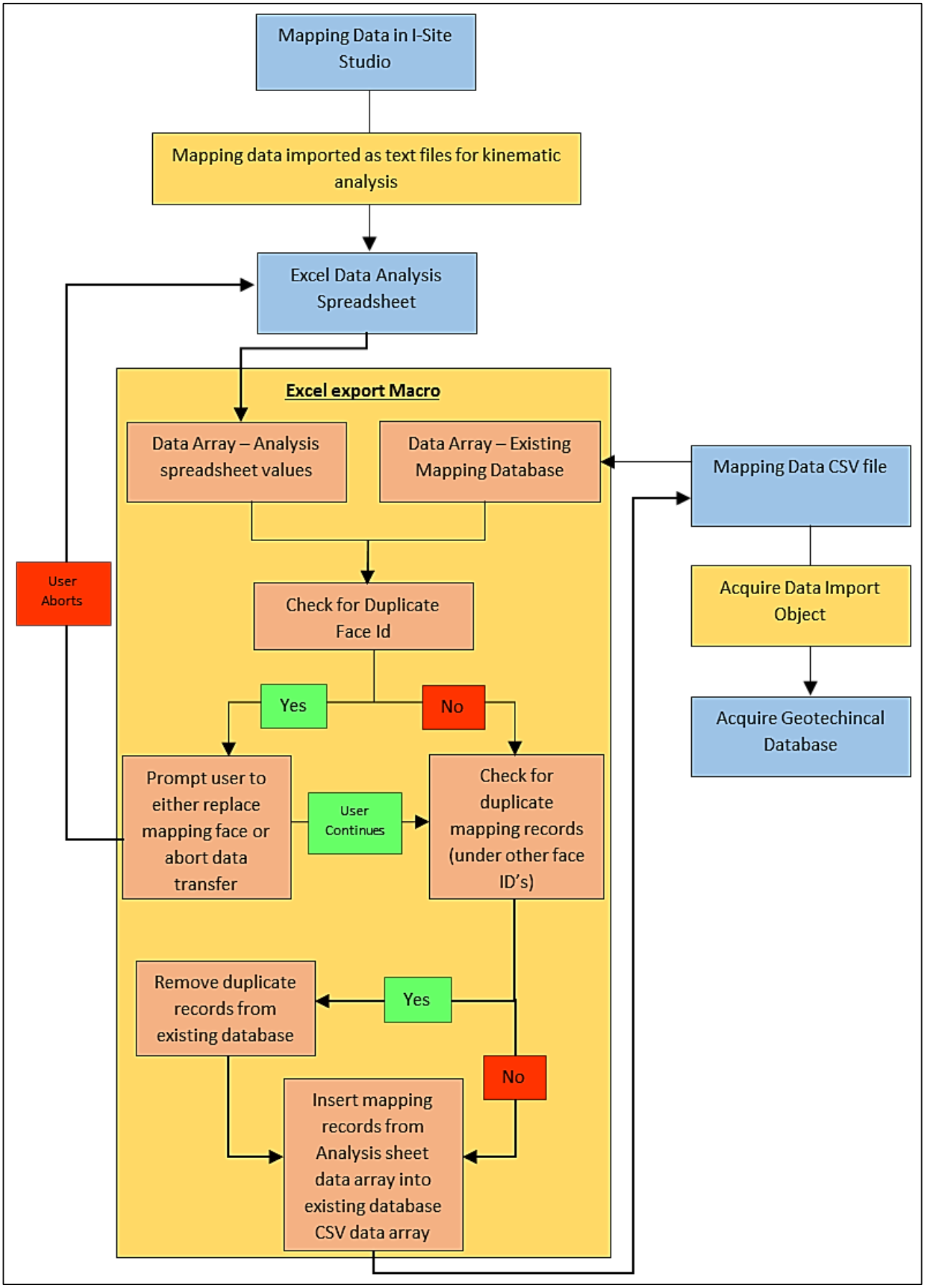

Figure 4.48: Theoretical mapping data flow path between I-Site Studio and Acquire.

4.2.7.7. Accessing, Querying and Reporting of Mapping Data Stored in Acquire

The most direct means of accessing and querying data in the Acquire database is through either a form or report database object within the Acquire front end software. A second option is to link with the required database fields through various third party software packages.

4.2.7.7.a. Accessing Data Directly Within Acquire

A form is based on a form definition that can be set up by the user to access specific data within the database. The form definition can either be based on individual tables within the Acquire Data Model or a compound definition.

A report object produces an output report that can be exported in various file formats (but typically as a pdf file). Report objects are designed by the user to produce summary values and charts representing the data in the desired database fields. Typically a report will consist of three components, an input sheet where required parameters and filters for the report output can be entered, a data sheet where the SQL script to access the required data is stored, and an output report sheet.

Forms allow for easy and rapid access of data in the database, usually for export to a package such as Excel for further manipulation and analysis. Reports are useful for routine reporting of a standard set of data out of the database such as monthly QAQC reports on assay samples. Their functionality is however limited and developing of a reporting object requires an in-depth knowledge of the Acquire Data Model and the front end software.

4.2.7.7.b. Creating a Database Link for Third Party Software

Directly accessing the Acquire database through third party software is in many instances the most practical way of querying and manipulating data. The Acquire front end software allows data client views to be set up that can be accessed by third party software. A data client view is simply the result of a stored query in the Acquire Database and is set up in the front end software by saving a form as a data client view in the database. Once saved the data client view can be accessed by any other software capable of creating an ODBC database connection.

4.2.7.7.c. Accessing Mapping Data Using Microsoft Excel

In order to access Sishen face mapping data in Microsoft Excel, the relevant database fields were included in Acquire form objects and saved to the database as data client views. One of the required outcomes of this research report is to compare and contrast values from face mapping and borehole data. Therefore, in a similar manner, data client views representing relevant borehole data were saved to the Acquire database for access in Excel.

4.2.7.7.d. Accessing Mapping Data Using Micromine Software

Analysis of the spatial relationship and orientations of mapped bedding planes, joint sets and larger structures with the pit design shell and existing structural data, forms an integral part of the slope design process. A structural model has been developed for Sishen Mine by external consultants based on several rounds of structural mapping on the mine. The existing structural model includes the following spatial data.

- Digital Terrain Models representing the faults planes mapped
- Lithological contacts incorporating interpreted fault throws from field mapping
- Geology clipped to the design final pit boundary
- Interpreted bedding dip and dip directions based on geological contacts, superimposed on the final pit boundary.

Micromine has the same functionality as Microsoft Excel that allows for ODBC links to be set up with the Acquire database. Data client views were set up specifically for Acquire mapping data to be accessed by Micromine, to allow the data to be plotted in 3D space along with data from the structural model, as well as other relevant mine planning, survey, geological and geotechnical data.

4.3. INTERGRATION OF MAPPING DATA IN THE GEOTECHNICAL DESIGN PROCESS

In order to provide lasting value as opposed to merely serving the requirements of isolated, area specific, stability assessments, mapping data needs to be integrated into the geotechnical design process in such a way that it can be reviewed and assessed in conjunction with rock mass strength data, structural models, geological models and the regional hydrogeological setting. The slope design process is by nature iterative throughout the life of an open pit mine. As the mine develops, pit shells change accordingly with refinement of the resource, geotechnical data confidence increases through borehole drilling and sampling, and understanding of the rock mass behaviour improves through monitoring of the mined out areas of the pit. A schematic diagram of the geotechnical data sources at Sishen Mine, and how they feed into a data analysis and reporting system and a 3D data modelling system, is indicated in Figure 4.49.

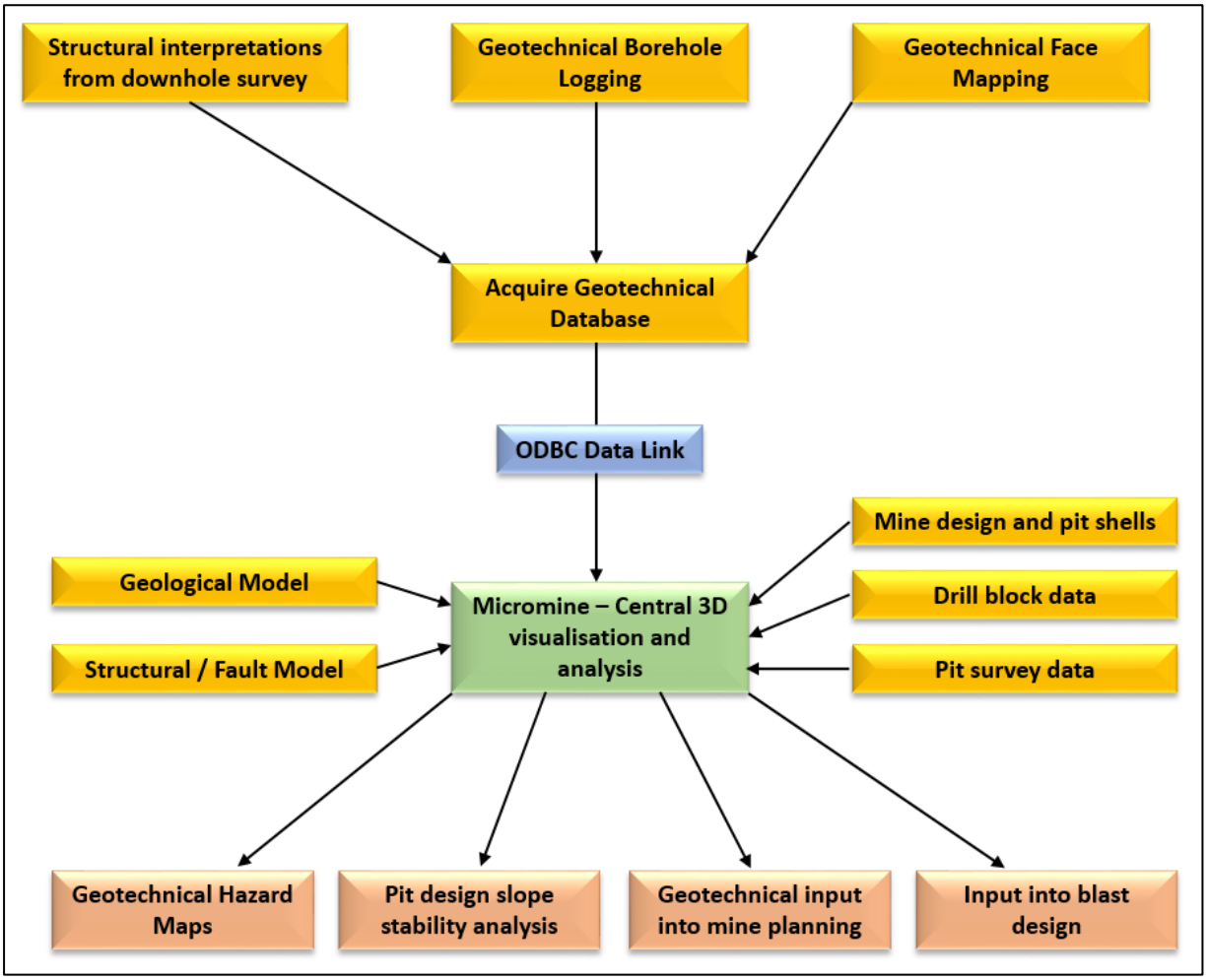

Figure 4.49: Geotechnical spatial data flow path at Sishen Mine.

4.3.1. Linking of Sishen's Geotechnical Data Sources with Micromine

The transfer of face mapping data from I-Site Studio to the Acquire Database System has been discussed in detail in Section 4.2 of this chapter.

In addition to direct face mapping data, the mine obtains structural data from geotechnical, exploration and dewatering boreholes through the use of optical and acoustic televiewer systems, employed during downhole surveys of the holes. During the downhole survey process the borehole sidewalls are either scanned optically (above the water table) or acoustically (below the water table). Orientated discontinuity traces can be extracted from the borehole sidewalls using this survey technique. Downhole surveys are carried out by specialist contractors that perform the on-site survey and carry out structural interpretations on the televiewer data. The mine receives a structural report for each surveyed borehole in CSV file format. Each report file contains depth, aperture, dip, strike and discontinuity type for all structures encountered in the borehole. This structural data is imported into the Acquire database in a similar manner to the face mapping data.

Borehole logging data is entered into the Acquire database through manual data entry on logging forms set up for use in the Acquire front end software. Laboratory test data is imported through a series of CSV import objects, in the same manner as for televiewer and face mapping data.

For planning and analysis purposes geotechnical data needs to be displayed in a 2D or 3D CAD package in conjunction with geological information, mine planning data and actual survey data from the mine. Sishen's Geotechnical Engineering section has selected the Micromine 3D CAD package to perform this function. One of the implicit aims of this research dissertation was to integrate mapping data, along with other available geotechnical data into such a system. For this reason, in addition to those defined for mapping data, Acquire data client views were created for other relevant data sources in the Acquire database such as borehole log information and televiewer structural data. An illustration of the data flow process between Acquire and Micromine is given in Figure 4.50.

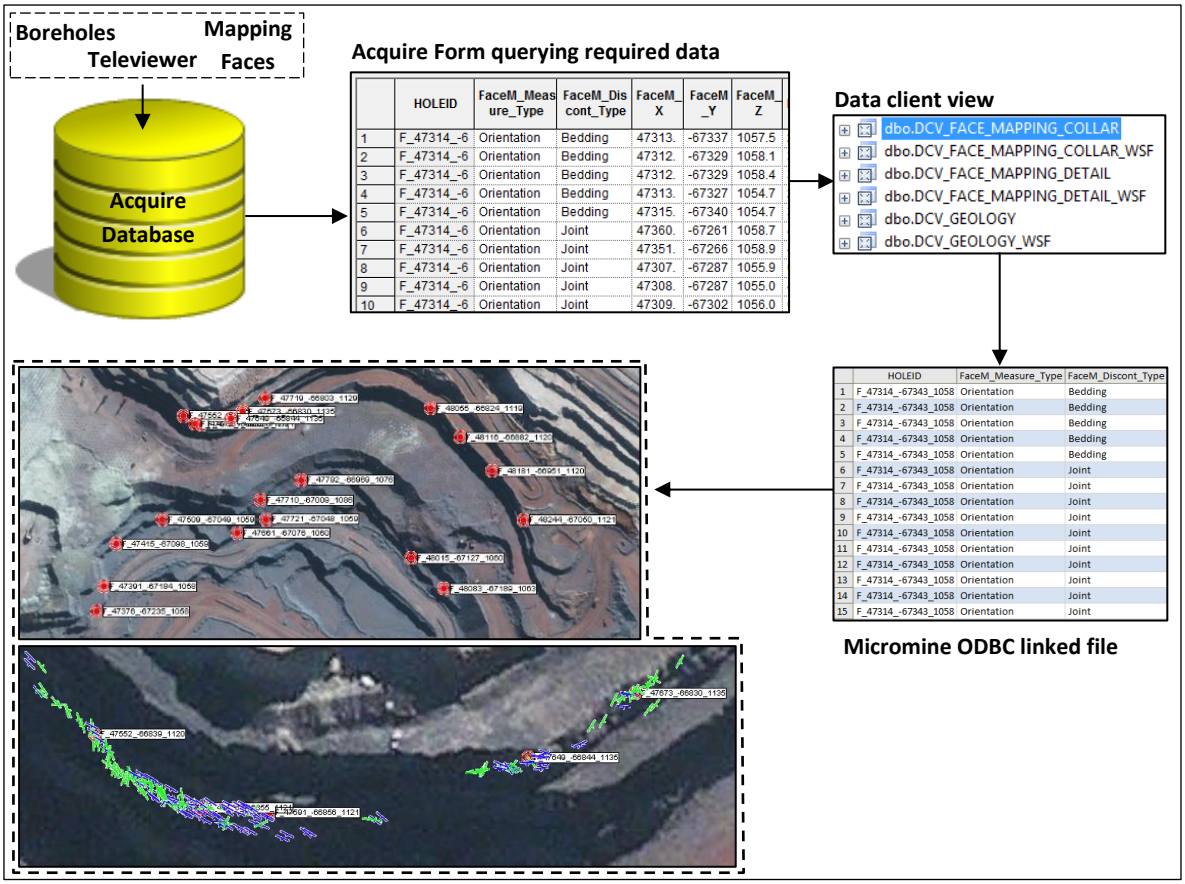

	HOLEID	FaceM_Measure_Type	FaceM_Discont_Type	FaceM_X	FaceM_Y	FaceM_Z
1	F_47314_-6	Orientation	Bedding	47313.	-67337	1057.5
2	F_47314_-6	Orientation	Bedding	47312.	-67329	1058.1
3	F_47314_-6	Orientation	Bedding	47312.	-67329	1058.4
4	F_47314_-6	Orientation	Bedding	47313.	-67327	1054.7
5	F_47314_-6	Orientation	Bedding	47315.	-67340	1054.7
6	F_47314_-6	Orientation	Joint	47360.	-67261	1058.7
7	F_47314_-6	Orientation	Joint	47351.	-67266	1058.9
8	F_47314_-6	Orientation	Joint	47307.	-67287	1055.9
9	F_47314_-6	Orientation	Joint	47308.	-67287	1055.0
10	F_47314_-6	Orientation	Joint	47309.	-67302	1056.0

	HOLEID	FaceM_Measure_Type	FaceM_Discont_Type
1	F_47314_-67343_1058	Orientation	Bedding
2	F_47314_-67343_1058	Orientation	Bedding
3	F_47314_-67343_1058	Orientation	Bedding
4	F_47314_-67343_1058	Orientation	Bedding
5	F_47314_-67343_1058	Orientation	Bedding
6	F_47314_-67343_1058	Orientation	Joint
7	F_47314_-67343_1058	Orientation	Joint
8	F_47314_-67343_1058	Orientation	Joint
9	F_47314_-67343_1058	Orientation	Joint
10	F_47314_-67343_1058	Orientation	Joint
11	F_47314_-67343_1058	Orientation	Joint
12	F_47314_-67343_1058	Orientation	Joint
13	F_47314_-67343_1058	Orientation	Joint
14	F_47314_-67343_1058	Orientation	Joint
15	F_47314_-67343_1058	Orientation	Joint

Figure 4.50: Data flow between Acquire and Micromine allowing for the automatic updating of Micromine plots as Acquire data is added.

4.3.2. Integration of Mapping Data With Other Geotechnical Data Sources

Face mapping data has the potential to add value to the slope design and geotechnical hazard assessment process when used in conjunction with the other available data sources outlined in Figures 4.51, 4.52 and 4.53.

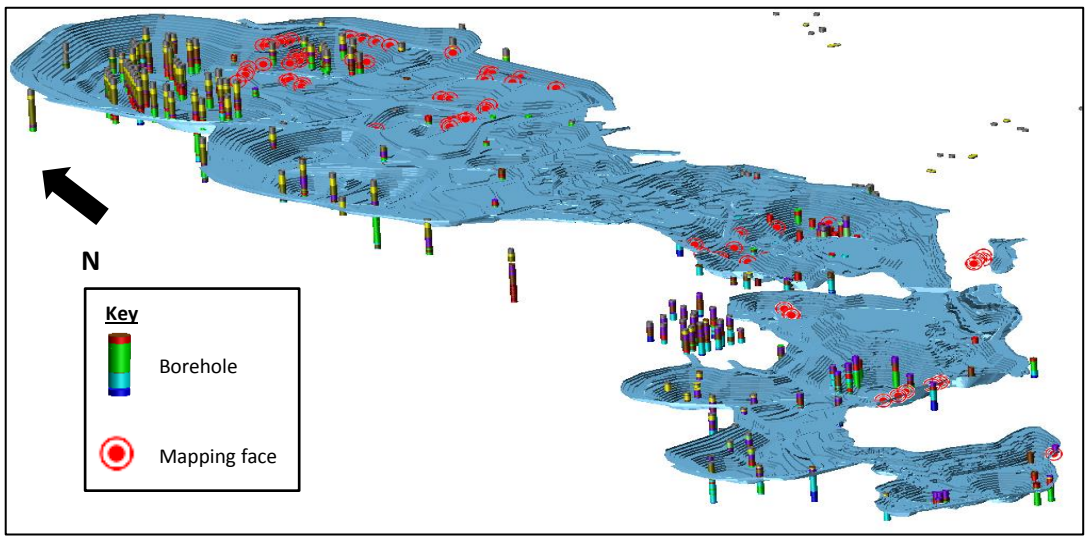

Figure 4.51: Geotechnical face mapping and borehole data overlain on Sishen's design pit shell.

The majority of the exposed rockmass in Sishen's interim and final pit boundaries consists of layered or bedded rock types such as Banded Iron Formation, shale and sandstone. Anisotropic strength properties, and the local orientation of rock strata relative to pit slopes, play a critical role in the stability of Sishen's highwalls. The Mine has an existing structural model developed by external consultants that details faulting on the mine, provides an interpretation of the position of geological contacts and interprets bedding orientations based on these contacts. Mapping plays an important role in ground proofing and verifying the accuracy of this data. Mapping data incorporated into Micromine can be used to verify inferred and interpreted structural data as illustrated in Figure 4.54.

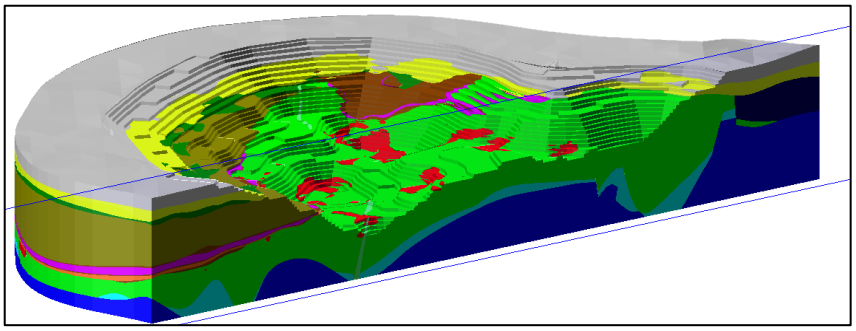

Figure 4.52: Section through the Sishen North pit structural geological interpretation.

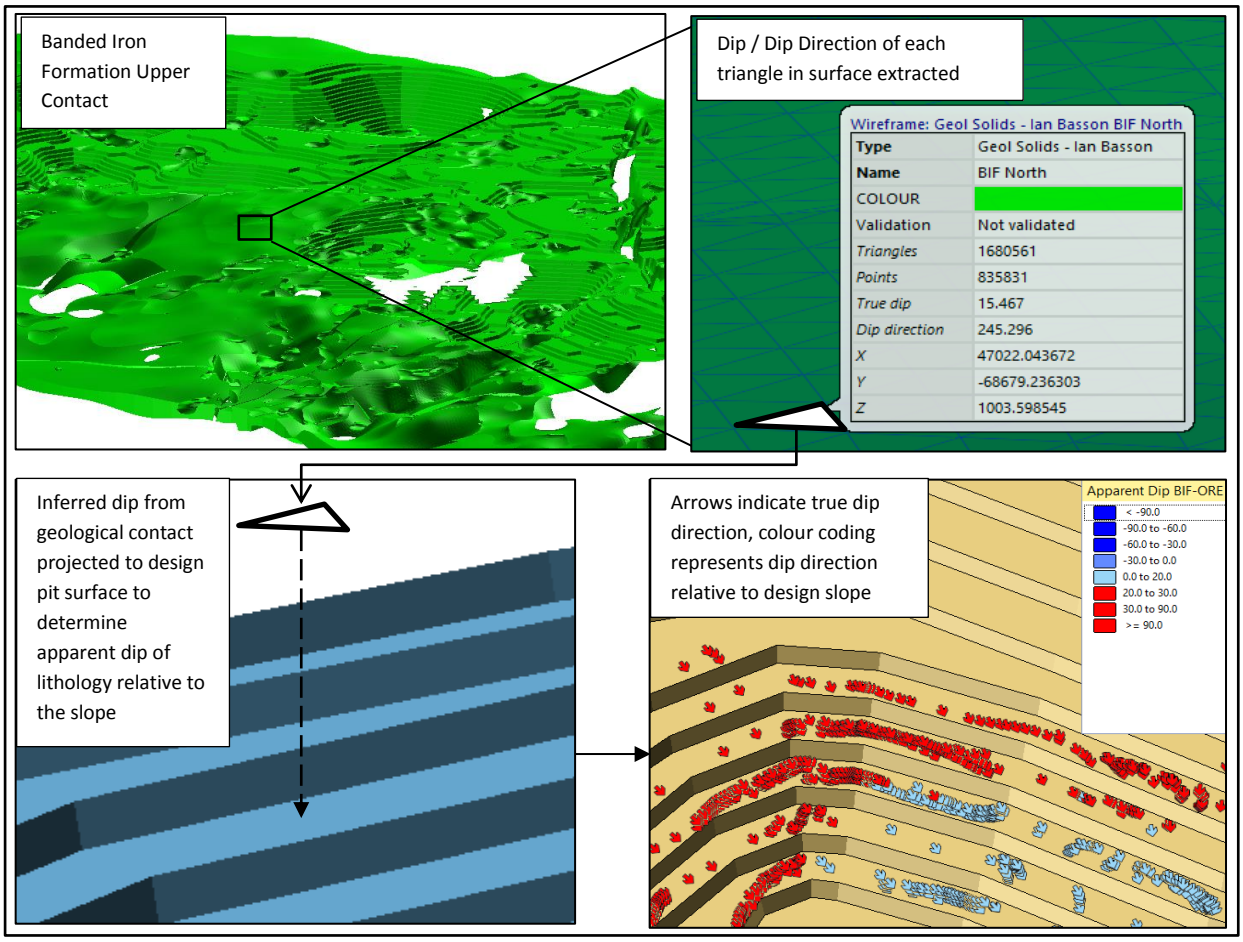

Figure 4.53: Process used to estimate bedding dip and dip direction based on modelled lithological contacts per fault block.

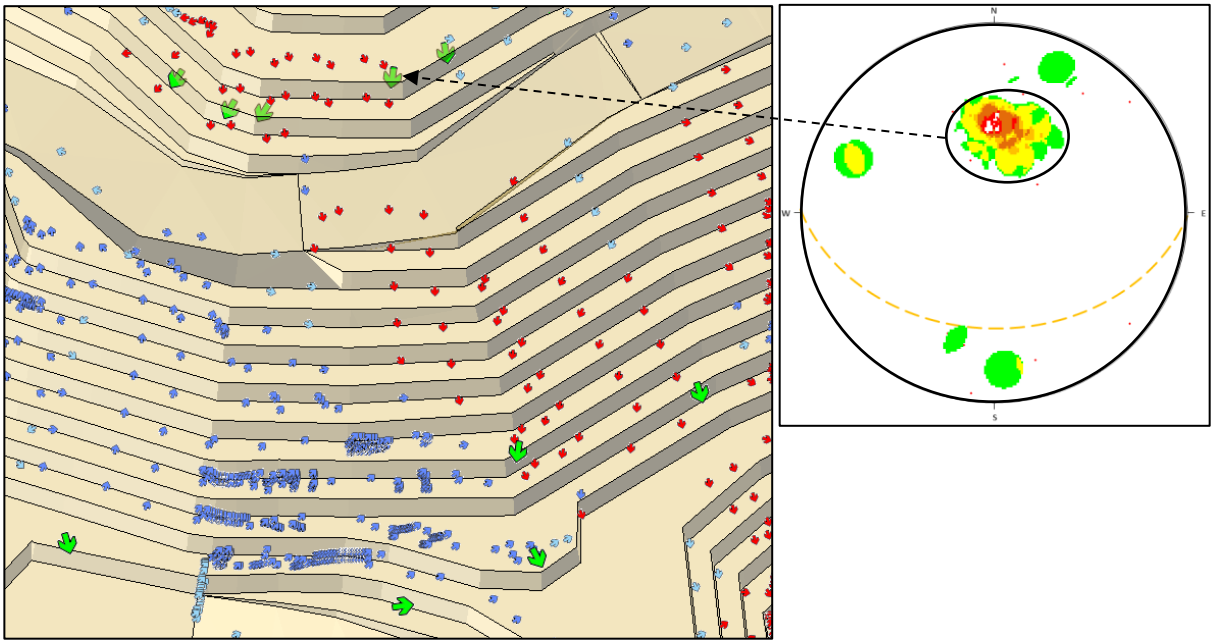

Figure 4.54: Inferred versus measured dip directions, green arrows represents bedding stereonet best fits per mapping faces, red/blue arrows represent inferred dip and dip directions.

A second major influence on slope stability at Sishen Mine, over and above bedding orientation, is faulting. The mine is intersected by numerous large faults that typically comprise zones of weathered, weakened material or clayey gouge. These fault zones have acted as releasing planes during large scale failures in the past at Sishen and are incorporated into any slope stability assessment done on the mine. As mentioned in the previous paragraph, structural interpretations have been carried out on the mine by external consultants. This exercise included the delineation of major fault planes, based on field measurement and interpretations from the mine's existing geological models and borehole database. In addition to mapping of smaller scale structures, laser scanner face mapping allows the orientations of larger faults to be established, if exposed over a 3D surface such as a multi-bench face. Faults mapped during routine face mapping are added to the Acquire database and incorporated into the integrated Micromine spatial dataset for comparison with inferred fault positions (Figure 4.55). This allows for the validity of the structural model to be checked, and any required update to be made.

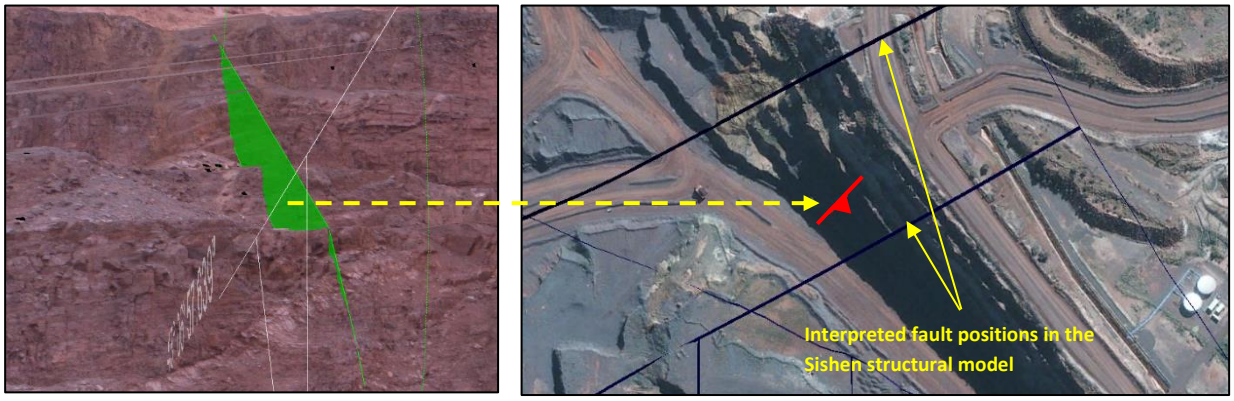

Figure 4.55: Measured versus interpreted fault planes overlain on an aerial photograph of the Sishen final pit boundary.

4.3.3. Influence of an Integrated Face Mapping Database on the Design Process

Geotechnical face mapping data has the potential to inform several aspects of the geotechnical design process. Areas of input within the design process that are evident from the face mapping and data management process developed for this dissertation and discussed thus far in this Chapter are summarised in Figure 4.56.

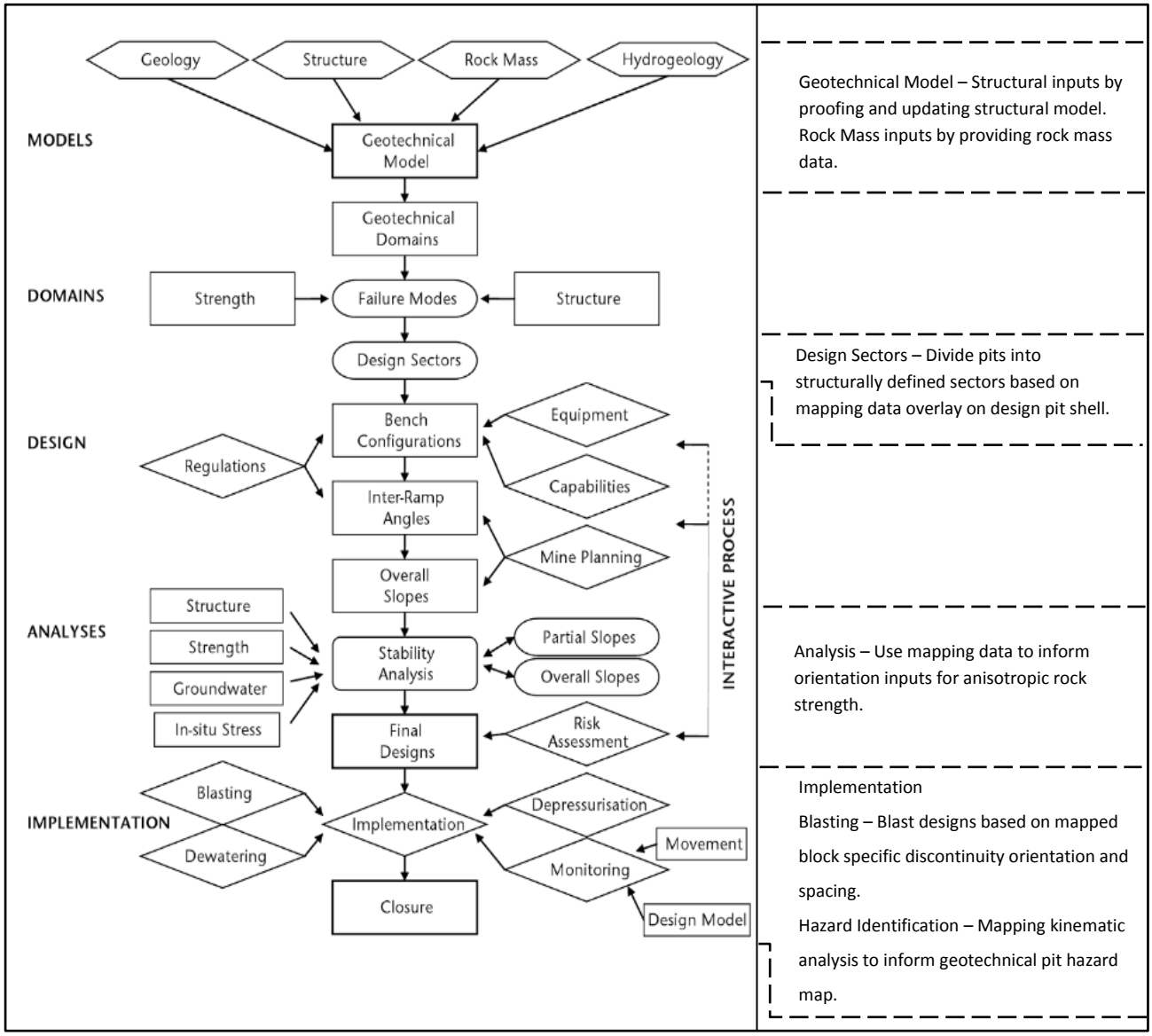

Figure 4.56: Summary of the potential face mapping inputs into the geotechnical design process (From Stacey, 2009).

4.4. REPORTING AND ANALYSIS OF ACQUIRE BOREHOLE AND MAPPING DATA

4.4.1. Tracking of Mapping Progress

The previous section outlines the spatial aspect of face mapping progress tracking through the use of Micromine system. A second aspect of face mapping tracking during the development and implementation of Sishen's face mapping protocol was a summary of mapping face data per lithology and per scanning time frame (Table 4.3 and Figures 4.57 and 4.58). Tracking of the geotechnical zones / rock types mapped serves as a means of determining where mapping data shortfalls lie and planning of areas of focus for future face mapping.

Table 4.3: Summary of face mapping statistics for faces scanned between September 2015 and May 2017.

Faces Mapped	**86**
Total Area Mapped (m^2)	**196445**
Orientation Measurements	**4022**
Spacing Measurements	**4726**
Persistency Measurements	**1302**
Roughness JRC Measurements	**116**

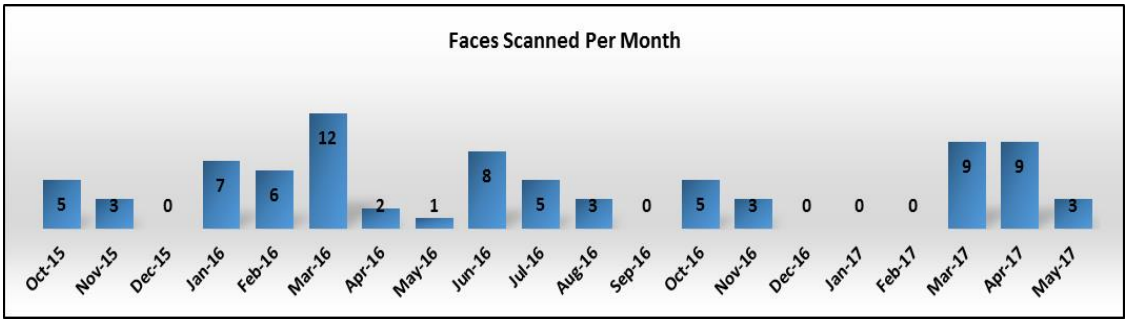

Figure 4.57: Summary of faces scanned per month between October 2015 and May 2017.

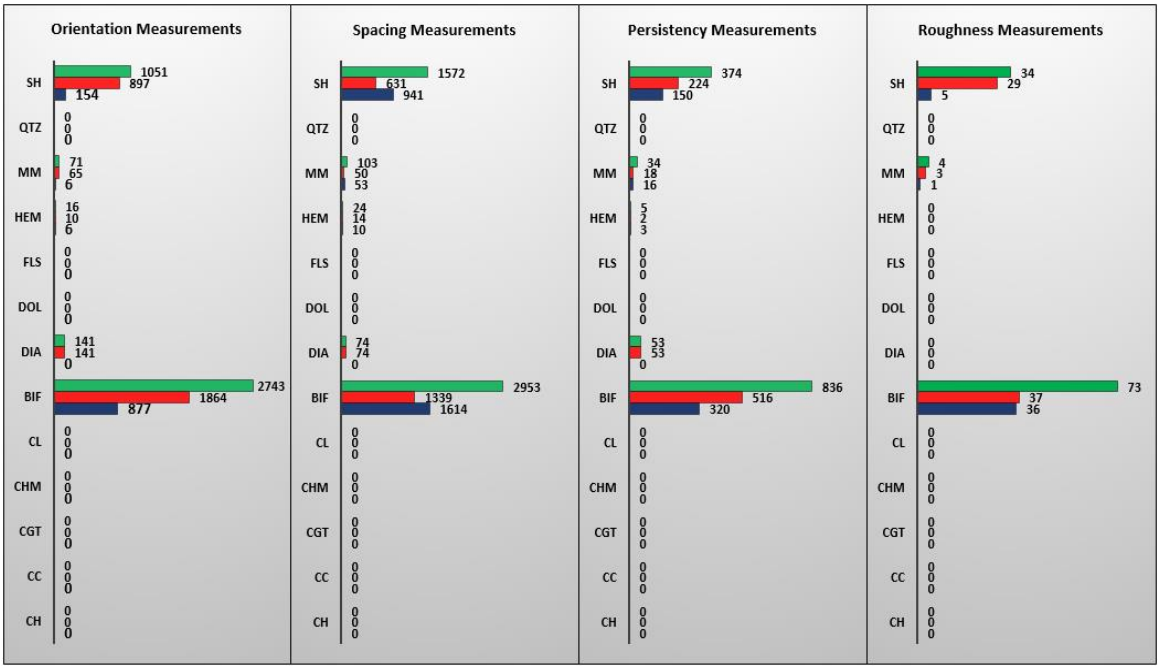

Figure 4.58: Summary of mapping measurement per lithology (Green – Total Measurements; Blue – Bedding Planes; Red – Joint Planes).

4.4.2. Reconciliation of Mapping and Borehole Data Statistics

As discussed in previous sections, mapping and geotechnical borehole data in the Acquire Database is made available to third party software using data client views. For the purpose of this research and to meet the general data analysis requirements a set of interactive excel spreadsheet templates were set to access and filter different combinations of geotechnical and mapping data. These data analysis templates form the basis for comparison between borehole and face mapping data, set out as one of the main research outcomes of this research report. Spreadsheets with ODBC links to the Acquire database have been set up to query all laboratory testing, borehole logging and face mapping parameters required for stability analysis. The spreadsheets have been set up to allow data to be queried per rock type / geotechnical domain (Table 4.4) and mining area (Figure 4.59). Export macros written within the spreadsheets allow for the export of the data sets from individual query outputs for further analysis, typically with statistical packages such as Oracle Crystal Ball. Examples of face mapping and borehole data reconciliation reports are given in Figures 4.60 and 4.61.

Table 4.4: Rock Types / Geotechnical Zones used for geotechnical purposes as Sishen. Groupings of logging codes are based on the geological groupings of rock types used in the mine's geological model.

Unit	Description
BIF (BIF, LY, LYT)	Banded Iron Formation
Calcrete (CC, KK)	Kalahari Group Calcretes
Conglomerate (CGT, KGT)	Conglomerate lenses on periphery of ore horizon and conglomeratic ore
Diabase (DI)	Large diabase dykes cross-cutting the mine
Dolomite (DOL)	Malmani Dolomites (Transvaal Supergroup)
Hematite (HEM, EKG, EL)	Laminated, conglomeratic and massive hematite ore
Lava (LAV, LAW)	Postmasburg Group mafic lavas
Manganese Marker (MN, MM, MNE, CH, CHM)	Manganese and chert rich breccia (Wolharkop Formation)
Quartzite (QTZ, FLS)	Gamagara Group quartzites and flagstone
Shale (SH, SHM, SHT, SKT)	Various shale layers in Sishen's stratigraphic column

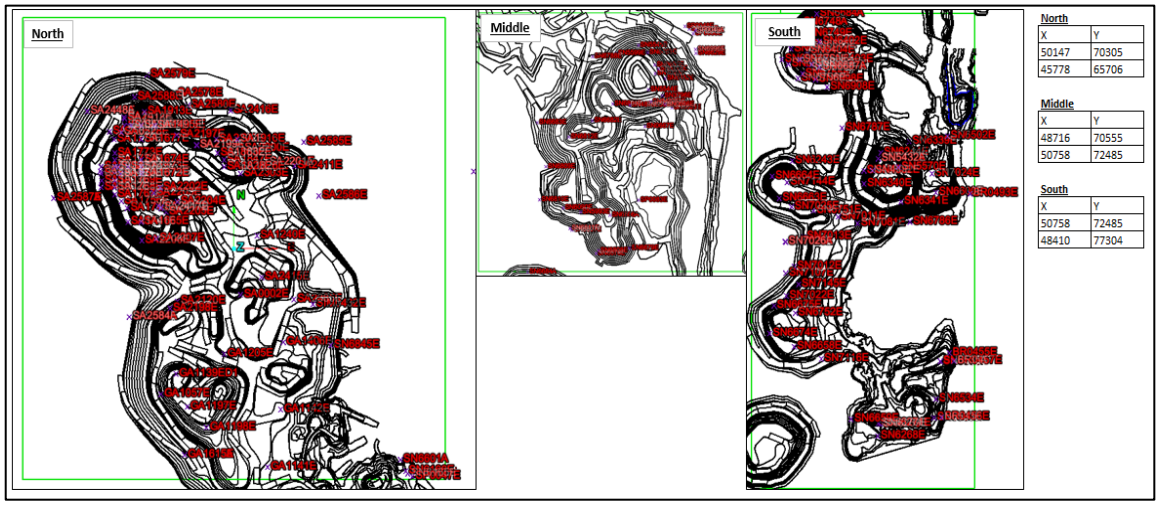

Figure 4.59: Mine divisions used for laboratory test, logging and mapping data queries.

BIF (BIF, LY, LYT) | All | All | North | Middle | South | RMR | GSI

MAPPING / LOGGING PARAMETER REPORT

Material Type BIF (BIF, LY, LYT)

Joint Spacing - Mapping

Count	2953
Min	0.02
Max	12.78
Average (Normal)	0.844
Std. Dev (Normal)	0.892
Average (Log Normal)	0.570
Std. Dev (Log Normal)	2.472
CV	105.64%

Joint Persistency - Mapping

Count	836
Min	0.14
Max	37.5
Average (Normal)	4.689
Std. Dev (Normal)	5.062
Average (Log Normal)	1.754
Std. Dev (Log Normal)	2.472
CV	107.95%

Fracture Frequency - Mapping

Count	2953
Min	0.0782
Max	50
Average (Normal)	2.705
Std. Dev (Normal)	3.343
Average (Log Normal)	2.837
Std. Dev (Log Normal)	2.904
CV	123.58%

Joint Spacing - Logging

Count	1746
Min	0.005
Max	70.85
Average (Normal)	0.926
Std. Dev (Normal)	2.459
Average (Log Normal)	0.389
Std. Dev (Log Normal)	3.512
CV	265.63%

Fracture Frequency - Logging

Count	584
Min	0.141
Max	122.22
Average (Normal)	9.115
Std. Dev (Normal)	8.412
Average (Log Normal)	0.000
Std. Dev (Log Normal)	0.000
CV	92.30%

Mapping RMR

Count	57
Min	51
Max	71
Average (Normal)	61.456
Std. Dev (Normal)	4.145
Average (Log Normal)	61.314
Std. Dev (Log Normal)	1.072
CV	6.74%

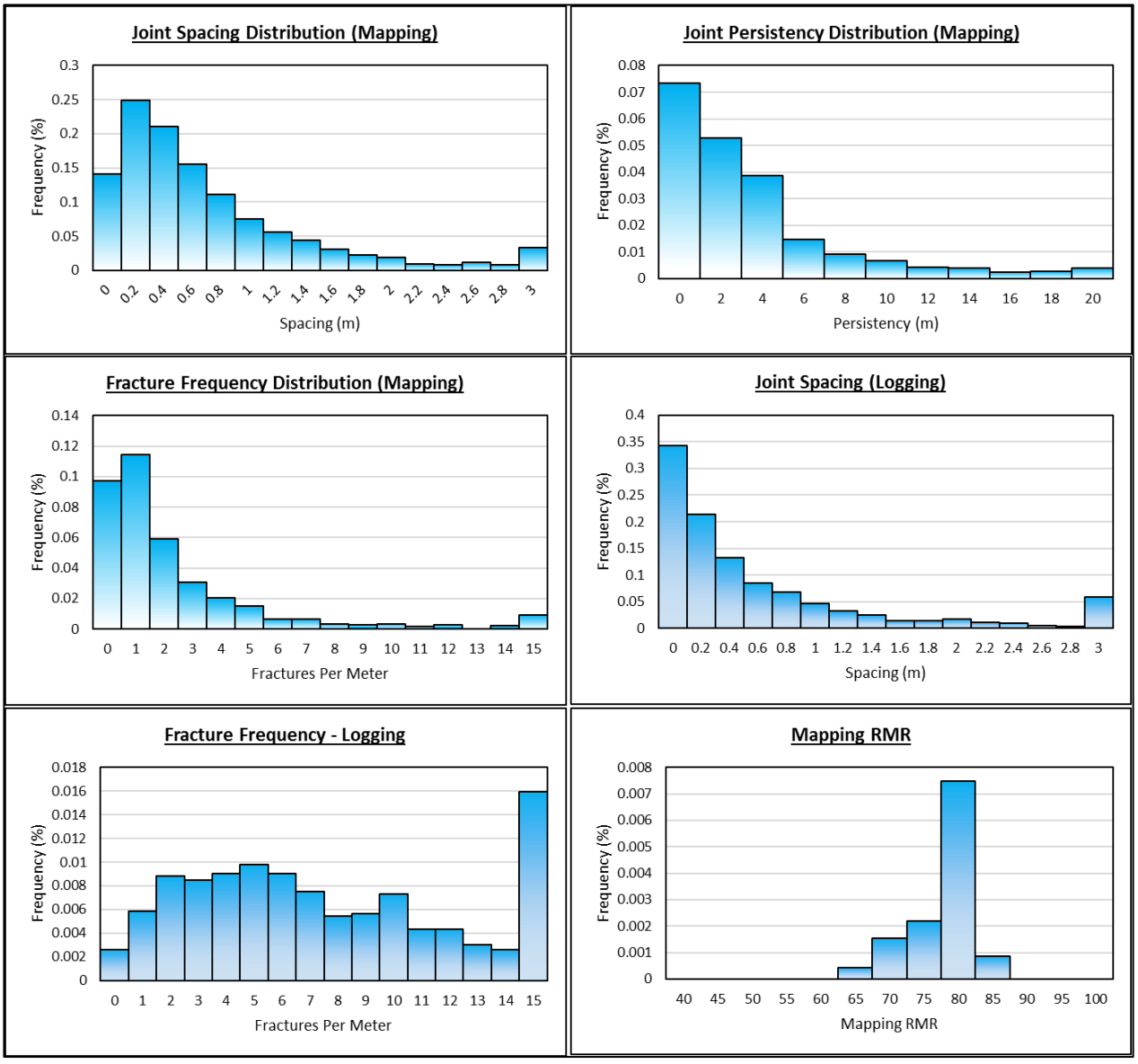

Figure 4.60: Mapping / Logging data query sheet.

BIF (BIF, LY, LYT) | All | North | Middle | South | Export

MATERIALS TESTING REPORT

Material Type	BIF (BIF, LY, LYT)	
Mi Calculation (UCS / UTB Paired Samples)	21	Target >10
Point Load UCS Factor (UCS / PLI Paired Samples)	50	Target >10

GSI / RMR	Mat
Count	579
Min	30
Max	83
Average	62.40
Std. Deviation	7.94
CV	12.72%

Point Load Index	Mat
Count	3145
Min	1
Max	719
Average	174.81
Std. Deviation	100.75
CV	57.63%

UCS	Mat
Count	82
Min	20.8
Max	650
Average	230.53
Std. Deviation	140.57
CV	60.98%

UTB	Mat
Count	63
Min	1.24
Max	51.10
Average	19.52
Std. Deviation	10.53
CV	53.94%

Youngs Modulus	Mat
Count	33
Min	11.2
Max	150
Average	87.76
Std. Deviation	26.71
CV	30.44%

Poissons Ratio	Mat
Count	33
Min	0.090
Max	0.408
Average	0.22
Std. Deviation	0.08
CV	36.30%

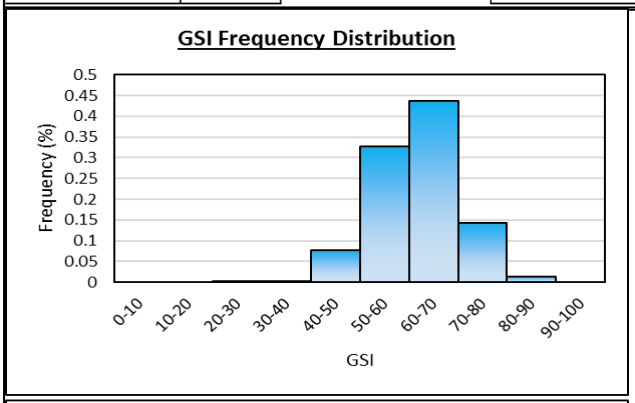

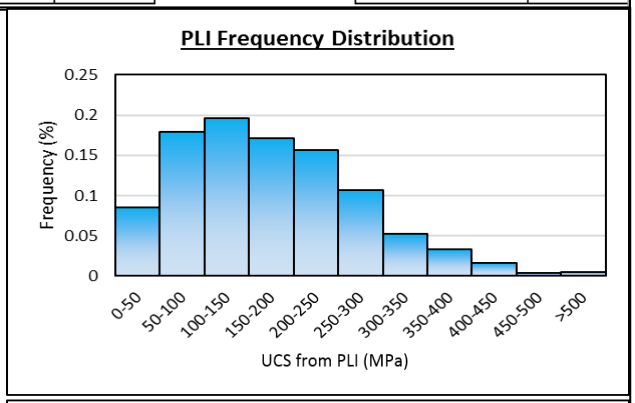

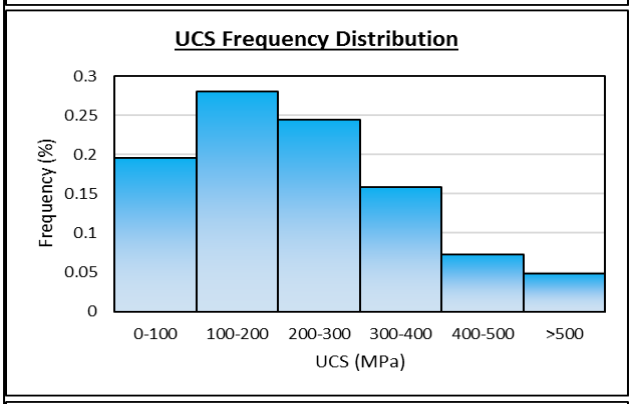

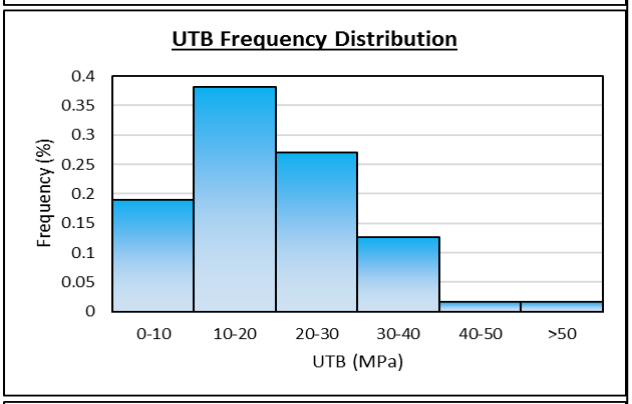

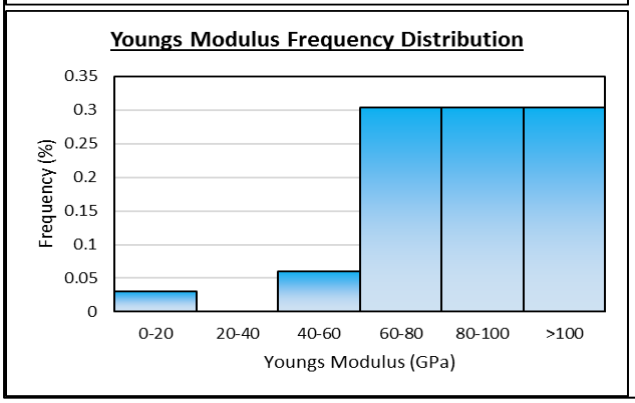

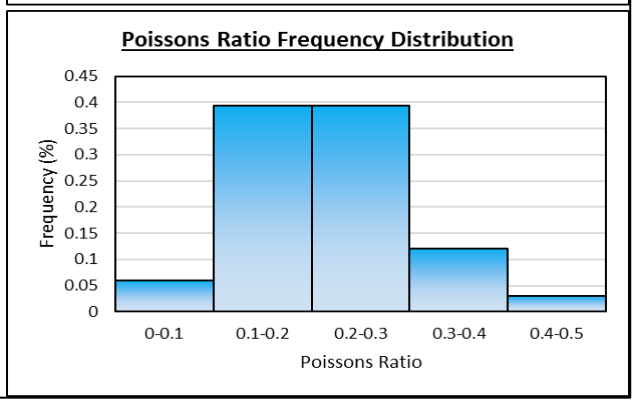

Figure 4.61: Laboratory testing data query sheet.

4.5. GEOTECHNICAL HAZARD IDENTIFICATION

The face mapping protocol discussed in the preceding sections in this chapter includes kinematic analysis and the generation of a face mapping report that contains analysis results and rock mass statistics for the mapped face. An example of a mapping report is given in Figure 4.62

FACE MAPPING ANALYSIS SHEET

Highwall ID	**F_47653_-67510_1045**
Mapped By	**T. Russell**
Pit	**GR80**
Area	**96**
Est. Base Friction Angle	**30**
Slope Dip	**65**
Slope Dip Direction	**215**
Approx Slope Face Area (m^2)	**977**
Approx Slope Face Length (m)	**64**

Output Summary

RMR = 73
Medium Jointed
Weathering - Slightly Weath.
High plain fail. potential
Low Wedge fail. potential

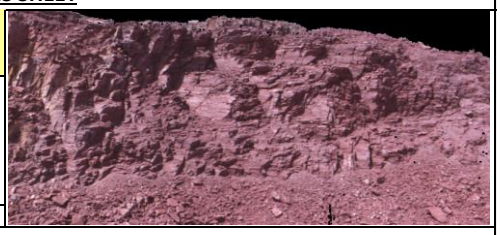

Slope Statistics

Mapping Statistics

Orientation		***Spacing***		***Persistence***	
Total Discontinuities Analysed	37	Total Spacing Measurements	54	Total Persistence Measurements	7
Bedding Planes	7	Bedding	35	Bedding	3
Joint Planes	30	Joints	19	Joints	4
0 - 30 Deg. (Shallow)	0	0 - 30 Deg. (Shallow)	30	0 - 30 Deg. (Shallow)	3
30 - 60 Deg. (Medium)	8	30 - 60 Deg. (Medium)	4	30 - 60 Deg. (Medium)	1
60 - 90 Deg. (Steep)	29	60 - 90 Deg. (Steep)	20	60 - 90 Deg. (Steep)	3
Average Area (m^2)	0.30	Average Spacing (m)	0.60	Average Persist. (m)	17.05
Average Length (m)	0.85	St.Dev	0.50	St.Dev	16.73

RMR Joint Space / Persist. Rating

Joint Spacing

Spacing - 0.6 = 10

Persistency

Persistency - 17.05 = 1

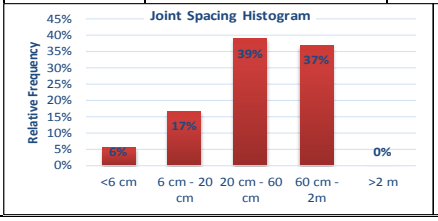

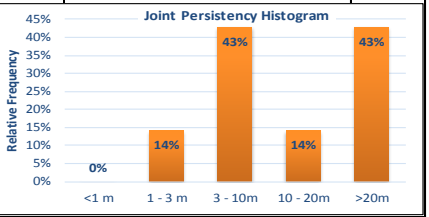

Slope Kinematics

Plane Failure Statistics		**Wedge Failure Analysis**	**Number**	**Percent**
Total Discontinuities Analysed	37	Total Intersection	666	
Potential Slipping Planes (%)	18.92%	Shallow Plunging (0 - 30 deg.)	340	51.05%
Favourable Slipping Planes (%)	18.92%	Medium Plunging (30 - 60 deg.)	162	24.32%
		Steep Plunging (60 - 90 deg.)	164	24.62%
		Kinematically Feasable Wedges	23	3.45%
		Large (>2m^2 area) Kinematically Feasable Wedges	0	0.00%

Major Planes	**Dip**	**Dip Direction**	**Plain Failure**	**Wedges**	**Intersection Line**	**Fail.**
Bedding	40	193	TRUE		18 / 125	FALSE
Joint	82	37	FALSE			

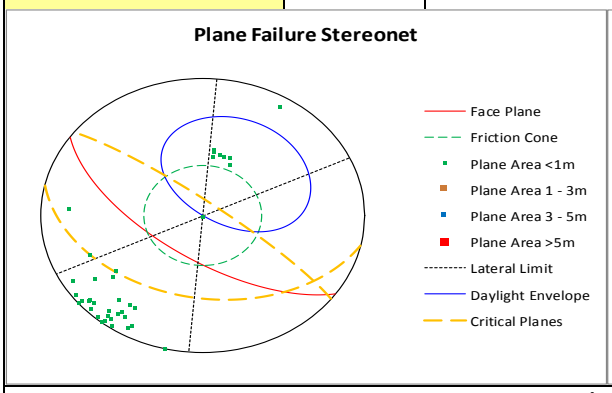

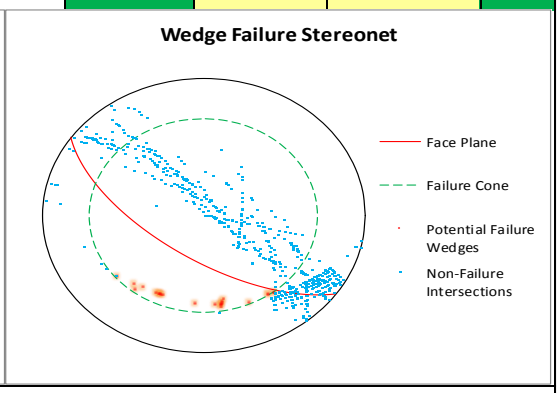

RMR / GSI

RMR Inputs	**Value**	**Rating**	**Joint Condition**	**Input**	**Rating**
Calc.RQD (3 Sets + Rand. assumed)	93	20	Persistency (m)	17.05	1
Estimated Rock Strength	Strong rock	7	Appeture	Closed	6
Calculated Joint Spacing	0.60	10	Roughness	Rough	5
Estimated Ground Water	Dry	15	Weathering	Slightly Weath.	9
RMR		**73**	Joint Condition Rating		21
GSI		**78**			

Figure 4.62: Face mapping analysis report.

Face mapping analysis and reporting has the function of feeding into the mine's monthly geotechnical hazard map by identifying plane and wedge failure hazards. A monthly geotechnical hazard map, developed from the assessment of face mapping as well as other sources of geotechnical data is produced on the mine. This map is distributed to the relevant personnel as part of ongoing geotechnical risk mitigation on the mine.

This chapter gives a detailed description of the functionality of the Maptek 8810 terrestrial laser scanner and associated software. The functionality and capabilities of the system are reviewed and the application of the system at Sishen Mine was outlined. The face mapping procedure and face mapping data management system developed during the course of this research project is described in detail.

The following chapter discusses some practical aspects of laser scanner face mapping, but focuses mainly on analysis of the data gathered during the course of this research project. Rock mass parameters captured during face mapping are compared with those obtained from geotechnical boreholes, with the effect on rock mass classification discussed. Inferred structural data from Sishen's geological models is compared with actual face mapping data as the integrity of the inferred data, and value of laser scanner face mapping as a ground proofing tool, is assessed. Finally, further applications of laser scanner face mapping relating to synthetic rock mass modelling, geotechnical block modelling and blast performance are discussed.

CHAPTER 5: RESULTS AND DISCUSSION

The previous chapter detailed the application of the Maptek 8810 terrestrial laser scanner system for geotechnical face mapping. Features of the system hardware and software were discussed and reviewed. The face mapping procedure and data management process developed for Sishen Mine was described in detail from the face mapping process to data analysis, storage and reporting.

In this chapter a review of the performance of the Maptek laser scanner system is given, outlining the practical constraints and merits of the system revealed during the data collection phase of this project. Rock mass data gathered from faces mapped during data collection will be compared with Sishen's geotechnical borehole dataset. Face mapping discontinuity orientation and fault trace data will be compared with inferred data from the mine's existing structural model. Use of face mapping data in synthetic rock mass models and potential future use in geotechnical block modelling and blastability analysis will be discussed.

5.1. OBSERVED ADVANTAGES AND DISADVANTAGES OF THE SYSTEM

5.1.1. Mapping of Scanned Faces and Data Capture

5.1.1.1. Safety and Accessibility

A significant benefit of laser scanner face mapping, as opposed to manual face mapping or stereo photo face mapping, which became immediately apparent when the Maptek system was first introduced on the mine, was the safety and accessibility aspect. In the open pit mining environment most mapping faces are recently exposed and have generally been damaged to a degree by the blasting process. The risks associated with falling rocks and bench scale failures are far higher in the immediate area below a mined out face than for natural outcrops, which are closer to an equilibrium state with respect to weathering and stability. Furthermore, access to benches is usually quickly cut off by the progression of mining activities in most open pits. Benches that are not on an active working level of the mine are generally not accessible.

Both manual face mapping and stereo photo mapping techniques require that either a geologist or surveyor have direct access to the mapping face. This increases exposure to the geotechnical risks present at the base of a mapping face and limits face mapping to accessible faces. Laser scanner face mapping requires no direct access to the mapping face for surveying of reference points or direct measurement of mapping parameters. The associated negative aspect of gathering all data

remotely is that some geotechnical parameters can only be obtained by physical contact with the mapping face. If laser scanner face mapping is to be used as a means of geotechnical data capture, ground proofing of estimated rock mass parameters should be carried out when the mapping face is safely accessible.

5.1.1.2. Data Capture Process

The mapping data capture process has been described in detail in Chapter 4. The data capture challenge encountered when setting up a laser scanner face mapping protocol is one often faced when capturing large amounts of geotechnical data, that of ensuring data capture is organized in such a way that meaningful information can be extracted when required. Data that is not referenced using a logical naming convention, is not date referenced, does not conform to a meaningful co-ordinate system, is incomplete in terms of parameters captured per data point or is stored in a disjointed filing system can be of little use in future analysis. Furthermore, a data management system needs to be documented in such a way that the system can be managed and understood by any new staff taking over the data management and administration role. As outlined in Chapter 4, the laser scanner face mapping protocol developed as part of this research consists of the following features.

- Laser scanner data and specialized software to allow for digital face mapping.
- A set of Microsoft Excel templates and macros to process and manage data exported from the face mapping software.
- A CSV data storage system to allow for importing into the Acquire Database System.
- The Acquire Geological Database system where mapping data is stored together with geotechnical borehole data and laboratory test data.
- The ODBC linked Micromine workspace where mapping and borehole data can be viewed in conjunction with geological, survey and mine planning data.

Over the course of the data collection phase of this project the data management system proved to be robust and effective, with all of Sishen's Geotechnical Engineering personnel using the system to carry out face mapping without any major issues. Data and analysis reports for all of the 86 faces mapped by the conclusion of the data collection phase of this project has proved to be easily accessible.

Although an excellent tool for facilitating data capture, analysis and manipulation, Microsoft Excel and VBA macro's have inherent disadvantages that are considered a major weak point in the above mentioned data capture system.

Firstly, the Excel Templates and macros that form part of the data capture system are reliant on the import data format from I-Site Studio. Any future release of I-Site Studio that adjusts the software's text file export format will result in errors in the Microsoft Excel import macros. Although functionality of the VBA code is documented in the Excel import template, the required programming skills to make the necessary adjustments may not be available.

Secondly, unless strict spreadsheet protection measures are put in place, functionality may inadvertently be affected by end users adjusting portions of the spreadsheet. Version and integrity control of Excel templates needs to be strictly maintained at all times for any system incorporating Microsoft Excel.

It can be concluded that the data management system developed as part of this research is adequate for capture and storage of routine laser scanner face mapping data. What would however be considered best practice is for the software vendor (Maptek) to extend I-Site Studio's internal Geotechnical Data Analysis module to include data reporting, management and export functionality. The proposed outline for such a system, based on the research described in this report is as follows.

5.1.1.3. Idealized I-Site Studio Kinematic Analysis Process

- **Discontinuity Capture**

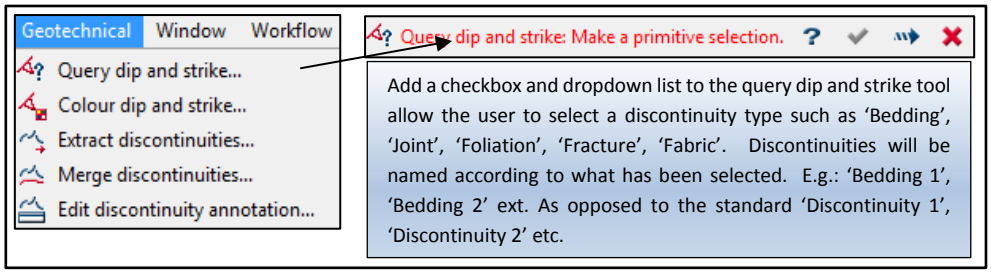

Figure 5.1: Conceptual changes to the I-Site Studio discontinuity orientation capture process.

- **Spacing and Persistency Capture**

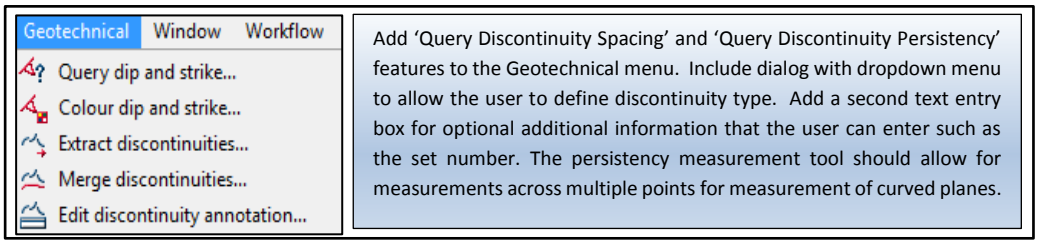

Figure 5.2: Conceptual addition of spacing and persistency query functions to I-Site Studio.

- **Data Import into Stereonet Report.**

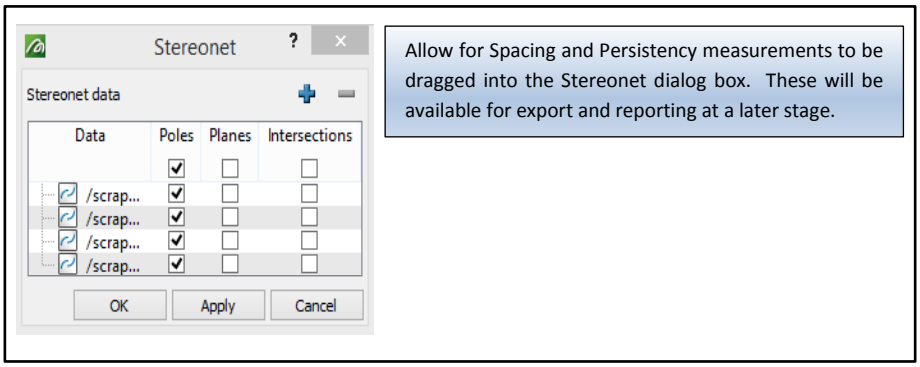

Figure 5.3: Conceptual addition to allow spacing and persistency measurements to be added to stereonet object for later reporting.

- **Stereonet Analysis (Figures 5.4 and 5.5)**

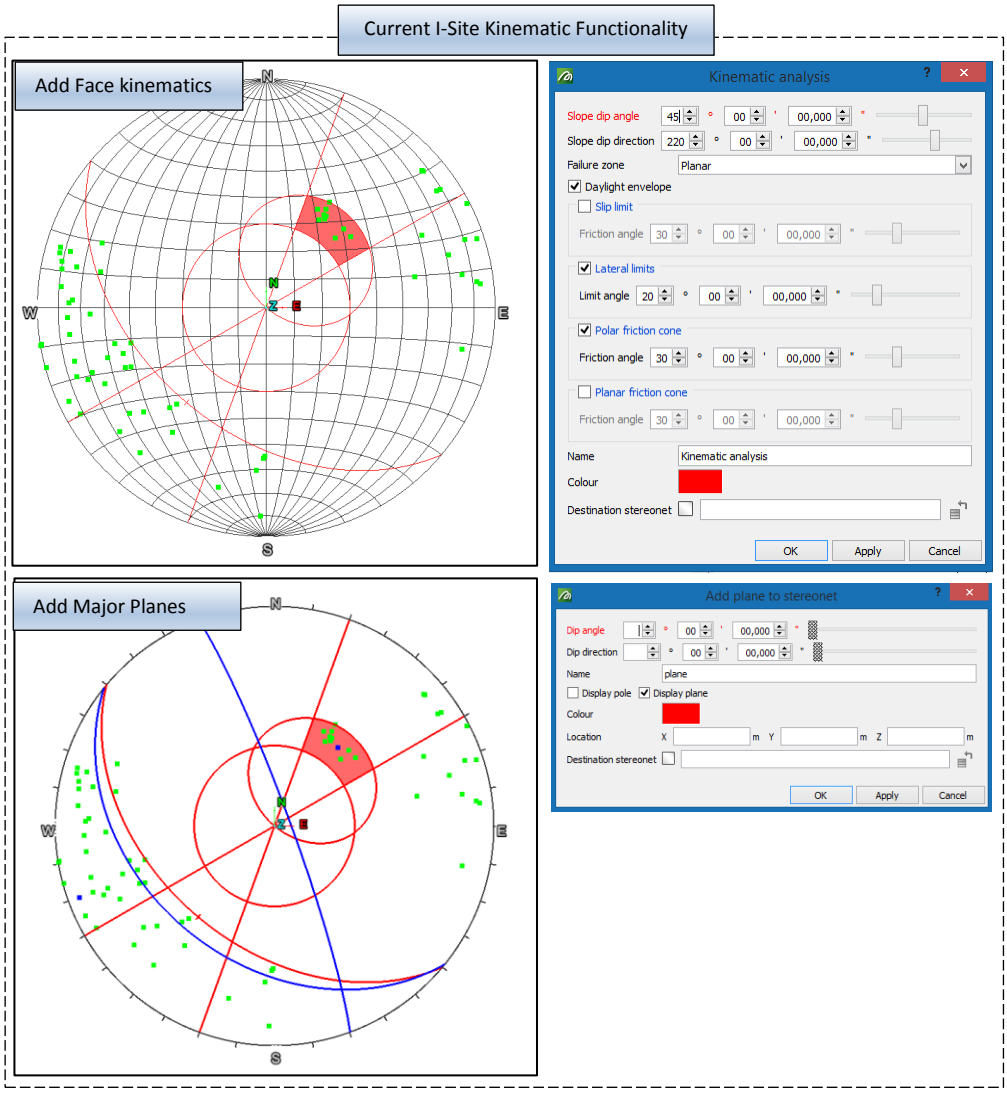

Figure 5.4: Actual I-Site Studio stereonet functionality.

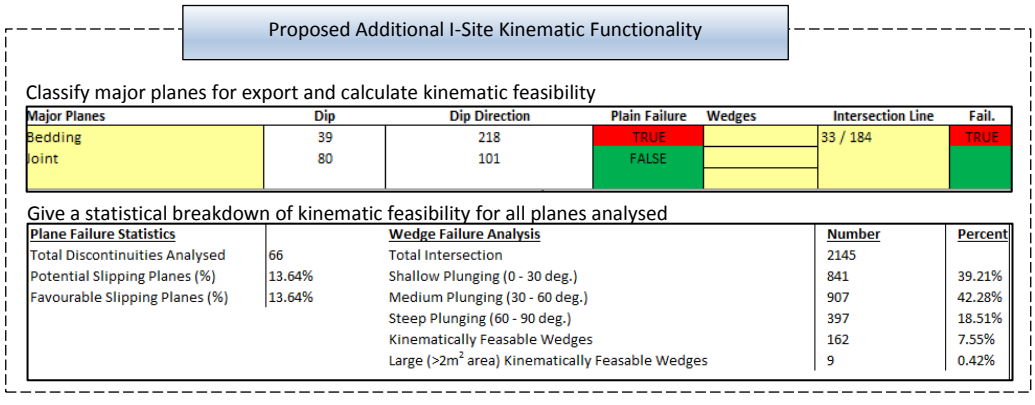

Figure 5.5: Possible I-Site Studio stereonet functionality extensions.

- **Rock Mass Classification**
  - Some form of rock mass classification such as a visual GSI assessment (Figure 5.6) or a dropdown list allowing RMR classification should be included in the analysis.

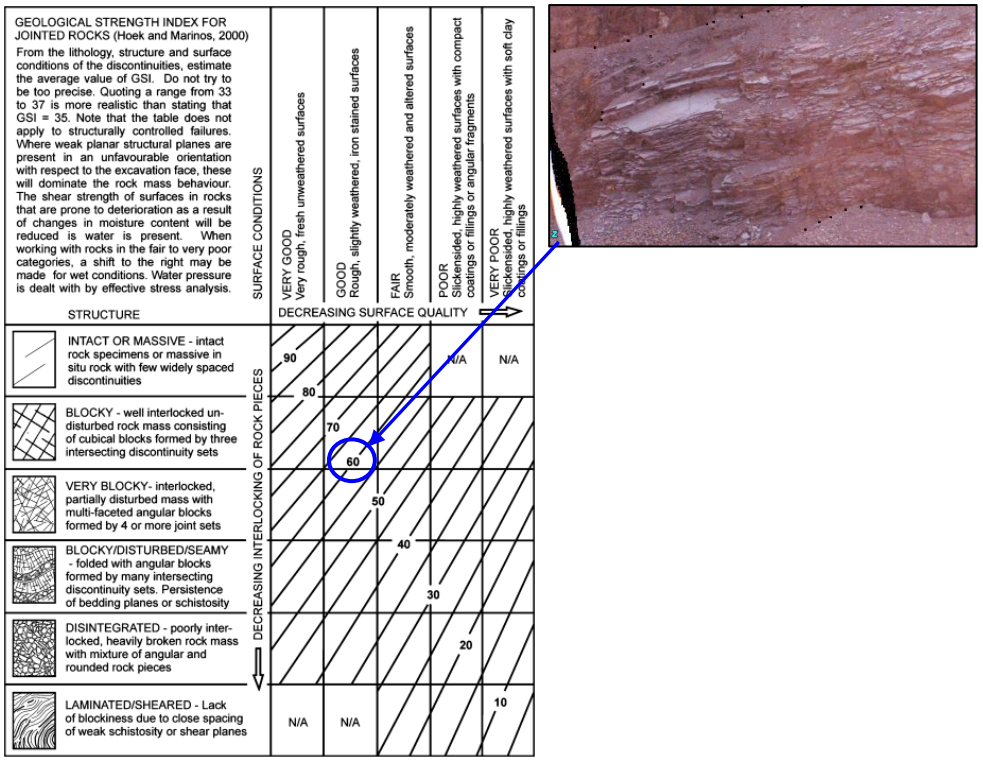

Figure 5.6: Potential GSI rating system to be incorporated into mapping analysis (Hoek et al., 2005).

- **Kinematic Analysis Reporting**
  - Allow for a report to be generated with all relevant data collected from the face (Figures 5.7, 5.8 and 5.9).

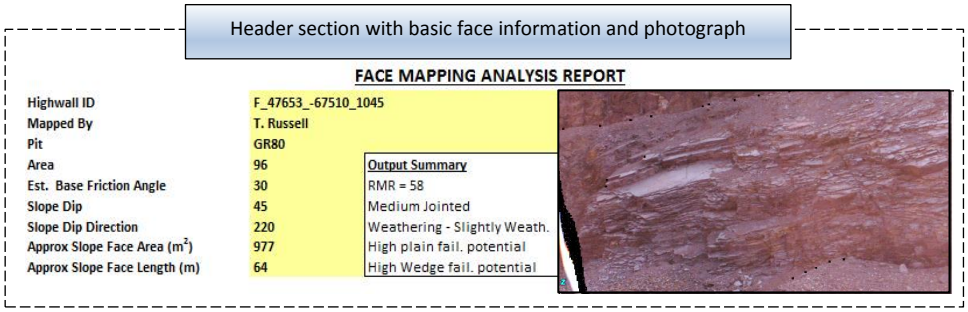

Figure 5.7: Example face mapping report header section.

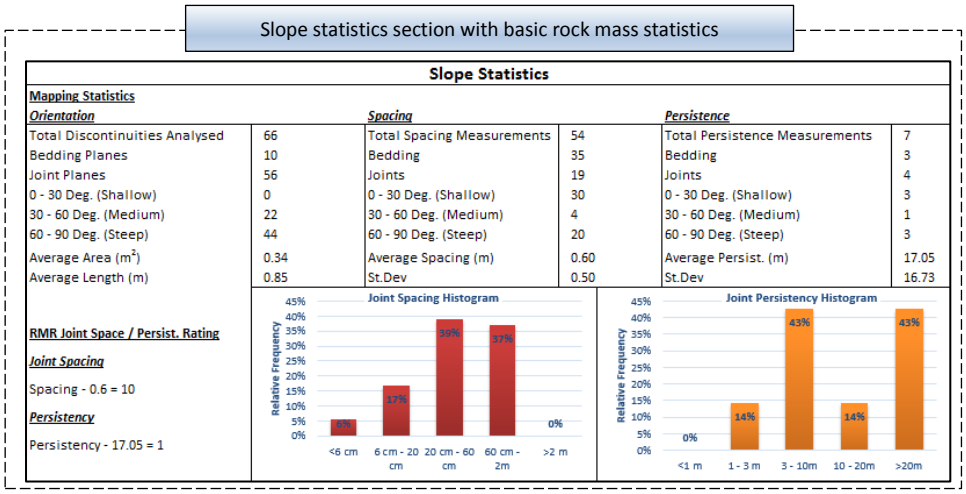

Figure 5.8: Example face mapping report rock mass statistics section.

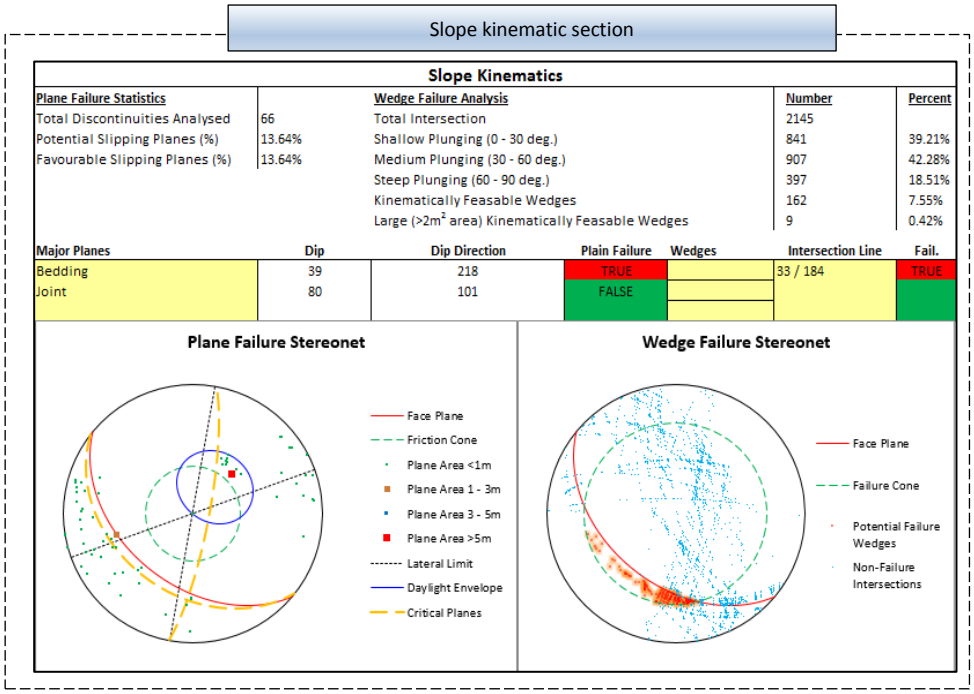

Figure 5.9: Example of face mapping report kinematic analysis section.

- **Data Export**

  All data should be exportable in a user defined CSV format that will allow individual sites to export kinematic analysis data according to their requirements. As discussed in Chapter 4, a separate collar and detail table format makes it possible to capture multiple records per face (for parameters such as orientation) and single records pertaining to the face itself (such as GSI) in an organized manner.

5.1.2. Economic and Practical Aspects of Laser Scanning

Sishen Mine represents a relatively large open pit mining operation in terms of the tonnages mined, the overall pit area and the rate at which mining areas are deployed. The extent of the operation, the economic gains from optimized slope angles and the potential consequences of slope failure have had the advantage that budget has never been an issue with respect to geotechnical data collection. The benefits of increased geotechnical confidence have always far outweighed the costs of investing in geotechnical drilling, materials sampling and any technology that can further improve geotechnical data confidence.

Purchase of the Maptek laser scanning unit at Sishen Mine was a worthwhile investment when considering the potential benefits in terms of geotechnical data confidence as well as the other survey functions of which the unit is capable. The relevance of the technology does however need to be considered in the context of smaller open pit mining operations and the variety of mining and civils projects that require geotechnical face mapping data. The cost of a single Maptek 8810 Scanner system is in the order of R2 000 000 (2017). This may well not be worth the investment for smaller projects where face mapping requirements are less and where dedicating available resources and personnel to manual face mapping exercises is feasible.

In addition to the economic aspect of laser scanner face mapping systems, there is also the practical aspect of who will operate and maintain the scanner system on site. The manufacturers of the system have done well to ensure that the scanner set-up, scanning and data processing can be done with relative ease. A short training course by the suppliers was enough for Sishen's Geotechnical Engineering Section to operate the system independently, without any outside assistance or inputs. Although easy to operate by an essentially untrained person, the data that the system produces is spatial in nature. For this reason the system should be operated by a qualified surveyor who has the relevant competencies to ensure that the system is operated properly and that the data produced is valid with respect to the co-ordinate system in use by the operation or project. Considering this, Sishen's Geotechnical Engineering Section handed over operation of the unit, as well as scan processing and registering, to the Sishen Mine Survey Department. An alternative to this approach in situations where a qualified surveyor is not available for scanning and processing of data would be to have a qualified person acting in an oversite role to ensure data integrity is maintained.

5.2. COMPARISON OF BOREHOLE AND FACE MAPPING DERIVED ROCK MASS RATING PARAMETERS

5.2.1. Discontinuity Spacing / Fracture Frequency

Fracture frequency and discontinuity spacing are inter linked parameters with the fracture frequency of a length of borehole core essentially representing the inverse of the average joint spacing. Comparisons made in this section will be based on the direct discontinuity spacing measurements that have been used to derive fracture frequency values. With the datasets available the following broad comparisons are considered appropriate.

- Bedding spacing per lithology
- Intermediate and steep discontinuity / joint spacing per lithology

Borehole joint spacing data has been captured to date on Sishen Mine based on a simple classification system that captures data as either 'Bedding / Laminations', 'Shallow Joints dipping between 0 – 30 degrees', Intermediate Joints dipping between 30 – 60 degrees', and steep Joints dipping between 60 – 90 degrees'. During logging the number of discontinuity planes conforming to each class is counted and recorded for each logged geotechnical zone. The approximate dip for each joint set present is also recorded. When joint count values are entered into the Acquire Database the apparent spacing is calculated by dividing the number of joints by the total length of the geotechnical zone in question for each joint set. The Terzaghi Correction is then applied to account for the angle between the borehole and discontinuity set, converting the apparent spacing into a true spacing value.

5.2.1.1. Bedding Spacing

The majority of rock types at Sishen are either sedimentary or meta-sedimentary, characterized by actual or relict bedding or lamination structures. Although faulted and folded with a wide variety of bedding dips most sedimentary features within the mines geological setting are shallow dipping. Shallow dipping joint sets and structural features are generally indistinguishable from sedimentary features, and for this reason the shallow (0 – 30 degree) discontinuity set has been logged interchangeably as either bedding or joints with no clear distinction between the two. For this analysis it is considered a fair assumption to use the 0 – 30 degree dipping discontinuity set as bedding, and discontinuities in the 30 – 90 degree dip range as joints. Bedding spacing statistics for laminated rocks from borehole and mapping data are given in Table 5.1, with comparative histograms presented in Figure 5.10.

Table 5.1: Statistical bedding spacing parameters for data acquired from borehole logging and face mapping.

	BIF		Shale	
Parameter	Borehole Log	Face Mapping	Borehole Log	Face Mapping
Count	966	1614	1074	940
Best Fit Distribution	Log Normal	Log Normal	Log Normal	Log Normal
Average (Normal)	0.89	0.65	0.52	0.58
Average (Log Normal)	0.36	0.42	0.42	0.37
Min	0.009	0.020	0.002	0.030
Max	70.85	12.78	11.59	5.59
St Dev (Normal)	2.90	0.79	0.88	0.70
St Dev (Log Normal)	3.41	2.53	2.53	2.56
Spacing Less than 10cm (%)	15%	6%	16%	7%

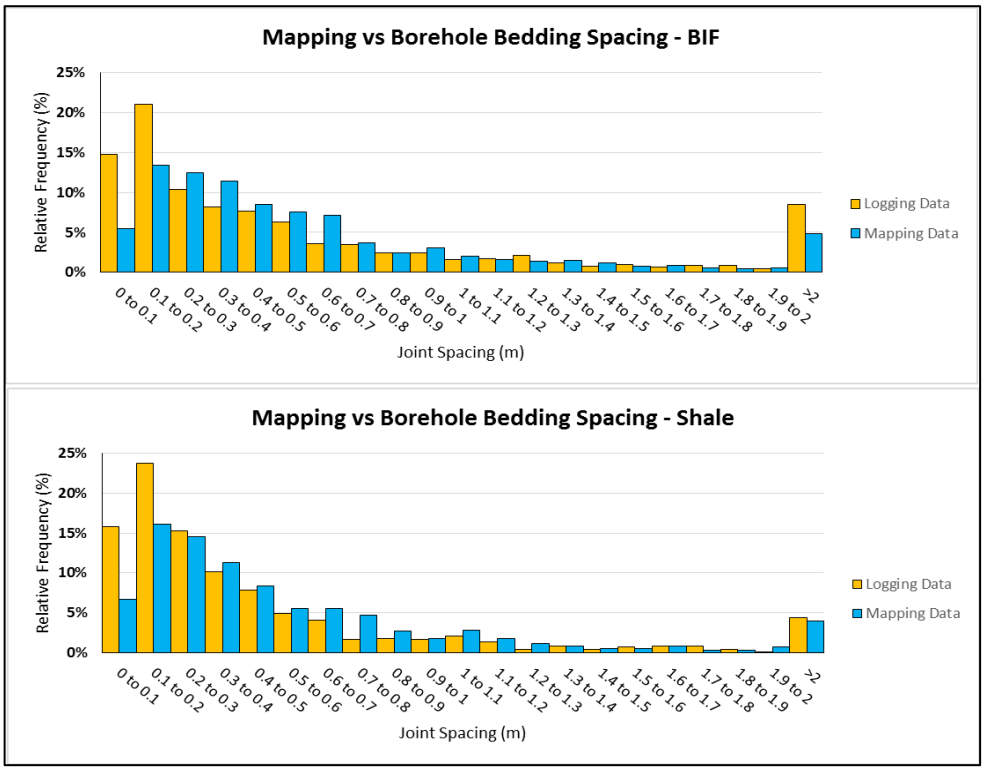

Figure 5.10: Comparison of bedding spacing data distributions for mapping and borehole logging data – laminated units.

With respect to non-laminated rock types, comparison between borehole and mapping data is restricted to the cherty and manganese rich collapse breccia of the Wolhaarkop Formation, as this was the only non-laminated unit exposed and mapped during the data capture phase of this project. As this unit is a brecciated material, the comparison is technically between the shallow dipping discontinuity planes as opposed to true sedimentary bedding structures. Bedding spacing statistics for Wolhaarkop Formation breccia is given in Table 5.2, with comparative histograms presented in Figure 5.11.

Table 5.2: Statistical bedding spacing parameters for data acquired from borehole logging and face mapping for the non-laminated Wolhaarkop Formation.

	Borehole	Mapping
Count	26	53
Best Fit Distribution	Log Normal	Log Normal
Average (Normal)	0.54	1.29
Average (Log Normal)	0.28	1.09
Min	0.030	0.200
Max	5.65	4.81
St Dev (Normal)	1.09	0.83
St Dev (Log Normal)	2.68	1.81
Spacing Less than 10cm (%)	4%	0%

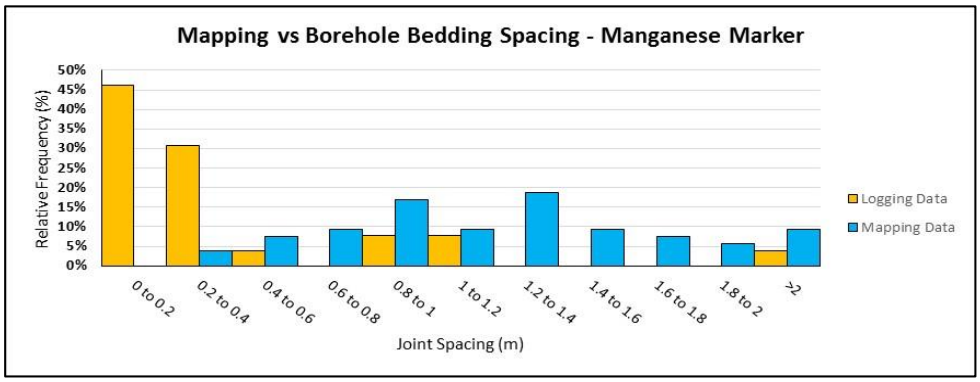

Figure 5.11: Comparison of bedding spacing data distributions for mapping and borehole logging data – non-laminated unit.

Comparison of the distributions of face mapping and borehole logging derived bedding spacing measurements, for both laminated and non-laminated units reveal the following.

- Spacing measurements generally conform to a lognormal distribution.
- The lognormal and arithmetic mean are higher for face mapping measurements than borehole measurements.
- Borehole measurements produce a wider distribution with more outliers at the high end of the spacing distribution.
- The difference between mapping and borehole derived spacing measurements is significantly greater for non-laminated rock types than for laminated rock types.

The higher spacing values acquired from face mapping data can be expected if some of the characteristics typical of borehole core and mapping faces are taken into account. Firstly, the drilling process can create additional fractures or open up healed fracture surfaces through the attrition and mechanical forces associated with

the drilling process. Secondly, stress release during drilling can result in fracturing, particularly along pre-existing weakness planes such as bedding laminations. The combination of mechanical attrition and stress changes in the borehole core has the effect of breaking up the core, creating further fracture planes over and above the natural in-situ discontinuity planes that will be picked up in a mapping face.

With respect to face mapping it was found during the course of this study that, although direct measurements of joint spacing on a photo overlay of a mapping face generally produce accurate and representative results, there is a practical lower measurement limit dictated by the resolution of the camera. This will typically result in fewer measurements of joints at the lower spectrum of the range, particularly on faces where the lighting for the photograph is not ideal.

5.2.1.2. Joint Spacing

As discussed previously in this section, borehole logging has generally been done at Sishen, classifying discontinuity planes in the 0 – 30 degree dipping range as bedding planes, with steeper discontinuities classified as joints. This is generally a reasonable assumption for sedimentary and metasedimentary rocks in the Sishen geological setting. Comparison of mapping and borehole logging derived joint spacing values are given in Tables 5.3 and 5.4, and Figures 5.12 and 5.13. It is important to note that borehole derived spacing values use the Terzaghi Correction to produce a true spacing value, and this can have a significant effect on steeply dipping joint sets which are orientated sub parallel to the borehole core axis.

Table 5.3: Statistical joint spacing parameters for data acquired from borehole logging and face mapping.

	BIF		Shale	
Parameter	Borehole Log	Mapping Face	Borehole Log	Mapping Face
Count	779	1339	924	631
Best Fit Distribution	Log Normal	Log Normal	Log Normal	Log Normal
Average (Normal)	0.96	1.08	0.75	1.18
Average (Log Normal)	0.43	0.82	0.82	0.88
Min	0.005	0.100	0.000	0.080
Max	27.34	9.02	13.35	19.41
St Dev (Normal)	1.76	0.95	1.21	1.24
St Dev (Log Normal)	3.58	2.06	2.06	2.09
Spacing Less than 10cm (%)	13%	0%	11%	0%

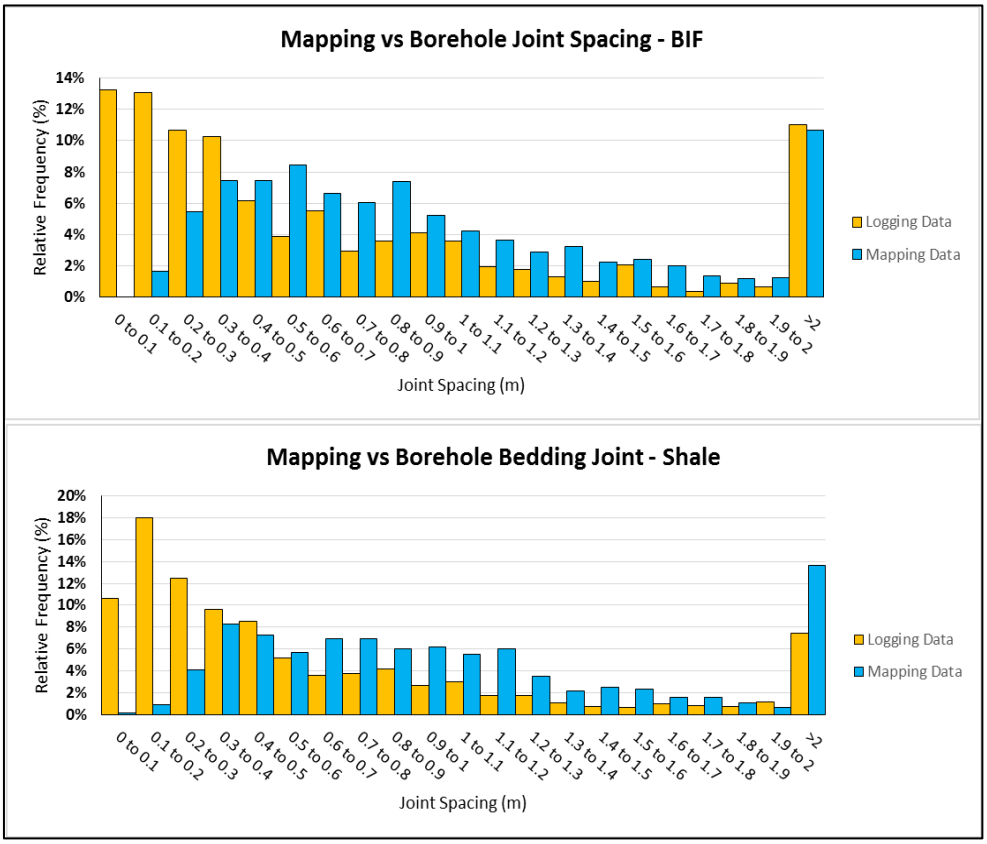

Figure 5.12: Comparison of joint spacing data distributions for mapping and borehole logging data – laminated units.

As for bedding spacing comparisons, the manganese and chert rich breccias of the Wolhaarkop Formation have been used to compare borehole logging and face mapping joint spacing values for non-laminated units.

Table 5.4: Statistical joint spacing parameters for data acquired from borehole logging and face mapping for non-laminated manganese marker unit.

	Borehole	Mapping
Count	46	50
Best Fit Distribution	Log Normal	Log Normal
Average (Normal)	1.74	1.18
Average (Log Normal)	0.95	1.04
Min	0.067	0.270
Max	18.82	4.88
St Dev (Normal)	2.80	0.71
St Dev (Log Normal)	3.11	1.64
Spacing Less than 10cm (%)	4%	0%

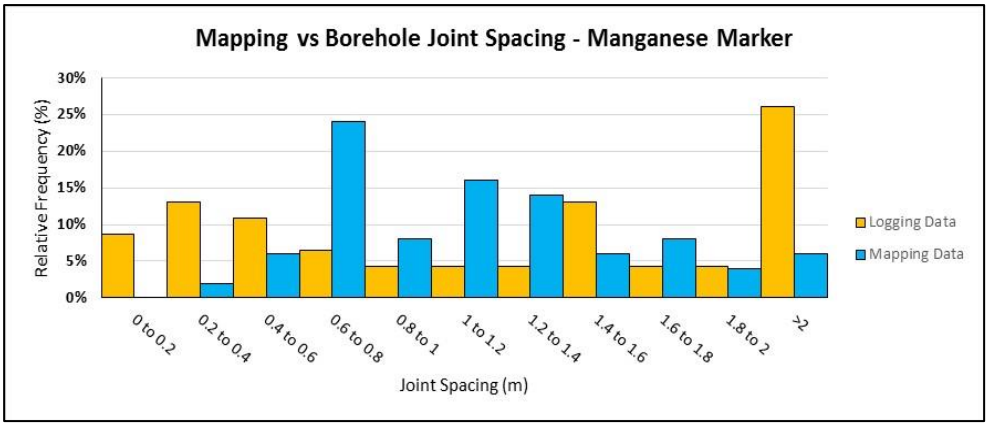

Figure 5.13: Comparison of joint spacing data distributions for mapping and borehole logging data – non-laminated unit.

As for bedding spacing values, the borehole derived spacing values tend to produce a wider distribution that those directly measured from mapping faces. In addition to the potential error sources mentioned in Section 5.2.1.1, errors associated with the acute intersection angle between steeply dipping discontinuities and the vertical drill holes used at Sishen appear to affect on the data spread. Adjustments according to the Terzaghi Correction are magnified as the angle between the borehole axis and discontinuity set reduces towards zero. In addition to this there is an element of chance as to whether a particular borehole will even intersect steeply dipping discontinuities. Outliers on the lower and upper end of the spacing spectrum can be attributed to the nature of drilling at low angles relative to the discontinuity planes and the attempt to correct for the orientation bias that arises therefrom. Overall, direct face mapping measurements are considered to be a more reliable means of determining the spacing of inclined and steeply dipping joint sets than measurement from vertically inclined boreholes.

5.2.2. RQD

The Rock Quality Designation (RQD) is a basic measurement to evaluate the conditions of a rock mass. When measured from borehole core, the RQD is calculated using the following formula.

$$\boldsymbol{RQD}(\%) = \left(\frac{\boldsymbol{Sum\ of\ pieces{>}10cm\ long}}{\boldsymbol{Total\ Core\ Run\ Length}}\right) \times \mathbf{100} \qquad \text{Deere et al. (1967)}$$

As discussed in Chapter 3 there are various empirical equations for deriving RQD from face mapping data. These include the following commonly applied empirical relationships.

RQD = 100 $e^{-0.1\lambda}$ (0.1λ + 1) Priest and Hudson (1976)

RQD = 115 – 3.3 Jv Palmström (1982)

RQD = 110 – 2.5 Jv Palmström (2005)

The relationship proposed by Priest and Hudson has been omitted from the analysis as most mean fracture frequency values (derived from mean discontinuity spacing) in the Sishen face mapping dataset fall below the lower limit of the range recommended by Priest and Hudson (1976).

Required inputs for each of the remaining two RQD formulae were gathered during routine face mapping as per the standard mapping procedure outlined in Chapter 4. RQD has been captured as a standard logging parameter in all geotechnical boreholes logged at Sishen Mine. Comparison of RQD values acquired from logging data and mapping data, per major lithology, are given in Table 5.5 and Figure 5.14. For comparison purposes only Shale and Banded Iron Formation values have been used, as the majority of mapping faces have been mapped in these lithologies.

Table 5.5: Statistical RQD parameters for data acquired from borehole logging and face mapping.

Geotech. Unit	Data Collection	Formula	Best Fit Distribution	Average	Min	Max	St Dev	CV
BIF and Shale	Mapping	RQD = 115 - 3.3Jv	Normal	94	60	100	8	9%
		RQD = 110 – 2.5Jv	Normal	95	68	100	7	7%
	Logging	RQD = (Sum >10cm)/TCR	Discrete Uniform	48	0	100	33	68%
BIF	Mapping	RQD = 115 - 3.3Jv	Normal	94	72	100	7	8%
		RQD = 110 – 2.5Jv	Normal	96	77	100	6	6%
	Logging	RQD = Sum >10cm/TCR	Discrete Uniform	48	0	100	33	69%
Shale	Mapping	RQD = 115 - 3.3Jv	Normal	91	60	100	11	12%
		RQD = 110 – 2.5Jv	Normal	92	68	100	9	9%
	Logging	RQD = Sum >10cm/TCR	Discrete Uniform	48	0	100	32	66%

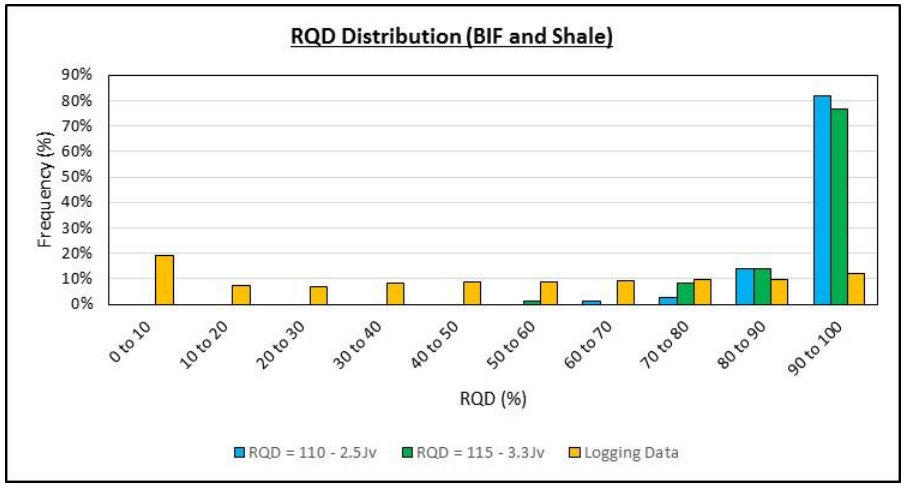

Figure 5.14: Comparison of RQD data distributions for mapping and borehole logging data.

Data presented in Table 5.5 and Figure 5.14 shows an obvious contrast between the RQD values acquired from face mapping and those obtained from the borehole logs. Face mapping derived values are significantly higher and tightly clustered close to the upper end of the RQD range while borehole logging values are relatively evenly distributed through the range. The poor reconciliation between borehole and face mapping RQD values can be explained in part in terms of the measurement / calculation procedure being used and in part due to the nature of the material being measured.

Face mapping RQD measurements are derived based on average joint spacing per mapping face. The default procedure applied on the face mapping calculation template uses the arithmetic mean joint spacing to derive a volumetric joint count (Jv) assuming 3 major joint sets and a random set. The volumetric joint count is then used to calculate RQD using the equation RQD = 115 – 3.3Jv as a default, as per the calculation method outlined by Palmström (1982). This should theoretically produce a similar result to those obtained during borehole logging. Figure 5.15 below gives a comparison of mean joint spacing (for an assumed 3 sets + random) and RQD when the Palmström (1982) formula is applied.

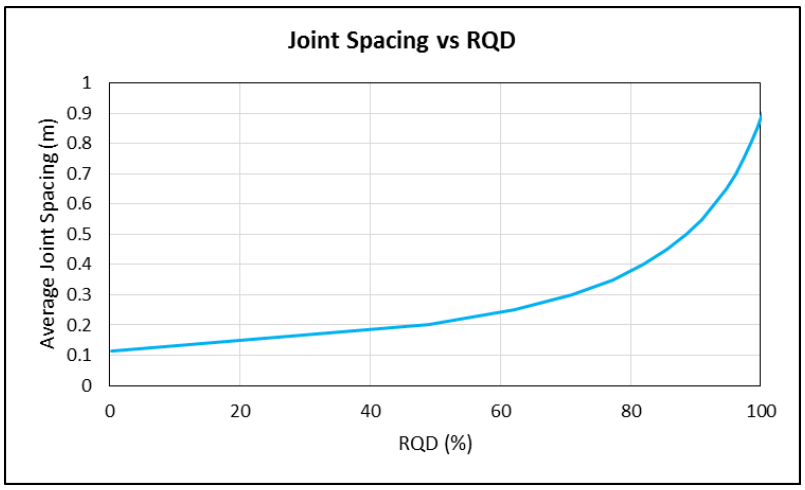

Figure 5.15: Relationship between RQD and Joint Spacing according to the equation RQD = 115 – 3.3Jv.

An analysis of measured joint spacing distributions from mapping data is given in Section 5.2.1. It is shown that the borehole and mapping derived joint spacing values conform closely to a lognormal distribution, with the majority of measured values falling below the arithmetic sample mean. By taking the arithmetic mean Palmström (1982) implies a normally distributed dataset, and logic dictates that this will over-estimate the joint spacing for lognormally or negative exponentially distributed data sets.

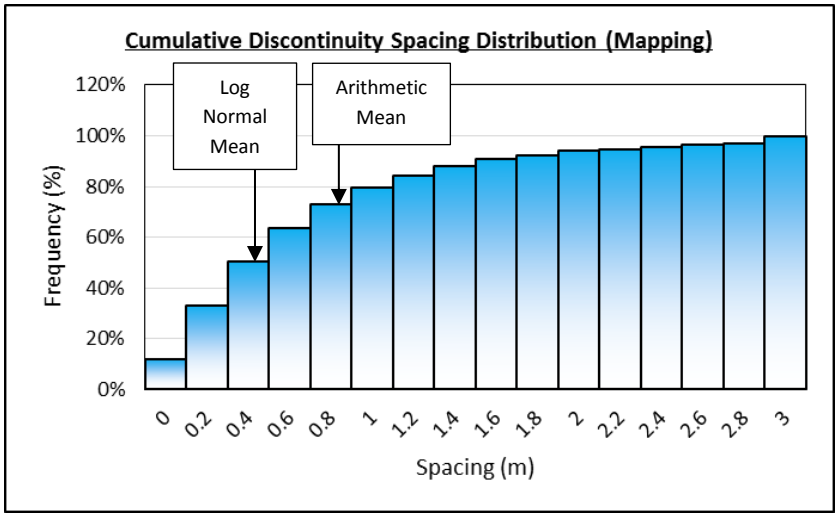

Figure 5.16: Cumulative joint spacing for Banded Iron Formation from mapping data with Arithmetic and Log Normal mean positions indicated.

As indicated in Figure 5.16 73% of the measured discontinuity spacing values for Banded Iron Formation are below the Arithmetic Mean of 0.85m. Use of the lognormal mean is considered a better representation of the population of the discontinuity data sets. A comparison of RQD values derived using the arithmetic and lognormal means for Banded Iron Formation is given in Table 5.6 and Figure 5.17.

Table 5.6: RQD statistics derived from the arithmetic and lognormal discontinuity spacing mean of each mapping face.

	Arithmetic Mean	Log Normal Mean
Average RQD	94	89
Standard Deviation	7	11
Min	72	54
Max	100	100
CV (%)	8%	13%

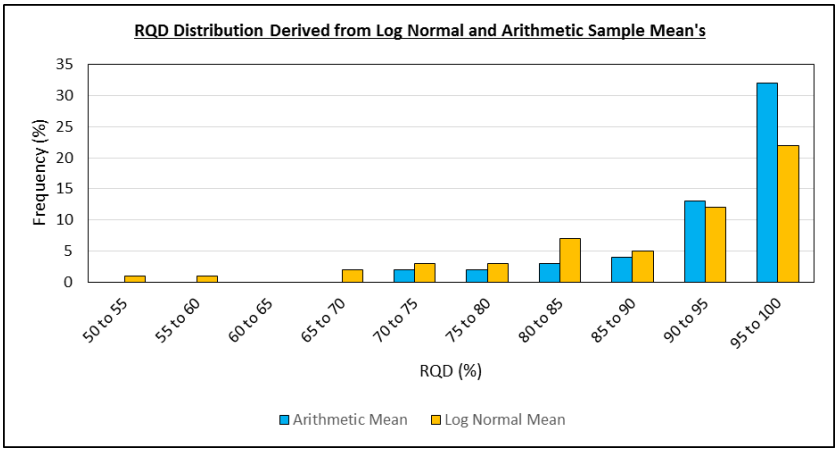

Figure 5.17: Comparison of face mapping RQD values derived from the Arithmetic and Log Normal discontinuity spacing mean of each mapping face.

Although there is a slight reduction in the average RQD when the true statistical distribution is used in deriving the Volumetric Joint Count as opposed to a simple arithmetic mean, calculated values remain generally higher than those derived from borehole logging.

Comparisons made in Section 5.2.1 between borehole and face mapping discontinuity spacing values showed a similar disparity. What was apparent from the analysis of bedding and joint spacing data was that in laminated rock masses the differences in mapping and logging measured spacing values was relatively small, while in non-laminated rocks, spacing values obtained from mapping faces was significantly higher than that derived from borehole core.

Factors such as applying the arithmetic mean as opposed to the lognormal mean in calculating Jv (Volumetric Joint Count), measurement disparities between logging and face mapping, and core degradation during the drilling process, can only partially explain the significant observed differences in RQD. It can be concluded that the relationships given by Palmström (1982) and Palmström (2005) are a relatively poor predictor of borehole drilling RQD for the Sishen rock mass. Figure 5.18 gives a comparison of back calculated average joint spacing values from Palmström (1982) and Palmström (2005) with true borehole RQD values. Although RQD values frequently appear at the lower end of the spectrum in borehole measurements, the equivalent theoretical average joint spacings are far lower than those observed in exposed faces for the same rock mass.

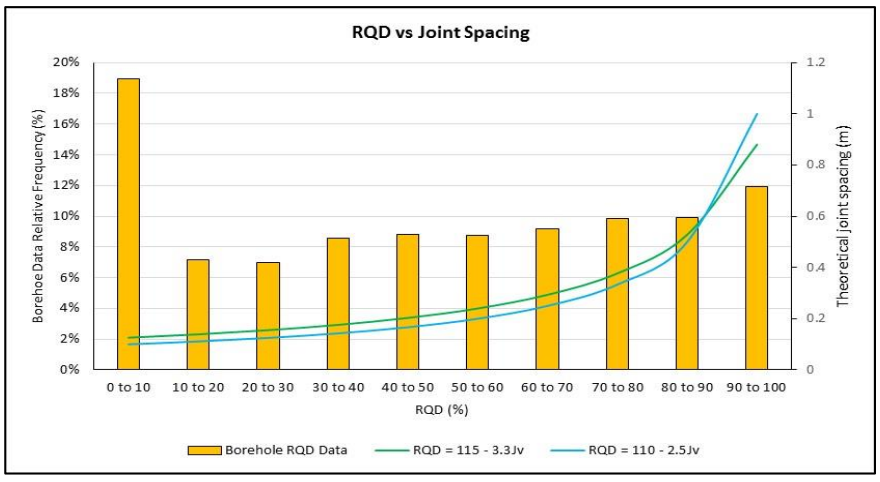

Figure 5.18: Actual RQD values measured from borehole core versus theoretical joint spacing values back calculated from the Palmström (1982) and Palmström (2005) formulae (assuming 3 joint sets + random).

As illustrated in Figure 5.18 a significant percentage of borehole RQD values fall in the 0 – 50% range, which would be equivalent to an average joint spacing of less than 0.2m according to the Palmström formulae. This is far lower than the measured results from faces mapped in the same rock types producing the borehole RQD values.

The significant difference between borehole and face mapping derived RQD values has a marked impact on the calculated RMR and GSI values for a particular rock mass. The RQD data presented in Table 5.5 shows a distinct difference in both the mean values and population spread between borehole and face mapping derived RQD values. If translated into the RMR input score according to Bieniawski (1989) the average RQD for face mapping will be 20. Furthermore, 80% of all the measured RQD values will translate to a score of 20. The average Bieniawski (1989) rating for borehole derived RQD for the BIF and Shale data analyzed is 8, with a relatively uniform spread between the minimum rating of 3 and maximum rating of 20. Considering that RQD is applied arithmetically to the overall RMR rating score, the differences seen between face mapping and borehole logging data will generally result in a significant variation of between 3 and 17 rating points for the same rock mass. This is due to the poor relationship between borehole and face mapping derived RQD values, with the wide uniform spread of borehole derived values in stark contrast with the mapping derived values that are clustered towards the upper end of the RQD spectrum.

5.2.3. Discontinuity Persistency

Discontinuity persistency measurements are incorporated into the mapping protocol outlined in Chapter 4. Prior to the introduction of laser scanner face mapping as a means of geotechnical data collection, no information pertaining to typical bedding and joint persistency values was available at Sishen. The mine's primary source of geotechnical information was borehole core, a data source that can inherently not be used for discontinuity persistency measurements. Joint persistency is however one of the source parameters used in the calculation of RMR (Bieniawski, 1989) and GSI (Hoek et al., 2013). To date a worst case scenario with persistency set to >20m has been used in rock mass rating calculations at Sishen. Face mapping data provides the opportunity to assess whether this is an accurate assumption for the Sishen rock mass, and if not, what effect applying measured persistency will have on the RMR and GSI. Persistency values captured during face mapping carried out for this dissertation are summarized in Tables 5.7 and 5.8 and in Figure 5.19.

Table 5.7: Bedding persistency statistics.

	Shale	BIF	Chert / Manganese Breccia	Diabase	Ore
Count	150	320	16	0	3
Best Fit Distribution	Log Normal	Log Normal	-	-	-
Average (Normal)	8.21	6.76	6.80	-	5.81
Average (Log Normal)	5.03	4.29	6.09	-	5.71
Min	0.18	0.21	2.43	-	4.61
Max	28.54	37.50	14.57	-	7.29
St Dev (Normal)	7.11	6.58	3.44	-	1.36
St Dev (Log Normal)	3.09	2.74	1.62	-	1.26
Cv (%)	87%	97%	51%	-	23%

Table 5.8: Joint persistency statistics.

	Shale	BIF	Chert / Manganese Breccia	Diabase	Ore
Count	224	516	18	53	2
Best Fit Distribution	Log Normal	Log Normal	-	Log Normal	-
Average (Normal)	3.40	3.40	5.15	-	2.56
Average (Log Normal)	2.50	2.20	3.82	-	2.36
Min	0.28	0.14	1.29	0.19	1.58
Max	20.02	26.51	26.93	12.51	3.54
St Dev (Normal)	2.78	3.24	5.81	1.04	1.39
St Dev (Log Normal)	2.28	2.77	2.02	2.84	1.77
Cv (%)	82%	95%	113%	-	54%

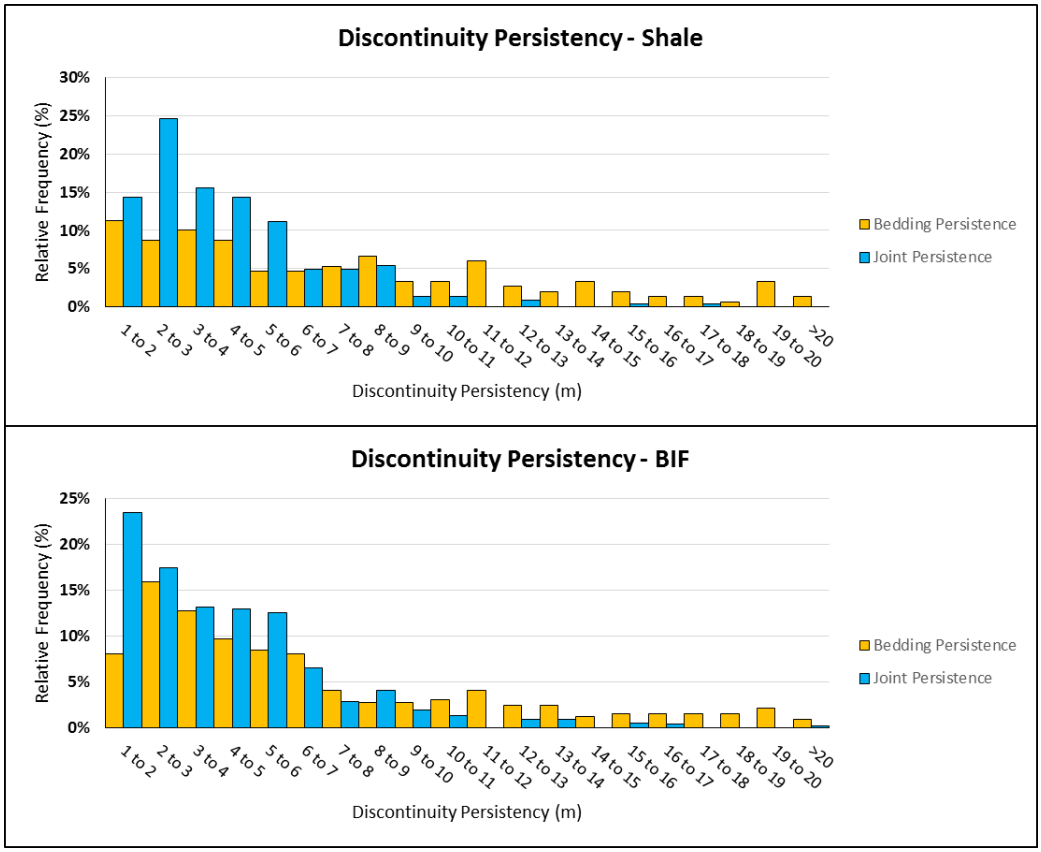

Figure 5.19: Distribution of bedding and joint persistency measurement taken during face mapping for Shale and BIF.

The use of discontinuity persistency in creating a synthetic rock mass model of the Sishen rock mass will be discussed in Section 5.3. With respect to the impact on calculated RMR and GSI values, application of the measured distribution as opposed to simply using a worst case scenario of >20m in terms of the Bieniawski (1989) will not have a significant impact on the overall rating. The measured persistency values given in Tables 5.7 and 5.8, and in Figure 5.19 generally fall in the range of 1 – 10m giving a score of 2 - 4 in terms of Bieniawski's (1989) rating as opposed to 0 for the default persistency of >20m used in borehole logging ratings. As persistency ratings are applied arithmetically to the overall

RMR score, it can be concluded from the measured values that borehole derived RMR ratings underestimate the RMR by 2 – 4 rating points by omitting measured persistency values.

The impact on the GSI (Hoek et al., 2013) rating will be slightly higher as the rating is defined by the following equation in which Bieniawski's (1989) joint condition rating is multiplied by 1.5.

$$\boldsymbol{GSI = 1.5 \times Joint\ Condition + {RQD}/{2}}$$

Applying joint condition ratings based on measured persistency values, as opposed to a default worst case scenario of >20m, will result in an increase in the calculated GSI value of 3 – 6 rating points.

5.2.4. Roughness Measurements

As part of this research a discontinuity roughness measurement procedure was set up, as outlined in Chapter 4. The distance between the laser scanner and mapping face plays a large role in the accuracy and resolution of the mapping surface produced. During the data collection phase of this project it was clear that the roughness of small scale discontinuities could not be reliably measured using laser scanner data under typical face mapping conditions. Based on scanner accuracy limitations stated by the manufacturer, and measurements of apparent irregularities on known flat surfaces in the field, the conclusion was reached that the laser scanner could only be reliably used to determine large scale waviness on discontinuity traces of 2m and longer.

From a practical perspective it was found that, in general, few clean, uninterrupted discontinuity surfaces that were large enough to produce the prerequisite minimum 2m long trace were exposed during the face mapping phase of this project. Out of the 86 faces that were mapped only 116 suitable joint roughness traces could be extracted.

A second aspect to consider was how roughness data could be processed and stored in a manner that could produce a meaningful outcome. As outlined in Chapter 4 there are many ways in which the roughness of a surface can be defined. I-Site Studio 6 was released with a built in tool designed to quantify the roughness of sections, through a selected area representing an exposed plane, by producing a measurement of the degree of waviness. A more simplistic approach was however adopted, whereby the amplitude of sections through selected discontinuities on the mapping face was used to generate a Barton JRC value, as per the Barton (1982) JRC versus asperity amplitude chart.

The JRC represents a practical value that was considered more useful within the mine design and analysis process than raw trace data or a statistical evaluation of the waviness of each individual joint set. In the context of the mine to design processs, large scale discontinuity roughness is often an important but unknown parameter. Sishen Mine exposes a predominantly anisotropic rock mass, where discontinuity strength and therefore large scale roughness / waviness, is a significant input in strength criteria such as the Snowden Modified Anisotropic Linear Strength Model (Rocscience, 2011), or in explicitly defining discontinuity properties in a modelled Synthetic Rock Mass (ITASCA, 2016).

Joint roughness data collected during the data collection phase of this research is presented in Tables 5.9 and 5.10 as well as Figures 5.20 and 5.21.

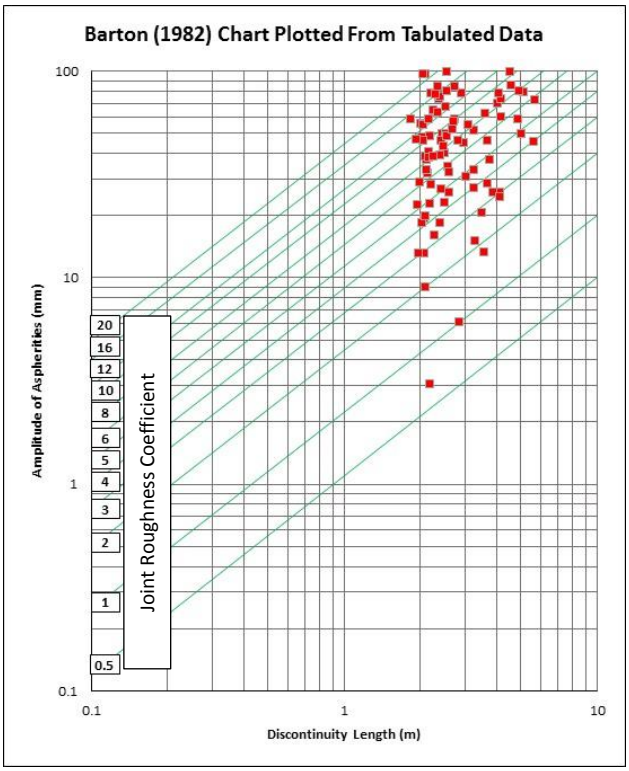

Figure 5.20: All discontinuity roughness data from the data collection phase of this project plotted on the Barton (1982) JRC calculation chart.

Table 5.9: Overall discontinuity Joint Roughness Coefficient statistics.

	Shale	BIF	Chert / Manganese Breccia	Diabase
Count	34	73	4	5
Best Fit Distribution	Normal	Normal	-	-
Average (Normal)	11.43	9.59	13.00	13.28
Min	3.05	0.69	6.92	5.18
Max	20	20	20	20
St Dev (Normal)	5.28	5.96	6.42	6.67
Cv (%)	46%	62%	49%	50%

Table 5.10: Joint and bedding plane Joint Roughness Coefficient statistics for Banded Iron Formation and Shale.

	Shale		BIF	
	Bedding	Joint	Bedding	Joint
Count	5	29	36	37
Best Fit Distribution	-	Normal	Normal	Normal
Average (Normal)	10.19	11.64	7.71	11.43
Min	3.05	3.94	0.69	2.18
Max	20	20	20	20
St Dev (Normal)	6.76	5.10	4.78	6.47
Cv (%)	66%	44%	62%	57%

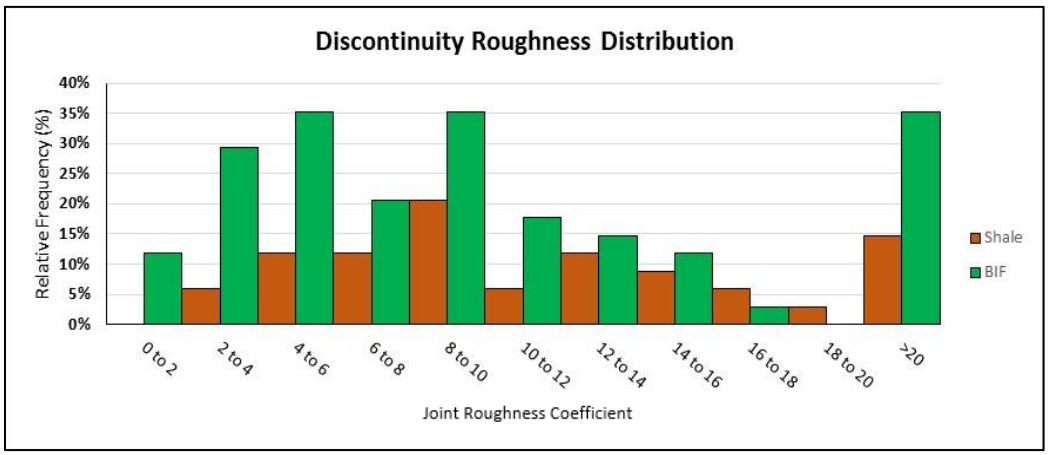

Figure 5.21: Roughness distribution for Banded Iron Formation and Shale.

Roughness data captured during face mapping shows large scale roughness generally conforms to a normal distribution when asperity amplitude is converted to JRC through the Barton (1982) JRC chart. Joint and bedding roughness values are relatively consistent for the shale dataset while BIF data shows higher JRC values for joint planes than for bedding planes. A significant portion of the asperity amplitude data (15% for shale and 35% for BIF) plotted above the JRC upper limit of 20 on the Barton (1982) JRC estimation chart.

As previously discussed, the roughness data obtained from face mapping can form a valuable input into models and analysis where joint strength is relevant for a particular rock type. In terms of rock mass rating systems it was found that in many cases no suitable planes could be sectioned for roughness rating on individual mapping faces. Joint roughness ratings for rock mass rating input were therefore applied subjectively by the face mapper, as per the face mapping protocol outlined in Chapter 4. A comparison of subjective borehole logging and face mapping roughness estimates is given in Figure 5.22 and Table 5.11. Although no distinction is made between individual rock types, for the sake of consistency the data is restricted to those present in both the face mapping and borehole logging databases.

Table 5.11: Comparison of subjective roughness assessments for RMR input from borehole core and mapping faces.

Count	Borehole Data	Face Mapping Data
Slickensided	630	0
Smooth	1824	3
Slightly Rough	1704	15
Rough	621	76
Very Rough	37	0

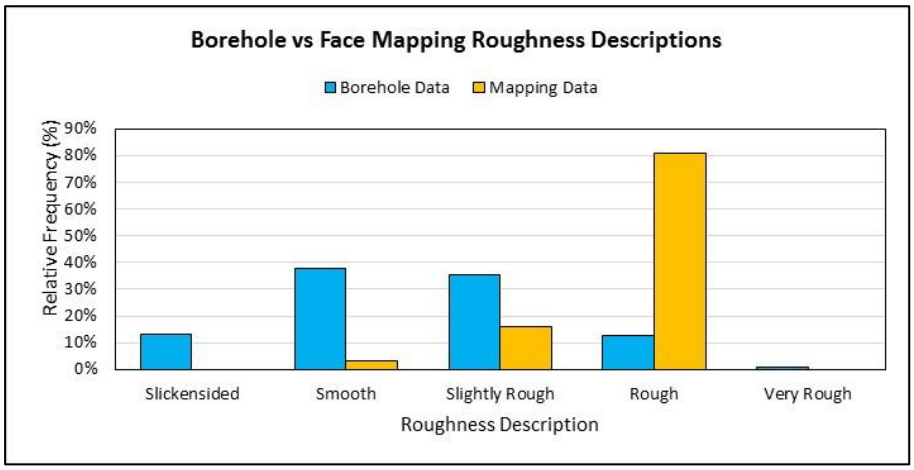

Figure 5.22: Borehole and mapping subjective roughness descriptions.

It is evident from the data presented in Table 5.11 and Figure 5.22 that roughness descriptions from mapping faces are generally higher than those from borehole core. Mapping roughness descriptions are essentially based on an assessment of a photographic image of the mapping face as opposed to a field assessment of the discontinuity surfaces, which are in most cases not safely accessible. It is therefore accepted that mapping roughness estimates are based on large scale discontinuity roughness (dictated by the resolution of the photograph) and are at best a broad estimate. If compared to the less readily available but more objective joint trace roughness profiles, the subjective roughness descriptions appear to correlate relatively poorly. The majority of descriptive face mapping roughness estimates fall within the slightly rough to rough descriptive range, which would suggest that the majority of measured joint profile values would plot towards the upper end of the JRC range in Figure 5.21. This is however not the case, and 58% of the total measured JRC values fall below 10, suggesting that subjective descriptions based on laser scanner photographs tend to overestimate roughness.

With respect to the contrast between borehole and mapping roughness, a distinct difference is apparent between the direct small scale observations on borehole core and the indirect large scale assessment of discontinuities on mapping faces. Borehole observations tend to classify joints across the full range of descriptive roughness values, reflecting the full range of JRC measurements taken from mapping faces. In contrast to this, subjective descriptions

taken from mapping face photographs for RMR and GSI classification are grouped almost exclusively in the slightly rough to rough range. When viewed in conjunction with borehole roughness values and mapping derived JRC values, it can be concluded that the subjective mapping roughness assessments tend to overestimate roughness. In the context of rock mass rating, this will result in an overestimation in the order of 2 to 4 rating points for the RMR Bieniawski (1989) system and 3 to 6 rating points for the GSI (Hoek et al, 2013) rating.

5.2.5. Rock Mass Rating Systems

5.2.5.1. Input Variability Between Face Mapping and Borehole Data

Variability between measured GSI and RMR input parameters from borehole core and face mapping surfaces are presented and discussed in the preceding sections. The individual impact each of these parameters will have on the overall rating outcome can be summarized as follows.

- There is a large disparity between borehole and face mapping derived RQD values for the same rockmass. Based on the available data it is apparent that face mapping derived RMR and GSI values will be 3 to 17 rating points higher.
- Borehole and face mapping derived spacing values were similar for the data analyzed and will generally not impact on the RMR or GSI score for either data capture technique.
- Using measured persistency values, as opposed to the default of >20m applied when calculating RMR and GSI from borehole logging data, will result in RMR and GSI values 2 – 3 and 3 – 6 rating points higher respectively.
- Subjective Roughness estimates are generally slightly higher for face mapping than borehole logging. RMR and GSI values will be 2 – 3 and 3 – 6 rating points higher respectively for face mapping ratings.

Analysis of the individual input parameters of common rock mass rating systems such as RMR, GSI, MRMR and Q shows that ratings will generally come out higher for the same rock mass when assessed from a mapping face as opposed to a borehole log. This pattern is substantiated in the actual face mapping and borehole derived rock mass rating data available for Sishen Mine.

5.2.5.2. Comparison of Face Mapping and Borehole Derived RMR and GSI Data

The first aspect to assess is whether the GSI, calculated as per the method outlined by Hoek et al. (2013), correlates with RMR_{89} values for borehole and face mapping data as per the generally accepted relationship as follows.

$$GSI = RMR_{89} - 5 \qquad \text{(Hoek and Brown, 1997)}$$

Figure 5.23 shows the distribution of the difference between GSI (Hoek, 2013) and RMR (Bieniawski, 1989) when individual values are directly compared for the same geotechnical zone or mapping face.

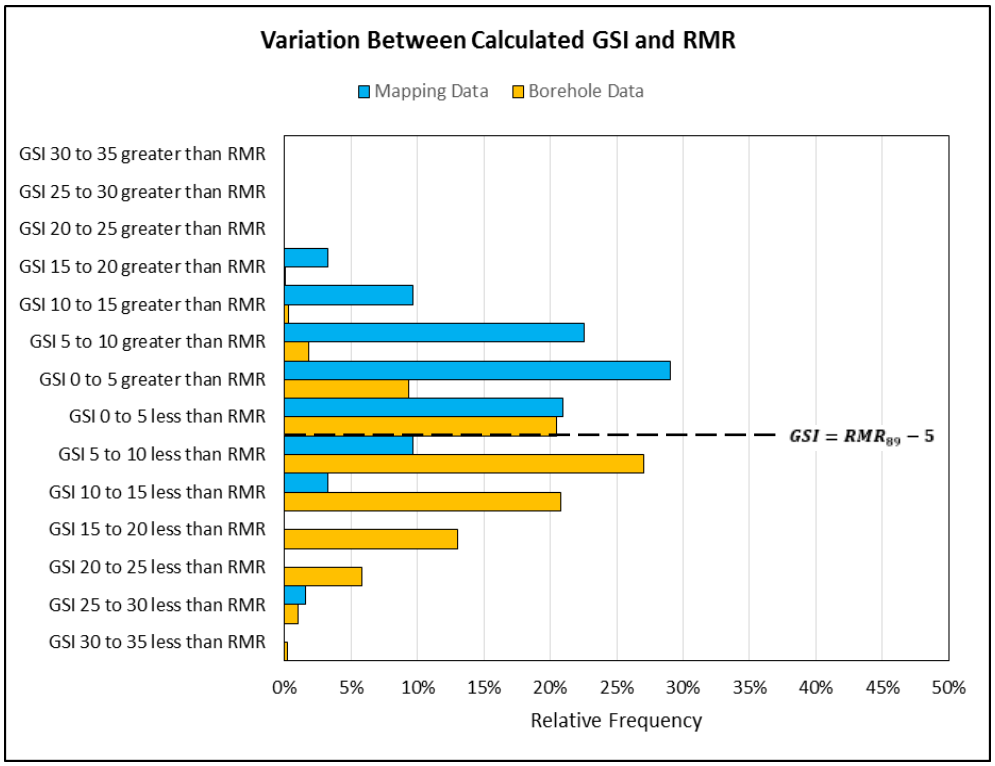

Figure 5.23: Difference between calculated RMR and GSI values for the same geotechnical zone or mapping face.

As indicated in Figure 5.23 most borehole derived GSI values conform relatively well with the relationship of GSI = RMR_{89} – 5 proposed by Hoek and Brown (1997), with 52% of all values falling between GSI = RMR_{89} and GSI = RMR_{89} – 10. 80% of all calculated borehole RMR/GSI values fall between GSI = RMR_{89} + 5 and GSI = RMR_{89} – 15. Face mapping data derived RMR and GSI values do not correlate as well with each other according to the Hoek and Brown (1997) relationship, with 64% of face mapping derived GSI values greater than the corresponding RMR value. This inconsistency between face mapping and borehole data can be attributed to the persistently high face mapping derived RQD value that are given a greater

weighting in the Hoek et al. (2013) GSI calculation than the Bieniawski (1989) RMR rating.

A further comparison can be made between borehole logging and face mapping derived rock mass rating values in terms of the consistency between the two for the same rock types. Based on an evaluation of the individual rating inputs, it stands to reason that face mapping derived RMR, GSI, MRMR or Q values will in general be higher than those obtained from borehole data for the same rock mass. GSI and RMR values per lithology from the available study data are compared in Table 5.12 and in Figure 5.24.

Table 5.12: Comparison of borehole and face mapping derived RMR and GSI values.

RMR (Bieniawski, 1989)										
	BIF		Shale		Ore		Diabase		Chert / Manganese	
	Log	Map	Log	Map	Log	Map	Log	Map	Log	Map
Count	546	57	696	21	348	1	28	2	360	3
Best Fit Distribution	Norm.	Norm.	Norm.	-	Norm.	-	Norm.	-	Norm.	-
Average (Normal)	62.8	76.5	57.4	72.2	62.8	79	62	81	65.6	71.7
Min	30	66	36	55	30	79	42	79	30	66
Max	83	86	78	84	85	79	81	83	85	79
St Dev (Normal)	7.69	4.15	7.45	7.07	7.34	-	10.5	2.83	8.25	6.66
Cv (%)	12%	5%	13%	10%	12%	-	17%	3%	13%	9%
GSI (Hoek et al., 2013)										
	BIF		Shale		Ore		Diabase		Chert / Manganese	
	Log	Map	Log	Map	Log	Map	Log	Map	Log	Map
Count	578	57	733	21	349	1	28	2	360	3
Best Fit Distribution	Norm.	Norm.	Norm.	-	Norm.	-	Norm.	-	Norm.	-
Average (Normal)	50.8	79.9	50.5	76	52	83	48.6	86	56.9	75
Min	14	66	6	52	7	83	11	83	2	68
Max	82	88	82	85	81	83	78	89	84	83
St Dev (Normal)	14.1	4.43	14.6	7.66	12.8	-	18.2	4.24	14.5	7.55
Cv (%)	28%	6%	29%	10%	25%	-	37%	5%	25%	10%

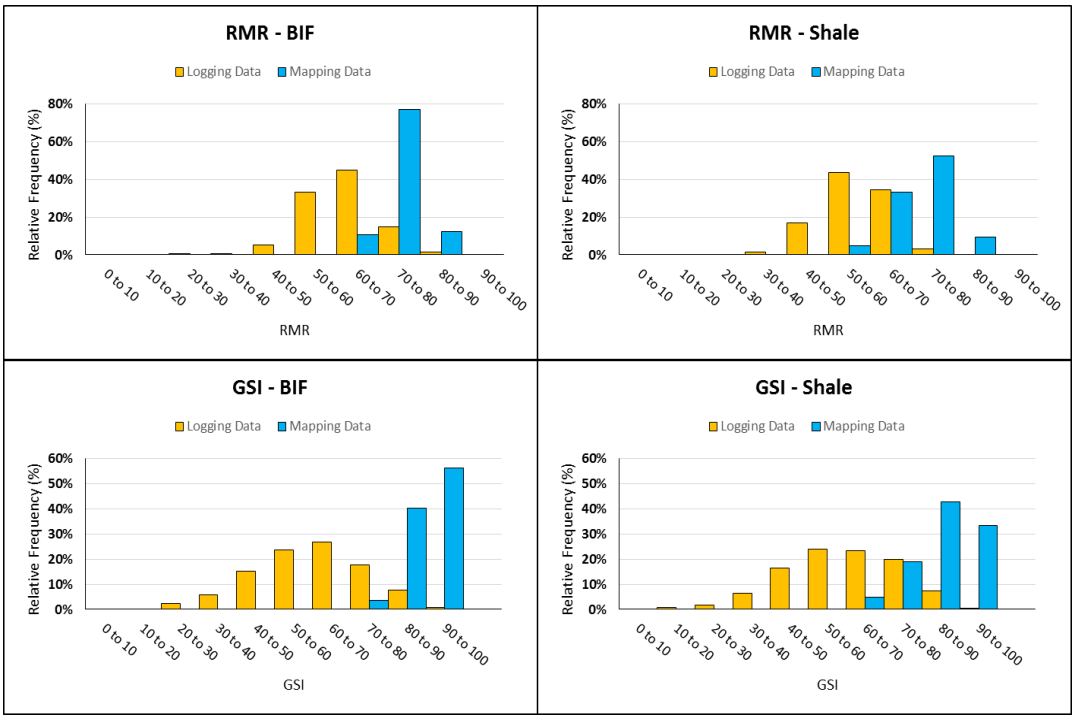

Figure 5.24: Face mapping and borehole derived GSI and RMR data for BIF and Shale.

Data presented in Table 5.12 and in Figure 5.24 confirms the conclusions of the preceding sections in this chapter that a face mapping derived rock mass rating will generally be higher than a borehole derived rating for the same rock mass. The data shows that a RMR score derived from a mapping face will typically be between 5 and 15 rating points higher than that from a borehole drilled into the same rockmass. Possible reasons behind this have been discussed and include differences between the two techniques in calculated RQD values, damage to borehole core due to stress relief and the mechanical forces involved in diamond drilling, and assumptions made regarding parameters such as discontinuity persistency. The following is evident when RMR (Bieniawski, 1989) and GSI (Hoek et al., 2013) are directly compared for borehole logging and face mapping.

- Within the analyzed dataset, face mapping RMR and GSI averages are far higher than those derived from borehole logging.
- There is a tighter distribution and smaller standard deviation for face mapping derived RMR values than for borehole logging values.
- The equation GSI = RMR_{89} – 5 is relatively accurate for RMR (Bieniawski, 1989) and (Hoek et al., 2013) GSI values for borehole derived data.
- Face mapping derived GSI values are generally higher than the face mapping derived RMR values for the same mapping faces, and do not correlate well with the equation GSI = RMR_{89} – 5.

- Differing RQD calculation methods are a major source in the discrepancy between borehole and mapping face derived RMR and GSI values.
- Due to various aspects of each data capture technique, borehole logging will tend to slightly underestimate RMR and GSI values while face mapping will tend to overestimate these values.

From the available data it can be concluded that, in general, face mapping derived RMR values calculated using the method outlined in this research report will produce higher results than borehole derived values. This is due to errors that are introduced with both measurement techniques. Laser scanner face mapping derived RMR values will be acceptable for good quality rock masses where parameters such as rock hardness and joint infilling are easier to estimate. Unless a completely subjective estimate is applied from the scanner photograph, laser scanner face mapping is of little use in assessing RMR for poor quality rock masses. For any site, there must be an awareness of the limitations of the system, and the potential for skewing of data sets by either omitting or overestimating RMR for mapping faces in poor quality rock masses.

GSI calculated using Hoek et al. (2013) produces reliable results from borehole data, but not from mapping faces. Face mapping derived GSI values are far higher than the equivalent borehole derived values, and the face mapping derived RMR values. The face mapping derived GSI values calculated during the data collection phase of this research are not considered representative of the rock mass. It is therefore concluded that, should a GSI rating be required from a mapping face, it should be obtained by either;

- Calculating RMR and applying the formula GSI = RMR_{89} – 5
- Using the Hoek et al. (2005) visual assessment chart in conjunction with the laser scanner photograph.

5.3. SYNTHETIC ROCK MASS MODELLING

The majority of Sishen Mine's design final pit boundaries expose laminated rock types such as Banded Iron Formation and Shale. The characteristic anisotropic strength properties of laminated rocks play a pivotal role in defining the strength characteristics of rock masses made up of such materials. The approach in assessing large scale slope stability at Sishen Mine has evolved into one which takes rock mass anisotropy into account, assessing slopes based not only on rockmass strength, but specifically on the relationship between the orientation of the slope and that of any underlying anisotropy that is present. This was first done by applying anisotropic strength criteria such as the Snowden Modified Anisotropic Linear Strength Model (Rocscience, 2011), but has been replaced by an approach whereby the rockmass is implicitly modelled to create a Discrete Fracture Network (DFN) from which a Synthetic Rock Mass (SRM) can be developed.

A Discrete Fracture Network can be defined as a means of representing rock mass fabric as accurately as possible in a 3-D volume by stochastically generating fractures from known distributions (Lisjak and Grasselli, 2014; ITASCA, 2016). Within a SRM sample, intact rock is represented as an assembly of bonded spheres, with intact material properties dependent on the stiffness and strength of the bonds between the spheres. A Discrete Fracture Network can be embedded within a SRM as a network of disk-shaped flaws, with joint properties applied to the DFN discontinuities (Pierce et al., 2007; Potyondy and Cundall, 2004). Incorporation of a DFN into a SRM sample allows the model to account for the effect of discontinuities on the models behavior (Lisjak and Grasselli, 2014).

In order to create a DFN orientation data as well as statistical distributions of discontinuity spacing and persistency need to be available. Kumba Iron Ore appointed ITASCA in 2016 to carry out the following analysis using the available structural, face mapping and rockmass strength data.

- Develop DFN's for shale and BIF
- Create sample Synthetic Rock Mass models of Shale and BIF to model specific anisotropic strength properties
- Apply anisotropic strength properties to assess stability for different structural domains within Sishen's North and Middle pits

The anisotropic slope stability analysis process and the role of face mapping data therein is outlined in Figure 5.25.

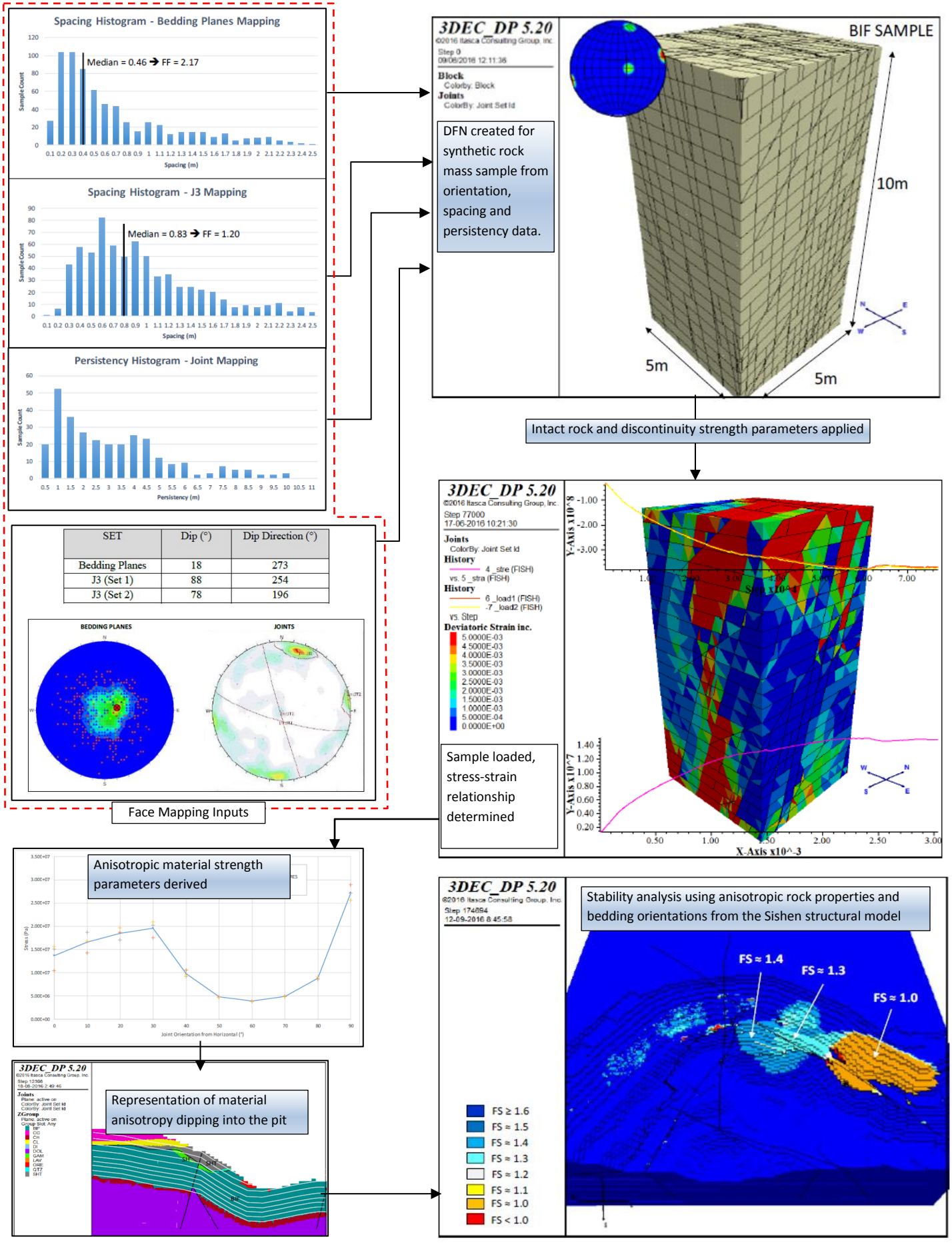

Figure 5.25: Illustration of the process used for modeling of slope stability with anisotropic strength (After Itasca, 2016).

5.4. FACE MAPPING FOR STRUCTURAL MODEL RECONCILIATION

As outlined in Chapter 2, Sishen Mine is situated in a complex structural setting characterized by both brittle and ductile deformation. The rockmass is cross cut by several large faults, and has been subjected to folding as well as low angle thrusts. The anisotropic nature of the laminated lithologies that are prevalent in the mine's permanent highwalls means that the structural setting, and in particular the bedding orientation within a particular structural domain, plays a critical role in determining overall slope stability, stack and bench stability, rockfall risk and limit blast performance. An accurate and reliable structural model of the mine therefore plays a crucial role in the geotechnical design process and in geotechnical risk management as the pit is mined out. Geotechnical face mapping, through integration into the mines spatial geotechnical data management system (Figure 4.49), has taken on the role of ground proofing and updating the interpreted structural model that is used to inform the geotechnical design and analysis process.

The Sishen Geotechnical Engineering Section has appointed specialist consultants to produce and update a structural model of the mine that defines predominant fault structures and bedding orientations throughout the mining area. As discussed in Chapter 4, this is based on field observations, borehole logs and an interpretation of lithological contact orientations from the mine's geological model. Figures 5.26 to 5.28 indicate the distribution of interpreted bedding orientations from the structural model versus actual measurement points acquired during face mapping.

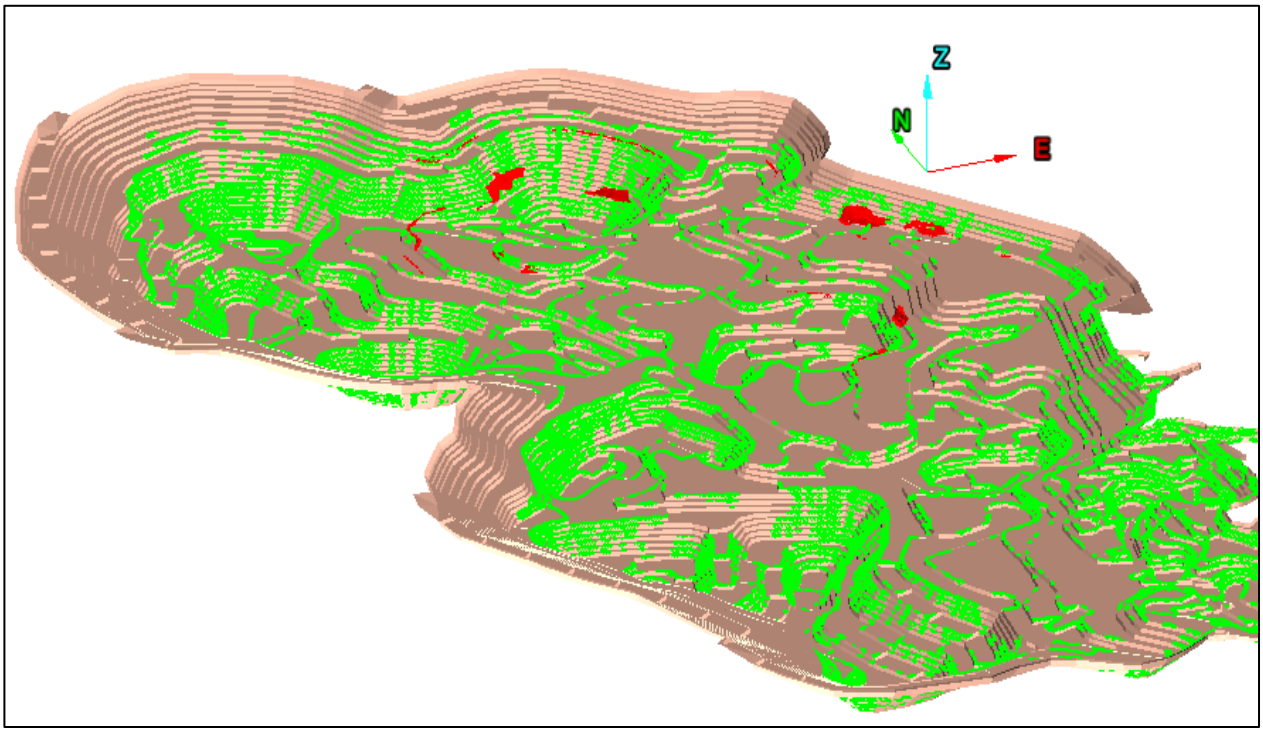

Figure 5.26: Sishen North Mine measured (Red) versus inferred (Green) bedding orientation data.

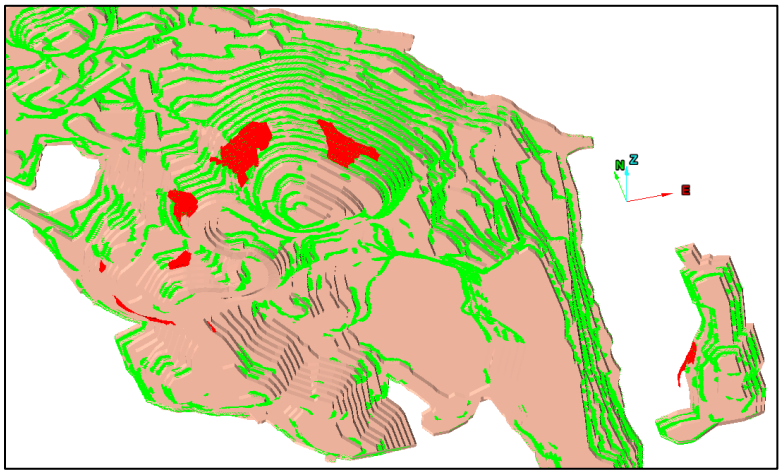

Figure 5.27: Sishen Middle Mine measured (Red) versus inferred (Green) bedding orientation data.

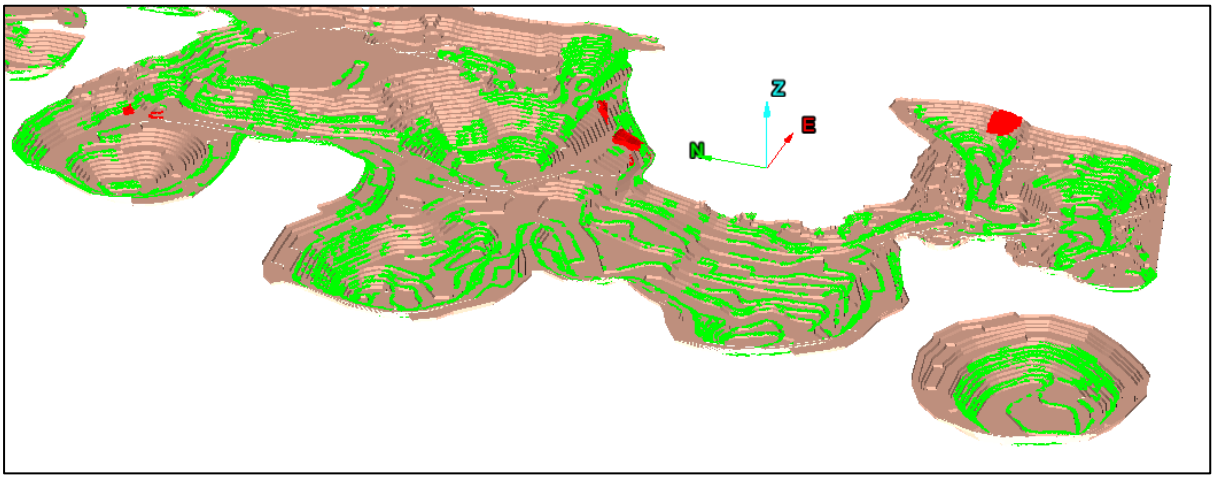

Figure 5.28: Sishen South Mine measured (Red) versus inferred (Green) bedding orientation data.

As indicated in Figures 5.26, 5.27 and 5.28, the majority of bedding orientation data is interpreted from geologic contacts. Face mapping data has to date played an important role in verifying the interpreted data upon which the mine's structural model, has been developed. By comparing actual measured orientations with those implied in the structural model the accuracy of the structural model, and degree of confidence in bedding orientations in unmapped or yet to be mined out areas, can be established. Figure 5.29 shows an example of an area where mapped data and interpreted bedding orientation have been overlain. Figure 5.30 indicates how well interpreted bedding orientations match with measured orientation in the mapped areas of the mine. Major bedding planes, as interpreted from stereonet data for each mapping face have been used as the basis for each comparison, with the closest mapping face centroid to each implied bedding data point being used. Only data within 100m of a mapping face centroid has been used for comparison, as indicated in Figure 5.31. Conformance between inferred and actual measurement points is relatively constant for data range cutoffs between 20m and 100m, which indicates that a radius of comparison of 100m is still representative of the mapping face centroid value.

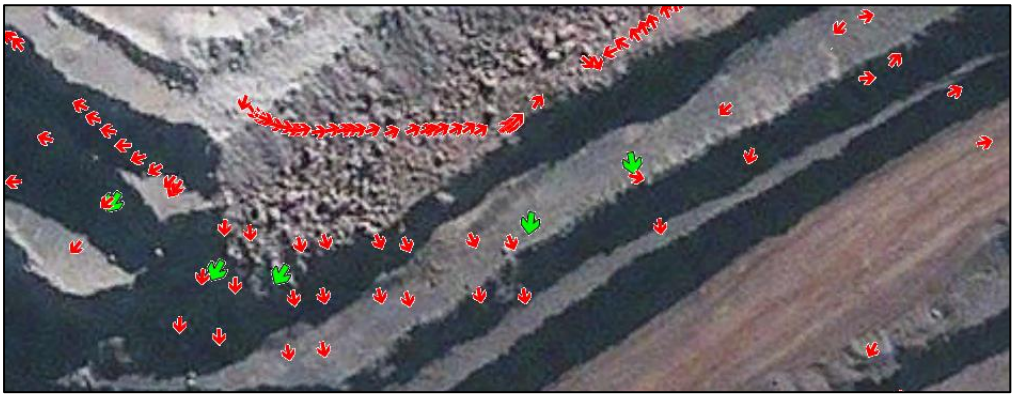

Figure 5.29: Interpreted (Red) and mapped (Green) bedding dip directions.

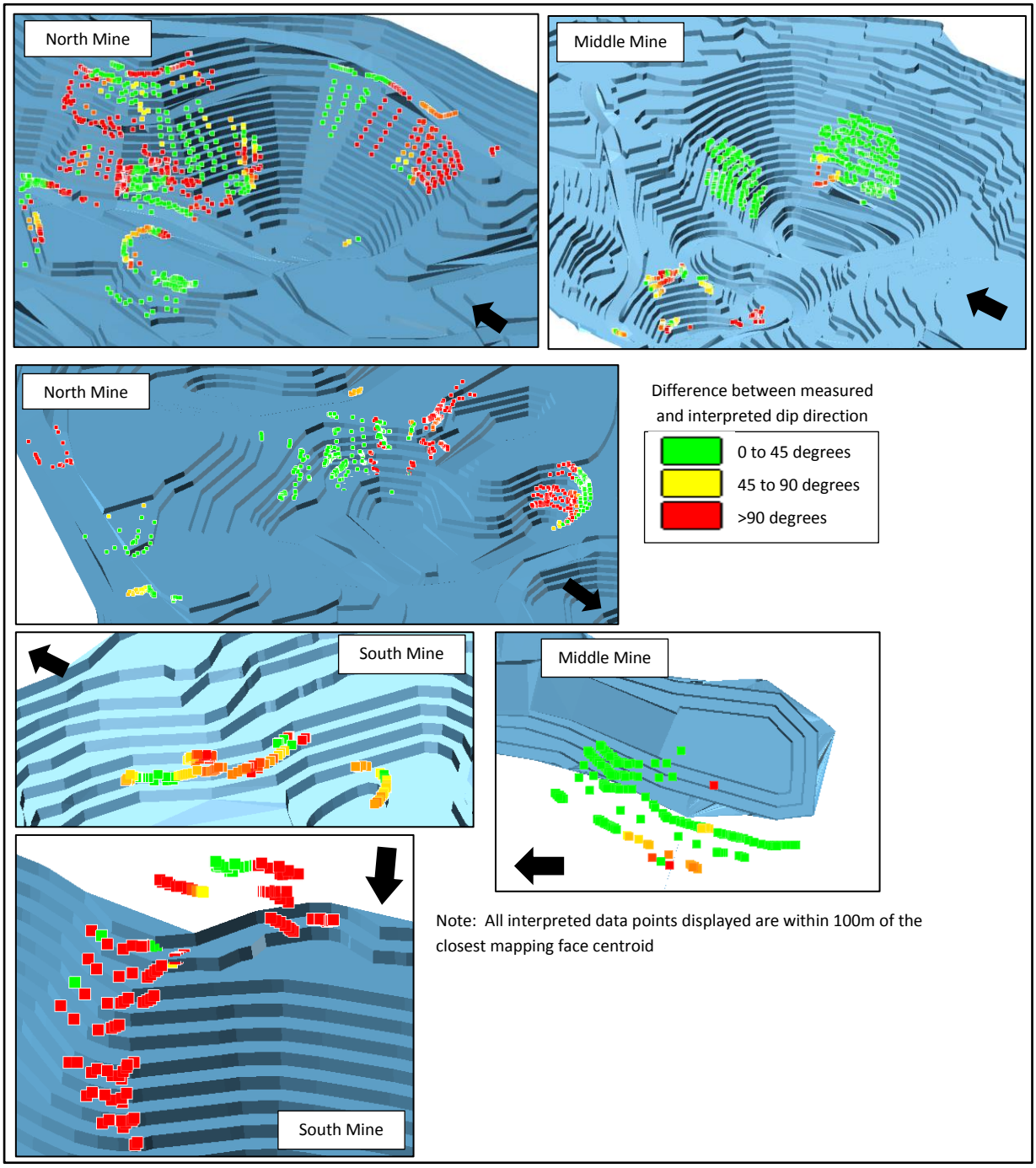

Figure 5.30: Difference in interpreted versus measured dip direction.

Figure 5.30 shows a relatively good correlation between measured and interpreted data in most instances. Figure 5.32 shows the percentage distribution of the error between interpreted and measured dip direction values.

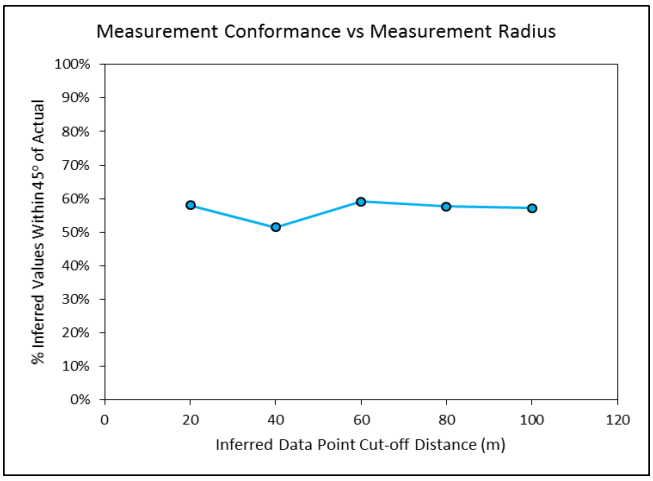

Figure 5.31: Percentage of inferred dip direction values within 45 degrees of measured values considering data points at a range of 20m, 40m, 60m, 80m and 100m

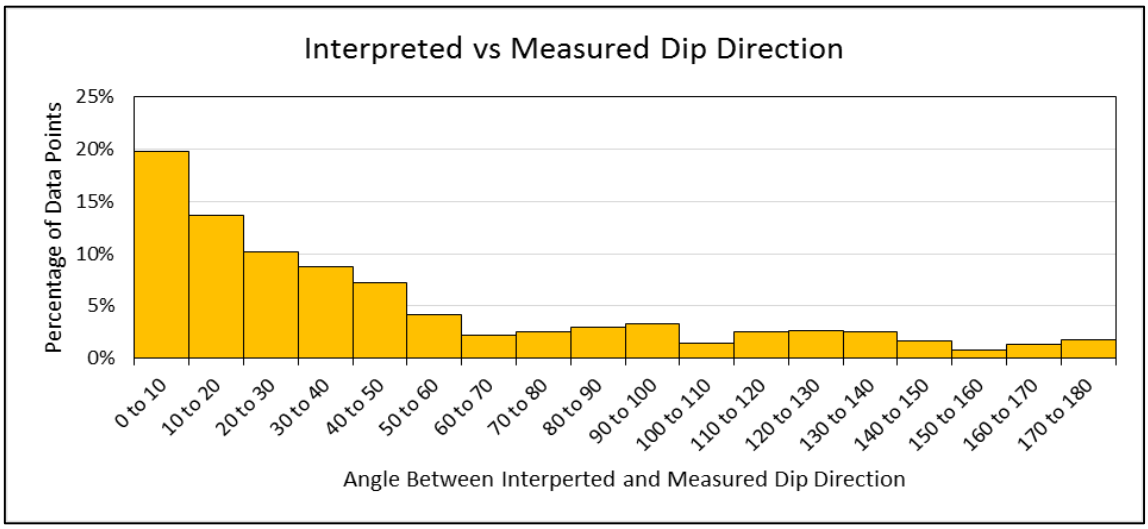

Figure 5.32: Distribution of error in interpreted data points from corresponding measured dip direction data.

Of the 5 223 interpreted dip direction values falling close enough to mapping faces for comparison, 57% have a dip direction within 45 degrees of the measured dip direction while 71% are within 90 degrees of the measured dip direction. It can be concluded from the comparison between measured bedding orientations with those interpreted from the mine's geological model that, for Sishen's rock mass, using geological contact orientations is relatively reliable as a means of establishing bedding orientations within the geological unit in question. As face mapping at the mine continues and the mapping database grows, interpreted data will progressively be replaced by measured data points for use in design and analysis.

5.5. POTENTIAL FUTURE DEVELOPMENTS

5.5.1. Geotechnical Block Modelling

Sishen's geotechnical block models are currently based on the lithological divisions in the mine's geological block models. Geotechnical block properties and design parameters are assigned based on the geotechnical dataset available for the assigned lithology for the block in question. An illustration of a block from within the Sishen geotechnical block model is given in Figure 5.33. Bench and stack angles prescribed by the geotechnical block model are incorporated into the mine planning cycle when designing an optimized and practical pit shell.

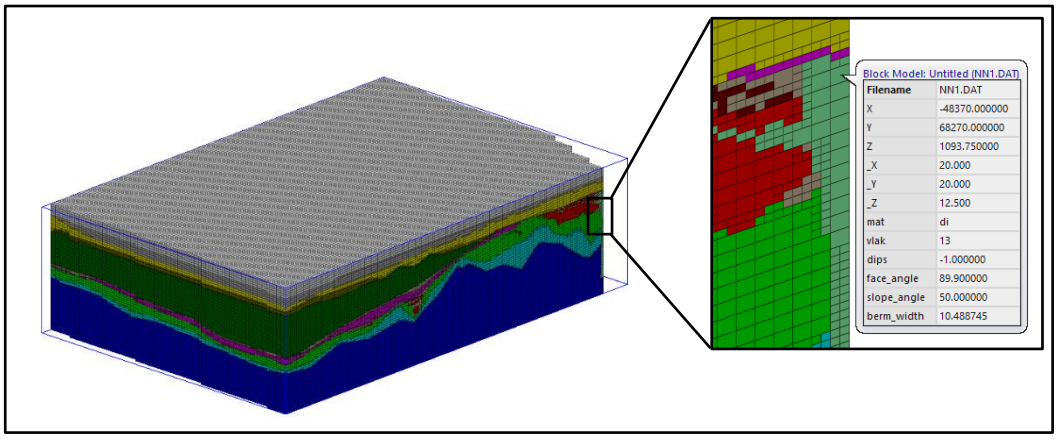

Figure 5.33: Design parameters from the Sishen geotechnical block model.

To date spatial structural data from the Sishen structural model or face mapping database has not been used to inform the geotechnical block model. This information is however invaluable in determining the optimum pit design angle, as it affects overall slope stability, bench development and bench scale stability.

Section 4.3 in Chapter 4 describes the process by which inferred bedding orientations are derived, based on the local dip of lithological contacts from the structural model, and projected vertically to the design pit shell. Comparison with actual measured orientations from face mapping data has shown that this is a relatively reliable method of estimating bedding orientations at a particular point in a rock mass. As a future development of the Sishen structural model and face mapping database, the Sishen Geotechnical Engineering Section is planning on incorporating fault and bedding orientation data into the geotechnical block model. This will be done first through the use of mapping data if available and secondly through the use of inferred orientations from lithological contacts to fill in the gaps. Fault data will be applied as per the discrete locations of large scale structures within the structural model.

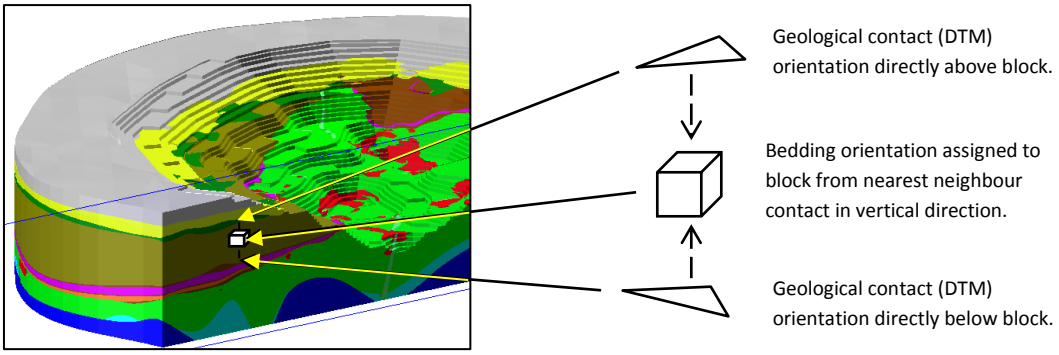

Figure 5.34: Illustration of populating a geotechnical block model with bedding orientation data.

5.5.2. Blastability Evaluation

Blastability and adjusting blast designs according to rock mass conditions is an area of considerable focus at any large open pit mining operation. Economics have dictated that large open pit mining operations adopt high energy blast designs to improve fragmentation and excavatability, thereby increasing the efficiency of the operation. A consequence of this increased blast energy has been to potentially damage and destabilize interim and final pit walls. Limit blast designs including trim blocks and pre-splitting or post-splitting are generally used to protect the pit highwalls from blast damage (Williams et al., 2009).

Williams et al. (2009) highlight the impact that discontinuity orientation has on limit blast performance and on the quality of bench faces produced. Different discontinuity orientations require different limit blast designs to achieve the best possible bench face conditions. The required blast pattern, hole angle and charge will differ with differing discontinuity orientations relative to the slope face (Williams et al., 2009).

As blast performance is so heavily influenced by geological conditions, it is logical that blast design be informed by the state of the rock mass. In addition to intact rock mass properties, blast performance is influenced by the following (Williams et al., 2009).

- Block size
- Spacing
- Persistency
- Discontinuity characteristics
- Discontinuity orientation relative to the batter face

Rock mass parameters are inherently variable and the application of a single blast design will inevitably yield mixed results on most sites. Sishen mine has experienced blasting

related problems from poor fragmentation of production blocks to highwall damage on final pit boundaries and floor elevation control issues. Face mapping and face mapping derived data have the potential to be used to rapidly and accurately assess local rock mass conditions, informing blast designs and thereby improving overall blast performance. The site specific orientation, spacing and persistency data collected during highwall face mapping can easily be adapted to mapping of a blast block free face, informing a blastability rating and blast design. In addition to measurements made prior to blasting, the accurate distance measurement and photographic overlay of the scan surface allows for post blast fragmentation analysis.

A direct assessment of a blast block face or adjacent highwall would be the ideal means of determining local rock mass conditions for blastability and blast design (Figure 5.35). The Sishen Blasting Section has looked into using the Maptek laser scanner for this purpose, but has run into the problem that, for most production blocks, the blast design needs to be finalized before the sides of the block have been exposed and are available for face mapping. In such cases, the planned extension to the geotechnical block model could represent the closest approximation for informing blast design with regard to intact rock, rock mass and structural orientation properties (Figure 5.36). With inferred discontinuity orientations from the structural model and rock mass properties from the borehole and face mapping databases applied to the geotechnical block model, blastability and the most appropriate blast design could be finalized prior to the blast block faces being exposed.

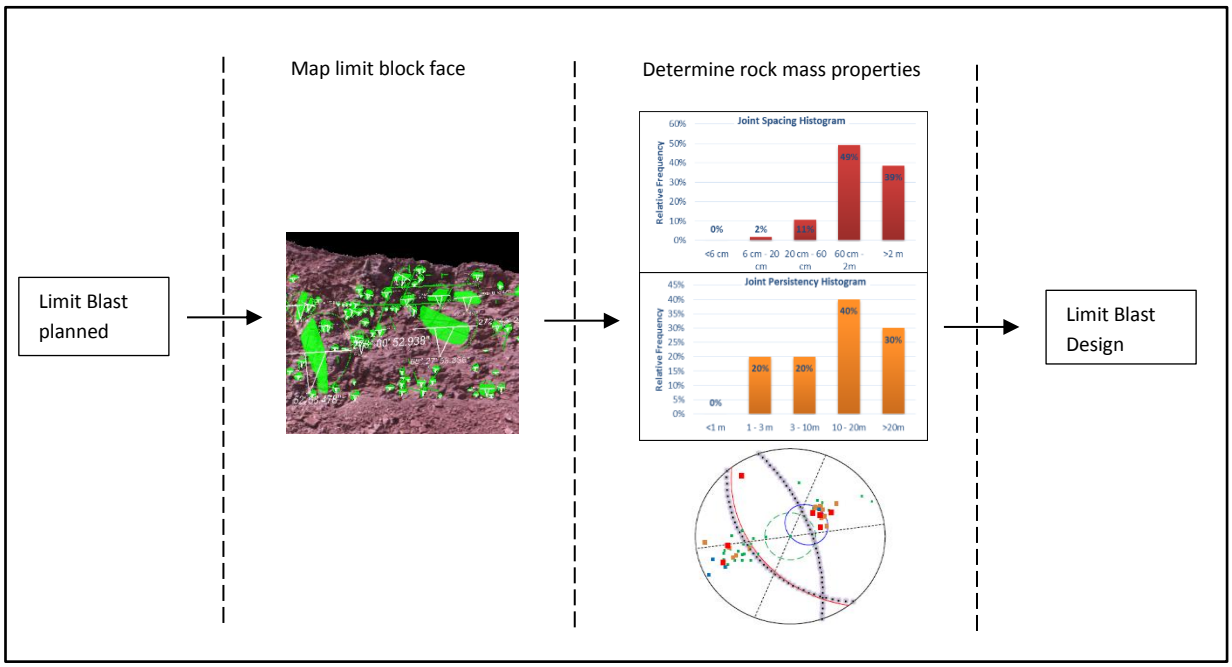

Figure 5.35: Conceptual process for determining limit block blast design from face mapping data.

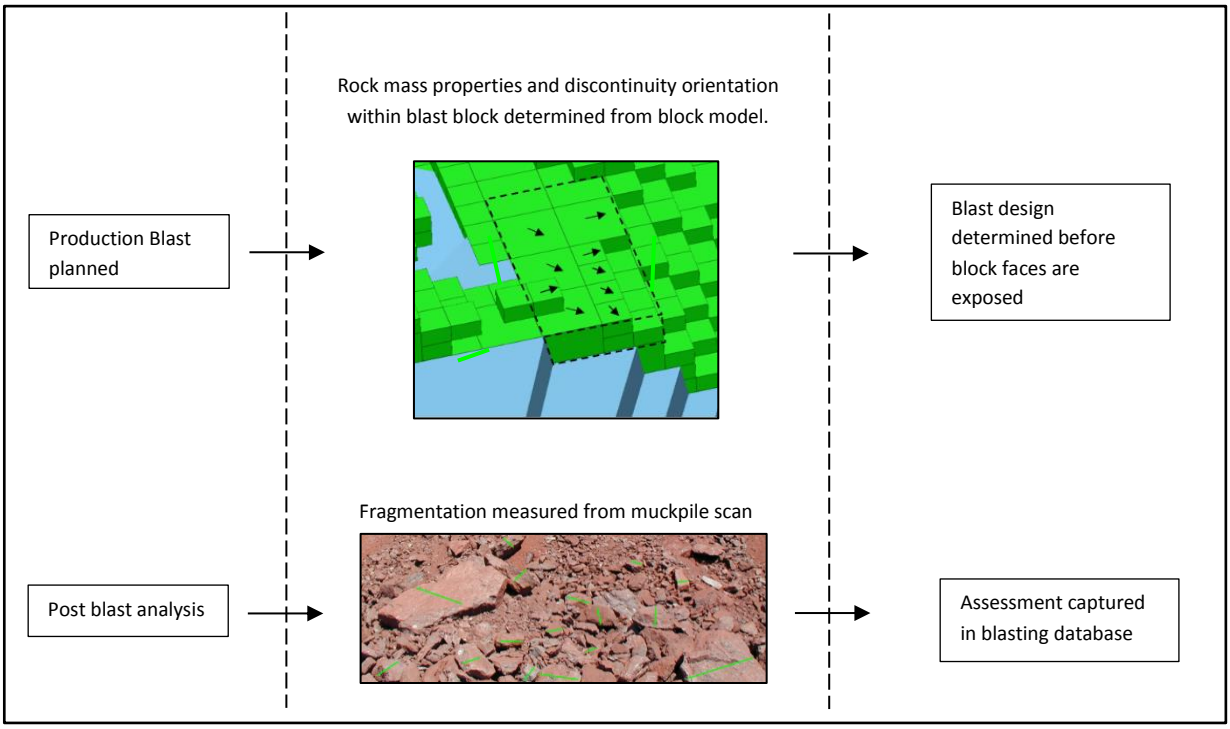

Figure 5.36: Conceptual process for determining production block blast design and carrying out post blast analysis.

This chapter gives an appraisal of the Maptek 8810 terrestrial laser scanner system based on experience gained during the data collection phase of this project. Rock mass data captured during the course of this research is analysed and compared with existing data in Sishen Mine's geotechnical borehole dataset. Face mapping orientation and fault trace data is similarly compared with inferred structural data from the mine's existing structural model. Usage of face mapping data in discrete fracture and synthetic rock mass modelling is discussed, and potential future uses of the system to inform geotechnical block models and blast designs is outlined.

CHAPTER 6: CONCLUSIONS

The Maptek 8810 laser scanner was initially purchased by Sishen Mine as a means of rapidly and safely collecting geotechnical face mapping data. This research report set out to explore the capabilities of the system, integrate face mapping data with the mine's existing geotechnical database and assess the impacts of incorporating face mapping data into the geotechnical design process at Sishen.

It is clear from the available literature, and experience gained during the data capture phase of this project, that the terrestrial laser scanner represent a far more practical and faster means of collecting face mapping data than manual techniques or using a stereo photo system such as Sirovision. No contact with the mapping face is required, which makes the system safer and allows for inaccessible rock faces to be mapped. The photographic overlay of the 3D mapping face automatically incorporated into the I-Site Studio software was found to be accurate and an excellent means of interpreting structural and rock mass features on the underlying scan surface. It was however concluded during the course of the project research, that relying on the remote data produced by the scanner was not always adequate on its own as a source of geotechnical information, and some form of ground proofing of rock mass conditions at the mapping face should be incorporated into a face mapping program.

With respect to data capture and processing, exporting mapping data from I-Site Studio into Microsoft Excel for further processing and analysis proved to be a robust and reliable system over the course of this project. VBA macro instructions incorporated into an Excel template were a powerful tool for importing and manipulating the raw CSV data exported by I-Site Studio. Although adequate for the duration of this project, there are concerns that using an Excel template to process data from I-Site Studio may represent a future weak point in the system, as maintenance of the template will be required with any changes in the I-Site Studio export system. The best solution would be for Maptek to extend I-Site's already capable geotechnical analysis functions to allow for capture of rock mass parameters, reporting of analysis results and customisable exports of geotechnical data.

The Acquire Geological Database system is used on Sishen Mine to store borehole data and is specifically designed for that purpose. Incorporating mapping data into the system required an approach whereby a mapping face was essentially viewed as a borehole collar with a unique ID and set of co-ordinates. Individual mapping features were added under the relevant face mapping collar in the same manner as logging intervals for a borehole, with feature co-ordinates taking the place of borehole depth intervals. The concept of incorporating a collar table with features relevant to the mapping face as a whole, and a details table for individual features within the mapping face, proved to be a simple and reliable data storage model for storing face mapping data. The Acquire system allows for 3rd party software application to access data from within the database through ODBC links with user defined data client views. This has allowed mapping data to be accessed for analysis with Microsoft

Excel and for spatial overlay with other geotechnical data, mine planning data and survey data, using the Micromine CAD package.

Comparison of mapping and borehole derived rock mass data indicates that, in general, face mapping derived ratings will tend to be higher than borehole logging derived values for the same rock mass. It can be concluded that face mapping will tend to overestimate the rock mass rating while, when using borehole derived data, the rock mass rating will tend to be slightly underestimated. This can be explained by the following.

- RQD from an exposed face and from borehole core is calculated using different methods that yield results that are inconsistent with each other.
- Persistency cannot be measured from borehole core and is generally assumed using a worst case scenario.
- Damage during the drilling process and stress relief of core tends to exaggerate the true fracture spacing of the rock.

While face mapping data has proven to be a useful addition to Sishen's geotechnical borehole data set, orientation data, and its application to verifying and updating the mine's structural model, is considered to be of greater value. In the anisotropic lithologies that are prevalent at Sishen, confidence in bedding orientation relative to design slopes is critical within the design and analysis process. Face mapping during the course of this project has proven invaluable in verifying the mine's structural model and will continue to add value as more pit boundaries are exposed and more faces are mapped.

In general the Maptek terrestrial laser scanner system has proved to be an invaluable tool for geotechnical data capture, geotechnical hazard assessment and structural mapping. With the current system of mapping and data capture in place at Sishen, future face mapping exercises will serve to increase geotechnical data confidence, improve geotechnical designs and enhance the mine's geotechnical risk mitigation capabilities.

REFERENCES

Alchin, D.J. (2008) Short note on the evaluation of the potential of an area west of the open pit, Sishen Iron Ore mine. Sishen Mine Internal Document. 18pp.

Alchin, D.J. and Botha, .W.J. (2005) The structural/stratigraphic development of the Sishen South (Welgevonden) iron ore deposit, South Africa, as deduced from ground gravity data modeling. Proceedings Iron Ore 2005 Conference, The Australasian Institute of Mining and Metallurgy, Melbourne, pp 29-41.

Altermann, W. and Hälbich, I.W. (1991). Structural history of the southwestern corner of the Kaapvaal Craton and the adjacent Namaqua realm: new observations and a reappraisal. Precambrian Research, Vol 52. 133-166.

Barton, N.R. (1973) Review of a new shear strength criterion for rock joints, Engng Geol., vol. 8. pp 287-332.

Barton, N. R. (1976) The shear strength of rock and rock joints. Int. J. Rock Mech. Min. Sci. and Geomech. Abstr., Vol. 13, no 9. pp 255-279.

Barton, N.R. (1982) Shear Strength Investigations for Surface Mining. 3rd Int. Conf. on Surface Mining. Vancouver, Canada. pp 171-196.

Barton, N.R. (1995). The influence of joint properties in modelling jointed rock masses. Keynote Lecture, 8th ISRM Congress (Tokyo), Balkema Publishers, Rotterdam.

Barton, N.R. and Bandis, S.C. (1982) Effects of block size on the shear behaviour of jointed rock. 23rd U.S. Symp. Rock Mech., Berkeley, California. pp 739-760.

Barton, N.R. and Bandis, S. (1990) Review of predictive capabilities of joint roughness coefficient and joint compressive strength model in engineering practice, Proc. International Symposium on Rock Joints, Balkema Publishers, Norway. pp 603-610.

Barton, N.R. and Choubey, V. (1977) The shear strength of joints in theory and in practice, Rock Mech., Vol. 10. pp 1-65.

Barton, N.R., Lien, R. and Lunde, J. (1974) Engineering classification of rock masses for the design of rock support. Rock Mechanics, Vol 6. pp 189-236.

Basson, I.J. (2010) Sishen Structural Study Part 1: Mapping, Analysis and 3D Modeling of the North Mine. Sishen Mine Internal Document. 54pp.

Beer, G., Oppriessnig, G., Gosler, H., Fasching, A. and Gaich, A. (1999) Geotechnical data acquisition, numerical simulation and visualization on site. Proc. 9th Int. Cong. Int. Soc. Rock Mech., Paris, Balkema Publishers. pp 1333-1338.

Beukes, N.J. (1983) Paleoenvironmental setting of iron-formations in the depositional basin of the Transvaal Supergroup, South Africa. In Iron-Formation: Facts and Problems. In: Trendall, A.C. and Morris R.C. (Editors) Developments in precambrian geology, Vol 6. Elsevier Science Publishers B.V. Amsterdam, Oxford, New York, Tokyo. 558 pp.

Bieniawski, Z.T. (1973) Engineering classification of jointed rock masses. Trans. S. Afr. Instn. Civ. Engrs., Vol 15, no.12. pp 335-344.

Bieniawski, Z.T. (1976) Rock Mass Classifications in Rock Engineering. Proceedings - Symposium on Exploration for Rock Engineering, Johannesburg. pp 97-106.

Bieniawski, Z. T. (1989) Engineering rock mass classifications : a complete manual for engineers and geologists in mining, civil, and petroleum engineering. Wiley-Interscience. 272 pp.

Bootsman, C.S. (1998). The evolution of the Molopo drainage. Ph.D Thesis, University of the Witwatersrand, Johannesburg, South Africa. 262pp.

Brady, B. H. G. and Brown, E. T. (1985) Rock Mechanics for Underground Mining: 1st Edition. George Allen & Unwin, London. 526 pp

Brady, B. H. G. and Brown, E. T. (1993) Rock Mechanics for underground mining: 2nd Edition. George Allen & Unwin, London 571 pp.

Brink, A.B.A and Bruin, R.M.H (2002) Guidelines for Soil and Rock Logging in South Africa. SAICE Geotechnical Division, Rivonia, South Africa. 45pp.

Butcher, R.J., Walker, D.J., Joughin W.C., Birtles, A.N., and Terbrugge, P.J. (2001) Methodology for the Safe Cleaning and Making Safe of Various Heights (10-35 m) Highwalls. SIMRAC Final Draft Project Report, Johannesburg. 343 pp.

Bye, A. R. and Bell, F. G. (2001) Stability assessment and slope design at Sandsloot open pit, South Africa. Int. J. Rock Mech. Min. Sci., Vol 38. pp 449-466.

Call, R. D. (1992) Slope stability. In Hartman, H.L. (Editor) SME Mining Engineering Handbook 2nd Edition, Volume 1. SME. Littleton, Colorado. 1840 pp.

Camonesa, L.A.M., Vargas, E.A., De Figueiredo, R.P. and Vellosoa, R.Q. (2013). Application of the discrete element method for modeling of rock crack propagation and coalescence in the step-path failure mechanism. Engineering Geology, Vol 153. pp 80-94.

Deere, D. U., Hendron, A. J., Jr., Patton, F. D. and Cording, E. J. (1967) Design of Surface and Near - Surface Construction in Rock. In Fairhurst, C. (Editors) Failure and Breakage of Rock. Society of Mining Engineers of AIME. New York. pp 237 - 302.

Dyke, G.P. (2006) A quantitative correlation between the mining rock mass rating and in-situ rock mass rating classification systems. M.Sc. Thesis - University of the Witwatersrand. 99 pp.

Eberhardt, E. (2016) Geotechnical Engineering. Practice & Design. Lecture 4: Kinematic Analysis. University of British Columbia Online Lecture Notes. https://www.eoas.ubc.ca/courses/ eosc433/ lecture-material/L4-KinematicAnalysis.pdf.

Eberhardt, E., Stead, D., Karami, A and Coggan, J. (2004) Numerical analysis of brittle fracture propagation and step-path failure in massive rock slopes. 57th Canadian Geotechnical Conference and the 5th joint CGS-IAH Conference, Quebec City, Quebec. Session 7 C, pp 1 -8.

Einstein, H.H., Veneziano, D., Baecher, G.B. and O'Reilly, K.J. (1983) The effect of discontinuity persistence on rock slope stability. Int. J. Rock Mech. Min. Sci. and Geomech. Abstr, Vol 20. pp 227-236.

Farr, J., Cheney, C., Baron, J., Peart, R. (1981) GS10 Project: Evaluation of Underground Water Resources, Final report. Botswana Geological Survey Department. 292 pp.

Fecker, E. and Rengers, N.F. (1971) Measurement of large scale rock planes by means of profilograph and geological compass. 1st Int. Symp. Rock Mech. Nancy. pp 1-18.

Feng Q. (2001) Novel methods for 3-D semi-automatic mapping of fracture geometry at exposed rock faces. Ph.D. Thesis - Division of engineering geology, Royal Institute of Technology (KTH), Stockholm, Sweden. 64 pp.

Feng, Q and Roshoff, K. (2006) Semi-automatic mapping of discontinuity orientation at rock exposure by using 3D laser scanning techniques. IAEG Paper no.751. 5 pp.

Franklin, J. A., Maerz, N. H. and Bennett, C. P. (1988) Rock mass characterization using photoanalysis. Engng. Geol., Vol 6, pp. 97-112.

Friese, A.E.W. (2007). Assessment of the tectono-structural evolution and its impact on mining in the lease area of Sishen Iron Ore Mine, Northern Cape, South Africa. Sishen Mine Internal Report. 121 pp.

Friese, AEW and Alchin, DJ, 2007. New insights into the formation, structural development, and preservation of iron ore deposits in the Northern Cape Province, South Africa. Proceedings Iron Ore 2007 Conference, The Australasian Institute of Mining and Metallurgy. Perth, Western Australia. pp 85-97.

Ghosh, S. K. (1993) Structural Geology Fundamentals and Modern Development. Pergamon Press Ltd., Oxford, United Kingdom. 376 pp.

Giani, G.P. (1992) Rock Slope Stability Analysis. Balkema Publishers, Rotterdam. 346 pp.

Goodman, R. E. (1980) Introduction to Rock Mechanics, 2nd Edition. Wiley. New York. 576 pp.

Google Earth (2017) Image ©2017 CNES/Airbus

Gumede, H. (2005). Development of data sets on joint characteristics and consideration of associated instability for a typical South African gold mine. M.Sc. Thesis - University of the Witwatersrand, Johannesburg, South Africa. 100 pp.

Haddon, I.G. (2005) The Sub-Kalahari Geology and Evolution of the Kalahari Basin. Ph.D. Thesis. University of the Witwatersrand, Johannesburg, South Africa. 295pp.

Haines, A. and Terbrugge, P.J. (1991) Preliminary Estimate of Rock Slope Stability using Rockmass Classification. Proc. 7th Int. Cong. Int. Soc. Rock Mech. Aachen, Vol 2. pp 887-892.

Hälbich, I.W., Scheepers, R., Lamprecht, D., van Deventer, J.L., De Kock, N.J. (1993). The Transvaal-Griqualand West banded iron formation: geology, genesis, iron exploitation. Journal of African Earth Sciences, Vol 16 (1,2). pp 63-120.

Harrison, J.P. (1993) Improved analysis of rock mass geometry using mathematical and photogrammetric methods. Ph.D. Thesis - Imperial College, London, U.K. 510 pp.

Hencher, S. (2015) Practical Rock Mechanics. CRC Press, Boca Raton, Florida. 356pp.

Hocking, G. (1976) A method for distinguishing between single and double plane sliding of tetrahedral wedges. Int. J. Rock Mech. Min. Sci. and Geomech. Abstr., Vol. 13, no 7. pp 225-226.

Hoek, E. (1994) Strength of rock and rock masses. News J ISRM Vol 2(2). pp 4-16.

Hoek, E. (2009) Fundamentals of slope design. Keynote address at Large Open Pit (LOP) Research Project, Slope Stability Conference 2009. Santiago, Chile. 25 pp.

Hoek, E and Bray, J. (1981) Rock Slope Engineering - Revised 3rd Edition. Institute of Mining and Metallurgy, London. 368 pp.

Hoek, E. and Brown, E.T. (1980) Empirical strength criterion for rock masses. J. Geotech. Engng Div., Vol 106. pp 1013-1035.

Hoek, E. and Brown, E.T. (1988) The Hoek-Brown failure criterion - a 1988 update. Proc. 15th Canadian Rock Mech. Symp. Toronto. pp 31-38.

Hoek, E. and Brown, E. T. (1997) Practical estimates of rock mass strength. Int. J. Rock Mech. Min. Sci. Vol 34 (8). pp 1165-1186.

Hoek, E., Carter, T.G. and Diederichs, M.S. (2013) Quantification of the Geological Strength Index Chart. 47th US Rock Mechanics / Geomechanics Symposium. San Francisco, USA. 8 pp.

Hoek, E. and Marinos, P. (2007) A brief history of the development of the Hoek-Brown failure criterion. Soils and Rocks, Vol 2. 13 pp.

Hoek, E., Marinos, P. and Benissi, M., (1998) Applicability of the geological strength index (GSI) classification for weak and sheared rock masses—the case of the Athens schist formation. Bull Eng Geol Env. Vol 57(2). pp 151-160.

Hudson, J. A. and Harrison, J.P. (2000) Engineering Rock Mechanics - An Introduction to the Principles. Elsevier, New York. 458 pp.

ISRM (1978) International Society for Rock Mechanics, Commission on Standardization of Laboratory and Field Tests. Suggested methods for the quantitative description of discontinuities in rock masses. Int. J. Rock Mech. Min. Sci. and Geomech. Abstr, Vol 15(6). pp 319-368.

ITASCA (2016) 3D Numerical Modelling for Kumba Iron Ore Operations Sishen Mine. Sishen Mine Internal Report. 45pp.

Jones, C.R. (1982) The Kalahari of southern Africa. In: Smiley, T.L. (Editor), The Geological Story of the Earths Deserts. Uppsala. pp 20-34.

Kersten, R.W.O. (1969) Structural analysis of fractures around underground excavations on a Witwatersrand Gold Mine. M.Sc Thesis, University of Pretoria, Pretoria.

Kliche, C.A. (1999) Rock Slope Stability. Society for Mining, Metallurgy, and Exploration, Inc. Littleton, USA. 253 pp.

Kumba Iron Ore (2015) Kumba Iron Ore Integrated Annual Report 2015.

Landmark, G. L. and Villaescusa, E (1992) Geotechnical mapping of Mount Isa Mines. Proc. Western Australia Conference on Mining and Geomechanics, Western Australian School of Mines. pp 329-333.

Laubscher, D. H. (1990) A geomechanics classification system for the rating of rock mass in mine design. J. S. Afr. Inst. Min. Metall., Vol 90. pp 257-273.

Laubscher, D.H. (1994) Cave mining - the state of the art. Jr. S. Afr Inst. Min. Metall., Vol 94(10). pp 279-293.

Lisjak, A. and Grasselli, G. (2014) A review of discrete modeling techniques for fracturing processes in discontinuous rock masses. J Rock Mech Geotech Eng, Vol 6, pp 301-314.

Lisle, R.J. (2004) Geological Structures and Maps: A Practical Guide. Butterworth-Heinemann. Burlington, Massachusetts. 106 pp.

Little, M. J. (2006) Geotechnical strategy and tactics at Anglo Platinum's PPRust open pit operation, Limpopo Province, South Africa. M.Sc. Thesis - University of the Witwatersrand. 176 pp.

Lorig, L., Stacey, P. and Read, J. (2009) Slope Design Methods. In: Read, J and Stacey, P (Editors) Guidelines for Open Pit Slope Design. CSIRO Publishing, Collingwood, Victoria. pp 1-15.

Maptek (2013) I-Site Studio Training Manual, Version 4.2. Sishen Mine Internal Maptek Training Course.

Marinos, P. and Hoek, E. (2000) GSI: a geologically friendly tool for rock mass strength estimation. Proceedings of the GeoEng2000 at the International Conference on Geotechnical and Geological Engineering, Melbourne. pp 1422-1442.

Marinos, P. and Hoek, E. (2001) Estimating the geotechnical properties of heterogeneous rock masses such as flysch. Bull. Eng. Geol. Environ., Vol 60. pp 82-92.

Marinos V., Marinos P. and Hoek E. (2005) The geological Strength index: applications and limitations. Bull. Eng. Geol. Environ. Vol 64. pp 55-65.

Markland, J.T. (1972) A useful technique for estimating the stability of rock slope when the rigid slide type of failure is expected. Imperial College of Science & Technology, London. 20 pp.

Marshak, S. and Mitra, G. (1988) Basic Methods of Structural Geology. Prentice Hall, California. 446 pp.

McQuillan, A. (2013) Comparison of photogrammetry and survey laser scanning output data for use in mapping joints in open cut highwalls. 13th Coal Operators' Conference, University of Wollongong, The Australasian Institute of Mining and Metallurgy & Mine Managers Association of Australia, 2013. pp 347-354.

Milne D., Germain P. and Potvin Y. (1992) Measurement of rock mass properties for mine design. Proc. Int. Conf. Eurock '92. Thomas Telford. London. pp. 245-250.

Milne, D. (2007). Problems with rock mass classification for empirical and numerical design. Proceedings of the International Workshop on Rock Mass Classification in Underground Mining. National Institute for Occupational Safety and Health (NIOSH). Atlanta, Georgia. pp 111-118.

Mohajerani, A. and Aust, M.I.E. (1989) Rock discontinuity spacing statistics: log-normal distribution versus exponential. Geomech N17. June 1989. pp 20-21.

Mortimer, B. (1995) Report on Structural Geological Analysis - Sishen. Sishen Mine Internal Report. 71pp.

Netterberg, F. (1980) Geology of Southern African calcretes: 1. Terminology, description, macrofeatures and classification. Trans. geol. Soc. S. Afr., Vol 83. pp 255-283.

Norman, N. and Whitfield, G. (2006) Geological Journeys, a traveller's guide to South Africa's rocks and landforms. Struik Publishers, Cape Town, South Africa. 323 pp.

Palmström, A. (1982) The volumetric joint count—a useful and simple measure of the degree of jointing. In Proceedings of the Fourth International Congress IAEG, New Delhi. pp 221-228.

Palmström, A. (1995) RMi - a rock mass characterization system for rock engineering purposes. Ph.D. Thesis. University of Oslo. Oslo, Norway. 409pp.

Palmström, A. (2001) Measurement and characterization system for rock mass jointing. In: Sharma, V.M. and Saxena, K. R. (Editors). In-situ characterization of rocks. Balkema Publishers. Oslo, Norway. pp 49-97.

Palmström, A. (2005) Measurements of and correlations between block size and rock quality designation (RQD). Tunnels and Underground Space Technology, Vol 20. pp 326-377.

Palmström, A. (2009) Combining the RMR, Q, and RMi classification systems. www.rockmass.net. 25pp.

Palmström, A. and Broch, E. (2006) Use and misuse of rock mass classification systems with particular reference to the Q-system. Tunnels and Underground Space Technology, Vol 21. pp 575-593.

Patton, F. D. (1966) Multiple modes of shear failure in rock, Proc. 1st Int. Cong. Int. Soc. Rock Mech., Colouste Gulbenkian Foundation, Lisbon, Vol. 1. pp 509-513.

Pierce, M., Cundall P. and Potyondy, D. (2007) A synthetic rock mass model for jointed rock. In: Eberhardt, E., Stead, D. and Morrison, T. (Editors). Rock Mechanics: Meeting Society's Challenges and Demands, Volume 1: Fundamentals, New Technologies & New Ideas. Taylor Francis Group. London. pp 341-349.

Piteau, D. R. (1970) Geological factors significant to the stability of slopes in cut rock. Proc. Sym. On Planning Open Pit Mines, Johannesburg. pp 33-53.

Piteau, D. R. (1973) Characterising and extrapolating rock joint properties in engineering practice. In: Müller L. (Editor) Geomechanics — Progress in Theory and Its Effects on Practice. Rock Mechanics. Vol 2. pp 2-31.

Potvin, Y., Dight, P.M. and Wesseloo, J. (2012). Some pitfalls and misuses of rock mass classification systems for mine design. J. S. Afr. Inst. Min. Metall., Vol 112. pp 697 - 712.

Potyondy, D.O. and Cundall, P.A. (2004) A Bonded-Particle Model for Rock. Int. J. Rock. Mech. Min. Sci. Vol 41. pp 1329 - 1364.

Price, N.J. (1966) Fault and Joint Development in Brittle and Semi-Brittle Rock. Pergamon, Oxford. 172 pp.

Priest, S.D., (1993) Discontinuity Analysis for Rock Engineering. Chapman & Hall, London. 381 pp.

Priest, S.D. and Hudson, J.A. (1976) Discontinuity spacings in rock. Int. J. Rock Mech. Min. Sci. & Geomech. Abstr., Vol 13. pp 135-148.

Raghu N. Singh, N.R. and Ghose, A.K. (2006) Engineered Rock Structures in Mining and Civil Construction. Taylor Francis Group, London. 520 pp.

Ramsay, J.G. (1967) Folding and Fracturing of Rocks. McGraw-Hill, New York. 410 pp.

Read, J., Jakubec, J. and Beale, J. (2009) Field Data Collection. In: Read, J and Stacey, P (Editors) Guidelines for Open Pit Slope Design. CSIRO Publishing, Collingwood, Victoria. pp 1-15.

Reid, T. R. and Harrison, J. P. (2000) A semi-automated methodology for discontinuity trace detection in digital images of rockmass exposures. Int. J. Rock Mech. Min. Sci., Vol 37. pp 1073-1089.

RocScience (2011) Snowden Modified Anisotropic Linear Strength. https://www.rocscience.com/help/slide/webhelp/slide_model/materials/Snowden_Modified_Anisotropic_Linear.htm.

RocScience (2012) Dips Kinematic Analysis Software (Version 6). https://www.rocscience.com.

Sen, Z. and Kazi, A.M. (1984) Discontinuity spacing and RQD estimates from finite length scanlines. Int. J. Rock Mech. Min. Sci. & Geomech. Abstr. Vol 21. pp 203-212.

Simangunsong, G.M., Matsui, K. and Shimada, H. (2004) Analysis of ground vibration and fragmentation by blasting: case study at limestone and shale-stone quarries of PT Indocement Tunggal Prakarsa, West Java, Indonesia. In Hardygóra, In M., Paszkowska G. and Sikora, M. (Editors) Mine Planning and Equipment Selection, Taylor Francis Group, London. pp 309 - 315.

Singh, B. and Goel, R.K. (1999) Rock mass classification - A practical approach in civil engineering. Elsevier, New York. 267 pp.

Singhal, B.B.S. and Gupta, R.P. (2010) Applied Hydrogeology of Fractured Rocks. Springer Science and Buisness Media B.V. 94 pp.

Slob, S. and Hack, H. R. G. K (2007) Fracture mapping using 3D laser scanning techniques. 11th Int. Cong. Int. Soc. Rock Mech. Lisbon, Portugal. pp 299 - 302.

Stacey, P. (2009) Fundamentals of Slope Design. In: Read, J and Stacey, P (Editors) Guidelines for Open Pit Slope Design. CSIRO Publishing, Collingwood, Victoria. pp 1-15.

Stacey T.R., (2007). Slope stability in high stress and hard rock conditions, Slope Stability 2007-Proceedings International Symposium on Rock Slope Stability in Open Pit Mining and Civil Engineering. Australian Centre for Geomechanics, 12-14 September 2007, Perth, Australia. pp 187-201.

Stead, D., Eberhardt, E., Coggan, J. and Benko, B. (2001) Advanced Numerical Techniques in Rock Slope Stability Analysis - Applications and Limitations. Landslides - Causes, Impacts and Countermeasures. Davos, Switzerland. pp 615-624.

Stowe, C.W. (1986) Synthesis and interpretation of structure along the north-eastern boundary of the Namaqua Tectonic Province, South Africa. Trans. geol. Soc. S. Afr., Vol 89. pp 185-198.

Terzaghi, R. D. (1965). Sources of Error in Joint Surveys. Geotechnique, Vol 15(3), pp 287- 304.

Tesfamariam, E.K. (2007) Comparing Discontinuity Surface Roughness Derived from 3D Terrestrial Laser Scan Data with Traditional Field-Based Methods. M.Sc Thesis, International Institute for Geo-Information and Earth Observation Science. 87 pp.

Van Schalkwyk, J.F. and Beukes, N.J. (1986) The Sishen iron ore deposit, Griqualand West. In: Anhaeusser, C.R. and Maske, S. (Editors) Mineral Deposits of Southern Africa, Vol. I. Geol. Soc. S. Afr., Johannesburg. pp 931-956.

Van Wyk, J.P. (1980). Die geologie van die Rooinekke-Matsap-Wolhaarkop in Noord-Kaapland met spesiale verwysing na die Koegas Subgroup en die Transvaal Supergroep. M.Sc. Dissertation (unpublished), Rand Afrikaans University, Johannesburg, South Africa. 159 pp.

Whitten, D.G.A. and Brooks, J.R.V. (1972) The Penguin Dictionary of Geology. Penguin Books Ltd., Harmondsworth, Middx. 495 pp.

Whitten, E.T.H. (1966) Structural Geology of Folded Rocks. Rand McNally and Co., Chicago, Illinois. 663 pp.

Williams, P., Floyd, J., Chitombo, G. and Maton, T. (2009) Design Implementation. In: Read, J and Stacey, P (Editors) Guidelines for Open Pit Slope Design. CSIRO Publishing, Collingwood, Victoria. pp 1-15.

Wines, D.R., Lilly, P.A. (2001) Measurement and analysis of rock mass discontinuity spacing and frequency in part of the Fimiston Open Pit operation in Kalgoorlie. Int. J. Rock Mech. Min. Sci., Vol 39. pp 589-602.

Wyllie, D.C. (2013) Foundations on Rock: Engineering Practice, Second Edition. CRC Press, London. 432 pp.

Wyllie, D.C. and Mah, C. (2004) Rock Slope Engineering: Fourth Edition. CRC Press, London. 456 pp.

Zhang, L. (2006) Engineering properties of rocks, second edition. Elsivier, Oxford. 112pp.